Properties of galaxies found in a deep blind neutral hydrogen survey

Robert Frank Minchin

A thesis submitted to the
University of Wales Cardiff
for the degree of

Doctor of Philosophy

May 2001

DECLARATION

This work has not previously been accepted in substance for any degree and is not being concurrently submitted in candidature for any degree.

Signed _____ (candidate)

Date _____

STATEMENT 1

This thesis is the result of my own investigations, except where otherwise stated.

Other sources are acknowledged giving explicit references. A bibliography is appended.

Signed _____ (candidate)

Date _____

STATEMENT 2

I hereby give consent for my thesis, if accepted, to be available for photocopying and for inter-library loan, and for the title and summary to be made available to outside organisations.

Signed _____ (candidate)

Date _____

Summary

The DEEP survey used the Parkes neutral hydrogen (HI) multibeam system to observe a $4^\circ \times 8^\circ$ region to a noise level of 4 mJy per 13.2 $\mathrm{km\,s^{-1}}$ channel, or 3.5 times the column-density sensitivity of previous surveys. A blind HI survey like DEEP avoids optical selection-effects such as discrimination against low surface-brightness (LSB) galaxies in defining the sample. HI parameters are presented for 69 galaxies found within this region. A deep optical image (eight 1-hour tech pan plates) was obtained, centred on the same position as the HI survey. Optical parameters from this data are presented for 54 galaxies uniquely identified as optical counterparts of the HI sources. No evidence was found for a population of low column-density galaxies that would be undetected in shallower surveys.

No high-luminosity, LSB galaxies have been found, however high HI mass, LSB galaxies were seen. That LSB galaxies make up more than 12% of the total population of high-luminosity galaxies can be ruled out with 95% confidence, however LSB galaxies could, to the same confidence level, contribute up to 46% of high HI mass galaxies. Luminosity is not a good guide to the total baryon content of LSB galaxies.

The surface-brightness distribution and the luminosity function have been found for the DEEP galaxies. The surface-brightness distribution is truncated at the high surface-brightness end, with the down-turn occuring near the 'Freeman-law' value while it is slowly increasing towards lower surface-brightnesses. The luminosity function is fairly flat, consistent with faint-end slopes for field galaxies from the literature. Further analysis of this data shows that low surface-brightness galaxies could make a significant contribution to the cosmic baryon density (19% to 71% at 1σ) and to the dynamical mass density of the Universe (27% to 90% at 1σ).

Acknowledgements

I would like to firstly thank my wife, Helen, for her unfailing help and support over the last few years and without whom this thesis may never have been finished. She was there at the start and she saw it through with me to the very end. I would also like to thank my parents who were always there with advice and assistance when I needed them.

This project would never have begun without my supervisor, Mike Disney, who has been a constant source of encouragement and interesting discussions. Without his advice I would have been stuck on a number of occasions and would not have followed up some interesting results. Gareth Banks also deserves my thanks both for initiating the DEEP survey and for showing me the ropes by involving me fully in his work. Peter Boyce has suffered more than most from having to read and re-read drafts of this thesis, yet hardly ever complained and made many useful comments. He also calibrated the optical tech-pan data which forms a major part of this work. I would also like to thank the other members of the research group in Cardiff for the many discussions we have had: Hugh Lang, Dan Zambonini, Marco Grossi, Diego Garcia and Catherine Vlahakis. Thanks also to our Starlink manager, Rodney Smith, who showed great patience in installing some particularly recalcitrant pieces of multibeam software, and to all the administative staff in the department who made things run smoothly and helped me with the paperwork.

The multibeam team in Australia accepted me into the working group and have provided much support in the way of software and observing techniques to this project. The staff at the ATNF were also very helpful. In particular I would like to thank my ATNF co-supervisor Ron Ekers for his encouragement and useful discussions along with Lister Staveley-Smith, Erwin de Blok, Alan Wright, Andrew Hunt, and Ian Stewart. I co-wrote PICASSO with Alan Wright during my time in Parkes and later while he was in Cardiff. Many people helped make my stay in Parkes enjoyable, in particular John Sarkissian, and Rick Twardy who helped me to escape from the observatory. I would also like to thank Ken Freeman and Helmut Jerjen at the ANU for help and advice on optical follow-up and spectroscopy and Virginia Kilborn at Jodrell Bank for useful discussions on HI astronomy. Quentin Parker made the optical observations without which this study would have been a lot poorer.

Numerous people in Cardiff have helped me by offering their friendship and hospitality while I was working on this thesis. I would like to thank Gareth Leyshon in particular for his support and prayers. There were many people at the Catholic Chaplaincy and St Peter's who welcomed me to Cardiff and helped me to become part of the community. They all too have my thanks. In particular, Rhodri and Eva Evans, Arthur Haythornthwaite, Clare Liddle, Christian Sachs and Frank Trombley often kept me entertained on Sunday evenings. Fr Graham Venn and Fr John Meredith were good friends to me and the members of CARIAD and Youth 2000 offered an opportunity to relax in a prayerful environment. I would also like to thank the users of the post-grad terminal room in Cardiff for some fascinating discussions and many others in the department for their support and friendship.

Last, but by no means least, I would like to thank the examination team of Jon Davies, Rod Davies,

Piet van der Kruit and Steve Eales for helping me relax on the day and for useful suggestions of future work.

Contents

List of Figures

List of Tables

Chapter 1

Introduction

1.1 Overview

The study and cataloguing of galaxies is one of the main activities in extra-galactic astronomy. Through this we learn about the properties of galaxies, and how these properties vary between different types of galaxy. Statistics can be used to test theories of galaxy formation and evolution against the observed population and thus further our knowledge of how the Universe has evolved.

However, it has become apparent over the last quarter of a century (e.g. Disney 1976; Disney & Phillipps 1983; Bothun, Impey, & McGaugh 1997) that we may be missing a significant number of galaxies, containing a significant amount of the matter in the Universe, from our catalogues. Low surface-brightness galaxies are hidden beneath the brightness of the night sky, leaving us to see only the fraction of galaxies that are visible and meet our selection criteria. It could be that most of the baryonic matter in the Universe is contained within these 'Crouching Giants', that our theories of galactic evolution fail to include.

In order to carry out good cosmology, it is important for us to know the baryon fraction (e.g. Fukugita, Hogan, & Peebles 1998). A significant proportion of baryons could, however, be contained within LSB galaxies (e.g. Impey & Bothun 1997) and thus missing from our census, which is limited to those galaxies easily found in optical surveys. We know that giant LSB galaxies exist – the serendipitous discovery of Malin 1 (Bothun et al. 1987) during a survey of dwarf galaxies in the Virgo cluster has shown this – but we do not yet have a large enough sample of such galaxies to draw any conclusions about their general

properties, nor do we know whether they will turn out to be numerous enough to contribute significantly to the baryon density of the universe. Malin 1 has a very high $M_{\rm HI}/L_{\rm B}$ ratio and similar examples could be discovered in blind HI surveys if they were equally gas rich, but there is no guarantee that this will be the case.

This thesis presents the results of the DEEP project, a long integration time blind survey for neutral hydrogen (HI). One of the aims of this survey is to identify whether there is a population of galaxies that can be detected in HI but are not included in optical catalogues. The survey would be capable of detecting Malin 1 over a volume of 14900 Mpc^3 and a similar $M^\star_{\rm HI}$ galaxy with a twelfth the amount of hydrogen over a volume of 10800 Mpc^3. It goes almost 4 times deeper than any previous HI survey in its sensitivity to low column-density objects, where the hydrogen is spread over a greater area than is normal, and therefore investigates previously unexplored areas of parameter space. The survey is also likely to turn up unexpected objects which could be very interesting in themselves. Previous blind-surveys at other wavelengths have often turned up unusual populations which were 'bright' at that wavelength, similarly it is probable that a large number of galaxies found by the DEEP survey will have a high gas-fraction – implying that they are relatively unevolved – and could therefore be important test-beds for theories of galaxy evolution and formation.

Section 1.2 discusses the strong selection effects that have been identified in the optical against low surface-brightness galaxies and also the possible discrimination against compact high surface-brightness (HSB) galaxies. Both of these populations may be detected in an HI survey, such as DEEP, while they would not be included in optical catalogues due to having a low isophotal magnitude (LSB galaxies) or being mistaken for stars (HSB galaxies). This section also discusses optical surveys for these LSB and HSB galaxies and their results.

Section 1.3 discusses the selection effects present in HI surveys and previous blind HI surveys that have been carried out. If HI column density is linked to optical surface-brightness (van der Hulst et al. 1993; de Blok, McGaugh, & van der Hulst 1996; Disney & Banks 1997), a large fraction of low surface-brightness galaxies may also have unusually low HI column-densities. These would therefore have evaded detection in previous HI surveys which did not reach particularly low column-density limits. Other issues, such as profile shape, could also lead to discrimination against LSB galaxies in HI surveys even though it is known (Romanishin et al. 1982; van der Hulst et al. 1993) that LSB galaxies cover the same range of HI masses as 'normal' galaxies.

Section 1.4 describes the importance of deep HI surveys in more detail and discusses the DEEP survey in particular, while Section 1.5 gives an outline of the thesis.

1.2 Optical Surveys & Selection Effects

1.2.1 Optical selection effects and Visibility

Freeman (1970) collated surface-photometry data on 36 disc galaxies that appeared in the literature between 1958 and 1970. On analysing this (non-statistical) sample, he found that "for twenty-eight of the thirty-six galaxies, $B(0)_c$ [the B-band central surface brightness, corrected for inclination] is nearly constant at $B(0)_c = 21.65 \pm 0.30(\sigma)$ mag per square second of arc along the entire sequence from S0 to Im, despite a range in absolute magnitude of nearly 5 mag." The surface-brightness distribution (SBD) from Freeman (1970) is shown in Figure 1.1. This distribution, $\mu_B = 21.65 \pm 0.3$, came to be known as 'Freeman's Law', even though Freeman never claimed it as a 'law' and, as it refers to the *corrected* central surface-brightness, it is not actually a description of the distribution of *observed* central surface-brightness.

Freeman (1970) asked in his conclusions, "Why is the surface-brightness scale for these disks approximately the same for about three-quarters of the sample?". Disney (1976) provided a possible answer – observational selection effects. He proposed that galaxies were included in catalogues based on the isophotal diameter – so LSB galaxies were discriminated against as only a small portion of the disk was above the limiting isophote, giving them a small isophotal diameter, and HSB galaxies were discriminated against as they were compact, again giving them a small isophotal diameter.

That there might be selection due to surface-brightness was not a new idea, see for instance Zwicky (1957), Arp (1965) and de Vaucouleurs (1974). In addition, although Freeman's result was the first direct measurement of the SBD, that it was highly peaked could be inferred from the result of Holmberg (1966) that there was a strong correlation between magnitude and log diameter. It can be seen (Figure 1.2) that Holmberg's result is well explained, at a qualitative level, by the simple selection effects proposed by Arp (1965), although Arp's selection band is considerably wider (10 magnitudes) than the distribution of Holmberg's sample and does not work at a quantitative level.

Disney (1976) was, however, the first to attempt to tie together the observed SBD and the selection effects in a quantitative manner. In addition to the result of Freeman (1970), which explicitly found a

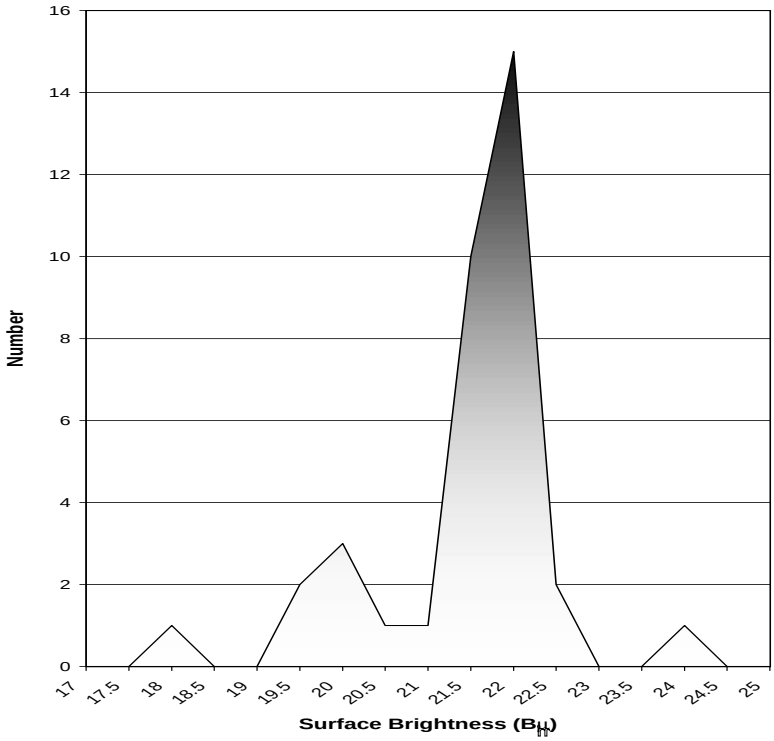

Figure 1.1: Surface Brightness distribution from Freeman (1970). It can be seen that the distribution is highly peaked at the 'Freeman's Law' value of $\mu_{\rm B} = 21.65 \pm 0.3$.

constant central surface-brightness for spiral galaxies, Disney analysed the results of Fish (1964) for elliptical galaxies. Fish had found that the binding energy of elliptical galaxies varied as their mass to the power 3/2: $\Omega \propto M^{3/2}$. Disney showed that the actual measurements made were of the luminosity (L) and the scale length (α), and that 'Fish's law' therefore implied $L_T/\alpha^2 =$ constant. However, $L_T/\alpha^2 \propto \sigma(0)$ – the central surface brightness, therefore Fish's result implied a constant central surface-brightness for ellipticals. Further analysis showed that the implied peak in the SBD was at 14.8 ± 0.9 Bμ (Bμ = B mags arcsec^{-2}).

Disney modelled spiral galaxies as face-on disks with exponential surface-brightness profiles and elliptical galaxies as having $r^{1/4}$ surface-brightness profiles (de Vaucouleurs, 1959). This gave a peak in the volume over which these galaxies could be seen – their visibility function, $V(\phi)$ – at $\mu_0 = \mu_L - 8.69$ for ellipticals

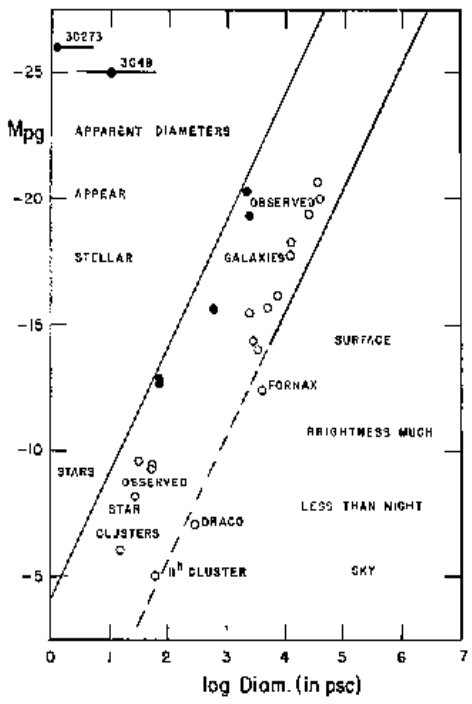

(a) Surface-brightness selection from Arp (1965)

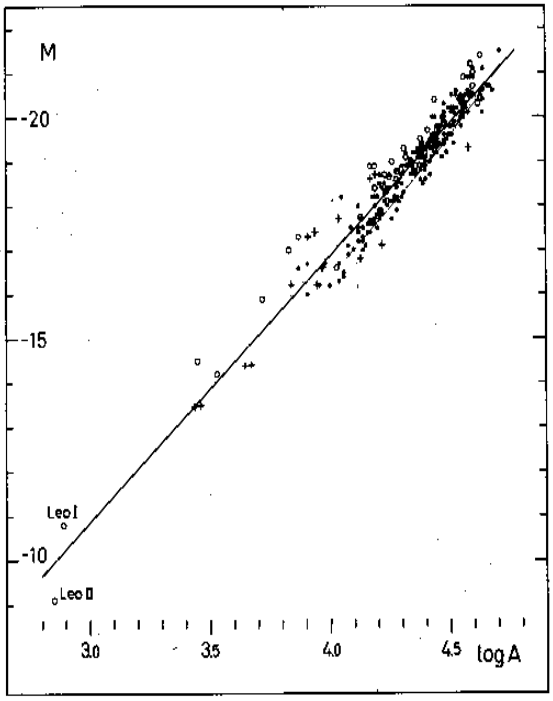

(b) Magnitude-diameter relationship from Holmberg (1966)

Figure 1.2: Surface-brightness selection from Arp (1965) and magnitude-diameter relationship from Holmberg (1966). It can be seen that Arp's selection effects explain the result of Holmberg (1966) at a qualitative level. However the selection band proposed by Arp has a width of around 10 magnitudes, considerably wider than the scatter seen by Holmberg.

and $\mu_0 = \mu_L - 2.17$ for spirals, where μ_L is the limiting isophote for detection. For the B_J Schmidt plates used in the sky surveys, Disney assumed that $\mu_L = 24$ B mags arcsec^{-2}, giving peaks at $\mu_B = 15.31$ for ellipticals and $\mu_B = 21.83$ for spirals. This can be seen to be close to the observed peaks in the SBDs at $\mu_B = 14.8$ and $\mu_B = 21.65$.

The effect of this discrimination due to size can be seen in an example by Bothun, Impey, & McGaugh (1997) of exponential disc galaxies with various central surface-brightnesses and scale lengths (see Table 1.1). In this example, galaxies A – D all have the same luminosity, while galaxy E is a dwarf galaxy with $1/10^{\text{th}}$

Table 1.1: Example galaxies from Bothun, Impey, & McGaugh 1997

	Scale Length	Central Surface-brightness	Inclusion distance[a]	Percentage of sample[a]
Galaxy A	0.5 kpc	16.0 Bμ	60 Mpc	9%
Galaxy B	5.0 kpc	21.0 Bμ	125 Mpc	72%
Galaxy C	25.0 kpc	24.5 Bμ	76 Mpc	18%
Galaxy D	50.0 kpc	26.0 Bμ	0 Mpc	0%
Galaxy E	5.0 kpc	23.5 Bμ	30 Mpc	1%

[a]For a survey where the selection is based on a minimum diameter of $1'$ at a limiting isophote of 25 B mags arcsec^{-2}

of the luminosity of the other galaxies but with the same physical size as the 'normal' galaxy B.

This example shows that a survey where no correction is made for visibility effects will be biased towards Freeman's Law galaxies, such as Galaxy B. In addition to this, the numbers of LSB galaxies (such as Galaxy C) and HSB galaxies (such as Galaxy A) detected will be small, so any correction made will be subject not only to difficulties in determining the correction to be applied but also to errors due to small-number statistics. For very low surface-brightness galaxies such as galaxy D, the statistics do not exist – the only known example of this class, Malin 1, was discovered serendipitously during an HI survey of Virgo dwarfs (Bothun et al. 1987), and even then only due to its bulge component – which may well not be present in other such giant LSB galaxies – being misidentified as a Virgo dwarf.

Kormendy (1977) offered an alternative explanation for 'Freeman's Law' – that it was an artefact of the fitting process used to determine the central surface-brightness of the exponential disc. Kormendy modelled disc and spheroidal contributions for a variety of true central disc surface-brightnesses and found that, except for particularly high surface-brightness discs, the spheroid dominated down to the isophotal limit and forced the fitted central surface-brightness to be close to Freeman's value.

Disney's conclusion that selection effects were responsible for the sharply peaked observed SBD and that there were probably numerous low surface-brightness galaxies remaining undiscovered in the local Universe

was opposed by Shostak (1977) who found no unambiguously extragalactic new sources in a neutral-hydrogen survey (see Section 1.3.3). Further doubt was thrown on the issue by Freeman (1978) who raised four objections to Disney's conclusion:

1. That the preferred value of μ_0 depended on the value of μ_{lim}, so that the newer IIIa-J emulsions with $\mu_{lim} \sim 26$ Bμ should have a lower preferred value and thus turn up large LSB galaxies – which were not being seen on those plates.

2. That the preferred value depended on the galaxies being selected by the light in their discs, but that most disc galaxies were dominated by the bulge at the $\mu = 24$ Bμ level – so selection should be dominated by the bulge.

3. That the approximate constancy of μ_0 only appeared after correction for inclination and galactic absorption – the uncorrected values of μ_0 fell over a much wider range from 19.6 to 23.1 Bμ. It is these uncorrected values that would influence selection.

4. That the selection effect is not strong enough to exclude nearby HSB galaxies, which have not been detected.

Allen & Shu (1979) re-analysed the data from Freeman (1970) and Fish (1964) and found a different position for the surface-brightness peak from those predicted by Disney (1976), in particular the difference between the peaks for disc and elliptical galaxies, found to be 6.85 magnitudes by Disney (1976) was re-calculated to be 7.83 magnitudes – rather different from the factor of e^6, or 6.52 magnitudes, predicted by Disney (1976). They also claimed that the data showed no evidence for discrimination against HSB galaxies, as the brightest such galaxies would be expected to have isophotal sizes considerably larger than the selection limit. Thus they wished to re-write 'Freeman's Law' and 'Fish's Law' to state that:

> Very few elliptical and spiral galaxies have extrapolated central isophotes which are brighter than, respectively, 12.0 Bμ and 19.5 Bμ.

However, re-analysis of their data shows that the same method they use to exclude galaxies with central surface-brightnesses brighter than 19.5 Bμ also excluded galaxies with μ_0 fainter than 23.4 Bμ. In addition to this, Allen & Shu had taken the limiting isophote of the plates to be 25 Bμ, if instead this is taken to

be 24 Bμ, as Disney (1976) and Freeman (1978) assumed, then their analysis would allow a range in central surface-brightness of approximately 17 to 23.5 Bμ.

Phillipps & Disney (1983) re-visited the work of Kormendy (1977) and showed that for galaxies with significant spheroidal components, fitting would give a central surface-brightness close to the Freeman value as the slope of the surface-brightness profile near $\mu = 25$ Bμ is the same for a spheroidal component as for a disc with $\mu_0 = 21.65$, as found by Kormendy (1977). Phillipps & Disney also showed that the hardest discs to 'hide' beneath a spheroidal component were those with $\mu_{lim} - \mu_0$ in the range 2 – 3, e.g. those near the Freeman value, as these have the largest apparent size – discs with either lower or higher surface-brightnesses than these appear smaller and are thus more easily dominated by spheroid. Domination by the spheroid, which is linked to the visibility of the disc, can therefore explain both the lack of LSB and HSB discs in Freeman's sample.

Disney & Phillipps (1983; DP 83) revised the visibility function to include selection based on magnitude as well as diameter, and showed that the isophotal magnitude was considerably lower than the total magnitude for low surface-brightness galaxies. This would lead to these galaxies being excluded from catalogues as they appeared less luminous than they truely were. They also showed that, for high surface-brightness galaxies, saturation of the photographic plates meant that the measured magnitudes were considerably less than the true total magnitudes.

Most catalogues will have both magnitude and diameter limits, in this case the two limits are applied simultaneously and the detection limit is the lower of the two limits at any given surface-brightness. This gives a very sharply peaked function with low surface-brightness galaxies being excluded as too faint and high surface-brightness galaxies being excluded as too small, DP 83 refer to the peak - at the surface-brightness where the two limits intersect - as the catalogue surface-brightness, μ_{cat}. For a limiting surface-brightness of $\mu_{\rm B} = 24$ mags arcsec^{-2} and catalogue limits of $m_{\rm B} = 15$ and $\theta = 20''$, the peak for spiral galaxies is at $\mu_{cat} \simeq 21$ Bμ, while for a limiting surface-brightness of $\mu_{\rm B} = 26$ mags arcsec^{-2} and slightly deeper catalogue limits of $m_{\rm B} = 16$ and $\theta = 20''$, the peak for spiral galaxies is at $\mu_{cat} \simeq 21.2$ Bμ.

The saturation of the central regions of high surface-brightness galaxies on photographic plates has no effect unless the diameter limit of the catalogue is very small and the magnitude limit is very bright, as the high surface-brightness galaxies that are affected are already excluded from most catalogues as being too small. This means that switching from photographic plates to CCDs has little effect on the visibility of HSB galaxies, as can be seen clearly from Figure 1.3. However, this saturation could affect nearby HSB galaxies

which would otherwise be large enough to be identified as such, as it will both lower their total magnitude and make them appear much more star-like.

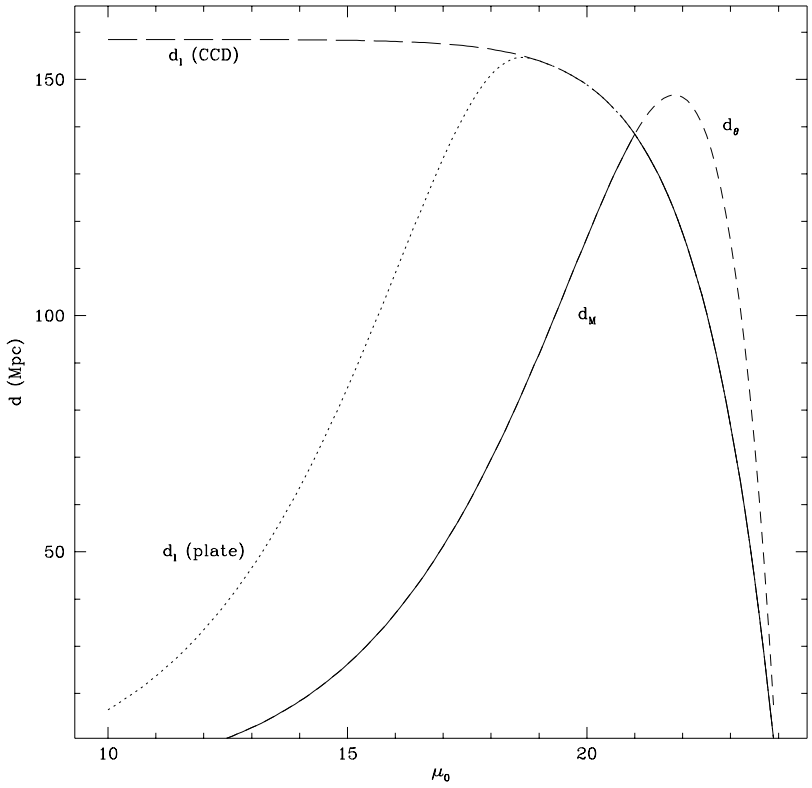

Figure 1.3: Distance limits from Disney & Phillipps (1983) for $\mu_{lim} = 24$ Bμ, $m_l = 15$ B mag, and $\theta_l = 20''$. It can be seen that the two limits intersect near the 'Freeman Law' value, so that discs with central surface-brightnesses near this value can be seen to greater distances. It should be noted that although CCDs do not saturate as quickly as plates, so d_l (CCD) does not turn down as d_l (plate) does, this has no effect on the distance limit, d_M.

This figure, modified from DP 83, shows how the limits due to apparent magnitude and angular-size intersect for galaxies with $M = -21$ B mag and catalogue limits of $m_l = 15$ B mag, $\theta_l = 20''$, and $\mu_l = 24$ B mag arcsec^{-2}. The maximum distance to which a galaxy can be seen, the minimum of d_l and d_θ, is given by d_M. It can be seen that LSB galaxies are excluded by the magnitude limit and HSB galaxies are excluded by the size-limit. The dashed line shows the situation for CCDs, where saturation is excluded. It can be

seen that this does not change the visibility of HSB galaxies as these galaxies are still excluded on the basis of their size.

The formal distance limits from DP 83 are

$$d_l = \left(\frac{L_{ap}}{L_T}\right)^{1/2} 10^{0.3(m_l - M + 5)} \tag{1.1}$$

for the luminosity limit, where L_{ap} is the isophotal luminosity, L_T is the total luminosity, m_l is the limiting apparent magnitude and M is the true absolute magnitude, and

$$d_\theta = \left(\frac{R_{ap}}{R_L}\right) \frac{10^{0.2(\mu_L - M + 5)}}{\pi^{1/2}\theta_l} \tag{1.2}$$

for the diameter limit, Where R_{ap} is the isophotal radius, and R_L is a normalising radius – the radius of a galaxy of luminosity L_T with a surface-brightness μ_L.

In these equation, L_{ap}/L_T is given by:

$$\frac{L_{ap}}{L_T} = X - (1 + 0.4 \ln 10\,(\mu_L - \mu_0))\, 10^{-0.4(\mu_L - \mu_0)} \tag{1.3}$$

and R_{ap}/R_L is given by:

$$\frac{R_{ap}}{R_L} = \left(\frac{0.4 \ln 10}{\sqrt{2}}\right) (\mu_L - \mu_0)\, 10^{-0.2(\mu_L - \mu_0)} \tag{1.4}$$

Where, in equation 1.3, $X = 1$ for unsaturated images and $X = \left(1 - s + 0.5s^2\right) e^{-s}$, with $s = 0.4 \ln 10\,(\Delta\mu - 2.5 \log N)$, for saturated images. N is the dynamic range of the detector (~ 100 for photographic plates) and $\Delta\mu$ is the difference in magnitudes between the limiting surface-brightness, μ_L, and the central surface-brightness, μ_0, e.g. $\Delta\mu = \mu_L - \mu_0$. If $\Delta\mu$ is greater than the dynamic range in magnitudes, $-2.5 \log N$, then the galaxy will be saturated in the centre and the measured luminosity will be an underestimate of the true luminosity.

These distances can be converted to volumes using $V = (\Omega/3)\, d_M^3$, where Ω is the angular area covered by a survey in steradians ($\Omega = 4\pi$ for the whole sky) and d_M is the lower of d_l and d_θ. Figure 1.4, modified from DP 83, shows the visibility function for the selection parameters used in Figure 1.3. The volume given is that for an all-sky survey covering both hemispheres and galaxies with $M_B = -21$, but the shape of the function is not affected be either the area or the magnitude chosen.

In 1987, Bothun et al. reported the discovery of the first giant LSB galaxy, Malin 1. This galaxy would not have been found if it were not for its bright central bulge region, which was mistaken for a dwarf in the

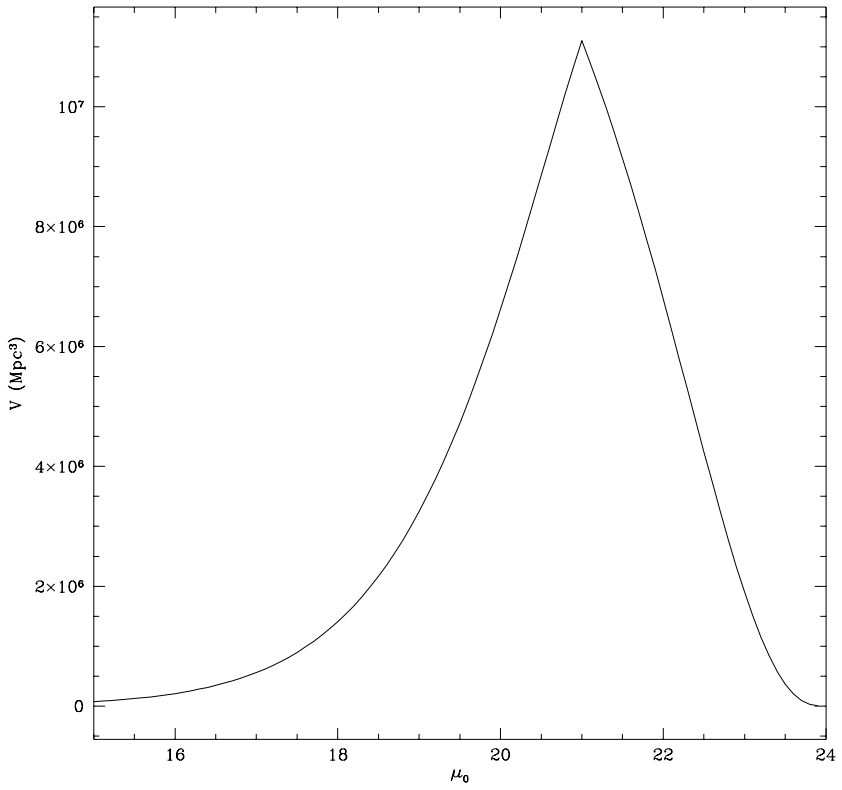

Figure 1.4: Visibility function from Disney & Phillipps (1983) for $\mu_{lim} = 24$ Bμ, $m_l = 15$ B mag, and $\theta_l = 20''$. It can be seen that this is strongly peaked in a similar manner to the surface-brightness distribution of Freeman (1970), with the peak coming where the limits due to luminosity and diameter intersect. These galaxies can be seen over a larger volume and are therefore expected to dominate numerically.

Virgo cluster. Stacking of three deep Schmidt plates revealed a LSB disc around this central bulge which would, if in Virgo, have a diameter of ~ 10 kpc. Optical spectroscopy using the 200-inch Palomar telescope showed that this central bulge had an emission-line redshift of ~ 25000 kms^{-1}– indicating that either this was a background emission-line galaxy which appeared to be the core of a foreground LSB spiral due to an coincidental alignment, or the emission lines were truely from the bulge of a giant LSB spiral.

In order to test out which of these was correct, Bothun et al. carried out HI observations using the Arecibo telescope. Searches at the redshifts of Virgo (500-3000 kms^{-1}) and Coma (5000-8000 kms^{-1})

revealed nothing, but when the telescope was tuned to the redshift of the emission lines – 25000 $\mathrm{km\,s^{-1}}$– HI emission from the disc was discovered, revealing Malin 1 as a giant background galaxy.

Malin 1 has a central disc surface brightness of 26.5 Bμ and an HI content of a few times $10^{10} M_{\odot}$. This remains the only known example of a giant low surface-brightness galaxy, the "Crouching Giants" predicted by Disney (1976), but the central surface-brightness of the disk is so low that it would escape detection in almost all optical surveys. were it not for the central bulge region. Additionally, if it had not been for the optical redshift of the bulge, HI observations would not have been made at high redshift and the galaxy, if detected, would have been catalogued as another gas-poor dwarf in Virgo.

In the same year as Malin 1 was discovered, van der Kruit (1987) published the results of a field survey that, he claimed, showed that the peak seen by Freeman (1970) in the SBD was real and could not be explained by surface-brightness selection effects. Van der Kruit's sample was selected by eye from IIIaJ Schmidt plates originally taken to image nearby bright galaxies. The selection criterion used was that the galaxies would have a size greater than $120''$ at the 26.5 $\mathrm{B_J}\mu$ isophote.

Van der Kruit found that his sample consisted solely of galaxies contained in the UGC catalogue (Nilson 1973) and gave an inclination-corrected SBD of $\mu_0 = 21.8 \pm 0.6 \mathrm{B_J}\mu$. If only spirals of types Sc or earlier were selected, then the SBD was μ_0 $21.5 \pm 0.4 \mathrm{B_J}\mu$ – very similar to the result of Freeman (1970). He argues that this peak cannot be explained using the visibility function of Disney & Phillipps (1983) using his assumed selection criteria.

However, van der Kruit did note that $< V/V_{max} >$ is significantly less than 0.5 for the dwarf galaxies in his sample, which are generally of lower surface-brightness, although the sample as a whole has $< V/V_{max} >= 0.46 \pm 0.04$. Curiously, no attempt is made to discuss the completeness in each surface-brightness bin – Davies et al. (1994) investigated this and found that for $\mu_0 > 22.3$ Bμ, $< V/V_{max} >= 0.35 \pm 0.08$, e.g the sample is incomplete for LSB galaxies.

This implies that there are selection effects that van der Kruit has failed to take into account – probably because he considers only selection by size and claims there is no selection by magnitude in his sample.

However, selection by eye is notoriously hard to quantify, and it seems highly likely that there was a further selection in finding the galaxies before they were measured which has led to discrimination against the LSB galaxies which have thus been excluded from his sample. In addition, he has assumed that his surface-brightness selection limit is the same as the isophotal limit to which the galaxies can be traced once

identified, if this was true then this IIIaJ plate survey would be deeper than virtually all of the CCD surveys carried out in the field! However, the selection limit is almost certainly substantially higher than the limiting isophote the galaxies can be traced to. It seems fairly certain that there are two selection processes at work here – the selection of the galaxies for measuring, done in an unquantifiably way by eye off the plates and with an unknown limiting isophote, and the selection from this sample of the galaxies larger than $2'$ at the $26.5 B_J \mu$ isophote. This survey does not prove that LSB galaxies do not exist, rather it shows how difficult it is to eliminate selection effects from a sample especially when that sample is selected in an intrinsically unquantifiable manner.

Davies (1990) addressed the problem of visibility for inclined galaxies and spiral galaxies with bulges, generalising from the pure face-on discs or $R^{1/4}$ ellipticals of DP 83. In addition, the effects of clustering upon the observed SBD were considered. Davies found that in general the shape of the visibility function from DP 83 was not substantially changed by considering inclination and adding bulges, although 'normal' spiral galaxies would (for a set total luminosity) have their visibility reduced as a higher fraction of the light was placed in the bulge, and LSB spirals could have their visibility increased by the same process, due to their initial very low visibility. The effect of clustering is to sharpen the peak of the observed SBD, as only the peak of the visibility function can be seen in distant clusters. Davies also addresses the problem of finding the correct central surface-brightness of a disc with a bulge, and finds (as Phillipps & Disney did in 1983) that the extrapolated central surface-brightness (μ_x) is forced by the fitting procedure to a value very close to the Freeman value for a wide range of true central disc surface-brightnesses and bulge fractions. Even relatively small bulges were found to have a major effect on μ_x.

McGaugh, Bothun, & Schombert (1995; MBS 95) proposed an alternative analysis of the visibility function. They re-arranged the equations of DP 83 to give the volume in terms of μ_0 and the scale-length, h, rather than μ_0 and M. They claim that as μ_0 and M are not orthogonal the analysis of DP 83 is misleading, while μ_0 and h are orthogonal and therefore their analysis gives a much better picture of the selection effects. A comparison on the two analysis is given in Figure 1.5, from Figure 1 of MBS 95.

This analysis still gives a strong discrimination against LSB galaxies, but it has no discrimination against HSB galaxies – in fact it gives the result that there will be discrimination in favour of HSB galaxies, if they exist. The authors therefore concluded that the SBD is truncated at the HSB end at $\mu_0^\star$, which they set at the 'Freeman's law' value of 21.65 Bμ.

However, de Jong & Lacey (1999) have shown that neither h nor M is orthogonal to μ_0, therefore the

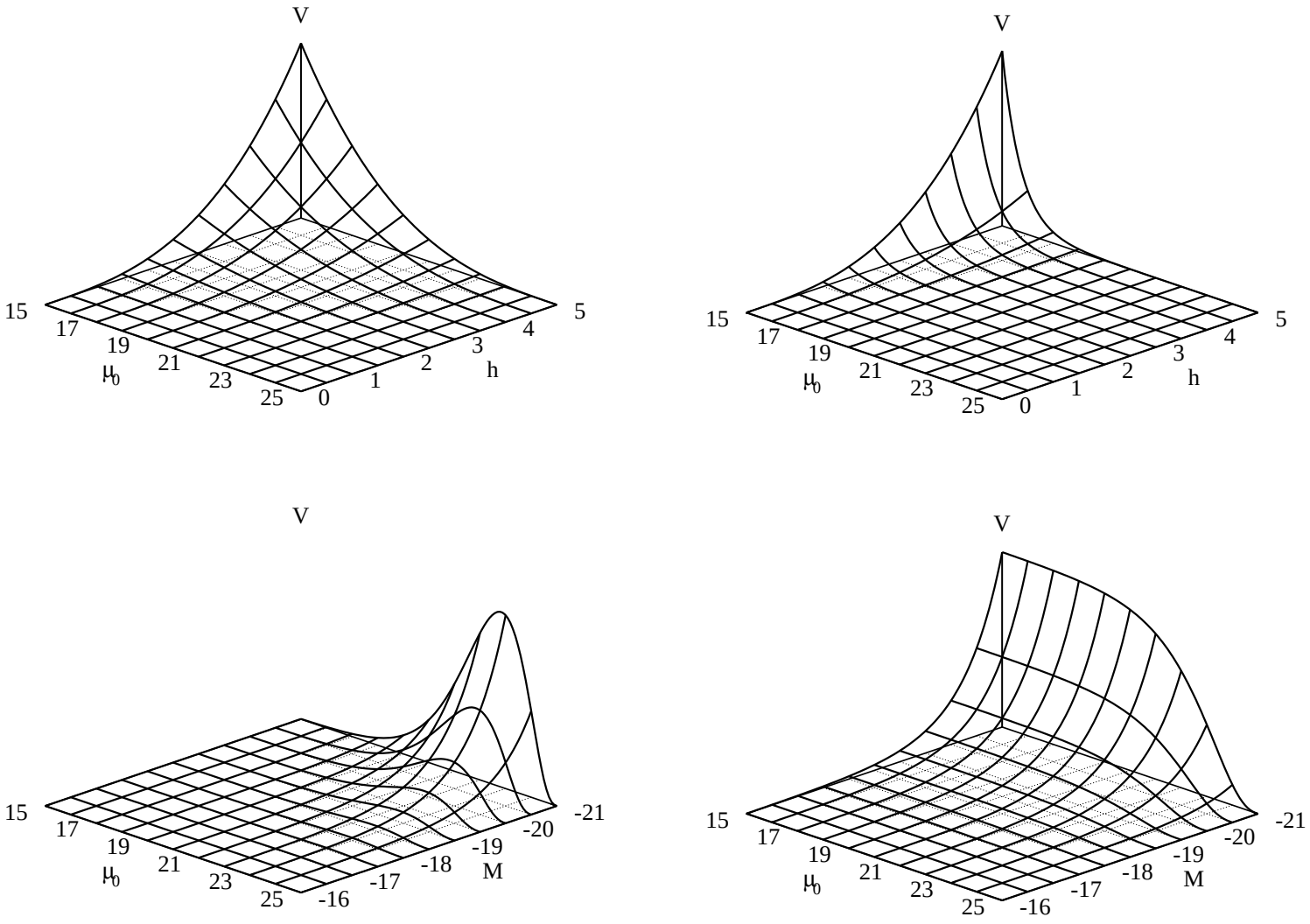

Figure 1.5: Different versions of Visibility, from McGaugh (1995). The Upper panels show visibility according to McGaugh, Bothun, & Schombert (1995), while the lower panels show visibility according to Disney & Phillipps (1983). The left-hand panels show selection by isophotal diameter, the right-hand panels show selection by isophotal magnitude (with saturation ignored), both with a limiting magnitude of $\mu_{\rm B} = 25$ Bμ. The general case where both magnitude and diameter limits apply was not considered. The two forms of visibility are actually identical, with McGaugh, Bothun, & Schombert preferring to plot h against μ_0 rather than M.

true visibility correction will be more complex than either DP 83 or MBS 95 imply – although it should be noted that both sets of authors realised that two parameters are required to properly correct for the visibility function. A measure of μ_0 alone will not do, except as a first approximation, but must be accompanied by a measurement of h or M – implying that the distance to a galaxy must be known before its visibility correction can be properly calculated. When this bivariate correction is made, the analyses of DP 83 and MBS 95 are identical, it is only when attempting to make corrections based solely on a measure of μ_0 that they differ.

1.2.2 Optical surveys for low surface-brightness galaxies

Since Freeman's original SBD (Freeman 1970), the number of galaxies for which we have photometry has increased greatly. A number of surveys have been carried out with the specific aim of finding galaxies which do not fit the 'Freeman Law' distribution. Most of these surveys have been aimed at finding LSB galaxies and it is now known that the number density of galaxies per magnitude of surface-brightness remains fairly constant in the field to at least $\mu_B = 23$ (see Figure1.9, from McGaugh 1999), and deep CCD surveys have failed to find a cut-off down to $\mu_B = 25$ (see Figure 1.8, from O'Neil & Bothun 2000). In clusters, it has been possible to push even further down in surface-brightness – Turner et al. (1993) found the number of galaxies per surface-brightness bin to be constant or slowly increasing down to $\mu_V = 26.4$ ($\mu_B \simeq 27$) in Abell 3574.

The earliest surveys to turn up a number of LSB galaxies were the David Dunlap Observatory catalogue (DDO; van den Bergh 1959) and the Uppsala General Catalogue of Galaxies (UGC; Nilson 1973). The DDO survey was aimed at finding dwarf galaxies and so most of its objects are low-mass local galaxies rather than large LSB galaxies. The UGC survey was not aimed specifically at finding LSB galaxies, but it used a large angular-size cut-off and therefore contained significantly more LSB galaxies than magnitude-limited catalogues such as that of Fisher & Tully (1981).

The first attempt to search specifically for LSB galaxies was made by Longmore et al. (1982). This survey attempted to find galaxies with diameters greater than 2 arcminutes on the UKST plates as the sky survey was carried out. To ensure completeness to 2 arcminutes, the diameter limit of the catalogue was set at 1.5 arcminutes. The size was estimated by eye using a hand-lens, which Longmore et al. estimate to introduce an error of 10%, with a further 10% error being introduced by variations between the plates. HI follow-up on these objects was carried out at Parkes Observatory. The survey concluded that LSB

galaxies were systematically of lower indicative mass than 'normal' (Freeman's law) galaxies of the same type, although they have similar HI masses and physical dimensions. As a result, LSB galaxies have a higher fractional HI mass than 'normal' galaxies. A similar conclusion, that LSB galaxies have a higher HI content relative to their luminosities than 'normal' galaxies, was reached by Romanishin et al. (1982), who studied galaxies from the UGC.

In the 1980s, a lot of work was carried out in clusters and groups such as Virgo (Bingelli, Sandage, & Tammann 1985; Impey, Bothun & Malin 1988) and Fornax (Phillipps et al. 1987; Davies et al. 1988; Irwin et al. 1990; Davies 1990) as well as important surveys of Abell 1367 (Davies, Phillipps, & Disney 1989a) and Abell 3574 (Turner et al. 1993) showing that the SBD remained constant down to the limits of survey sensitivity. The Virgo survey of Impey, Bothun, & Malin (1988) found that the observed relationship between central surface-brightness and absolute magnitude broke down for dwarf galaxies ($M_B < 16$). These LSB dwarf galaxies were generally gas-poor dwarf elliptical galaxies, rather than LSB spirals.

One particularly important cluster survey is that of Davies (1990) in Fornax, and the volume along the line of sight of the cluster. This reported on part of the Automated Plate Measuring (APM) project (Cawson et al. 1987; Phillipps et al. 1987; Davies et al. 1988; Kibblewhite et al. 1989; Evans, Davies, & Phillipps 1990; Disney et al. 1990; Irwin et al. 1990) which used an automatic technique to enhance the Schmidt plates for the UK Schmidt Telescope and thus reach surface-brightnesses than had previously only been possible by co-adding multiple exposures ("Malinising") the plates. The survey covered both HSB and LSB ends of the SBD, covering 21 Bμ $\lesssim \mu_0 \lesssim$ 24 Bμ and so spanning the Freeman-law value, and both angular-size and flux limited samples were constructed.

This sample was the most complete sample available for a long period and was used by McGaugh (1996) in constructing his model SBD. This is shown in Figure 1.6. It can be seen that this gives a turn-down in the SBD at the HSB end, at approximately the Freeman-law value, while the numbers fall off slowly towards the LSB end.

This lack of large LSB spirals in clusters does not necessarily imply a similar lack in the field – simulations have shown that the dense environment of clusters will lead to the disruption of large LSB galaxies (e.g. Moore et al. 1998), so if these simulations are correct, these objects would not be expected to be found in such surveys. Field surveys are therefore more likely to find large LSB galaxies than the cluster surveys, where large LSB galaxies are only likely to be found by serendipitous discoveries either in the foreground or the background of the cluster (such as Malin 1).

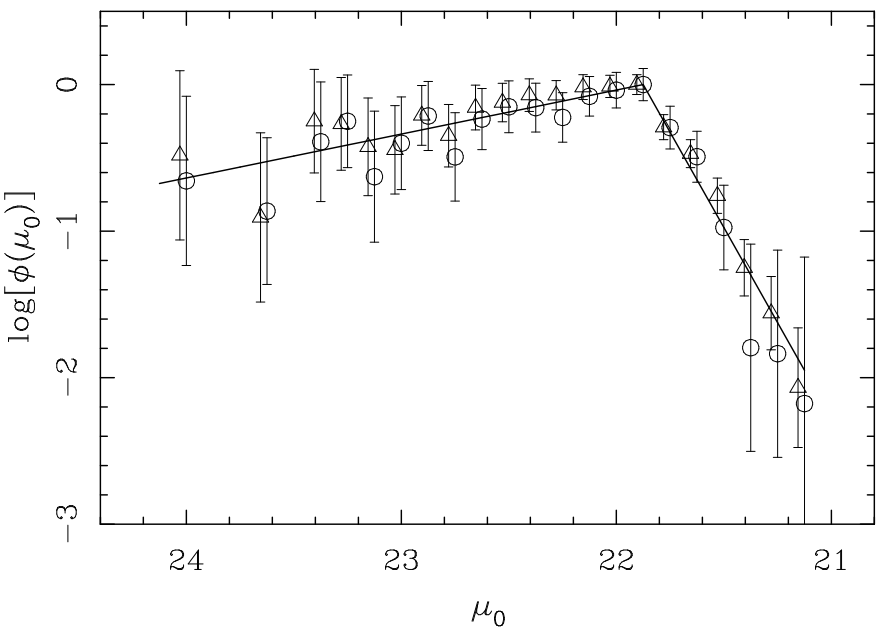

Figure 1.6: Model SBD from McGaugh (1996) with points from Davies (1990) angular-size limited (circles) and magnitude limited (triangles) samples. This shows a sharp truncation in the SBD at the high surface-brightness end, while there is a slowly-decreasing number of galaxies per magnitude bin towards lower surface-brightnesses. The SBD is fitted by a broken power-law, with the break occuring at $\mu_B^\star = 21.9$ Bμ, this give a slope of $\phi \propto \mu_0^{-0.9}$ towards low surface-brightnesses, $\mu_0 > 21.9$, and $\phi \propto \mu_0^{2.6}$ towards higher surface-brightnesses.

Important recent surveys in the field are described below, these are split fairly evenly between CCD surveys and enhanced plate surveys:

- Catalogue of Low-Surface-Brightness Objects (Schombert & Bothun 1988; Schombert et al. 1992): This survey uses plates from the blue (B_J) Second Palomar Sky Survey plates, which have an average limiting surface-brightness of 26 Bμ. The catalogue covers a strip between declinations of 0° and +25° and is divided into two parts - the primary catalogue of LSB objects with diameters greater than $1'$ and the secondary catalogue of LSB objects with diameters between $0.5'$ and $1'$. The survey suffers from being on plates which are, by their very nature, of variable quality, and from being manually selected. This means that the selection criteria can not be precisely defined.

  The survey found 198 objects in the primary catalogue and 140 objects in the secondary catalogue.

Distances to these galaxies have been found using HI follow-up observations, which detected a total of 171 galaxies taken from both catalogues (an 80% detection rate). The survey showed that LSB galaxies cover all Hubble types and all masses, although late-types dominate. The LSB objects were found to trace large-scale structure, although they avoid the cores of clusters, and did not fill in the voids.

The primary catalogue can be compared directly to the UGC, as both are angular-size limited catalogues with a diameter limit of $1'$. The UGC has an average surface-brightness limit about 1 mag arcsec^{-2} brighter than Schombert et al.'s primary catalogue, and the comparison between the two reveals that there is an 11.5% incompleteness in the UGC. This is in contrast to the study of van der Kruit (1987), also using Palomar plates, which only found objects contained in the UGC. The distribution of HI masses is found not to be significantly different to that of UGC galaxies, implying that HI surveys may well sample a wide range of surface-brightnesses better than optical surveys.

- Davies et al. (1994): Davies et al. searched through deep CCD data using an algorithm optimised to find large low surface-brightness galaxies. This algorithm will preferentially select galaxies with scale-sizes of around 50 kpc and central surface-brightnesses about 4 magnitudes below the sky (around 25.7 Vμ, equivalent to around 26.3 Bμ for B-V colours of 0.6 mags as assumed in this paper).

  The survey found 19 extended LSB objects, and the authors conclude that LSB galaxies in the range $-22 < M_v < -19$ are at least an order of magnitude less common than their 'normal' surface-brightness counterparts.

- Schwartzenberg et al. (1995): This survey covers 1.2 square degrees near the south galactic pole using the same CCD data as Davies et al., but uses a connected-pixel algorithm to search for smaller LSB galaxies. The threshold was set at 2.5σ, giving a limiting isophote of 26.6 ± 0.6 Vμ (approximately equivalent to 27.2 Bμ) in most of the fields, and the minimum area for the LSB candidates was set at nine $0.98''$ pixels (8.6 arcsec^2). Any object detected by this algorithm will therefore have a signal to noise ratio of $2.5 \times \sqrt{9} = 7.5$. Further limits were applied to the detected objects of $\mu_0 \geq 22.5$ Vμ and $\alpha \geq 2''$ in order to remove high surface-brightness galaxies and stars from the sample.

  The survey found that LSB galaxies significantly outnumber 'normal' bright galaxies (brighter than 0.1 $L^\star$) by a factor between 5 and 25 (depending on the value assumed for the maximum scale-size of LSB galaxies, $a^\star$ – these limits are for $a^\star = 2h^{-1}$ kpc and $a^\star = 5h^{-1}$ kpc respectively). These LSB galaxies appear to be medium-sized galaxies with scale-sizes of $\approx 1h^{-1}$ kpc, however they would have

typical luminosities of around 0.01 $L^\star$ and so would not dominate the total luminosity of the Universe even though they appear to dominate numerically.

- de Jong & van der Kruit (1994), de Jong (1996a;b;c): This survey uses a statistically complete sample selected from the UGC and followed-up in B, V, R, I, H, & K bands. The 86 galaxies selected have a minimum diameter of $2'$ and an axis ratio of $b/a > 0.625$. A two-dimensional decomposition technique was used to separate the components of the galaxy into a bulge, disc, and (where necessary) a bar. Distances were calculated from the galactic standard of rest velocities in the RC3, which were available for all the galaxies.

  De Jong found that the SBD fell away slowly towards surface-brightnesses lower than the Freeman-law value, and that there was a cut-off at the high surface-brightness end. This is similar to the result found by Davies (1990) for the Fornax cluster. He also found a correlation between surface-brightness and Hubble type, with later types being of lower surface-brightness. Bivariate brightness distributions in B and K band were constructed, and show that there is a tendency for lower surface-brightness galaxies to be lower-luminosity – there are no giant LSB galaxies in the sample.

- Low Surface Brightness Galaxies in the Local Universe (Impey et al. 1996, Sprayberry et al. 1997): This survey uses the Automated Plate Measuring (APM; Kibblewhite et al. 1984) machine to search on UK Schmidt Telescope (UKST) B_J survey plates. The use of the APM machine allows the selection parameters to be well defined and therefore for the incompleteness of the survey to be measured, and it also allows a wide area of sky (786 deg^2) to be covered. The catalogue is limited to galaxies with $\mu_0 \gtrsim 22$ Bμ and is divided into two parts using the isophotal diameter at the limiting isophote to which the galaxies could be traced (about 26 Bμ, the first part containing 513 galaxies with $D \gtrsim 30''$ and the second 180 galaxies with $D \lesssim 30''$. The detection threshold is set at the 2σ level, $\mu = 24.5 \pm 0.5$ Bμ.

  For one of the survey plates, all the galaxies found, including the 'normal' galaxies, have been catalogued and the observed SBD corrected for the measured incompleteness. This gives a peaked function with a peak at 21.75 Bμ, which, after the addition of the LSB galaxies from the rest of the survey to improve the statistics, has been corrected using the visibility function from DP 83 with the appropriate parameters for this plate. This corrected SBD, reproduced in Figure 1.7, shows a peak at 21.75 Bμ with a FWHM of approximately 3 Bμ. The peak is skewed rather than normal and falls off rapidly towards the LSB end of the distribution before levelling off at around 20 – 25% of the peak height at around 23 Bμ, while there is a much gentler slope towards the HSB end.

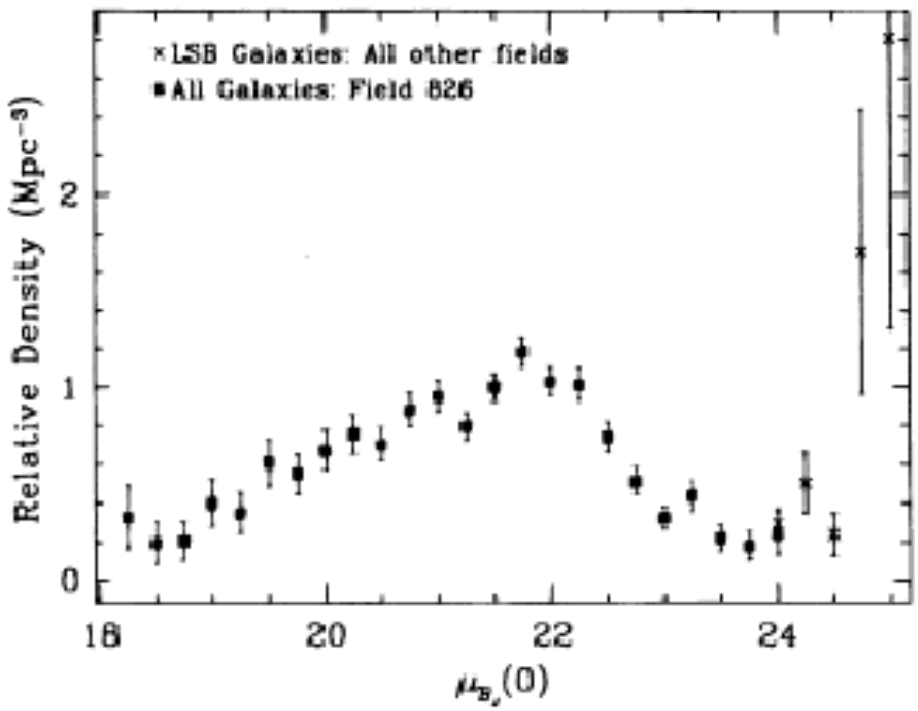

Figure 1.7: Surface Brightness distribution, from Sprayberry et al. (1997). This is considerably flatter than that found by McGaugh (1996) using the data of Davies (1990), in particular the fall-off towards higher surface-brightnesses is not as severe. The peak at 21.75 Bμ has a FWHM of $\approx$ 3 Bμ, considerably wider than the Freeman law, and the SBD is approximately flat for surface-brightnesses lower than 23 Bμ.

- Wide Field CCD Survey for Low Surface Brightness Galaxies (O'Neil, Bothun, & Cornell 1997; O'Neil et al. 1997): These papers present a multi-colour (U,B,V,R,I) CCD survey down to a limiting detection isophote of 26 Bμ aimed towards the Cancer and Pegasus clusters and towards known galaxies outside of clusters. The survey covers 27 square degrees, half of which is in the two clusters.

  The first paper found that the SBD is flat down to 24 Bμ, after which there is a sharp cut-off, and attributed this to the inability of LSB galaxies to survive within clusters. However, no attempt was made to correct for surface-brightness selection effects – the authors apparently believed their sample to be complete down to the detection limit – and Monte-Carlo simulations presented in the second paper showed that it was not possible to distinguish between a flat SBD and a Gaussian distribution

which fell off at 24 Bμ.

A major result of this survey was that it discovered red LSB galaxies which had not been found in previous surveys – almost certainly because most of these surveys had been carried out using blue plates (see McGaugh 1994). The LSB galaxies found in this survey covered the same range of colours as 'normal' galaxies.

The use of multi-colour filters allows inclination to be plotted against colour. If there is a significant amount of dust in LSB galaxies then this will show up as a reddening of the more inclined galaxies. As this is not seen, it is concluded that LSB galaxies have a low dust content, consistent with the observed low metallicity of LSB galaxies (van der Hulst et al. 1993) and the model that LSB galaxies are relatively unevolved systems.

The survey was further analysed by O'Neil, Bothun, & Schombert (2000) who used the refurbished Arecibo to make HI observations of 43 of the LSB galaxies found, and by O'Neil & Bothun (2000), who re-examined the SBD of the galaxies.

O'Neil, Bothun, & Schombert find that there appears to be a lack of large, luminous, low surface-brightness galaxies (e.g. Malin-1 type galaxies) in the sample. This could be an environmental effect, as the survey did not probe very low-density environments, or it could indicate that the space-density of such objects is low. They also find that their sample does *not* fit well to the Tully-Fisher (TF) relationship.

Tully & Fisher (1977) found a relationship between the HI profile width (which is distance independent) and absolute magnitude – thus giving a velocity-independent measure of distance. Zwaan et al. (1995) investigated this relationship for LSB galaxies from the UGC (Nilson 1973) and from the catalogue of Schombert et al. (1992) and found that these LSB galaxies also fell on the TF relationship. However, other surveys have seen deviations from this relationship – Matthews, van Driel, & Gallagher (1998) found that most of their sample of extreme late-type spiral galaxies fell below the normal Tully-Fisher relation and that the deviation increased with decreasing luminosity and size, implying that these lowest luminosity spirals may be a distinct class of objects that follows a different relationship from 'ordinary' spirals. These deviations from the TF relationship could not be resolved by adding in the HI content of the galaxies, implying that they are not due simply to the galaxies having evolved more slowly and preserved a larger reservoir of neutral gas than 'ordinary' spirals.

Unlike the deviations seen by Matthews, van Driel, & Gallagher (1998), the deviations found by O'Neil,

Bothun, & Schombert are seen in high velocity-width galaxies (above 200 $\mathrm{km\,s^{-1}}$). Only 40% of the galaxies fall within the 1-σ limits of the TF relationship defined by Zwaan et al. (1995) and only 77% within the 2-σ limits. The authors find that there appears to be a link between the distance these galaxies lie off the TF relationship and their fractional gas masses, $M_{\rm HI}/L_{\rm B}$. This indicates that a 'Baryonic Tully-Fisher relation' may well still exist for larger galaxies, as proposed by McGaugh et al. (2000).

McGaugh et al. (2000) proposed the Baryonic TF relations as they found that field galaxies with velocity-widths below 90 $\mathrm{km\,s^{-1}}$ fell below the normal T-F relation (similar to those found by Matthews van Driel, & Gallagher 1988) for galaxies drawn from a number of surveys. McGaugh et al. found, contrary to Matthews et al., that plotting the baryonic disc mass ($M_d = M_\star + M_{gas}$) in place of luminosity restored the TF relationship. In this, M_{gas} is taken to be $M_{\rm HI}$ with a correction for helium and metals, so $M_{gas} = 1.4 M_{\rm HI}$. $M_\star$ has been calculated using the model of de Jong (1996c) for a 12 Gyr old population with solar metallicity, a constant star formation rate, and a Salpeter initial mass function (Salpeter 1955). This gives mass-to-light ratios of $\Upsilon^I_\star = 1.7$, $\Upsilon^H_\star = 1.0$, $\Upsilon^{K\prime}_\star = 0.8 M_\odot/L_\odot$ which were used to calculate $M_\star$.

O'Neil & Bothun (2000) use the distance information from the HI observations of O'Neil, Bothun, & Schombert to derive a bivariate volume correction to the sample. This is possible as the distances to the galaxies are known from the HI observations, so the scale-length and the absolute magnitude for each galaxy can be found and the volume over which it would be included in the catalogue can be calculated. When this correction is applied, it gives a flat SBD out to 25 Bμ, and shows that a significant proportion of the mass in galaxies is contained in the low surface-brightness population. This adds weight to the idea put forward by Impey & Bothun (1997) that the missing baryon problem could be resolved by baryons contained in low surface-brightness galaxies. The SBD from O'Neil & Bothun is given in Figure 1.8 plotted with data from previous surveys, which have been corrected using the visibility function of MBS 95 (see section 1.2.3).

- Dalcanton et al. (1997): Dalcanton et al. surveyed 17.5 square degrees of sky to a limiting detection isophote of 25 Vμ ($\approx$ 25.5 Bμ, assuming B-V $\approx$ 0.5 as found by McGaugh & Bothun 1994 and de Blok, van der Hulst, & Bothun 1995) by drift-scanning with a CCD. This method gives much better flat-fielding than ordinary pointed observations, as each point on the sky has passed through many pixels and the flat-field averages out. Good flat-fielding is very important for detecting LSB galaxies,

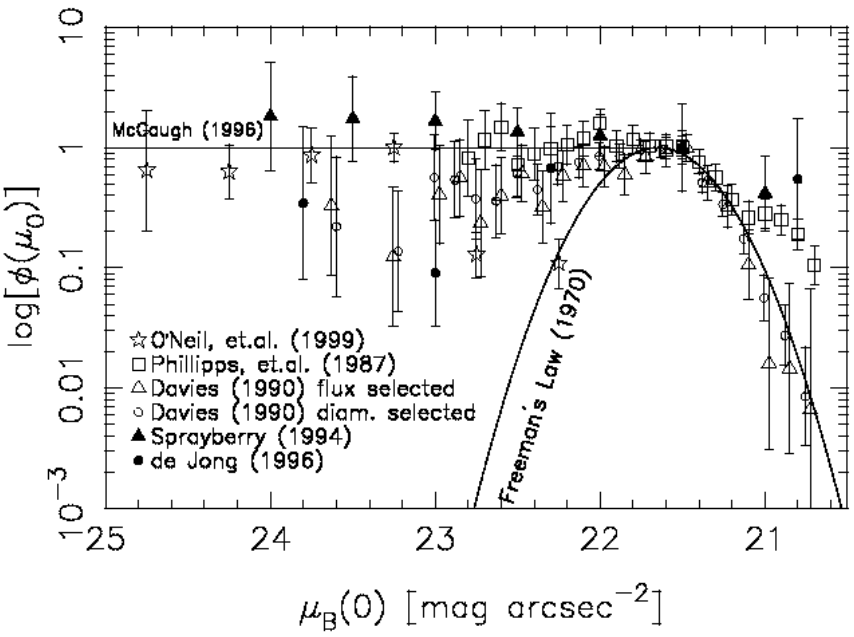

Figure 1.8: Surface Brightness distribution, from O'Neil & Bothun 2000. This SBD looks very similar to that found by McGaugh (1996), with the number per magnitude bin remaining flat down to at least 25 Bμ, where statistics for galaxies run out, and turning down at the high surface-brightness end. However, as the HSB end is dominated by the same data from Davies (1990) used by McGaugh (1996), this is unsurprising.

as variations of a few percent in the sky can hide galaxies that have surface-brightness that are only a few percent of the sky.

Dalcanton et al. detected 14 galaxies with central surface-brightnesses in the range $23 < \mu_V < 25$. The galaxies found all have smooth exponential profiles, as is expected as the procedure for removing higher surface-brightness objects will have also removed any low surface-brightness galaxies with bulges or bright HII regions. Redshifts of the LSB galaxies were found using optical spectroscopy.

Simulations were used to correct for selection effects in the detection and classification of the LSB galaxies. This gives the result that the number-density of LSB galaxies in the surface-brightness range

examined is greater than that of 'normal' galaxies with either the same range of luminosities or the same range of scale-lengths by a factor of around two. This is without including any LSB galaxies with high surface-brightness features. With these included the contribution from LSB galaxies would be even more significant.

- Automated search for nearby low-surface-brightness galaxies (Morshidi 1998; Morshidi-Esslinger, Davies, & Smith 1999a, Morshidi-Esslinger, Davies, & Smith 1999b): This survey used an automated technique to search APM scans of UKST plates over 2187 square degrees in the Fornax cluster and the NGC 1400, Sculptor and Dorado groups as well as in the field between these groups. The search algorithm was optimized using the Fornax data to find LSB dwarf elliptical (dE) galaxies.

  An average of 32 galaxies were detected per plate in the field, of which an average of 19 per plate are found to be background galaxies ($cz > 5,000$ kms^{-1}). This leaves an average of 13 galaxies per plate, much less than the ~ 60 required for LSB dEs to be the local faded counterparts of the Faint Blue Galaxies found at high redshifts according to the fading model of Driver (1994).

  It is also found that the dEs trace the same large scale structure as high-luminosity, high surface-brightness galaxies but with weaker clustering. The clustering is, however, stronger than that predicted by Dekel & Silk (1986) using the biased galaxy formation theory. The number counts are consistent with those from Dalcanton et al. (1997; see above) for a flat SBD.

Only one optical survey has been carried out that has turned up large numbers of high surface-brightness galaxies, a spectroscopic survey of all objects (stellar and non-stellar) in Fornax (Drinkwater et al. 1999; Drinkwater et al. 2000) using the 2df fibre spectrometer on the Anglo-Australian Telescope. This found 13 compact galaxies with magnitudes in the range $16.5 < \mathrm{B}_J < 19.7$, or 7 ± 3 deg^{-2}. These galaxies are generally luminous, with $L \sim L^\star$, and represent $2.8 \pm 1.6\%$ of local ($z < 0.2$) galaxies.

1.2.3 The surface-brightness distribution

From the many attempts made to find LSB galaxies, we can now be fairly certain that the SBD is flat or slowly-falling from the 'Freeman's Law' peak of 21.65 Bμ down to at least 25 Bμ. Beyond this, little is known in the field, although in clusters the SBD is known to be flat down to at least 27 Bμ. There is considerably less data about the HSB end, although what data there is does appear to imply a cut-off brighter than the Freeman-law value.

The DP 83 analysis, which holds luminosity constant while varying the surface-brightness, indicates that there is a strong discrimination against high surface-brightness as well as against low-surface-brightness galaxies. However, the analysis of MBS 95, where the scale-length is held constant, finds an even stronger discrimination against low surface-brightness galaxies, but no discrimination at all against high surface-brightness galaxies – saying even that if these existed they would be preferentially selected over Freeman-law galaxies. McGaugh (1999) presented an analysis of various surveys corrected using the analysis of MBS 95 to get the SBD given in Figure 1.9.

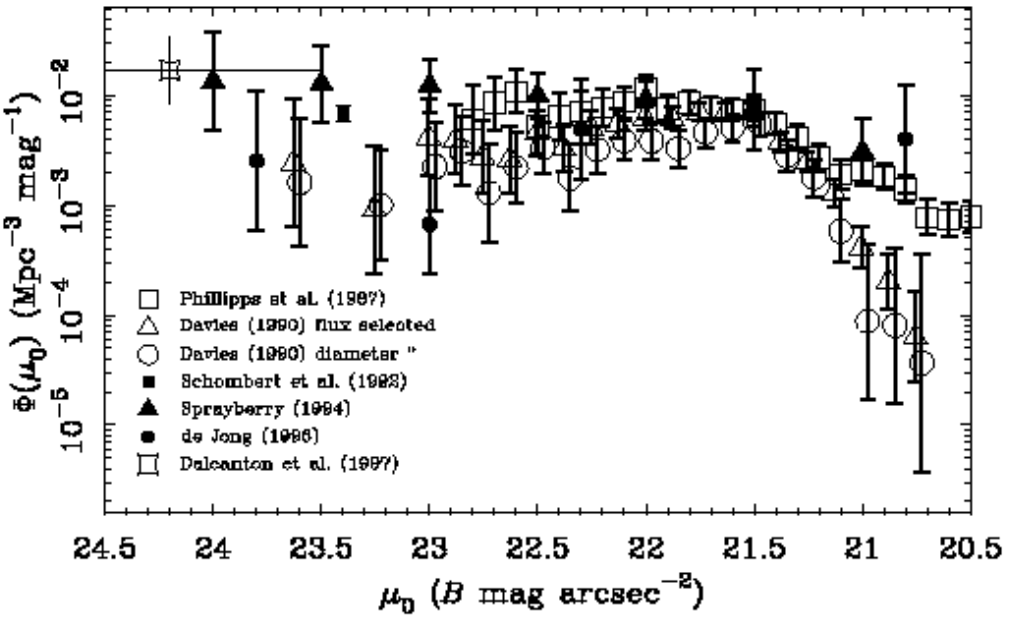

Figure 1.9: Surface Brightness distribution, from McGaugh 1999. This is in good agreement with the SBD of O'Neil & Bothun (2000), but as most of the data-points are common to the two figures this is unsurprising. It can be seen that the number density is flat or slowly falling towards lower surface-brightnesses and falls away more quickly for surface-brightnesses higher than the Freeman-law value. The slope of this HSB fall-off is uncertain, the data of Davies (1990) gives a fairly steep slope while a shallower slope is found by Phillipps et al. (1987) and is hinted at by de Jong (1996) and Sprayberry (1994).

De Jong (1999) has argued that neither of these analyses is correct, as it is incorrect to hold either scale-length or luminosity constant and allow the other to vary. The actual visibility function is more complicated than a simple relationship between volume and surface-brightness as such a relationship depends

on assumptions made about the distribution of galaxies in either surface-brightness – luminosity space or surface-brightness – scale-length space.

The down-turn in the SBD seen at $\mu_0 \lesssim 21.5$ Bμ in Figure 1.8 and in Figure 1.9 is not investigated by O'Neil & Bothun. The magnitude of this down-turn, even in the analysis of MBS 95 which has been used to create this SBD, is not clear. The results of Davies (1990) appear to fall roughly as predicted by Freeman's Law at the HSB end, yet the down-turn is much weaker in the surveys of Phillipps et al. (1987), Sprayberry (1994) and de Jong (1996b).

An HI survey should investigate the distribution of HSB galaxies, if these contain neutral hydrogen. However, star-like objects are unlikely to be chosen as the optical counterparts of Parkes sources as the errors on the positions are fairly large and another galaxy in the region may be mis-identified as the source. Interferometry and spectroscopic follow-up of uncatalogued sources will minimise this effect, but it is not possible to be completely certain that galaxies are not being missed.

1.3 Blind HI Surveys and Selection Effects

There have been a number of blind HI surveys since the 1970s. The first was Mathewson, Cleary, & Murray (1974), who used the Parkes 18-m dish to survey an area around the Magellanic Clouds and discovered the gas bridge of the Magellanic Stream which links the clouds to our galaxy. The first attempt to use HI to find LSB galaxies was carried out by Shostak (1977), who looked originally in the off-beams of pointed observations of known galaxies and followed this with two blind drift-scan surveys and a pointed absorption survey toward bright QSOs.

However, one shortcoming of many HI surveys is their inability to detect low column-density objects. All surveys have a column-density limit: they can only detect galaxies which have more than a certain number of atoms per square centimetre along a column through a source of a given velocity width. Below this limit, the mass in the beam falls below the detection limit, even if the total mass of the object is greater. Disney & Banks (1997) showed that the column density limit was dependent only on the integration time of the survey, the system temperature of the detector, and the velocity width of the source:

$$N_{\rm HI}({\rm atoms\,cm^{-2}}) = 10^{18} T_s \sqrt{\frac{\Delta V({\rm km\,s^{-1}})}{t_{int}({\rm s})}} \tag{1.5}$$

The reason for the lack of correlation between the telescope size and the column density limit is that larger telescopes have proportionally tighter beams, so the area of the beam is proportional to D^2. This then cancels out the increase in sensitivity, which is proportional to the size of the collecting area and therefore also proportional to D^2 (see Figure 1.10).

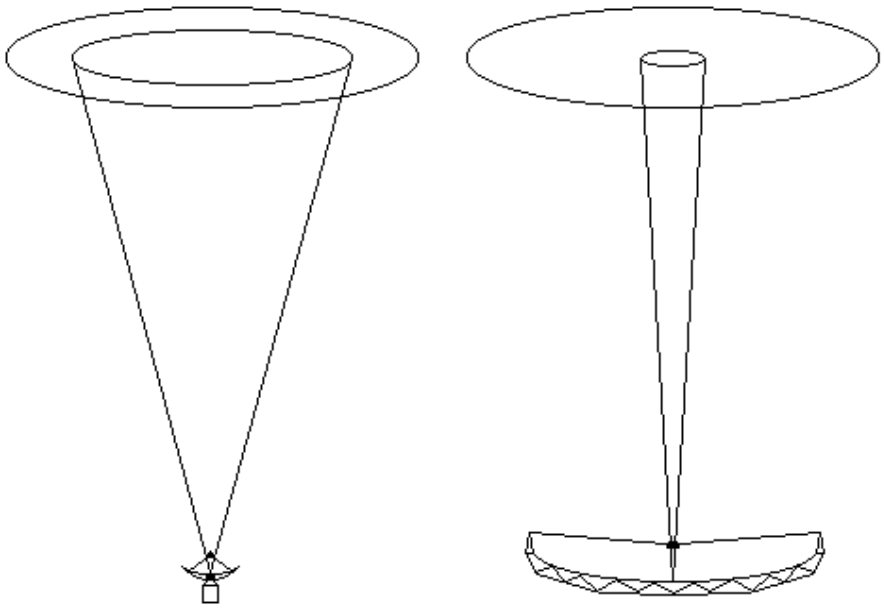

Figure 1.10: A smaller telescope (a) is less sensitive by a factor D^2, however it has a wider beam and so, in the column-density limited regime, picks up D^2 more hydrogen than a large telescope (b). These factors cancel, so for the same integration time, $T_{\rm sys}$, etc., the two telescopes will have the same limiting column density.

It is known (Schombert et al. 1992) that LSB galaxies cover the same range of HI masses as 'normal' galaxies, so a simple expectation would be that they would be detected equally in an HI survey. However, as LSB galaxies have lower column densities than 'normal' galaxies (de Blok, McGaugh, & van der Hulst 1996), they are more likely to fall beneath the limiting column-density. A simple scaling relationship between the average surface-brightness and the average column density over the HI disc was derived by Disney & Banks (1997):

For any given region the HI surface density and the optical surface brightness are related by:

$$\Sigma_{\rm HI}\left(M_\odot {\rm pc}^{-2}\right) = \left(\frac{M_{\rm HI}}{L_{\rm B}}\right) \times \Sigma_{\rm B}\left(L_\odot {\rm pc}^{-2}\right) \tag{1.6}$$

where $\Sigma_{\rm HI}$ is the HI surface density and $\Sigma_{\rm B}$ is the B-band optical surface brightness, averaged over the region, and $M_{\rm HI}$ and $L_{\rm B}$ are the HI mass and the B-band luminosity within the same region. As 1 $M_\odot$ pc^{-2} is approximately equal to an HI column density of $10^{20.1}$ atoms cm^{-2} and 1 $L_\odot$ pc^{-2} is approximately equal to a surface-brightness of 27.05 B mags arcsec^{-2}, this gives the scaling relationship found by Disney & Banks (1997):

$$N_{\rm HI} \simeq 10^{20.1}\left(\frac{M_{\rm HI}}{L_{\rm B}}\right) 10^{(0.4(27-\mu_{\rm mean}))} \tag{1.7}$$

which is known as the Disney-Banks scaling. $N_{\rm HI}$ is the HI column density in units of atoms cm^{-2} and μ_{mean} is the average optical surface brightness in units of mags arcsec^{-2} taken over the same area as $N_{\rm HI}$. This can be re-written as:

$$\mu_{\rm mean} \simeq 2.5\left(30.1 + \log\left(\frac{M_{\rm HI}}{L_{\rm B}}\right) - \log\left(N_{\rm HI}\right)\right) \tag{1.8}$$

This relation can be adapted to relate the central surface-brightness of a galaxy to its average HI column density if certain assumptions are made about the size of the HI disc. Cayatte et al. (1994) found that $R_{\rm HI} \simeq 1.7R_{25}$. This scaling will obviously not hold for LSB galaxies, some of which may not even have a $\mu_B = 25$ isophote, but for a Freeman's law galaxy $R_{25} = 3.1$ scale lengths and it therefore seems reasonable to assume that $R_{\rm HI} = 3.1 \times 1.7 = 5.25$ scale lengths. Assuming also that $M_{\rm HI}/L_B = 0.3M_\odot/L_\odot$ (average value from Roberts & Haynes 1994), we get:

$$\mu_0 \simeq 2.5\left(28.95 - \log\left(N_{\rm HI}\right)\right) \tag{1.9}$$

which can be used to work out an approximate equivalent central surface-brightness limit for HI surveys.

In addition to the column-density limit, there is another effect that could cause LSB galaxies to be less readily detected in HI surveys that their 'normal' counterparts. De Blok, McGaugh, & van der Hulst (1996) found that LSB galaxies have slowly rising rotation curves, as opposed to the flat rotation curves observed in 'normal' galaxies. This means that a by-eye inspection of HI data cubes may miss LSB galaxies near the limit of detection while including HSB galaxies of the same HI flux. This should be seen in the results as a trend towards higher surface-brightness at lower integrated fluxes and at lower ratios of peak flux to

integrated flux, so it should be possible to check for this effect. In order to attempt to lessen the effect of by-eye selection, we have used an automated galaxy finder (see Chapter 2) which selects by integrated-flux rather than by peak-flux.

Another HI selection effect is that wider galaxies have a lower signal to noise ratio than narrower galaxies. The error of N measurements is given by $\sqrt{\sum_{i=1-N} \sigma_i^2}$, for a Gaussian error in measurement k of σ_k. For a spectrum, the noise can be taken to be a constant, σ, this then gives a noise over N channels of the spectrum of $\sigma\sqrt{N}$, or $\Delta V^{-1/2}$. The signal to noise of a galaxy with a given flux is then proportional to $1/\sqrt{N}$, giving a lower signal to noise for narrower line-width galaxies. However, it is known that LSB galaxies fall on the same Tully-Fisher relation as HSB galaxies (Zwaan et al. 1995), so the proportionality of L to ΔV does not depend on surface-brightness. The implication of this is that discrimination against higher line-width galaxies will be independent of surface-brightness and so should not affect the SBD of galaxies found in HI surveys.

1.3.1 Ionisation effects

Obviously, for a galaxy to be detected by this method, it must contain neutral hydrogen. However, it has been proposed (Corbelli & Salpeter 1993) that neutral hydrogen will be ionised below a critical column density, very close to the Kennicutt (1989) critical density for star-formation, following observations of a cut-off at $\sim 2 \times 10^{19}$ atoms cm^{-2} in Messier 33 and NGC 3198 (Corbelli, Schneider, & Salpeter, 1989; Maloney 1993). However, clumping of HI may well mean that galaxies with an average surface-density below the threshold will still contain neutral hydrogen, and the low number of observations means that the ionisation limit cannot yet be well determined. The closeness of the ionisation limit to Kennicutt's critical density implies that all galaxies detected in HI will contain stars and, with the exception of gas clouds associated with galaxies and a single, relatively nearby, object from HIPASS (Kilborn et al. 2001) this appears to be the case.

However, LSB galaxies do contain stars and are believed to have ongoing star formation, albeit at a much lower rate than in 'normal' galaxies. This implies that LSB galaxies do contain neutral hydrogen, but as LSB galaxies are generally more spatially extended than 'normal' galaxies, this HI is spread over a larger area, and the *average* column density seen within the beam of a single-dish telescope may therefore be well below the ionisation limit. It is also quite possible that the ionisation limit will not be the same for all galaxies, as the intergalactic UV field may well vary – e.g. surveys of HVCs show that they have a cut off at $\sim 5 \times 10^{18}$ atoms cm^{-2} (Colgan, Salpeter, & Terzian 1990). This might also have the effect of some regions

being more 'LSB-friendly' than others where the gas in LSB galaxies is ionised before stars can form.

1.3.2 The HI Mass Function

One of the aims of blind HI surveys has often been not just to find out whether there are galaxies detectable in HI but also to determine the HI mass function. The HI mass function (HIMF) is the neutral-hydrogen equivalent of the optical luminosity function, and is often parameterised in the same way using a Schecter function (Schecter 1976):

$$\Psi\left(\frac{M_{\rm HI}}{M^{\star}_{\rm HI}}\right)\ {\rm d}\left(\frac{M_{\rm HI}}{M^{\star}_{\rm HI}}\right) = \Psi^{\star}\left(\frac{M_{\rm HI}}{M^{\star}_{\rm HI}}\right)^{-\alpha} e^{-(M_{\rm HI}/M^{\star}_{\rm HI})}\ {\rm d}\left(\frac{M_{\rm HI}}{M^{\star}_{\rm HI}}\right) \tag{1.10}$$

where Ψ is the number per bin of HI mass per unit volume, $M^{\star}_{\rm HI}$ is the mass of galaxies at the knee of the Schecter function, equivalent to the optical $L^{\star}$, $\Psi^{\star}$ is the normalization – the number of $M^{\star}_{\rm HI}$ galaxies per unit volume, and α is the faint-end slope, as in the optical luminosity function.

Determining the HIMF accurately for local galaxies allows the HI density of the local Universe, $\Omega_{\rm HI}$, to be calculated. Both $\Omega_{\rm HI}$ and the HIMF itself are important for modelling cosmology and the evolution of galaxies. If the HIMF is determined from an optically-selected sample there is the possibility that low-luminosity, HI rich galaxies could be missed so determination from an HI selected sample is preferable. In addition to this, the HIMF from an HI selected sample can be compared to HIMFs from optically-selected samples to determine whether these are different – which would indicate that a significant population of HI rich galaxies was missed by optical catalogues. Recent determinations the HIMF include $\alpha = -1.2$, $M^{\star}_{\rm HI} = 10^{9.8}$ (Zwaan et al. 1997), $\alpha = -1.32$, $M^{\star}_{\rm HI} = 10^{9.75}$ (Kilborn, Webster, & Staveley-Smith 1999), and $\alpha = -1.52$, $M^{\star}_{\rm HI} = 10^{10.1}$ (Kilborn 2001) It should be noted that for the first two of these, the value of $M^{\star}_{\rm HI}$ has been corrected to $H_0 = 75$ kms^{-1}Mpc^{-1} from the value of $H_0 = 100$ kms^{-1}Mpc^{-1} used in the analysis, value of α is unchanged by this. Schneider et al. (1998) have found some evidence for a turn-up at the faint-end of the HIMF, similar to that seen in optical luminosity functions, however this has not been seen in other surveys.

1.3.3 Single-beam HI surveys

Banks (1998) gives a full summary of all the HI surveys leading up to HIPASS, here I concentrate on those that are important in the search for LSB galaxies. That is, the surveys of Sorar (1994) – the Arecibo HI

Strip Survey (AHISS), Spitzak (1996) – the Arecibo Slice, and Henning (1995). I also include the more recent survey of Rosenberg & Schneider (2000) – the Arecibo Dual-Beam Survey (ADBS) and, for historical reasons, the survey of Shostak (1977).

Table 1.2 gives the parameters for these surveys. As the column density limits are proportional to the square root of the velocity width, ΔV, I have chosen a 'standard' velocity width of 200 km s^{-1}. This allows realistic comparisons to be made between the surveys and what they might be expected to find. Shostak (1977) reports on 4 different sets of observations each of which has different parameters, the range of the values is given in the table.

- Shostak (1977) uses data from 4 surveys – two drift scans (Shostak 1973, unpublished, and Shostak & Davies 1974, unpublished), a survey of the off-beams of pointed observations of known galaxies (Shostak & Roberts 1973–1974, unpublished), and an absorption survey pointed at 50 strong QSOs (Shostak & Condon 1974, unpublished).

  The two drift scan surveys contain between them over 90% of the volume over which an $M^{\star}_{\rm HI}$ galaxy can be detected. Shostak (1977) calculates that in these surveys the average detected flux of a galaxy will be 42% of the total flux of that galaxy, the noise figures for the drift scans have been adjusted accordingly. The deeper of the two drift-scans reaches an equivalent central surface-brightness of $\mu_B = 22.7$ Bμ and is band-pass limited for $M^{\star}_{\rm HI}$ galaxies at $14h^{-1}$ Mpc. The shallower drift-scan reaches an equivalent central surface-brightness of $\mu_B = 22.3$ Bμ over a much larger volume of detection for $M^{\star}_{\rm HI}$ galaxies.

  The volume of the off-beam pointings cannot be calculated from the data given in Shostak (1977) as the pointings are at different red-shifts. However, Shostak does say that the frequency coverage is nominally 5 MHz wide at $\sim$ 1413 MHz, if these frequencies are used to calculate the volume of the survey then it can detect $M^{\star}_{\rm HI}$ galaxies over $\sim 8.6h^{-3}$ Mpc^3 to an equivalent central surface-brightness of $\mu_B = 23.9$ Bμ. Shostak (1977) calculates that the detected flux of a galaxy will, on average, be 48% of its total flux and the noise has been adjusted accordingly.

  The absorption survey, aimed at 50 strong QSOs, covers a cylinder 140 Mpc long with the area of a galaxy, rather than a beam-cone as is the case for emission-line surveys, and so covers a negligible volume over which it is not surprising that no galaxies were seen.

  One previously uncatalogued source was detected in these surveys, with a velocity of -353 km s^{-1}. This cannot be unambiguously defined as extra-galactic. The source is less than 5° from the galactic plane

Table 1.2: Blind HI surveys for LSB galaxies prior to HIPASS

	AHISS	Arecibo Slice	Shostak (1977)	Henning (1995)	ADBS
Telescope	Arecibo	Arecibo	NRAO 300 ft.	NRAO 300 ft.	Arecibo
Channel separation ($\mathrm{km\,s^{-1}}$)	16	16	11	22	33.8
Velocity range ($\mathrm{km\,s^{-1}}$)	-700 – 7,400	100 – 8,340	-775 – 11,000	-400 – 6,800	-654 – 7,977
Noise/channel/beam (mJy)	0.75	2	18 – 105	3.4	3 – 4
Ind. Sight-lines	6,000	14,130	6,050	7,200	181,000
FWHM	$3.3'$	$3.3'$	$10.8'$	$10.8'$	$3.3'$
New Detections[a]	36	33	1	18	81
Total Detections[a]	66	75	Not Given	37	265
Area ($\mathrm{deg^2}$)[b]	13	33.6	154	183	430
M_{HI} limit ($M_\odot d^2_{\mathrm{Mpc}}$)	5.3×10^4	1.3×10^5	$1.0 - 5.8 \times 10^7$	2.6×10^5	3.4×10^5
N_{HI} limit ($\mathrm{cm^{-2}}$)	9.8×10^{18}	1.7×10^{19}	$1.3 - 10 \times 10^{19}$	4.5×10^{18}	6.2×10^{19}
Vol ($M^\star_{\mathrm{HI}}$) (1000 $\mathrm{Mpc^3}$)[c]	1.4	4.7	0.27	13.9	52.5
μ_0 limit (Bμ)	24.9	24.3	22.4 – 24.6	25.7	22.9

[a] Includes any detections outside FWHM area
[b] Area within FWHM of beam
[c] for $H_0 = 75\ \mathrm{km\,s^{-1}Mpc^{-1}}$

and is at a galactic velocity of -163 $\mathrm{km\,s^{-1}}$ and so may well be a high velocity cloud. The column-density limit of the drift-scans is too high to expect LSB galaxies to be found, while the pointed observations do not cover sufficient volume to unearth a hidden population – for a galaxy density for $M^{\star}_{\mathrm{HI}}$ of $1.4 \pm 0.5\ 100h^{-3}$ Mpc^3, as found by Zwaan et al. (1997), the volume would have to be over 8 times larger before even a single galaxy detection was expected.

- AHISS (Sorar 1994; Zwaan et al. 1997; Zwaan 2000) was the deepest survey prior to the multibeam surveys. It makes use of the wide side-lobes of the Arecibo telescope, giving a strip $15'$ wide, covering a total area of 65 deg^2, but with a variation of a factor of ten in sensitivity from the beam centre to the edges of the side-lobes. In this region (which crosses the Zone of Avoidance (ZOA) twice) 66 galaxies were found, of which 36 were previously uncatalogued. Zwaan et al. (1997) give the distance from the centre of the beam for each source in their Table 1 (from VLA follow-up), this can be used to work out which galaxies fall within the FWHM of the main beam (radius $100''$). Inside the FWHM there are 29 detections, of which 23 were previously uncatalogued. Excluding those galaxies identified by Zwaan et al. as being within the ZOA, this leaves 26 detections, of which 20 are uncatalogued, within the FWHM area.

  Schneider, Spitzak & Rosenberg (1998) discuss the sensitivity of AHISS, pointing out that the Arecibo sidelobes which were included in the AHISS have asymmetries and temperature dependencies which make the sensitivity uncertain and so they only consider the 45 main-beam sources when comparing AHISS with the Arecibo Slice. They also point out that the method of checking the detections by examining each day's data individually means that the limit is closer to 7σ than 5σ, raising the effective surface-brightness limit to 24.0 Bμ

  The main result of the AHISS is the HIMF, which has a faint-end slope of $\alpha = -1.2$. This is consistent with HIMFs from optically-selected samples, which Zwaan et al. interpret as meaning that there is not a large population of gas-rich LSB or low-luminosity galaxies which are not included in optically-selected galaxies. This seems to contrast with 80% of the galaxies in the full-sensitivity region being new detections, even when those galaxies near the galactic plane are excluded. The uncatalogued galaxies cover a range in HI masses from $8.3 \times 10^7 M_{\odot}$ to $2.6 \times 10^9 M_{\odot}$, while the catalogued galaxies cover a range from $1.3 \times 10^8 M_{\odot}$ to $4.4 \times 10^9 M_{\odot}$ $\left(H_0 = 100 \mathrm{km\,s^{-1}\,Mpc^{-1}}\right)$. It should be remembered that the Schecter function (Schecter 1976) is dominated by the statistics of galaxies around the 'knee' at, for the HIMF, $M^{\star}_{\mathrm{HI}}$. Because of this, a new population of lower-mass galaxies may well not cause

a significant change in α.

The analysis of the HIMF in Zwaan et al. also indicates that most of the neutral HI gas in the Universe is found in galaxies with $10^9 M_\odot < M_{\rm HI} < 10^{10} M_\odot$ $(H_0 = 100 {\rm km\,s^{-1} Mpc^{-1}})$, or $\log(M_{\rm HI}/M_\odot) = \log(M^\star_{\rm HI}/M_\odot) \pm 0.5$, e.g. $L^\star$ galaxies. Of the 33 galaxies in the survey that fall in this mass range, 10 are uncatalogued. However, 2 of these are inside the ZOA and so we would not expect these galaxies to be included in optical catalogues. This leaves 8 out of 31 galaxies, or 26%, which are uncatalogued in this dominant region of the mass function. Within the main-beam FWHM the situation appears even more extreme, with 4 out of the 8 galaxies in this mass range being uncatalogued and another one (F 477-01) being omitted from the major diameter-limited and magnitude-limited optical catalogues. This might possibly be due to the higher column-density limit in the side-beams, which may prevent the detection of LSB galaxies which have a lower column-density.

The density of galaxies with $\log M_{\rm HI}/M_\odot = \log M^\star_{\rm HI}/M_\odot \pm 0.5$ in the FWHM region is therefore $1.4 \pm 0.5\ 100h^{-3}$ Mpc^3. This matches the density found for $M^\star_{\rm HI}$ galaxies in the HIMF by Zwaan et al., and the density for $M_{\rm HI}$ galaxies in optically selected samples. This implies that these detections are being added through greater flux sensitivity rather than greater column-density sensitivity. Looking at the fluxes for these galaxies confirms that the 4 uncatalogued galaxies have lower fluxes than all of the catalogued galaxies (with the exception of F 477-01), and are therefore likely to be less luminous in the optical and thus less easy to detect.

In the AHISS, 5 of the 33 previously uncatalogued galaxies have no optical counterpart on the photographic sky-survey plates. However, all of the galaxies can be seen on CCD images made at the 2.5-m Isaac Newton Telescope on La Palma, and none of the galaxies has a central surface-brightness fainter than 24 Bμ – the limit predicted by the Disney–Banks scaling. Zwaan et al. also found that there were no galaxies in the AHISS with $N_{\rm HI} < 10^{19.7}$ cm^{-2}. This column-density limit is important as it is close to both the limit for star-formation found by Kennicutt (1989) and the limit for ionisation by the inter-galactic UV field found by Maloney (1993) and Corbelli & Salpeter (1993).

- The Arecibo Slice survey (Schneider, Spitzak & Rosenberg 1998; Spitzak & Schneider 1998) is sensitive to low-mass objects over a wider area than AHISS. Despite this, the survey is not particularly sensitive to low column-density objects due to the small size of the Arecibo beam. The survey covers approximately 55 square degrees, with a sensitivity variation over the region of a factor of 3 to 4 (note that this is larger than the area given in Table 1.2, as this gives the area within the half-power beam

width).

Out of the 75 detections, 35 are in 'major' magnitude-limited catalogues (NGC/IC – Dreyer 1888,1895 & 1908, CGCG – Zwicky et al 1961, 1963, 1965, 1966, 1968a, 1968b, & MCG – Vorontsov-Vel'Yaminov & Krasnogorskaya 1962; Vorontsov-Vel'Yaminov & Arkhipova 1963, 1964, 1968, & 1974) of which 28 are also in the diameter-limited (1′) UGC (Nilson 1973). The UGC also includes 2 galaxies missed by the magnitude-limited catalogues. The Flat Galaxies Catalogue (Karachentsev, Karachentseva, & Parnovskij 1993; FGC), diameter-limited at 40″, adds a single galaxy to this. Of the remaining 37 detections, 4 are found in the LSB searches of Schombert et al. (1992) and Eder et al. (1989). Of the remaining 33 detections, all but one were found in CCD follow-up observations. The undetected galaxy is close to a bright star, but if it is at the position indicated by follow-up at the VLA then it must have a surface-brightness lower than 25 Bμ to have remained undetected.

The major result from the Arecibo Slice is the HIMF, which indicates a turn-up in the lowest mass bin due to two galaxies found in that bin. The 95% confidence limit from Poisson statistics in this bin rules out the slope of $\alpha = -1.2$ found by Zwaan et al. (1997) with AHISS. This up-turn could indicate that there is a large population of gas-rich LSB galaxies which are missed by optical surveys, especially as one of the galaxies in the lowest mass bin is the object that has remained optically undetected despite being confirmed as real by the VLA.

- The Henning (1995) survey (also Henning 1992, Henning & Kerr 1989, and Kerr & Henning 1987) is sensitive to $M^{\star}_{\rm HI}$ galaxies over a larger volume than the other surveys. However, 60% of this volume is within the Zone of Avoidance and the region outside the ZOA was observed mainly during the daytime and so is of lower sensitivity than the other observations. The sensitivity also varies with declination, as points were observed for 4 minutes sec δ – the longest possible observation for something moving through the 1° east-west across the sky that was accessible to the NRAO 300 ft.

  There were 39 sources detected, 2 of which were classified as high velocity clouds (HVCs) due to their negative velocities. Out of the 37 sources classified as galaxies, 16 lie within $|b| < 10°$ and 21 lie in the field. Of the 19 catalogued galaxies, only 2 are within $|b| < 10°$ with the other 17 being in the field. This leaves 4 previously uncatalogued galaxies outside the ZOA, 3 of these are in the mass range $10^8 M_{\odot} < M_{\rm HI} < 10^9 M_{\odot}$ and one is in the range $10^9 M_{\odot} < M_{\rm HI} < 10^{10} M\odot$ (for $H_0 = 100 {\rm km s}^{-1-1}$ Mpc^{-1}).

  The survey finds no galaxies with $M_{\rm HI} < 10^8 h^{-2} M_{\odot}$, indicating that the sensitivity of the survey

may have been over-estimated as these should have been detectable in a volume of about 400 Mpc^3. The noise level given here is calculated from detection limits given in Henning (1992). Banks (1998) gives a noise limit for this survey of 14 mJy per channel per beam, which would lead to galaxies to $M_{\mathrm{HI}} = 10^8 h^{-2} M_\odot$ being detected only over 50 Mpc^3. This would give a general mass limit of $1.1 \times 10^6 d^2_{\mathrm{Mpc}}\ M_\odot$ and a column-density limit of $1.9 \times 10^{19}\ \mathrm{cm}^{-2}$ for galaxies with a width of $\Delta V = 200$ $\mathrm{km\,s}^{-1}$.

The HIMF from Henning (1995) rules out the existence of a large population of low-mass, LSB dwarf galaxies, but is inconsistent with the results of HIMFs from optically-selected samples (e.g. Briggs & Rao 1993; Solanes, Giovanelli, & Haynes 1996) which do detect low HI mass objects. This indicates that these objects should be found in a blind HI survey, as indeed they are in the Arecibo Slice and the AHISS. Banks (1998) suggests that this inconsistency could be due to the survey sensitivity being poorly understood and that the true detection limit was too high for the low-mass dwarfs to be detected.

- The ADBS (Rosenberg & Schneider 2000) covers a large area compared to previous blind surveys, this combined with the sensitivity of the Arecibo Telescope makes it very useful for discovering low-mass objects – 7 galaxies are found with $M_{\mathrm{HI}} < 10^8 M_\odot$. Of the 81 previously uncatalogued sources, 11 are heavily obscured by the galaxy ($\mathrm{A}_v > 2$ mags). There remain 11 objects without obvious counterparts on the plates (generally POSS-II, although a few are POSS-I), although the authors identify 3 of these as being in regions of high stellar density and a further 3 as being near bright stars (2 of these with possible nebulosity behind the star). Of the remaining 5 sources, 1 is possibly associated with a nearby bright galaxy and the other 4 have multiple faint sources.

  The survey initially identified 407 candidate sources, this was reduced to 265 confirmed sources by follow-up at the VLA and at the refurbished Arecibo. The sources were picked out from the survey using a mixture of the human eye – for regions where only a single scan existed – and an automated technique based on SExtractor (Bertin & Arnouts 1996) – for regions where there were two scans making cross-correlations possible. The follow-up confirmation observations mean that it will have been possible to push further down into the noise than is normally possible, so the figures in Table 1.2 may be high as these are based on a 5σ detection limit.

  Although the ADBS is sensitive to low-mass objects, the small size of the Arecibo beam means that it does not reach a particularly low column-density. Despite this, the ADBS turns up a number of LSB galaxies – it is possible that these are primarily HI rich dwarf galaxies.

1.3.4 Multibeam HI surveys

Multibeam surveys allow larger areas to be covered much more quickly than was previously possible and so can cover large areas to a low limit. Table 1.3 gives the parameters for current and proposed HI surveys – the HI Parkes All Sky Survey (HIPASS), a long integration-time survey carried out at Parkes (DEEP), the proposed northern extension of HIPASS (HIPASS-NE), and the northern sky survey at Jodrell Bank Observatory (HIJASS).

These surveys are summarised in Table 1.3. The noise figures have been measured off the data cubes produced by the three surveys (it is assumed that the northern-extension of HIPASS will have the same noise figures as the main survey). The figures for DEEP are for the data to 12.5×HIPASS. The DEEP survey has since been extended to 20×HIPASS, which will give a 27% increase in sensitivity if the noise continues to fall as $\sqrt{t}$, as it is has done so far.

It can been seen by comparison with Table 1.2 that the multibeam surveys cover much larger areas to a high sensitivity level than previous surveys. Between HIPASS, the northern extension of HIPASS, and HIJASS the whole sky will be covered to a mass-sensitivity of around $10^6 d^2_{\rm Mpc}$ $M_\odot$ and a column-density sensitivity of around 10^{19} atoms cm^{-2}.

The sensitivity of these surveys to low-mass objects will not be as good as some of the deeper surveys that have been carried out previously, but the much greater volume it will cover will compensate for this in terms of number of galaxies found. This means that HIPASS will be able to tie down the HIMF more accurately than has previously been possible (see Kilborn, Webster, & Staveley-Smith 1999, Kilborn 2001).

The DEEP survey is described in more detail in section 1.4 and in chapter 2. It is a much smaller survey than HIPASS and is of a much longer integration time which should enable it to detect low surface-brightness galaxies with central surface-brightnesses of around 26.5 Bμ, even if these galaxies are not particularly HI rich. Despite covering a much smaller area than HIPASS, it is still sensitive to $M^\star_{\rm HI}$ galaxies over more than 10,000 Mpc^3 and covers 32 square degrees of sky, so it should be able to place strong limits on the space-density of very low surface-brightness galaxies.

Table 1.3: Multibeam HI surveys

	HIPASS	DEEP	HIPASS-NE	HIJASS
Telescope	Parkes	Parkes	Parkes	Lovell
Channel separation ($\mathrm{km\,s^{-1}}$)	13.2	13.2	13.2	13.2
Velocity range ($\mathrm{km\,s^{-1}}$)	-1000 – 12,700	-1000 – 12,700	-1000 – 12,700	-2500 – 10,000
Noise/channel/beam (mJy)	14	4	14	16
Ind. Sight-lines	446,000	670	167,000	378,000
FWHM	14.8	14.8	14.8	12.5
Area (square deg.)	21,300	32	8,000	12,900
$M_{\rm HI}$ limit ($M_\odot d^2_{\rm Mpc}$)	8.5×10^5	2.4×10^5	8.5×10^5	9.7×10^5
$\mathrm{N_{HI}}$ limit ($\mathrm{cm^{-2}}$)	7.8×10^{18}	2.2×10^{18}	7.8×10^{18}	1.2×10^{19}
Vol ($M^\star_{\rm HI}$) (1000 $\mathrm{Mpc^3}$)[a]	1170	11.5	439	580
μ_0 limit (Bμ)	25.1	26.5	25.1	24.7

[a] for $H_0 = 75$ km s^{-1} Mpc^{-1}

1.3.5 The Centaurus A surveys

Two multibeam surveys were carried out in the region of the Centaurus A group. The first of these was a HIPASS survey of 600 square degrees (Banks 1998, Banks et al. 1999), the second was the initial part of the DEEP survey to a depth of 4.5 × HIPASS of 32 square degrees in the neighbourhood of Messier 83.

The HIPASS survey of Centaurus A detected 18 of the 21 previously known members within the survey area. In addition, 10 new group members were found – an increase of almost 50% on the number of known galaxies in the group.

Of these 10 new galaxies, one was a previously catalogued high surface-brightness elliptical galaxy that had a measured optical redshift which placed it beyond the Centaurus A group, three were previously catalogued low surface-brightness dwarf galaxies with no previous redshifts, and one was previously identified as a possible galaxy in the ESO catalogue, despite being behind 2 magnitudes of galactic extinction in the B-band and suffering severe stellar contamination. The other five were completely new detections by HIPASS.

These new detections added 30% to the HI mass in dwarf galaxies, but only 6% to the total HI mass in the group and around 4% to the total B-band luminosity of the group. The HI Mass Function (HIMF; the HI equivalent of the optical Luminosity Function) has a slope of $\alpha = -1.30 \pm 0.15$ which is consistent with that found in the field by previous surveys (e.g. Zwaan et al. 1997, Spitzak & Schneider 1998).

Although this survey showed the potential of HIPASS to find new galaxies, it did not add significantly to either the light or the HI in the group. For these to be changed there would either need to be a significant upturn in the HIMF at the faint end, indicating that as yet undiscovered dwarfs could come to dominate the group, or large low surface-brightness galaxies would have to have been found which could have added significantly to the HI mass and luminosity of the group.

The intermediate DEEP survey uncovered only a single new source in the Centaurus A group – DEEP J1337-3320. Extrapolating from the HIMF of Banks et al. (1999) gives the number of expected new detections in Centaurus A in the DEEP survey to 12.5 × HIPASS of $1.5^{+0.5}_{-0.3}$ (Banks 1998). Taken with the previously known companion of Messier 83, UGCA 365, there are two sources which would not have been detected by HIPASS, therefore there is no evidence for a sharp steepening of the HIMF at $\sim 10^6 - 10^7 M_\odot$.

The Centaurus A galaxies detected in the DEEP survey, including DEEP J1337-3320, are given in Table 1.4. The positions are taken from Banks (1998) but the HI properties have been re-determined using the

Table 1.4: DEEP sources in the Centaurus A group

ID	RA (J2000)	DEC (J2000)	V	$\int S\mathrm{d}v$	ΔV_{50}	ΔV_{20}	M_{HI}
	h m s	°′″	$\mathrm{km\,s^{-1}}$	$\mathrm{km\,s^{-1}}$	$\mathrm{km\,s^{-1}}$	$\mathrm{Jy\ km\,s^{-1}}$	$10^6 M_\odot$
NGC 5253	13 39 56	-31 38 54	404	38 ± 2	64	102	110 ± 6
ESO 444-G084	13 37 21	-28 02 36	585	17.5 ± 0.8	55	75	50 ± 2
Messier 83	13 37 00	-29 54 40	523	1888 ± 2	257	285	5450 ± 6
DEEP J1337-3320	13 37 02	-33 20 34	591	1.1 ± 0.1	25	41	3.1 ± 0.4
UGCA 365	13 36 22	-29 14 15	569	1.8 ± 0.1	30	45	5.1 ± 0.3
HIPASS J1328-30	13 28 05	-30 26 00	205	2.8 ± 0.5	31	63	8.2 ± 1.3

more advanced *mbspect* routine in MIRIAD which was not available at the time. Spectra of these galaxies are given in Figure 1.11.

1.4 Deep HI Surveys

1.4.1 Why go deep?

As shown in section 1.3, Disney & Banks (1997) found that the column-density limits of HI surveys are linked primarily to the integration time of the survey and are not related to the size of the telescope used. This lack of sensitivity to low column-density objects is likely to be translated into a lack of sensitivity to low surface-brightness objects. If there is a direct correlation between HI column-density sensitivity and surface-brightness sensitivity, then going to longer integration times will allow lower surface-brightness galaxies to be detected. This will allow new populations to be explored, or show that the low column-density regime is unpopulated.

Table 1.5: Equivalent surface-brightnesses for different column-densities and different HI mass to light ratios. It can be seen that if $M_{\rm HI}/L_B$ rises as the surface-brightness falls, it is possible to reach low surface-brightnesses without reaching low column-densities.

	$M_{\rm HI}/L_{\rm B}$ $(M_\odot/L_\odot)$				
$N_{\rm HI}$	0.1	0.3	1	3	10
10^{21} cm^{-2}	18.7	19.9	21.2	22.4	23.7
3×10^{20} cm^{-2}	19.9	21.2	22.4	23.7	24.9
10^{20} cm^{-2}	21.2	22.4	23.7	24.9	26.2
3×10^{19} cm^{-2}	22.4	23.7	24.9	26.2	27.4
10^{19} cm^{-2}	23.7	24.9	26.2	27.4	28.7
3×10^{18} cm^{-2}	24.9	26.2	27.4	28.7	29.9
10^{18} cm^{-2}	26.2	27.4	28.7	29.9	31.2

HIPASS reaches to a lower column-density limit than any previous survey (taking the values for the Henning (1995) survey from Banks (1998)), yet it is only marginally deeper than previous surveys. The DEEP survey has an integration time 12.5 times that of HIPASS. This allows it to reach the equivalent of almost 1.4 optical magnitudes fainter and thus explore the area between 10^{18} and 10^{19} HI atoms cm^{-2} which has been virtually unobserved. The equivalent central surface-brightness from the Disney-Banks scaling (Disney & Banks 1997; see section 1.3) for different column-densities and HI mass to light ratios is given in Table 1.5.

1.4.2 The DEEP survey

The DEEP survey covers 32 square degrees in a $4^\circ \times 8^\circ$ region centred on ($13^h40^m00^s$,-30°00′00″), near M83 in the Centaurus A group. The survey builds on observations described in Banks (1998) which reached an integration time of 1980 seconds (33 minutes) and the choice of the target region is described there. To this have been added 3600 seconds of observations taken during 1998 for a total integration time of $\sim$ 56000 seconds (over 1.5 hours). This is around 12.5 times longer than a standard HIPASS integration, giving $\sim$ 3.5 times higher sensitivity. A further 3430 seconds of observations were made during 1999 but, due to software and hardware problems in reducing this much data, these have not yet been added to the data set. When this data is reduced, the full data set will have an integration time of $\sim$ 9000 seconds (2.5 hours), or around 20 times longer than a standard HIPASS integration.

The survey region lies in the supergalactic plane and cuts through the Centaurus cluster at 4000 $\mathrm{km\,s^{-1}}$ and the Centaurus A group at 500 $\mathrm{km\,s^{-1}}$ The observations are described in more detail in chapter 2. This thesis deals only with the portion of the cube above 1000 $\mathrm{km\,s^{-1}}$, below this velocity there was only one new detection in the DEEP survey – DEEP J1337-3320 in the Centaurus A group. This galaxy is described in Banks (1998) and in Section 1.3.5 and this single new detection is consistent with the HIMF for the group found from HIPASS by Banks et al. (1999).

1.5 Outline of the Thesis

Chapter 2 discusses the HI sample selection and the HI properties of the galaxies. It describes the observations and the reduction of the HI data, and a semi-automated galaxy finder that was used to analyse the data.

Chapter 3 discusses the optical properties of the sample, and the optical observations and data reduction.

Chapter 4 discusses the analysis of the data and the results of the thesis.

Chapter 5 presents the conclusions of the thesis and discusses future extensions of this work

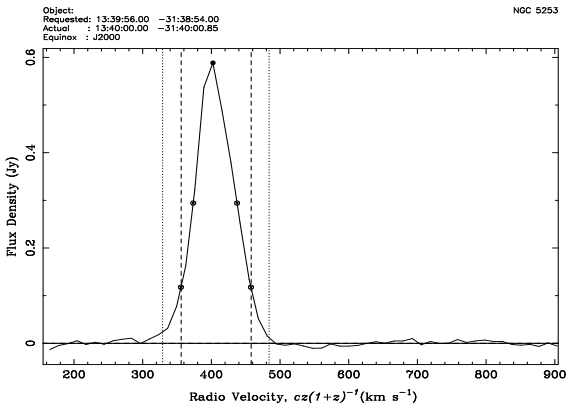

(a) NGC 5253

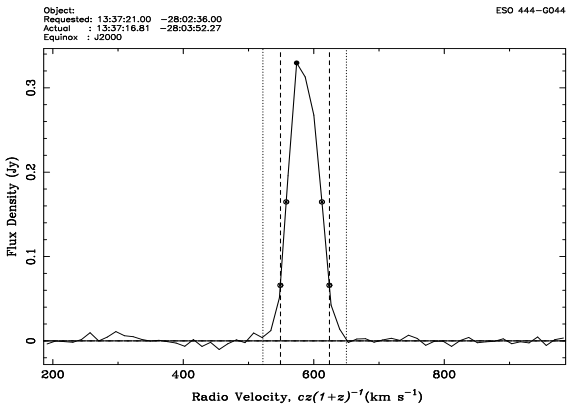

(b) ESO 444-G044

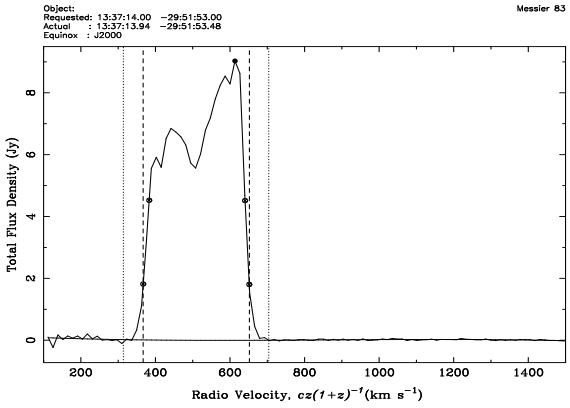

(c) Messier 83

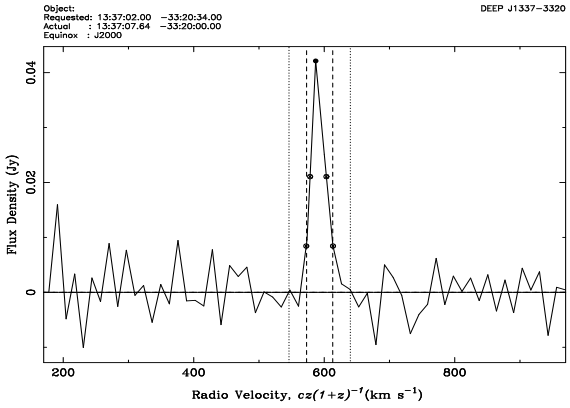

(d) DEEP J1337-3320

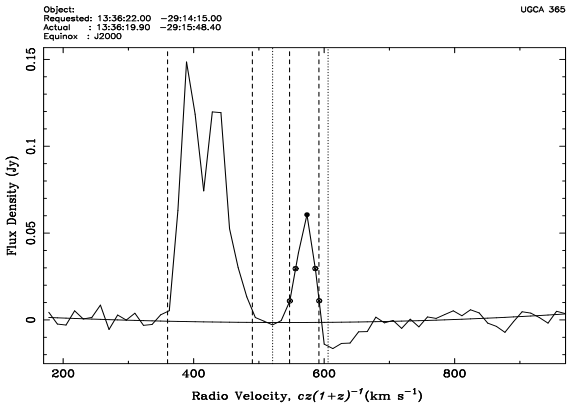

(e) UGCA 365 (right-hand source)

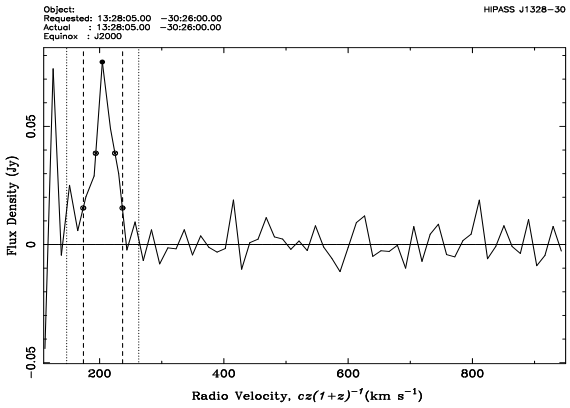

(f) HIPASS J1328-30

Figure 1.11: Spectra of sources in the Centaurus A group detected in DEEP

Chapter 2

HI Data

2.1 Summary of Chapter 2

This chapter presents the radio HI data for the DEEP survey. The observations and the reduction path are described in Section 2.2 and the problem of extended sources is discussed. Section 2.3 describes the semi-automated galaxy finder, PICASSO, used in this project. Section 2.4 describes how the sample was selected and discusses $(1+z)$ effects, as well as giving the HI properties of the sources and their association with known optical galaxies. A comparison with values from the literature is given in Section 2.5 and the velocity-width – HI mass relationship is explored in Section 2.6. Interferometry follow-up using the Australia Telescope Compact Array (ATCA) is discussed in Section 2.7. A discussion of large scale structure in the DEEP survey and a comparison with the Third Revised Shapely-Ames Catalogue (RC3; de Vaucouleurs et al. 1991) is given is Section 2.8. Spectra of all the DEEP sources are given in Section 2.9.

2.2 Parkes HI Observations and Reduction

Observations for the DEEP project were made using the Parkes HI Multibeam system between 1996 and 1998 by Gareth Banks and Robert Minchin of Cardiff University and Peter Boyce (now at the University of Bristol) and other members of the DEEP team. The observations were all made during night time, in order to prevent the data being affected by radiation from the Sun entering the receiver via reflection off

the tripod legs of the Parkes Telescope and thus adding to the noise. The data has an integration time per pixel of $\sim$ 5600 seconds, or 12.5 times longer than HIPASS. This makes it around 3.5 times as sensitive as HIPASS. DEEP is therefore sensitive to objects at any given mass over a substantially larger volume (6.6 times larger for sources that are flux-limited in both surveys) than a HIPASS-depth survey of the same area. In addition, DEEP is more sensitive to low column-density objects, pushing the column-density limit down to $\simeq 2 \times 10^{18}$ atoms cm^{-2}.

2.2.1 The Multibeam System

The Parkes HI Multibeam system (Staveley-Smith et al. 1996) is a 13-beam system arranged to give a fairly uniform coverage of the sky when it is scanned at an angle of 15° (see Figure 2.1 from Banks 1998). Multiple scans are carrid out with slight offsets between them in order to ensure uniform sensitivity and that. Each individual beam samples at a closer spacing than that required for Nyquist sampling. There are two polarisations per beam, resulting in a total of 26 input channels.

The multibeam correlators, in the configuration used, have a bandwidth of 64 MHz which is split into 1024 frequency channels. When centred at 1394.5 MHz, this gives a velocity range of cz = -1200 to 12,700 km s^{-1} and a channel seperation of $13.2(1+z)^2$ km s^{-1}.

The standard observing procedure is to actively scan the multibeam receiver along strips in declination at 1° per minute. Integrations are taken every 5 seconds, or every 5′ on the sky, and each declination strip contains 104 integrations. This results in a total scan length of 8°40′, however as the multibeam array has a radius of around 48′ when projected on the sky, this results in a 'half-power' scan length of around 8°.

2.2.2 Data Reduction

The data were reduced using the standard multibeam reduction techniques (Barnes et al. 2001). Online bandpass removal and calibration was carried out using LiveData (Barnes 1998; Barnes et al. 1998). The bandpass is robustly estimated by median-combining the raw spectra taken immediately befora and after the spectrum being corrected. This estimate of the bandpass is then subtracted from that spectrum. The DEEP observations were reduced using the default settings – spectra taken within 120 seconds of the spectrum to be corrected were used as reference spectra and median combined to form the bandpass, with any spectra taken within 15 seconds being rejected. As the telescope is driven at 1′ per second in declination, this means that

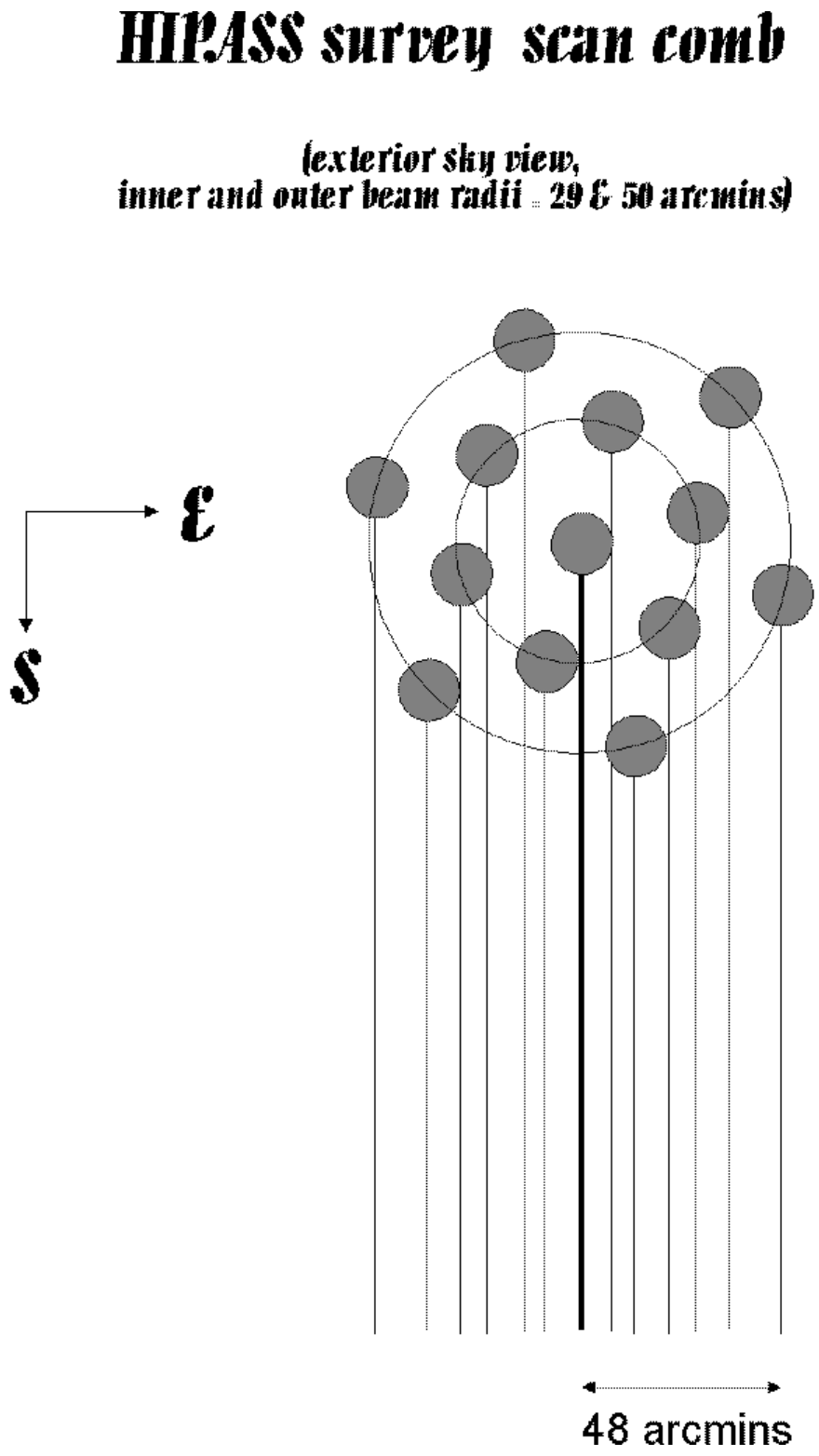

Figure 2.1: Beam scan pattern used for DEEP

the baseline spectra are taken over 4° and that the rejection window is sufficiently wide that a point-source in the spectrum being corrected will not contaminate the reference spectra. Only spectra from the same scan are used as reference spectra, which leads to less reference spectra being used when correcting spectra near the ends of a scan. This does not appear to noticeably increase the noise in these regions. The data are also calibrated by LiveData and the effects of Gibbs ringing in the correlator is reduced by the application of a 25% Tukey filter. This degrades the spectral resolution to ~ 18 kms^{-1}.

The spectra were combined into a datacube using the standard multibeam gridding software developed by the ATNF (Gridzilla), this is described in detail in Barnes et al. (2001) and de Blok, Barnes, & Staveley-Smith (1998; private communication). Again, the default settings were used with the exception that 32-bit integers were used in the data cube rather than the truncated 16-bit integers used in HIPASS cubes. This was to minimise quantisation noise, which could otherwise be significant at the noise levels reached by the DEEP survey. Gridzilla median combines all spectra within $6'$ of a pixel centre onto a grid of $4'\times4'$ pixels. The spectra are corrected for the shape of the Parkes beam in order to correctly reconstruct the flux for point sources in the cube. The output DEEP cube is 100 pixels $\times$ 160 pixels and has 1024 velocity planes.

After the data has been gridded, it is further processed to remove ripple due to on-beam continuum sources. These sources set up a characteristic ripple with a frequency of 5.7 MHz ($\simeq 1200$ kms^{-1}) on the spectra due to standing waves with a wavelength of 52 m set up between the prime-focus cabin and the dish surface and also give a rise in flux towards the low-frequency end of these spectra. The amplitude of the ripples and of the rise in flux is proportional to the strength of the sources, and the phase of the ripple is constant for on-beam sources, it is therefore possible to remove these ripples using a scaled-template. An algorithm to do this (Luther) has been developed at Parkes Observatory by Ian Stewart and Alan Wright and is described in Barnes et al. (2001). The effectiveness of this technique is shown in Figure 2.2, showing the noise in the interquartile ranges (in RA and DEC) of the DEEP cube before (panel (a)) and after (panel (b)) 'luthering'. Much of the noise in panel (a) comes from the strong continuum source associated with Messier 83, but there is a significant contribution from smaller continuum sources. It can be seen that the noise does increase towards the ends of the bandpass, even after the continuum is removed. The spikes seen in panel (b) are generally associated with galaxies – the Milky Way at 0 kms^{-1}, Messier 83 at a few hundred kms^{-1}, and the Centaurus Cluster between 4000 – 5000 kms^{-1} are particularly obvious features. The slight increase in noise around 8000 – 9000 kms^{-1} may be due to residual interference from GPS satellites which transmit very strongly in this frequency range.

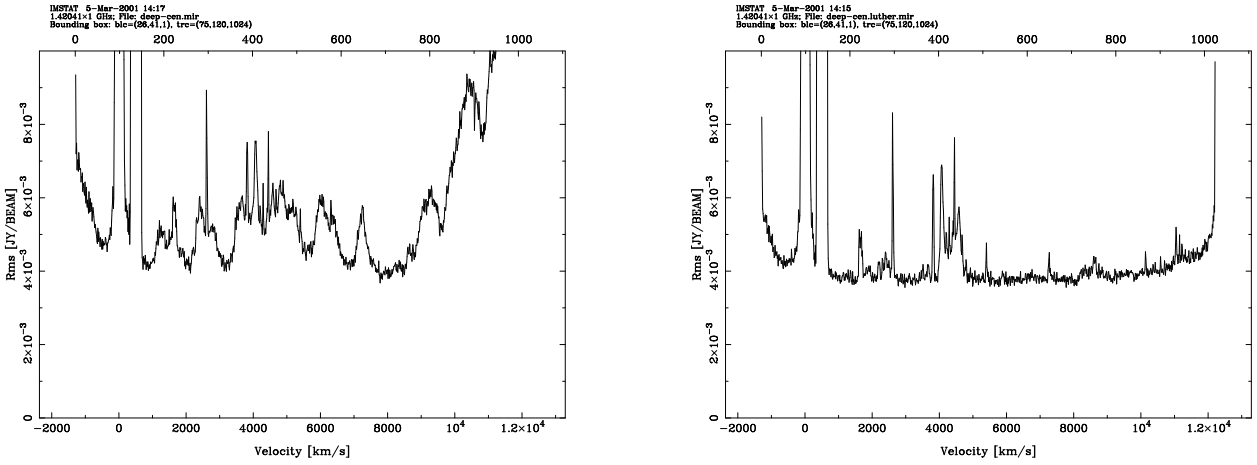

(a) Noise in the DEEP cube – before 'luthering'

(b) Noise in the DEEP cube – after 'luthering'

Figure 2.2: Noise in the interquartile region of the DEEP cube as measured by the MIRIAD task *imstat*. It can be seen that the noise after 'luthering' (panel b) is considerably lower and has less variation than before 'luthering' (panel a). There is still a turn-up in the noise near the ends of the bandpass, but it occurs much closer to the ends and is less severe. Most of the structure seen in panel (b) is due to real sources within the cube, although the structure near 8500 $\mathrm{km\,s^{-1}}$ may be due to interference from GPS satellites.

The 'luther' algorithm does not remove off-beam continuum sources, nor does it remove ripple caused by the Sun, as these ripples have a phase-shift relative to the on-beam sources and so are not well fitted by the template. As the DEEP observations were taken at night, the cube is not contaminated by solar ripple. However there is some residual ripple due to the strong continuum source Centaurus A (NGC 5128) which is $\sim 15°$ away from the DEEP region.

2.2.3 Extended Sources

Most of the reduction software for the multibeam has been written with the object of preserving the flux of 'point sources' (roughly speaking, this means sources smaller than the Parkes beam). Barnes et al. (2001) assume that over 90% of the sources that will be found in HIPASS are point sources, and also give a table of the corrections that need to be applied to extended sources in order to find their correct flux. However, as low column-density galaxies may well be more extended than 'normal' galaxies, it is possble that the DEEP survey will find a greater fraction of extended sources, some of which may be potentially interesting.

The sample presented here is cutoff at the low velocity end at 1000 $\mathrm{km s^{-1}}$, beyond the Centaurus A group at 3.5 Mpc which covers the range $\simeq 200 - \simeq 800$ $\mathrm{km s^{-1}}$. At the cutoff velocity, for an assumed value of $H_0 = 75$ $\mathrm{km s^{-1}}$ $\mathrm{Mpc^{-1}}$, the FWHM of the Parkes beam is ~ 60 kpc. Pickering et al. (1997) have investigated the HI content of four giant LSB galaxies – F568-6, UGC 6614, NGC 7589, and Malin 1 – using the VLA. All of these galaxies have sufficient HI content to be detected over the full bandpass of the DEEP survey. Pickering et al. give radially averaged surface-density profiles for all four of these galaxies, which show that although they would be bigger than the beam at 1000 $\mathrm{km s^{-1}}$, they would become smaller than the beam at approximately 3500, 2500, 1500, and 3500 $\mathrm{km s^{-1}}$ respectively. All of these giant LSB galaxies have sufficient HI content to be detected over the full bandpass of the DEEP survey, out to 12,700 $\mathrm{km s^{-1}}$. Even the largest known low surface-brightness galaxies would only be larger than the beam over $\sim 2 - 3\%$ of the volume of the survey. It is therefore unlikely that we will have missed any significant population of giant LSB galaxies due to the members being extended sources.

2.3 PICASSO

Any blind HI survey relies on being able to identify sources in HI data that are not associated with previously catalogued galaxies with known positions and, to a certain extent, velocities. The main method for this has been to look through the data by eye – similar to the methods used in optical astronomy to identify galaxies until the recent development of automated techniques to search through digital data. Seaching by eye, however, does not give well understood selection effects and may miss high velocity-width sources where the signal is spread over many channels, or sources without strongly peaked profiles.

An ideal automated source finder would be highly reliable with well defined selection criteria. It would not select on the basis of peak flux, but rather in terms of the total signal to noise ratio of a source, and would only be affected by the width of a galaxy in terms of its impact on the signal to noise ratio. Such a finder does not currently exist, the best finders that have been developed so far are 'PICASSO' (Minchin 1999) and 'MultiFind' (Kilborn 2001).

This latter finder has been used to determine the sample for the HIPASS Bright Galaxy Catalogue (Koribalski 2001; BGC). This catalogue contains ~ 700 galaxies, of which only 60 were previously uncatalogued – most of these being in the Zone of Avoidance where the lack of a previous identification is probably due to high absorption in our own galaxy rather than anything intrinsic to the sources. The reason for this could be that the catalogue was selected primarily by peak HI flux, rather than total flux or signal to noise ratio. This could have led to discrimination against LSB galaxies as these galaxies have continuously rising velocity curves rather than the flat velocity curves of 'normal' galaxies (de Block, McGaugh, & van der Hulst 1996) and therefore will not have as strongly peaked an HI profile as these 'normal' galaxies – the gas, and thus the HI signal, is spread across many channels in the LSB galaxy while it falls mainly in a small number of channels at the flat rotation velocity of a 'normal' galaxy (see Chapter 4 for an analysis of the peakiness of DEEP galaxies).

PICASSO was developed in Cardiff by Robert Minchin and Alan Wright and has been designed to select sources by their overall signal-to-noise ratio, rather than their signal-to-noise ratio in a single channel. The main parts of the program are the *finder* routine, which identifies potential sources and assigns them a 'quality', and the *fitter* routine which carries out a 3D fit with a 2D gaussian in the spatial directions and a top-hat in the velocity direction in order to fit an accurate position and velocity.

The quality level output by *finder* is defined as being the signal measured in the pixel being examined,

summed over a number of velocity channels, divided by the noise measured in a surrounding annulus, taken over the same number of channels. The quality of a source is therefore its signal to noise as seen by the finder. For comparison with other selection techniques, a quality of $Q = 7$ is equivalent to a source two channels wide with a 5-σ flux in each channel, or a source 16 channels wide (~ 200 km s^{-1}) with a 1.8-σ flux in each channel.

PICASSO was tested on a HIPASS data cube with real noise and simulated sources. A blank cube was formed by subtracting the two polarisations during gridding, rather than combining them. This should leave a cube with real noise while removing all the sources, as these are expected to be unpolarised. The blank cube was then injected with simulated point sources (spatially gaussian with the FWHM of the Parkes beam) with top-hat velocity profiles. It was found that the sources could be found reliably down to a quality level of $Q = 7$ and across a range of velocity widths of 2 – 32 channels (26 – 422 km s^{-1}), as shown in Figure 2.3.

However, when the finder was tested on real data – HIPASS level cubes of the DEEP region which had *not* been 'luthered' – it proved to be considerably less reliable. There were three times as many unreliable sources as were found in the cube used for the simulation. These were mainly associated with the baseline ripple due to continuum sources, which had been removed by the subtraction of the polarizations in the test cube. As most of the unreliable sources were beyond 8000 km s^{-1}, the finder was tested again using just the region below 8000 km s^{-1}.

The sources in this region were then checked by eye on the deep cube and a judgement made as to their reliability. This showed that a catalogue produced with a limit of $Q = 7$ was approximately 70% reliable. A comparison of this catalogue with a by eye catalogue of the same cubes showed that they found roughly the same number of sources with $\sim 75\%$ overlap between the two catalogues.

PICASSO was run with a limit of $Q = 5$ on the 'luthered' DEEP data cube. This gave a total of 401 detections, of which 73 (18%) were judged to be real when examined by eye on the cube. Figure 2.4 shows how the reliability – defined as the fraction of sources which were judged to be real in a by eye examination – drops with decreasing quality. It also shows the reliability of a catalogue down to a certain limiting quality – it can be seen that at the $Q = 7$ level a Picasso catalogue of the DEEP cube has a reliability of $\sim 75\%$.

The two dips in quality at $Q = 9 - 9.5$ and at $Q = 11 - 11.5$ appear to be associated with residual ripple from strong continuum associated by the 408 and 2700 MHz radio survey of Wright & Otrupcek (1990;

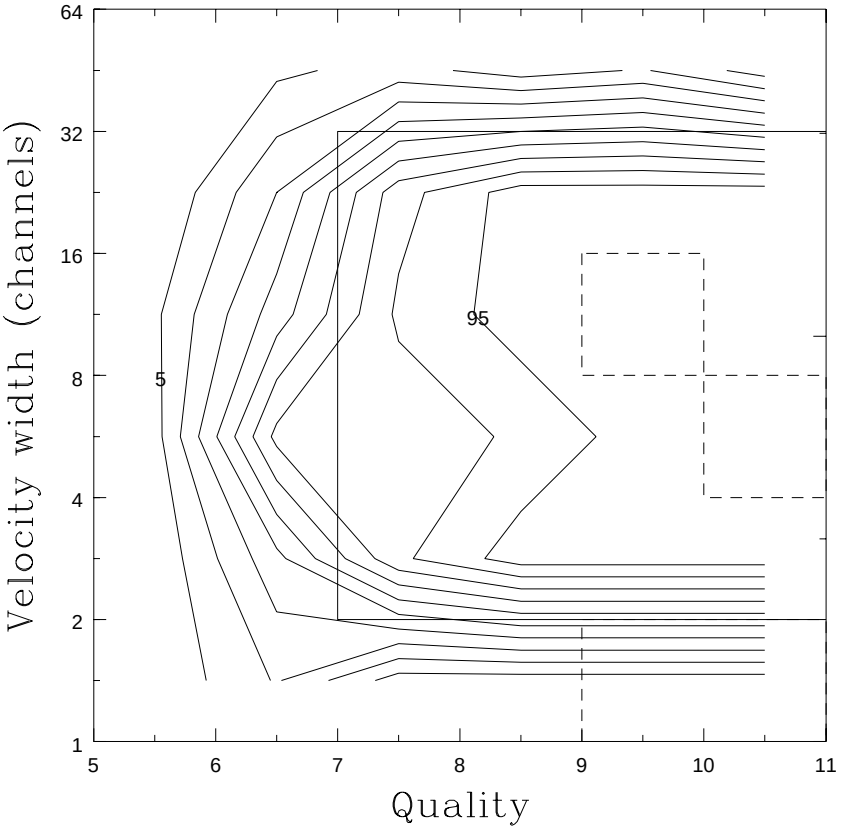

Figure 2.3: Contour map of reliability from simulation, showing quality against velocity width. Contours are from 5% to 95% reliability at intervals of 10%. Dashed-off regions indicate that there were no sources found in this area of parameter space and values have been interpolated. This figure shows how the reliability increases dramatically between Quality 5 and Quality 7 and then increases more slowly above this level, and also how the reliability falls off for low and high velocity width sources. The region enclosed by the solid box is that generally taken as reliable, with velocity widths of between 2 and 32 channels and a quality greater than 7.

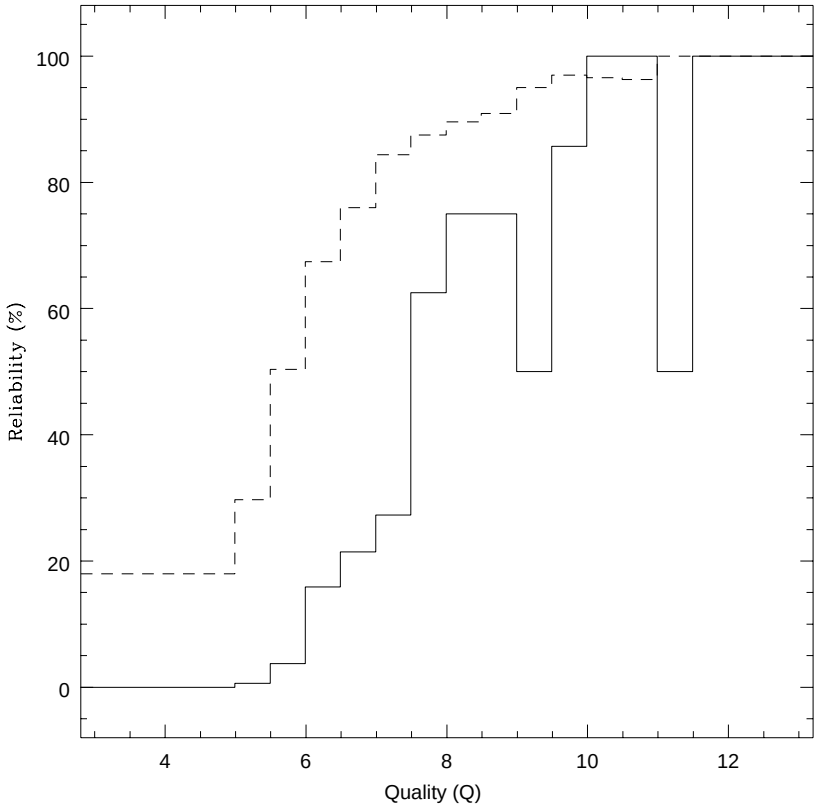

Figure 2.4: Reliability versus Quality for the DEEP data cube. The solid line shows the reliability of sources in that quality bin, while the dashed line shows the reliability of a catalogue down to (but not including) that bin. It can be seen that at the $Q = 7$ level a Picasso catalogue of the DEEP cube has a reliability of $\sim 75\%$, while by $Q = 5$ this has fallen to 18%.

PKSCAT 90) with the radio lobes of IC 4296. However, one of these sources, with a quality of $Q = 11.3$, is (by its *fitter* position) only 3.9′ away from ESO 383-G030 and has a velocity of $cz = 3784$ kms^{-1}, compared with a velocity from the literature for ESO 383-G030 of 3834 kms^{-1}. Careful re-examination of the cube by eye did not pick out anything except the ripple, but when a fifth-order polynomial is fitted to the baseline using *mbspect* the galaxy can be seen. The dip in the $Q = 11 - 11.5$ bin is therefore *not* a real dip in reliability, but is due to PICASSO finding a source that was not detected in the by-eye examination of the cube. It is possible that other sources that have been judged unreal in the by-eye examination are also true sources – Figure 2.5 implies that some low flux, high velocity-width sources may have been omitted due to their having low peak fluxes (see Section 2.4).

2.4 The HI Sample

2.4.1 Defining the Sample

The HI sample was selected from the DEEP data cube using a semi-automated finder (PICASSO - see Section 2.3). In order to ensure that all sources were detected, the finder was run with a low threshold quality ($Q = 5$, equivalent to a $\sim 3.5\sigma$ detection in two channels). This turned up 401 sources which were examined by eye firstly as spectra and then, where there was doubt about whether a source was real or unreal from the spectrum, on the cube. Seventy four of the sources were judged to be real, giving a reliability for the finder down to this quality level of $\sim 18\%$. A total of 69 unique sources were found, some of these being detected twice due to their double-horned profiles. For those sources detected twice, the velocity-width measured by the finder was replaced by a width measured by eye on the data cube at the 20% level for the initial stages of the data analysis. Although the velocity widths used in the final analysis have all been determined using the *mbspect* routine in MIRIAD.

Figure 2.5 shows the selection limits in the DEEP survey. Panel (a) shows the limits in flux – HI mass space. Here, the solid lines indicate 'hard' limit which cannot be broken at the outer end of the bandpass (12,700 kms^{-1}) and at the low redshift cutoff (1000 kms^{-1}). The dashed line indicates the flux limit, but is a 'soft' limit as it may be crossed by galaxies which have a velocity width smaller than that implied by the $\Delta V - M_{\rm HI}$ relationship (see Section 2.6) or which are in an area of the cube with a noise lower than 4 mJy per channel.

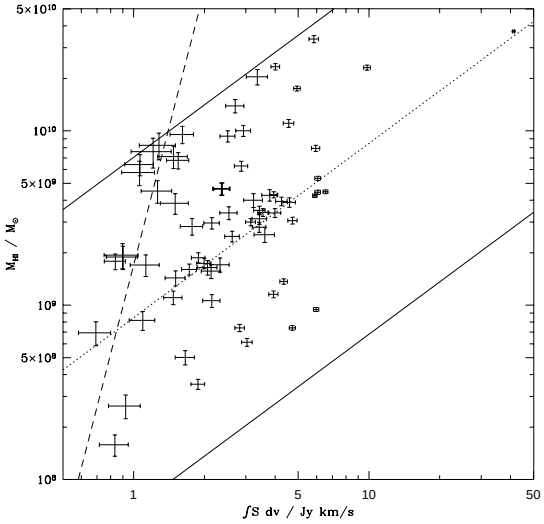

(a) Selection limits in flux – mass space. Solid lines indicate the bandpass limits on detection, while the dashed line indicates the 5σ flux limit for $\Delta V_{20} \propto M_{\rm HI}^{0.34}$, as found in Section 2.6, and a constant noise of $\sigma = 4$ mJy. The Centaurus cluster can be seen as an overdensity of galaxies approximately half way between the upper and lower bandpass limits. It can be seen that there are no obvious regions of the selection plot that are less populated than would be expected.

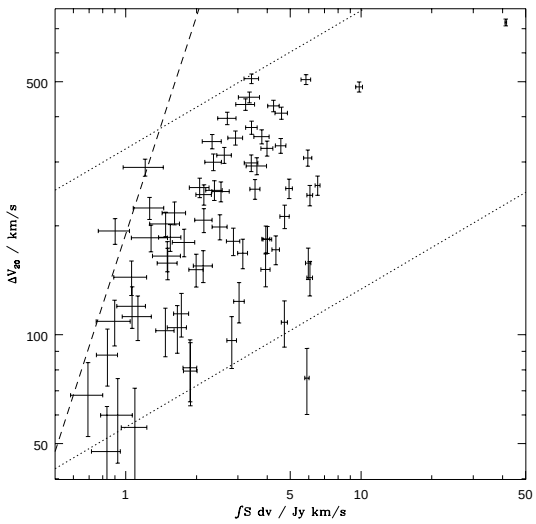

(b) Selection limits in flux – velocity width space. The dotted lines indicate the bandpass limits for $\Delta V_{20} \propto M_{\rm HI}^{0.34}$, as found in Section 2.6, while the dashed line indicates the 5σ flux limit for a constant noise of $\sigma = 4$ mJy. The underpopulated region at the low-flux, high velocity width corner may due to a peak-flux selection at an equivalent peak flux for sources with top hat profiles of ≈ 6 mJy. For real sources, this is likely to translate to a peak flux of $\approx 8-12$ mJy, e.g. $\approx 2-3\sigma$. That a low-level peak-flux selection was present would be unsurprising as all the detections by Picasso were checked by eye and judged real or unreal, this indicates that some lower flux, higher velocity-width galaxies have been omitted from the DEEP survey.

Figure 2.5: Selection limits for flux, mass, and velocity width in the DEEP survey

Panel (b) shows the limits in flux – velocity width space. The dashed line again indicates the flux limit, for a uniform noise of 4 mJy per channel. Galaxies in regions with lower noise than this may lie to the left of this line. The dotted lines indicates the bandpass limit at 12,700 $\mathrm{km\,s^{-1}}$ and the low redshift cutoff at 1000 $\mathrm{km\,s^{-1}}$. These are 'soft' limits on this graph as they rely on the $\Delta V - M_{\mathrm{HI}}$ relationship from Section 2.6 so outliers from this relationship may cross these lines. There appears to be an underdensity of large velocity width, lower flux galaxies, near the intersection of the flux limit and the upper bandpass limit. This could be due to a peak-flux limit entering the selection of the sample due to the by-eye checking, the underdensity can be explained as being due to an equivalent peak flux for sources with a top hat profile of ≈ 6 mJy. This is likely to translate to a true peak flux of $\approx 8 - 12$ mJy, or a $2 - 3\sigma$ peak in the data. This does not seem like an unreasonable level to expect to see a peak-flux cutoff entering the sample selection, and implies that some high velocity-width sources removed during the by-eye checking were in fact real sources. The selection limits in this figure could also be explained by a limit of the form $\int S \, \mathrm{d}v_{limit} \propto \Delta V_{20}^{0.9}$ as can be seen in Figure 2.6.

This figure shows that although the limit of $\int S \, \mathrm{d}v_{limit} \propto \Delta V_{20}^{0.9}$ works well in velocity-width – flux space, it does not work well in velocity-width – SNR space, and that the combined SNR and peak-flux limit does work in velocity-width – SNR space. It appears that the DEEP survey is signal to noise ratio limited for $\Delta V_{20} \lesssim 200$ $\mathrm{km\,s^{-1}}$, and peak-flux limited at an equivalent top-hat peak flux of 6 mJy for larger velocity-width galaxies.

2.4.2 HI Analysis

Once the sample had been defined, accurate positions were determined by fitting a gaussian to a zeroth-order (intensity) moment-map using the *imfit* task in MIRIAD. Further measurements were made using the *mbspect* task in MIRIAD. This routine was used to fit a fifth order polynomial to the baseline over the range $V \pm 1000$ $\mathrm{km\,s^{-1}}$, with the section of baseline occupied by the galaxy or other signals (such as other sources or RFI) masked out. This removed any residual ripple left from 'luthering', such as ripple from off-beam sources. The masking was carried out manually, with sources being masked at 20% of their peak height. A fifth order polynomial was used to make the baseline fit, as this allows four turning points to be fitted – necessary for the removal of ripple with a wavelength of ~ 1200 $\mathrm{km\,s^{-1}}$. This was an iterative process, as it was often the case that masking those points with fluxes greater than 20% of the peak height caused the baseline fit, and thus the points to be masked, to change.

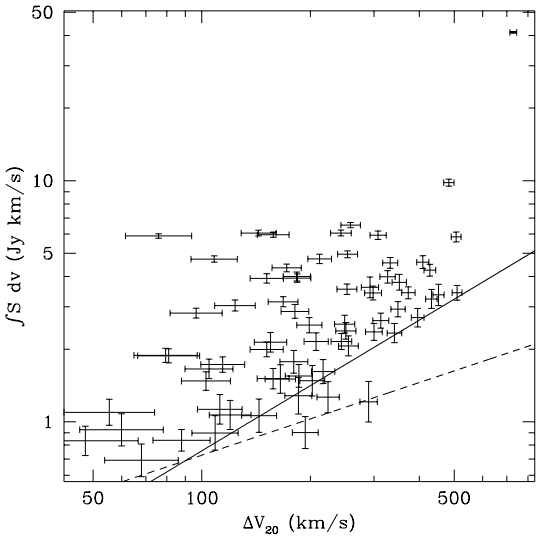

(a) Selection limits in velocity-width – flux space. Selection based on constant signal to noise ratio is shown by the dashed line and a selection limit of $\int S \, \mathrm{d}v_{limit} \propto \Delta V_{20}^{0.9}$ is shown by the solid line. It can be seen that the solid line appears to give a fairly good approximation of the selection limit, without the necessity for a second flux-limit component to explain the lack of low-flux, high velocity-width sources.

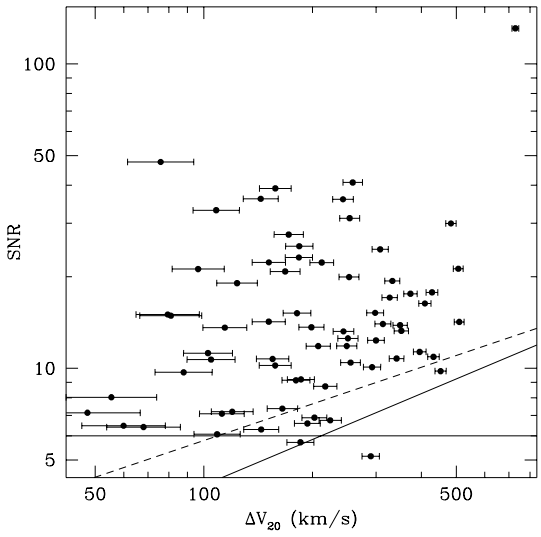

(b) Selection limits in velocity-width – signal to noise ratio (SNR) space. SNR is defined as the measured flux of a source divided by the error on that flux. The solid lines show limits of SNR = 6 and equivalent top-hat peak flux = 6 mJy and can be seen to fairly well explain the selection. The dashed line shows a selection limit of $\int S \, \mathrm{d}v_{limit} \propto \Delta V_{20}^{0.9}$, it can be seen that this does not well explain the selection in this plot.

Figure 2.6: Selection limits of the DEEP survey. It can be seen that although a selection limit of $\int S \, \mathrm{d}v_{limit} \propto \Delta V_{20}^{0.9}$ works well in velocity-wdith – flux space, it does not explain the selection well in velocity-width – SNR space.

The routine was used to measure the velocity widths at 50% and 20% of the peak height (ΔV_{50} and ΔV_{20}), the zeroth moment (integrated flux) of the source ($\int S_\nu \mathrm{d}v$), the first moment (radial velocity) of the source (V), the peak flux (S_{peak}) and the noise on the baseline section of the spectrum (σ). The moment measurements were made over a window of width $\Delta V_{20} + 53$ km s^{-1}, centred on the central velocity of ΔV_{20}, e.g. to two channel widths beyond the 20% level on either side. This gave an error on the total flux of $\sigma(\Delta V_{20} + 53)^{1/2}(13.2)^{1/2}$. The error on the systematic velocity was estimated as $\sim$ 16 km s^{-1} from comparing the measurement of the first order moment (used at the best indicator of the systematic velocity of the neutral hydrogen) with the centres of ΔV_{20} and ΔV_{50}. This is consistent with the scatter of 16 km s^{-1} seen when the velocities are compared with HI velocities from the literature. Similar analysis of the scatter for ΔV_{20} and ΔV_{50} gives errors of 16 km s^{-1} and 7 km s^{-1} respectively (see Section 2.5).

The flux limit on the DEEP survey is approximately 1 Jy km s^{-1}. This is obtained for a 'standard' velocity width of 200 km s^{-1} and a 'standard' noise of 4 mJy. This limit is shown in Figure 2.7, where it can be seen that almost all the sources fall in the decade of mass above this limit, at whatever distance they are located. There are some sources below the limit. These sources are either narrower than 200 km s^{-1} or are in regions of the cube where the noise is less than 4 mJy. The figure also shows the lower velocity cut off at 1000 km s^{-1} as a dashed line.

The distribution of masses for sources found in the DEEP survey is given in Figure 2.8. Using the relationship found between ΔV_{20} and $M_{\rm HI}$ (see Section 2.6) it is possible to calculate that, for a noise per channel of 4 mJy and a minimum signal-to-noise ratio for detection of 5, the transition from flux-limited to bandpass-limited occurs at $10^{10} M_\odot$, although it will occur earlier for sources that are narrower than implied by this relationship. For an $M^\star_{\rm HI}$ galaxy to be bandpass-limited, it would have to have a velocity width of less than 120 km s^{-1}. It can also be seen that there is a paucity of low-mass sources. This is partly due to the bandpass cut-off at 1000 km s^{-1}, which removes the Centaurus A group from the survey, but primarily due to the lack of volume in which these low-mass sources could be detected.

2.4.3 $(1 + z)$ effects

As the DEEP sample covers a velocity range of 1000 – 12,700 km s^{-1}, it reaches a redshift of $z \simeq 0.04$. At this redshift, $1 + z$ effects can become important and must be taken into account. In the radio convention, velocity is based on a measurement of the frequency, giving

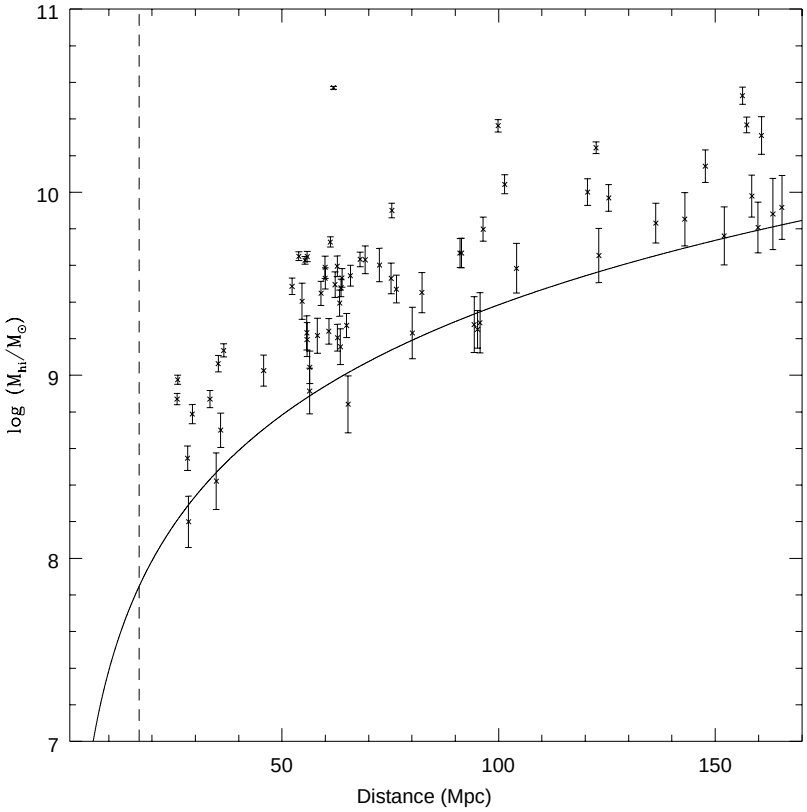

Figure 2.7: Selection limit for DEEP sources and distribution of sources by mass and distance. The solid line shows the detection limit for a limiting flux of 1 Jy km s^{-1}, a velocity width of 200 km s^{-1}, and a noise of 4 mJy. In reality, the noise varies across the cube and the velocity width is related to the mass of the galaxy, so this serves only as a first approximation. However, it can be seen that it is a fairly good approximation and most sources are clustered above the line. As the volume sampled increases with greater distance, higher mass sources (which are rarer) are generally found only at larger distances, leading to most sources being in the decade of HI mass directly above the selection line. The lower velocity cut off at 1000 km s^{-1} is indicated by a dashed line at 17 Mpc, below this is the Centaurus A group at $\approx$ 3.5 Mpc and 200 – 800 km s^{-1}.

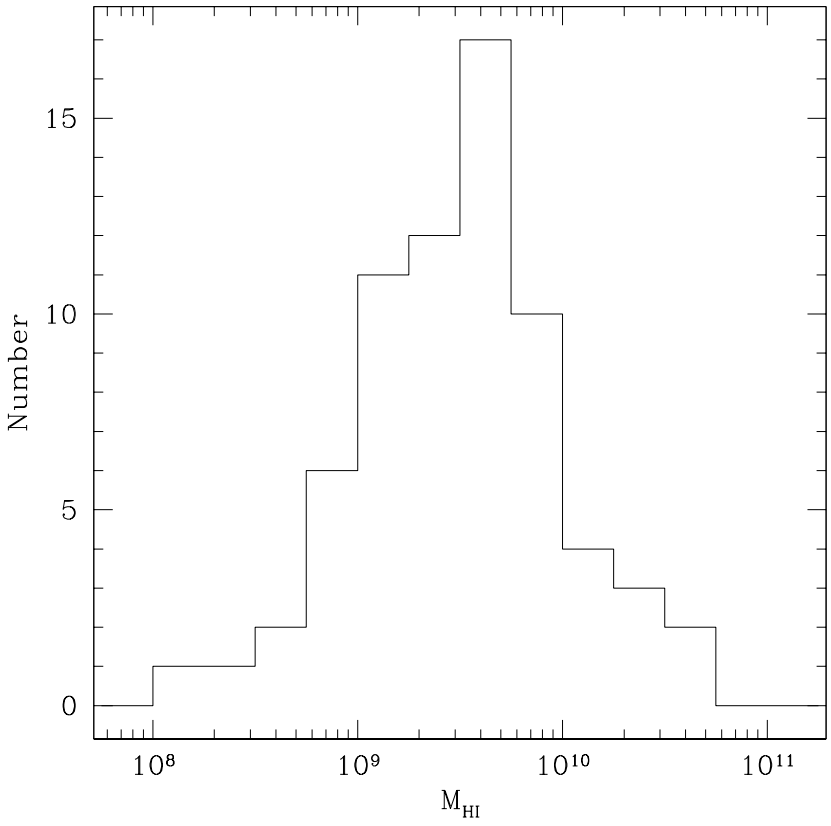

Figure 2.8: Distribution of HI masses from the DEEP survey. There is a peak in the bin $10^{9.5} < M_{\rm HI} < 10^{9.75}$, where expected from the value found by other authors (e.g Zwaan et al. 1997) for $M^{\star}_{\rm HI}$ of $10^{9.75} M_{\odot}$ (for $H_0 = 75$ kms^{-1} Mpc^{-1}). Lower mass galaxies than this are too faint to be seen over large volumes, and there are therefore fewer of these galaxies in the sample, while higher mass galaxies are too rare to be seen in large numbers. The transition from flux-limited to bandpass-limited occurs at $M_{\rm HI} \approx 10^{10} M_{\odot}$ for a galaxy following the relationship found between $M_{\rm HI}$ and ΔV (as indicated in panel a of Figure 2.5). For an $M^{\star}_{\rm HI}$ galaxy to be bandpass limited, it would need to have a velocity width of less than 120kms^{-1}.

$$v_{radio} = c\frac{\Delta\nu}{\nu_0} \tag{2.1}$$

where ν_0 is the rest frequency of the line and $\Delta\nu$ is the shift in frequency. However, velocities are generally measured in the cz convention defined by

$$cz = c\frac{\Delta\lambda}{\lambda_0} \tag{2.2}$$

where λ_0 is the rest wavelength of the line and $\Delta\lambda$ is the shift in wavelength. These two velocity conventions can be related as $\Delta\lambda = \lambda_1 - \lambda_0$, where λ_1 is the observed wavelength of the line, and $\Delta\nu = \nu_0 - \nu - 1$, where ν_1 is the observed frequency of the line. This gives:

$$v_{radio} = \frac{cz}{1+z} \tag{2.3}$$

This can be used to convert the velocity to the cz convention by inverting the equation to get

$$cz = \frac{c}{\frac{c}{v_{radio}} - 1} \tag{2.4}$$

In addition to this correction to the velocity, a correction to the velocity width must also be made. If the velocity width is thought of as being considerably smaller than the velocity, then a differential form can be used:

$$v_{radio} = \frac{cz}{1+z} \tag{2.5}$$

$$\frac{\mathrm{d}v_{radio}}{\mathrm{d}z} = \frac{(1+z)\frac{\mathrm{d}(cz)}{\mathrm{d}z} - cz\frac{\mathrm{d}(1+z)}{\mathrm{d}z}}{(1+z)^2} \tag{2.6}$$

$$= \frac{c(1+z) - cz}{(1+z)^2} \tag{2.7}$$

$$= \frac{c}{(1+z)^2} \tag{2.8}$$

$$\mathrm{d}v_{radio} = \frac{c\mathrm{d}z}{(1+z)^2} \tag{2.9}$$

At the redshifts reached by the DEEP project the $(1+z)$ effects are non-negligible in the radio frame and it is therefore necessary to convert velocities and velocity widths to the cz frame before they are used for analysis. The total effect of the $(1+z)$ terms, after conversion of the radial velocity to the cz frame, is substantially smaller than the measurement error on the mass and so can be neglected.

Cosmological $(1+z)$ effects can therefore be neglected from the HI analysis, although it will be necessary to include these in the optical analysis where they enter the luminosity as $(1+z)^2$ (up to 0.09 mags) and the surface-brightness as $(1+z)^4$ (up to 0.18 mags), or around the level of the error in the optical photometry. (see Chapter 3)

2.4.4 HI Properties

The HI properties of sources found in the DEEP cube are given in Table 2.1. Columns 1 and 2 give the DEEP identifcation for the source and the standard catalogue name, where the source can be associated with a previously catalogued galaxy. Columns 3 and 4 give the right ascension and declination of the HI source from fitting to the zeroth order moment map. Columns 5–7 give the noise (rms dispersion around the baseline, σ), the zeroth order moment (integrated flux, $\int S_\nu \mathrm{d}v$), and the peak flux (S_{peak}), all as measured by *mbspect*. Columns 8–10 give the first order moment (barycentric velocity, $V_\odot$), the velocity width at 50% of the peak flux (ΔV_{50}), and the velocity width at 20% of the peak flux (ΔV_{20}), all measured by *mbspect* in the radio frame and converted to cz. Column 11 gives the distance in Mpc calculated from the CMB rest-frame velocity of the sources with conversion from the barycentric to CMB frame carried out using the velocity conversion tool in NED (NASA/IPAC Extragalactic Database; http://nedwww.ipac.caltech.edu), this gives $V_{\rm CMB} \simeq V_\odot + 280\,\mathrm{km\,s^{-1}}$, although the exact correction varies across the field. Column 12 gives the HI mass calculated using the flux from column 6 and the distance from column 11 using the standard equation $M_{\rm HI} = 2.356 \times 10^5 \int S_\nu \mathrm{d}v \; d^2_{\rm Mpc} \; M_\odot$. Column 13 gives the 'quality' of the source as detected by PICASSO (see section 2.3). Column 14 gives the offset to the assumed optical counterpart, either to the catalogued position for catalogued galaxies, to a counterpart identified by ATCA observations (see Section 2.7), or to the assumed counterpart on the tech pan plate (where available) or the blue DSS – the source of the optical counterpart is given in footnotes to the table.

Table 2.1: HI Properties of DEEP sources

DEEP ID	Catalogue Name	α_{J2000} h m s	δ_{J2000} ° ′ ″	σ mJy	$\int S\,dv$ Jy km s^{-1}	S_{peak} mJy	$V_\odot$ km s^{-1}	ΔV_{50} km s^{-1}	ΔV_{20} km s^{-1}	D Mpc	$M_{\rm HI}$ $10^8 M_\odot$	Q	Offset ′
1	2	3	4	5	6	7	8	9	10	11	12	13	14
DEEP J1330-3212	ESO 444-G059	13 30 29	-32 12 28	3.6	1.10 ± 0.17	32	3948	40	55	56	8.2 ± 1.0	9.5	0.2[1]
DEEP J1331-3205	Abell 3558:[MGP94]3325	13 31 35	-32 05 55	3.2	0.83 ± 0.12	27	1851	32	48	28	1.6 ± 0.2	7.0	0.9[1]
DEEP J1331-3155	ESO 444-G066	13 31 49	-31 55 10	2.8	3.15 ± 0.15	36	4492	152	168	64	30.0 ± 1.4	14.2	0.5[2]
DEEP J1332-2943	IC 4275	13 32 01	-29 43 34	2.7	6.06 ± 0.17	42	4304	185	243	61	53.35 ± 2.5	24.6	2.2[2]
DEEP J1332-2726	ESO 509-G048	13 32 28	-27 26 45	3.1	2.70 ± 0.24	15	10791	377	396	148	139.0 ± 12.3	9.3	1.4[2]
DEEP J1332-3158	ESO 444-G070	13 32 47	-31 58 35	3.3	1.06 ± 0.17	12	11127	106	144	152	57.7 ± 9.2	6.3	0.6[2]
DEEP J1333-3401	ESO 383-G018	13 33 03	-34 01 43	3.8	2.14 ± 0.20	22	3910	105	155	56	15.7 ± 1.5	9.7	4.9[2]
DEEP J1333-2729	IRAS F13304-2714	13 33 12	-27 29 10	3.7	1.48 ± 0.21	12	10435	172	202	143	71.2 ± 10.3	9.6	1.2[1]
DEEP J1333-3347		13 33 15	-33 47 44	3.7	0.93 ± 0.14	26	2337	33	60	35	2.6 ± 0.4	9.7	0.1[3]
DEEP J1333-3243	ESO 444-G071	13 33 29	-32 43 38	3.3	3.99 ± 0.23	25	4223	310	327	60	33.8 ± 2.0	14.7	0.4[2]
DEEP J1333-2742	IC 4286	13 33 30	-27 42 09	3.0	1.55 ± 0.17	19	9934	144	186	136	67.8 ± 7.4	7.7, 6.0	4.6[1]
DEEP J1334-3223	Abell 3558:[MGP94]4312/4317[3]	13 34 09	-32 23 53	3.0	1.88 ± 0.13	34	1839	60	81	28	3.5 ± 0.2	14.7	2.4[1,4]
DEEP J1334-2809	IRAS F13312-2754	13 34 11	-28 09 49	3.2	2.52 ± 0.18	20	9120	156	199	125	93.2 ± 6.8	13.3	1.2[2]
DEEP J1334-3329	ESO 383-G024	13 34 27	-33 29 46	3.1	2.15 ± 0.18	18	3157	171	207	46	10.6 ± 0.9	6.8	1.1[2]
DEEP J1334-2859		13 34 51	-28 59 46	3.0	2.82 ± 0.13	39	2220	78	96	33	7.4 ± 0.3	21.3	0.5[3]
DEEP J1335-2802	IC 4290	13 35 22	-28 02 20	2.8	3.94 ± 0.16	34	4818	162	184	68	43.0 ± 1.7	18.9	1.1[2]
DEEP J1335-3352	ESO 383-G030	13 35 36	-33 52 54	5.3	3.61 ± 0.36	19	3825	280	292	55	25.4 ± 2.5	11.3	4.0[2]
DEEP J1335-3410	ESO 383-G031	13 35 31	-34 10 37	3.9	9.82 ± 0.33	56	7219	175	483	100	230.8 ± 7.7	11.8, 8.3	2.7[2]
DEEP J1335-2807	IRAS F13329-2751	13 35 42	-28 07 45	4.0	1.28 ± 0.22	15	12121	148	185	165	82.6 ± 14.5	5.7	1.7[2]
DEEP J1335-3051	ESO 444-G075	13 35 42	-30 51 23	2.8	3.55 ± 0.18	25	4509	199	252	64	34.1 ± 1.7	14.8	1.7[2]
DEEP J1335-2729		13 35 52	-27 29 05	2.9	2.93 ± 0.21	15	8755	340	350	121	100.3 ± 7.2	8.3	1.4[5]
DEEP J1335-3025	ESO 444-G077	13 35 52	-30 25 41	3.0	5.90 ± 0.12	111	3867	55	76	55	42.5 ± 0.9	39.5	0.3[2]
DEEP J1336-3327	NGC 5220	13 36 03	-33 27 41	2.9	1.48 ± 0.13	27	3958	51	103	56	11.1 ± 1.0	10.5	1.4[2]
DEEP J1336-2635	IC 4298	13 36 11	-26 35 04	3.2	0.90 ± 0.15	14	6891	75	109	96	19.4 ± 3.2	10.1	5.5[2]
DEEP J1336-2933		13 36 16	-29 33 12	2.7	1.73 ± 0.13	20	4430	104	114	63	16.1 ± 1.2	11.9	2.1[3]
DEEP J1336-3029	[QRM95]1330-30 01	13 36 31	-30 29 58	2.7	2.00 ± 0.14	19	4282	133	151	61	17.4 ± 1.2	8.8	1.2[2]
DEEP J1337-3259	ESO 383-G044	13 37 23	-32 59 00	2.5	6.54 ± 0.16	43	3768	234	258	54	44.7 ± 1.1	13.5, 6.0	1.7[2]
DEEP J1337-2839	IC 4303	13 37 22	-28 39 34	3.4	3.94 ± 0.18	38	2366	134	151	35	11.6 ± 0.5	12.7	0.9[1]

Table 2.1: HI Properties of DEEP sources (continued)

DEEP ID	Catalogue Name	α_{J2000} h m s	δ_{J2000} ° ′ ″	σ mJy	$\int S\,dv$ Jy kms^{-1}	S_{peak} mJy	$V_\odot$ kms^{-1}	ΔV_{50} kms^{-1}	ΔV_{20} kms^{-1}	D Mpc	$M_{\rm HI}$ $10^8 M_\odot$	Q	Offset ′
1	2	3	4	5	6	7	8	9	10	11	12	13	14
DEEP J1337-2907		13 37 39	-29 07 58	2.6	2.15 ± 0.16	18	5449	213	244	76	29.6 ± 2.2	6.7	0.1[6]
DEEP J1337-3035		13 37 55	-30 35 57	3.4	1.13 ± 0.16	18	5727	83	112	80	17.0 ± 2.4	7.5	0.8[3]
DEEP J1338-3054		13 38 06	-30 54 59	2.9	5.97 ± 0.15	51	1668	141	158	26	9.5 ± 0.2	16.4	0.5[3]
DEEP J1338-3120	ESO 444-G088	13 38 12	-31 20 13	3.3	3.04 ± 0.16	38	1921	95	124	29	6.1 ± 0.3	19.8	2.3[1]
DEEP J1338-2732		13 38 27	-27 32 33	2.4	0.90 ± 0.14	10	6794	175	193	94	18.9 ± 2.9	8.2	0.8[6]
DEEP J1338-2828		13 38 37	-28 28 49	3.1	1.26 ± 0.19	11	8953	206	224	123	45.1 ± 6.7	7.0	0.9[6]
DEEP J1338-3053	ESO 444-G090	13 38 43	-30 53 58	3.6	4.74 ± 0.21	33	3648	193	212	52	30.6 ± 1.4	21.5	1.0[1]
DEEP J1339-3021		13 39 03	-30 21 44	2.8	1.51 ± 0.15	18	4485	126	158	63	14.3 ± 1.4	8.7	1.2[6]
DEEP J1339-3131	IRAS 13365-3116[7]	13 39 39	-31 31 46	2.0	0.84 ± 0.09	14	6860	75	88	95	17.8 ± 1.8	7.1	3.7[2]
DEEP J1339-3141	CSRG 0737	13 39 23	-31 41 19	3.1	4.00 ± 0.17	38	11522	166	183	157	233.3 ± 10.1	15.4	0.8[2]
DEEP J1339-3205	ESO 445-G003	13 39 32	-32 05 13	3.4	2.87 ± 0.19	24	6957	159	181	96	62.8 ± 4.1	15.0	1.2[2]
DEEP J1340-3253	ESO 383-G059	13 40 06	-32 53 46	3.3	4.56 ± 0.24	24	7333	311	333	101	110.5 ± 5.7	10.1	0.7[2]
DEEP J1340-3142	ESO 445-G007	13 40 22	-31 42 08	3.1	4.73 ± 0.14	55	1661	93	108	26	7.4 ± 0.2	31.1	0.2[8]
DEEP J1340-3339	ESO 383-G060	13 40 36	-33 39 36	3.3	6.06 ± 0.17	54	3918	118	144	56	44.5 ± 1.2	32.8	1.1[2]
DEEP J1341-3303	WMMA 219	13 41 03	-33 03 52	2.7	2.63 ± 0.19	20	4478	284	313	63	24.8 ± 1.7	11.4	1.4[2]
DEEP J1341-3151		13 41 30	-31 51 05	3.1	1.61 ± 0.19	12	11610	207	217	158	95.4 ± 10.9	6.0	1.9[3]
DEEP J1341-3200	ESO 445-G011	13 41 46	-32 00 52	2.8	2.36 ± 0.19	17	6585	237	300	91	46.5 ± 3.8	5.7	4.0[2]
DEEP J1341-3209		13 41 53	-32 09 38	3.1	1.07 ± 0.15	19	11720	76	120	160	64.2 ± 8.9	6.0	4.8[3]
DEEP J1341-3235		13 41 54	-32 35 59	3.5	1.21 ± 0.24	17	11977	205	290	163	76.1 ± 14.8	8.2	1.3[3]
DEEP J1342-2901		13 42 06	-29 01 32	3.4	1.66 ± 0.16	23	2411	95	105	36	5.0 ± 0.5	13.7	0.3[3]
DEEP J1342-3024		13 42 17	-30 24 55	2.7	0.69 ± 0.11	19	4620	37	68	65	6.9 ± 1.1	5.4	1.9[6]
DEEP J1342-3104	ESO 445-G015	13 42 17	-31 03 17	2.8	3.43 ± 0.24	22	4395	358	510	62	31.3 ± 2.2	8.7	1.0[2]
DEEP J1342-3405		13 42 31	-34 05 14	3.8	1.40 ± 0.20	19	7543	148	165	104	38.4 ± 5.2	6.4	1.4[9]
DEEP J1343-2901	IC 4318	13 43 41	-29 01 04	2.5	4.95 ± 0.16	33	8911	222	253	122	175.0 ± 5.6	11.7	5.1[2]
DEEP J1343-2944	ESO 445-G020	13 43 39	-29 44 06	3.3	3.42 ± 0.22	20	4150	280	298	59	28.0 ± 1.8	11.5	1.0[1]
DEEP J1343-2948	IC 4319	13 43 35	-29 48 22	2.6	3.43 ± 0.20	19	4660	312	373	66	35.0 ± 2.0	8.3	1.9[2]
DEEP J1343-3253	ESO 383-G067	13 43 44	-32 53 28	3.1	2.06 ± 0.20	15	4096	217	255	58	16.5 ± 1.6	5.9	1.9[2]
DEEP J1344-3341		13 44 03	-33 41 04	3.5	1.77 ± 0.19	17	5908	166	180	82	28.3 ± 3.1	7.5	1.0[3]

Table 2.1: HI Properties of DEEP sources (continued)

DEEP ID	Catalogue Name	α_{J2000} h m s	δ_{J2000} ° ′ ″	σ mJy	$\int S\,dv$ Jy km s^{-1}	S_{peak} mJy	$V_\odot$ km s^{-1}	ΔV_{50} km s^{-1}	ΔV_{20} km s^{-1}	D Mpc	$M_{\rm HI}$ $10^8 M_\odot$	Q	Offset ′
1	2	3	4	5	6	7	8	9	10	11	12	13	14
DEEP J1344-2719	ESO 509-G100	13 44 07	-27 19 07	3.0	2.38 ± 0.19	19	6553	195	251	91	46.6 ± 3.7	10.4	4.2[2]
DEEP J1344-2801	MGC -05-32-072	13 44 12	-28 01 56	3.4	2.54 ± 0.21	16	5362	235	249	75	33.8 ± 2.9	7.6	1.0[1]
DEEP J1344-3003	ESO 445-G023	13 44 46	-30 03 17	3.0	1.89 ± 0.13	35	4596	63	79	65	18.7 ± 1.2	10.0	0.9[2]
DEEP J1345-2839	IC 4323	13 45 11	-28 39 38	2.9	4.35 ± 0.16	37	2466	140	172	37	13.7 ± 0.5	9.5	1.0[1]
DEEP J1346-3052	ESO 445-G026	13 46 41	-30 52 43	3.7	3.23 ± 0.30	22	5166	397	433	72	40.0 ± 3.7	7.8, 6.6	1.8[2]
DEEP J1347-3024	NGC 5291	13 47 18	-30 24 02	3.0	41.24 ± 0.31	115	4371	637	729	62	372.0 ± 2.8	61.3, 22.1	1.5[2]
DEEP J1347-2818	IC 4330	13 47 20	-28 18 57	3.2	5.84 ± 0.28	21	11448	481	507	156	336.2 ± 15.8	9.0	1.5[2]
DEEP J1347-3055	NGC 5292	13 47 46	-30 55 09	3.0	4.25 ± 0.24	30	4437	417	428	62	39.4 ± 2.2	5.8	1.8[2]
DEEP J1347-2923	IC 4325	13 47 50	-29 23 49	3.0	2.33 ± 0.22	25	3907	298	342	56	17.1 ± 1.6	9.7	3.2[2]
DEEP J1347-3049	Abell 3574:[R84]0453[10]	13 47 55	-30 49 48	4.2	3.36 ± 0.34	19	11780	388	453	161	204.2 ± 20.9	8.1	3.2[1]
DEEP J1348-3012	IC 4327	13 48 42	-30 12 16	3.5	5.94 ± 0.24	26	5382	281	308	75	79.5 ± 3.2	12.1	0.9[2]
DEEP J1349-2802	ESO 445-G048	13 49 05	-28 02 38	3.9	3.79 ± 0.29	24	4918	332	352	69	42.7 ± 3.2	10.8	2.4[2]
DEEP J1349-3303	ESO 383-G088	13 49 38	-33 03 43	3.6	4.59 ± 0.28	19	4234	347	409	60	38.9 ± 2.4	6.2	1.1[2]

[1] Offset to assumed previously catalogued counterpart without a previous redshift.
[2] Offset to previously catalogued counterpart with a matching optical redshift
[3] Offset to ATCA-identified previously uncatalogued counterpart
[4] Two possible sources, indistinguishable without optical spectroscopy
[5] Offset to only obvious counterpart on Tech Pan plate – ESO 509-G075, which has an optical velocity of $cz = 16302 \pm 50$ km s^{-1} (Quintana et al. 1995)
[6] Offset to assumed previously uncatalogued counterpart on Tech Pan plate
[7] FGCE 1090 is at the same offset but has no velocity measurement
[8] Offset to previously catalogued counterpart with a prior HI single-dish redshift but no prior optical redshift
[9] Offset to assumed previously uncatalogued counterpart on on blue DSS
[10] ESO 445-G034 is closer at 1.5′, but has an optical velocity of $cz = 4130 \pm 60$ km s^{-1} (Willmer et al. 1991)

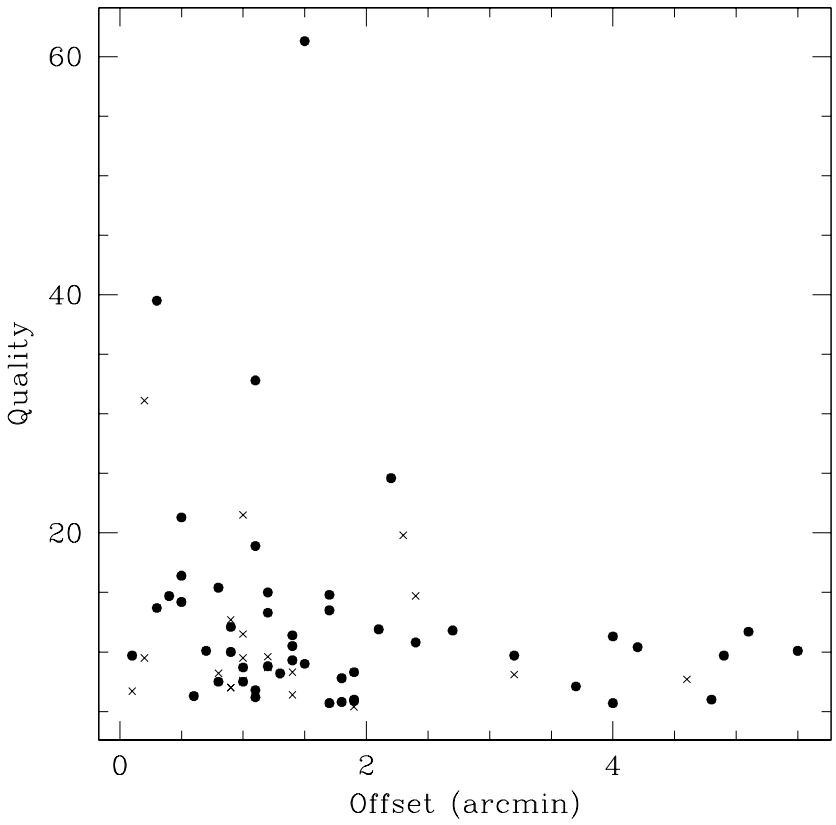

Figure 2.9: Comparison between angular offset to the assumed optical counterpart and finder 'Quality'. The 'Quality' is a measure of the detection signal to noise ratio, it can be seen that there is only a weak trend for higher Quality sources to have a smaller offset. Filled circles indicates offsets to candidates where I am confident of the detection – where there a matching previously catalogued redshift or an accurate position from interferometric follow-up, crosses indicate offsets to less certain candidates.

2.4.5 Identification of optical counterparts

Analysis of the optical properties of an HI selected sample must include the identification of optical counterparts to the HI sources. For many of the sources there are catalogued galaxies nearby, a large number of which have redshifts in the literature that match the velocity of the HI source – these can be assumed to be fairly firm detections. There are also some sources for which HI follow-up has been carried out using the Australia Telescope Compact Array (ATCA) to get accurate HI positions. Where this gives a possible optical counterpart within the errors on the ATCA position, we can again be confident that the correct galaxy has been selected. However, there are some previously catalogued galaxies without redshifts and some previously undetected sources without ATCA follow-up. For these galaxies, it is necessary to select the most likely counterpart from optical images of the region around the HI position.

Figure 2.9 shows how the offsets to the optical counterparts varies with finder Quality (see Section 2.3. It has been predicted from modelling (Barnes 1998) that the positional accuracy should be $\sim 15'/SNR$, however this is not seen here – the number of higher Quality sources at large offsets is substantially higher than given by this model.

Figure 2.10 shows a cumulative distribution of the offsets divided into two datasets, that of offsets to counterparts where I am confident about the identification – where there are redshifts in the literature or ATCA positions as detailed above, and those offsets to candidates where the identification is less certain. Analysis of these shows that the median for the 'confident' offsets is $1.4'$, with a semi-interquartile range of $0.6'$and that of the 'less certain' offsets is lower (although not significantly) at $1.0'$, with a semi-interquartile range of $0.5'$. Analysing the data sets with the Kolmogorov-Smirnov test shows that the two data sets cannot be shown to come from different parent populations, it therefore seems likely that the 'less certain' identifications can be trusted.

Figure 2.11 shows that there is no relationship between the distance to a source and the angular offset between the HI source and the galaxy identified as its optical counterpart. This is expected, as it is thought that the distribution of offsets is due to the poor resolution (FWHM $\sim 15'$) of the Parkes telescope rather than being due to physical extension of the galaxies, but it does provide a useful check on this. Had there been systematically larger offsets for nearby galaxies, this would have indicated that the HI in these galaxies has a very different morphology from the light thus giving it a different centroid, while systematically larger offsets for distant galaxies would have indicated that bright, high visibility, galaxies were being mis-identified

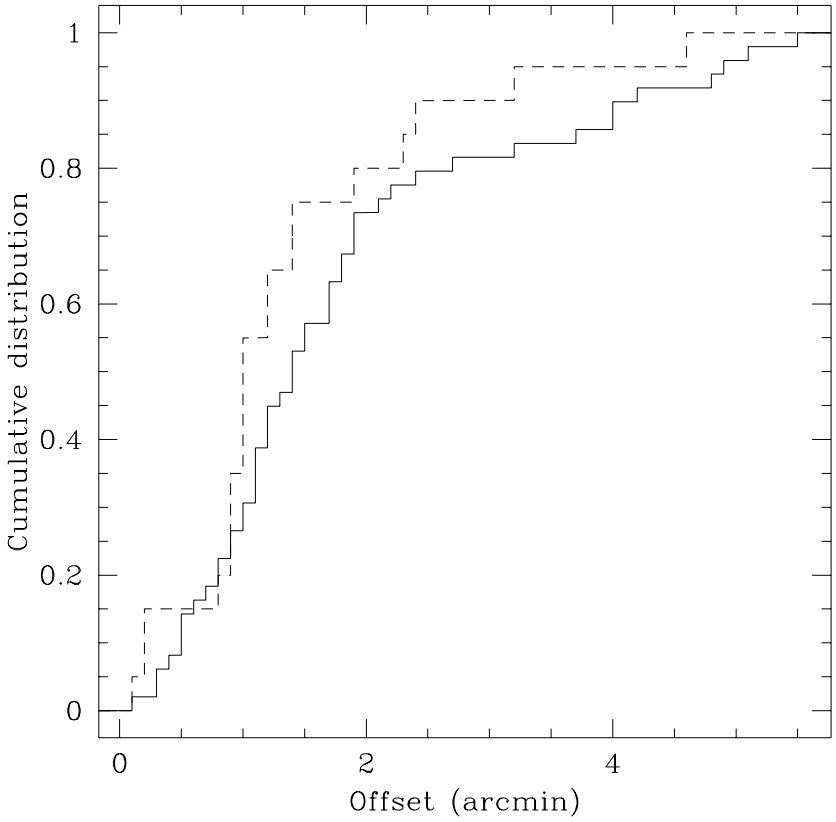

Figure 2.10: Comparison between cumulative distributions of offsets for those galaxies where I am confident of the identification (solid line) and for those galaxies where the identification is less certain (dashed line). The Kolmogorov-Smirnov test indicates that these two samples cannot be shown to come from different parent populations, implying that the 'less certain' identifications can be trusted.

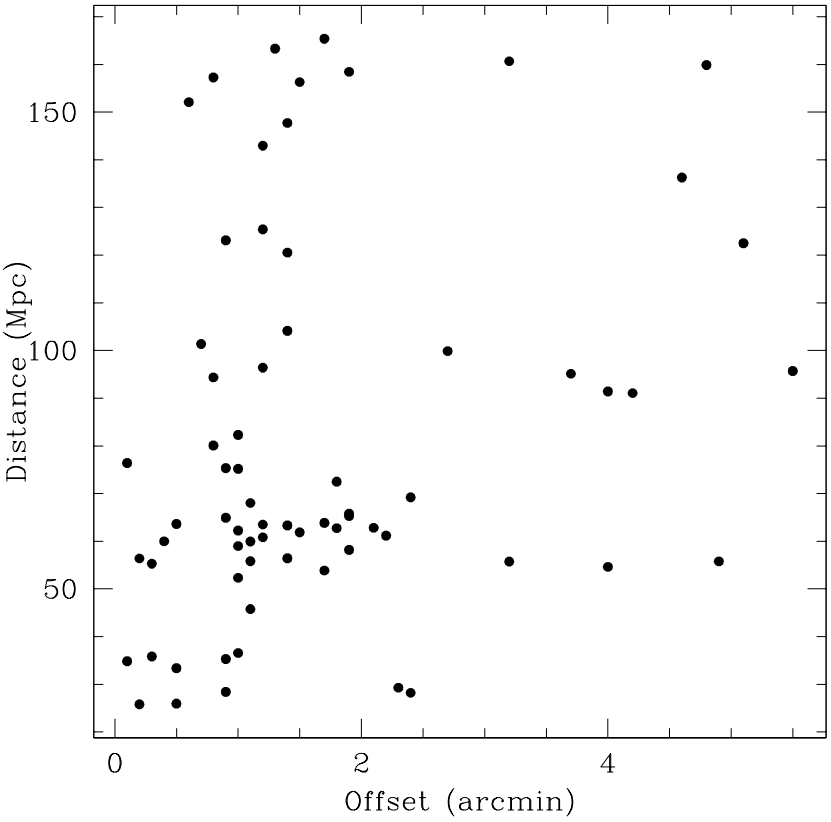

Figure 2.11: Comparison between angular offset to the assumed optical counterpart and the assumed radial distance to the source. It can be seen that there is no relationship between these two quantities, indicating that the errors in the positions are primarily due to the poor resolution of the Parkes telescope rather than any physical cause.

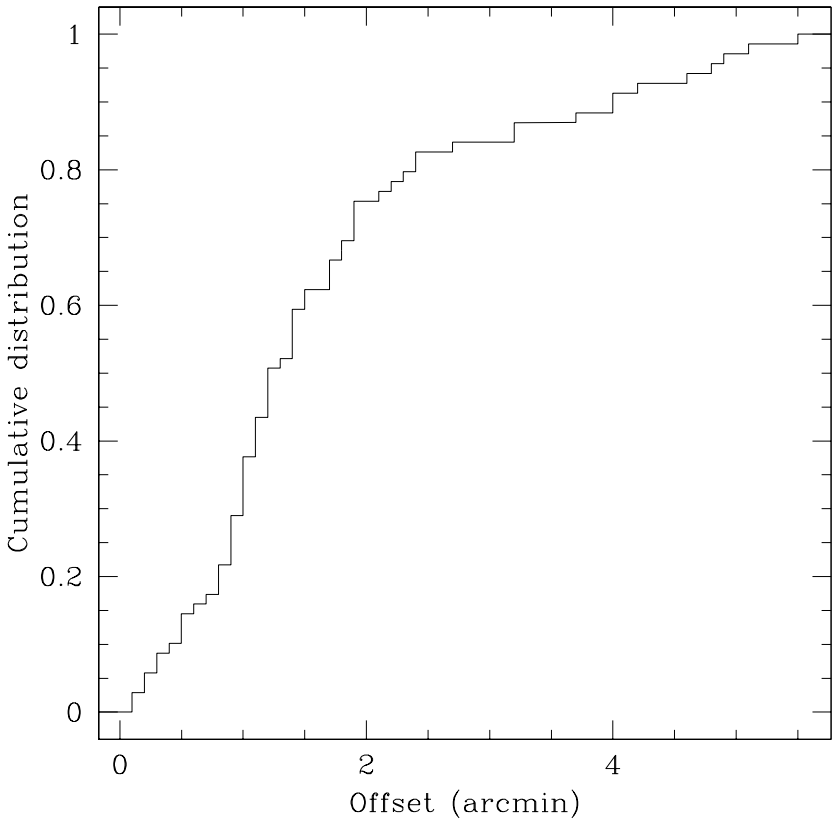

Figure 2.12: Cumulative distribution of angular offsets. It can be seen that most optical counterparts lie within 1.2′ of the HI position and 90% lie within 4.0′. That most optical counterparts are close to the fitted positions of the sources gives some confidence that correct identifications can generally be made, however the long tale – ≈ 25% of sources fall between 2′ and 6′ – indicates that mistakes are possible.

as the sources.

Figure 2.12 shows the cumulative distribution of offsets. The median offset to the galaxies is $1.2' \pm 0.5$ (errors showing the semi-interquartile range), while the mean is $1.7' \pm 1.3'$. Almost all the galaxies (90%) have offsets of less than 4.0′, with 98% having offsets less than 5.0′. The offsets are generally fairly small (for the full data set, the 'confident' data set, and the 'less-certain' data set – see Figure 2.10), indicating that in general the region that must be searched for counterparts is similarly small and thus the risk of mis-identifications is low. Where there is an uncertainty in the identification this has been noted in Table

2.1.

2.5 Comparison with the Literature

For those sources in the DEEP survey that were near catalogued galaxies, previously catalogued redshifts (where available) have been compared with those measured in the survey. This has been used to divide the survey sources into 3 classes – ID (identification, 40 galaxies), where there is both a positional match with a previously catalogued galaxy and a match between the velocity measured in DEEP and one in the literature, GCNV (Galaxy Close No Velocity, 12 galaxies), where there is a positional match with a previously catalogued galaxy but there is no velocity available in the literature, and NOF (No Object Found, 17 HI sources), where there is no previously cataloged galaxy nearby. Nearby galaxies which have non-matching redshifts were excluded, where there was no other nearby galaxy with a matching redshift this has been noted in Table 2.1

There are optical redshift for 39 of the 52 previously catalogued galaxies associated with the HI sources (see Table 2.2) and HI measurements of the total flux, velocity, and velocity width for 18 of these 52 galaxies (see Table 2.3). There is one galaxy (ESO 445-G007) which has a previous HI measurement but no optical redshift, with this exception all the IDs are those with velocities in Table 2.2 and the GCNVs are those without velocities in that table. This gives a total of 40 IDs (58%), 12 GCNVs (17%). and 17 NOFs (25%). Of the 52 associated galaxies, four are only found in the IRAS catalogue and have been omitted by optical catalogues and a further seven are from sources other than the ESO/IC/NGC catalogues.

The correspondence between the HI properties in the literature and those found in this survey is shown by Figure 2.13. It can be seen that there are two galaxies that fall well above the line of slope unity in both velocity width and flux (NGC 5220 and IC 4298). These two galaxies both appear single peaked in the DEEP survey but have presumably been identified as double peaked by Theureau et al (1998). These second peaks are not visible in the DEEP data. These same two galaxies fall away from the line of slope unity in velocity, being the source with a significantly higher literature velocity at a DEEP velocity of around 4000 $\mathrm{km\,s^{-1}}$ and the source with a significantly lower literature velocity at a DEEP velocity of around 7000 $\mathrm{km\,s^{-1}}$. These deviations are presumably also due to the inclusion of a second peak.

With these two galaxies removed, 16 remain. These have been used to analyse the error in the velocity and the velocity widths, taking into account the published errors on these variables. This was done by

Table 2.2: Optical velocities for DEEP sources

Catalogue ID	Velocity $km\,s^{-1}$	Reference
ESO 444-G059	No optical velocity	
Abell 3558:[MGP94]3325	No optical velocity	
ESO 444-G066	4425 ± 95	Dressler 1991
	4505 ± 44	da Costa et al. 1987
IC 4275	4383 ± 37	Richter 1987
	4376 ± 50	Quintana et al. 1995
ESO 509-G048	10789 ± 40	da Costa et al. 1986
ESO 444-G070	11106 ± 31	Willmer et al. 1999
ESO 383-G018	3721 ± 17	Willmer et al. 1999
IRAS F13304-2714	No optical velocity	
ESO 444-G071	4137 ± 95	Dressler 1991
	4301 ± 40	da Costa et al. 1986
IC 4286	No optical velocity	
Abell 3558:[MGP94]4312	No optical velocity	
Abell 3558:[MGP94]4317	No optical velocity	
IRAS F13312-2754	9173 ± 50	Quintana et al. 1995
ESO 383-G024	3270 ± 79	Willmer et al. 1999
IC 4290	4859 ± 95	Dressler 1991
	4869 ± 26	da Costa et al. 1987
	4960 ± 75	Fairall, Vettolani, & Chincarini 1989
ESO 383-G030	3873 ± 38	Sandage 1978
ESO 383-G031	7101 ± 10	Mathewson & Ford 1996
IRAS F13329-2751	12334 ± 50	Quintana et al. 1995
ESO 444-G075	4657 ± 95	Dressler 1991
	4569 ± 40	da Costa et al. 1986
ESO 444-G077	3872 ± 95	Dressler 1991
	3847 ± 53	da Costa et al. 1987
NGC 5220	4213 ± 20	Willmer et al. 1999
IC 4298	6593 ± 95	Dressler 1991
	6732 ± 39	da Costa et al. 1998
[QRM95]1330-30 01	4507 ± 50	Quintana et al. 1995
ESO 383-G044	3989 ± 90	Penston et al. 1977
IC 4303	No optical velocity	
ESO 444-G088	No optical velocity	
ESO 444-G090	No optical velocity	
IRAS 13365-3116	6932 ± 47	Willmer et al. 1999
CSRG 0737	11574 ± 24	Willmer et al. 1999

Table 2.2: Optical velocities for DEEP sources (continued)

Catalogue ID	Velocity $km\,s^{-1}$	Reference
ESO 445-G003	6969 ± 43	Willmer et al. 1999
ESO 383-G059	7364 ± 28	Willmer et al. 1999
ESO 445-G007	No optical velocity	
ESO 383-G060	3932 ± 95	Dressler 1991
	3850 ± 100	Fairall et al. 1989
WMMA 219	4494 ± 44	Willmer et al. 1999
ESO 445-G011	6634 ± 60	Willmer et al. 1999
ESO 445-G015	4489 ± 95	Dressler 1991
	4417 ± 26	da Costa et al. 1987
	4387 ± 10	Mathewson, Ford, & Buchhorn 1992
IC 4318	8881 ± 95	Dressler 1991
	46 ± 29	Menzies, Coulson, & Sargent 1989
	8780 ± 100	Fairall et al. 1989
ESO 445-G020	No optical velocity	
IC 4319	4653 ± 10	Mathewson, Ford, & Buchhorn 1992
ESO 383-G067	4093 ± 10	Mathewson, Ford, & Buchhon 1992
ESO 509-G100	6502 ± 95	Dressler 1991
MCG -05-32-072	No optical velocity	
ESO 445-G023	4620 ± 10	Côté et al. 1997
IC 4323	No optical velocity	
ESO 445-G026	5096 ± 54	Richter 1984
	5201 ± 10	Mathewson & Ford 1996
NGC 5291	4302 ± 112	Richter 1984
	4366 ± 31	Sandage 1978
IC 4330	11381 ± 10	Mathewson & Ford 1996
NGC 5292	4548 ± 95	Dressler 1991
	4478 ± 14	Menzies, Coulson, & Sargent 1989
	4485 ± 29	Richter 1984
	4482 ± 41	Sandage 1978
IC 4325	3801 ± 40	da Costa et al. 1986
Abell 3574:[R84]0543	No optical velocity	
IC 4327	5600 ± 40	Fairall et al. 1989
	5413 ± 36	da Costa et al. 1987
ESO 445-G048	4679 ± 26	de Souza, de Mello, & Dos Anjos 1997
ESO 383-G088	4062 ± 95	Dressler 1991
	4233 ± 10	Mathewson, Ford, & Buchhorn 1992

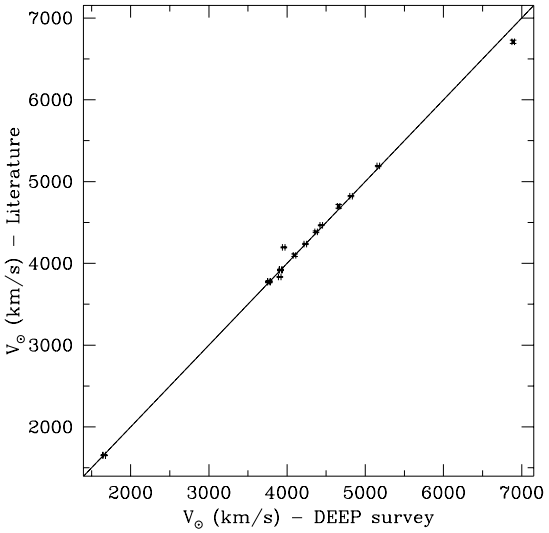

(a) Comparison between HI velocities from DEEP and previous observations

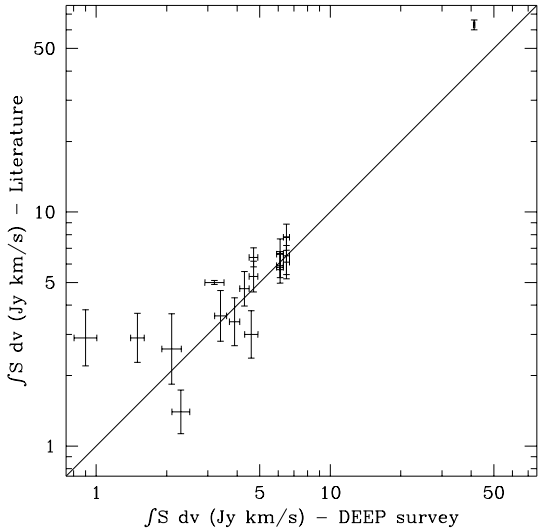

(b) Comparison between HI fluxes from DEEP and previous observations

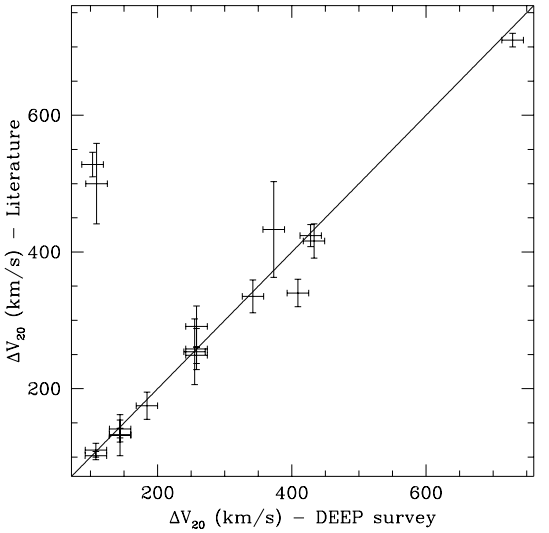

(c) Comparison between ΔV_{20} from DEEP and previous observations

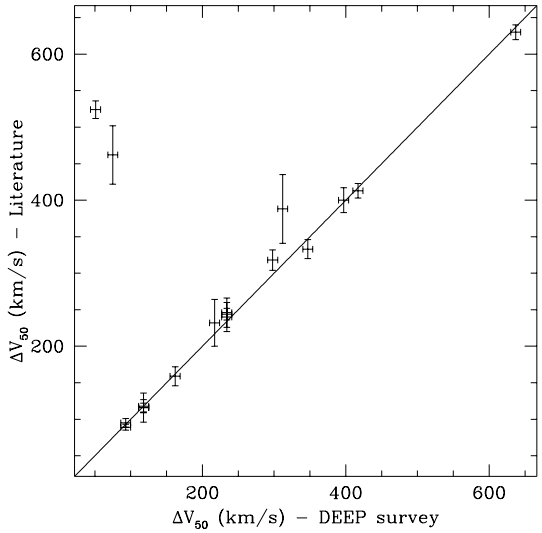

(d) Comparison between ΔV_{50} from DEEP and previous observations

Figure 2.13: Comparison between properties from the DEEP survey and from the literature. The line on each graph shows a slope of unity passing through the origin, it can be seen that this matches the data fairly well except for two galaxies (NGC 5220 and IC 4298) that fall off this line in every graph.

Table 2.3: HI values from the literature for galaxies found in the DEEP survey.

Catalogue ID	$\int Sdv$ (Jy km s^{-1})	Velocity (km s^{-1})	ΔV_{20} (km s^{-1})	ΔV_{50} (km s^{-1})	Reference
IC 4290	3.4 ± 0.8	4822 ± 7	175 ± 20	159 ± 13	Theureau et al. 1998
NGC 5220	2.9 ± 0.7	4195 ± 6	528 ± 18	524 ± 12	Theureau et al. 1998
IC 4298	2.9 ± 0.8	6709 ± 20	500 ± 59	462 ± 40	Theureau et al. 1998
ESO 383-G044	6.1 ± 1.0	3779 ± 4	249 ± 12	244 ± 8	Theureau et al. 1998
	7.8 ± 1.0	3775 ± 10	258 ± 30	246 ± 20	Mathewson, Ford, & Buchhorn 1992
	6.5 ± 1.2	3771 ± 10	291 ± 30	240 ± 20	Fouqué et al. 1990
ESO 445-G007	6.4 ± 0.6	1650 ± 2	102 ± 6	89 ± 4	Huchtmeier et al. 2000
	5.2 ± 0.8	1657 ± 3	110 ± 10	95 ± 6	Fouqué et al. 1990
ESO 383-G060	5.9 ± 0.7	3920 ± 3	132 ± 10	116 ± 6	Theureau et al. 1998
	5.8 ± 0.9	3920 ± 10	132 ± 30	116 ± 20	Mathewson & Ford 1996
ESO 383-G060	6.6 ± 1.0	3919 ± 4	141 ± 13	118 ± 9	Fouqué et al. 1990
IC 4319	3.6 ± 0.9	4697 ± 16	433 ± 70	388 ± 47	Theureau et al. 1998
ESO 383-G067	2.6 ± 0.9	4099 ± 16	254 ± 48	232 ± 32	Theureau et al. 1998
ESO 445-G026	5.0 ± 0.1	5190 ± 8	416 ± 25	400 ± 17	Theureau et al. 1998
NGC 5291	63.0 ± 3.0	4386 ± 10	710 ± 10	630 ± 10	Longmore et al. 1979
NGC 5292	4.7 ± 0.8	4466 ± 5	424 ± 16	413 ± 10	Theureau et al. 1998
IC 4325	1.4 ± 0.3	3834 ± 7	335 ± 24	318 ± 14	Theureau et al. 1998
ESO 383-G088	3.0 ± 0.7	4236 ± 7	340 ± 20	333 ± 13	Theureau et al. 1998

finding the scatter around a line of slope unity. The scatter is given by

$$\text{scatter} = \frac{\chi^2}{\sum_i 1/\sigma_i^2} \tag{2.10}$$

where σ_i are the errors on each point. For a line of slope unity, as is expected here, χ^2 is given by

$$\chi^2 = \sum \left(\frac{x_i - y_i}{\sigma_i} \right)^2 \tag{2.11}$$

This gives a scatter in velocity of 16 $\mathrm{km\,s^{-1}}$, which is consistent with the internal scatter between the 1st moment and the centres of the 50% and 20% velocity widths. It also gives a statistical error for the 20% velocity width of 16 $\mathrm{km\,s^{-1}}$ and for the 50% velocity width of 7 $\mathrm{km\,s^{-1}}$. These values have therefore been adopted as the errors for this project.

2.6 The HI mass – velocity width relationship

A correlation between HI mass and velocity width of the form $\Delta V \propto M_{\mathrm{HI}}^{\beta}$ is expected in the DEEP data as it has been seen in optically-selected samples (e.g. Briggs & Rao 1993) and as it would be the HI equivalent of the Tully-Fisher relationship. The relationship seen by Briggs & Rao is found in data that has not been corrected for inclination – that the relationship is seen in the observed data provides a useful tool for analysing the selection effects in HI surveys where velocity width plays an important role.

That this relationship can be seen in the DEEP data is shown in Figure 2.14. The solid lines shown here are for the best-fits of $\Delta V_{20} = 0.15^{+0.26}_{-0.09} M_{\mathrm{HI}}^{0.34\pm0.05}$ (panel (a)) and $\Delta V_{50} = 0.13^{+0.27}_{-0.09} M_{\mathrm{HI}}^{0.34\pm0.05}$ (panel (b)). The dashed line on both graphs shows $\Delta V = 0.16 M_{\mathrm{HI}}^{1/3}$ as found by Briggs & Rao (1993). The best fit slopes found to the DEEP data are statistically indistinguishable from this, indicating that the relationship seen in the DEEP data is consistent with that seen in optically-selected samples.

2.7 ATCA HI data

Follow-up observations of a number of NOFs were carried out at the Australia Telescope Compact Array (ATCA) in November 1999 (21 hours) and January 2000 (52 hours) by Erwin de Blok of the Australia

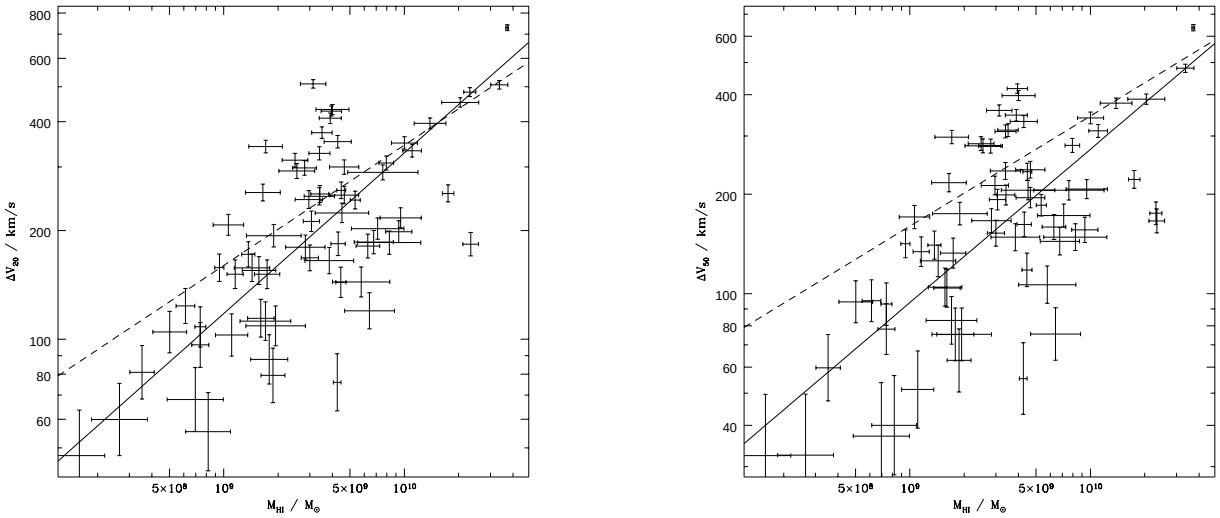

(a) Relationship between $M_{\rm HI}$ and ΔV_{20}

(b) Relationship between $M_{\rm HI}$ and ΔV_{50}

Figure 2.14: HI mass – velocity width relationship for DEEP sources. It can be seen that there is a correlation between velocity width and HI mass for both ΔV_{50} and ΔV_{20}. The best fits to the DEEP data are shown by solid lines, while the fit of $\Delta V = 0.016 M_{\rm HI}^{1/3}$ (Briggs & Rao 1993) is shown as a dashed line. The slope of this is statistically indistinguishable from the fits to the DEEP data, although the constant appears a little high in comparison.

Telescope National Facility. Both sets of observations were carried out with the ATCA in the 375-m configuration, this offers 10 baselines (excluding the 6-km fixed antenna) ranging between 31 and 459 metres. This gives a beam size of approximately $1.6' \times 3.2'$ at -30°, which means the positions of the sources can be fitted with an accuracy of around $15''$, thus allowing a definite identification of the HI source with an optical counterpart. This smaller beam size does, however, make detections more difficult as the flux is spread among a number of pixels, thus reducing the signal to noise ratio.

The November 1999 run was unfortunately scheduled when the Sun was only around 20° from the DEEP field, with the result that around 25% of the data had to be rejected as bad, including most of the short baselines. Of seven candidates observed, only two solid detections and one dubious detection ($\sim 2\sigma$, but near the likely optical candidate) were made.

In the January 2000 run, twelve sources were observed. This consisted of seven previously unobserved sources along with the four sources that were observed in the November 1999 run but remained undetected and the 'dubious' source from the November 1999 run that was detected but with a low signal to noise. This resulted in the confirmation of the 'dubious' detection from November and the 'dubious' detection, at a lower signal to noise than would have been preferred, of two of the previously undetected sources. Of the seven new sources, four solid detections were made and one 'dubious' detection, with two sources remaining undetected. A summary of the ATCA observations and the positions derived from them is presented in Table 2.4. There were a total of 7 definite detections, 3 'dubious' detection, and 4 non detections after the January 2000 run.

2.8 Large scale structure in the DEEP cube - comparison with RC3 data

The Third Reference Catalogue of Bright Galaxies (RC3; de Vaucouleurs et al. 1991) was searched in the DEEP region ($13^h30^m46^s < \alpha_{J2000} < 13^h49^m14^s$ and $-34° < \delta_{J2000} < -26$). This gave a total of 72 sources, 56 of which had optical or HI velocities in the range covered by DEEP (1,000 – 12,700 $\mathrm{km\,s^{-1}}$).

A comparison between the DEEP sources and RC3 galaxies in velocity – right ascension and velocity – declination is given in Figure 2.15. It can be seen that both surveys clearly detect the Centaurus Cluster in the velocity range 3000 – 5000 $\mathrm{km\,s^{-1}}$. It can also be seen that DEEP detects more galaxies in the field

Table 2.4: Summary of ATCA observations

Source ID	Peak flux	November 1999			January 2000		
	(mJy)	Status	α	δ	Status	α	δ
DEEP J1333-3347	26	Not observed			Detected	13 33 15	-33 47 35
DEEP J1334-2859	39	Not observed			Detected	13 34 52	-29 00 13
DEEP J1335-2729	15	No detection			No detection		
DEEP J1336-2933	20	Detected	13 36 08	-29 34 17	Not observed		
DEEP J1337-3035	18	Not observed			Detected	13 37 56	-30 35 13
DEEP J1338-2732	10	Not observed			No detection		
DEEP J1338-3054	51	Detected	13 38 08	-30 55 02	Not observed		
DEEP J1338-2828	11	Not observed			No detection		
DEEP J1341-3209	19	Dubious	13 41 32	-32 11 44	Detected	13 41 31	-32 10 42
DEEP J1341-3151	12	No detection			Dubious	13 41 36	-31 52 24
DEEP J1341-3235	17	Not observed			Dubious	13 41 53	-32 34 38
DEEP J1342-2901	23	Not observed			Detected	13 42 05	-29 01 48
DEEP J1342-3405	19	No detection			No detection		
DEEP J1344-3341	17	No detection			Dubious	13 44 00	-33 40 13

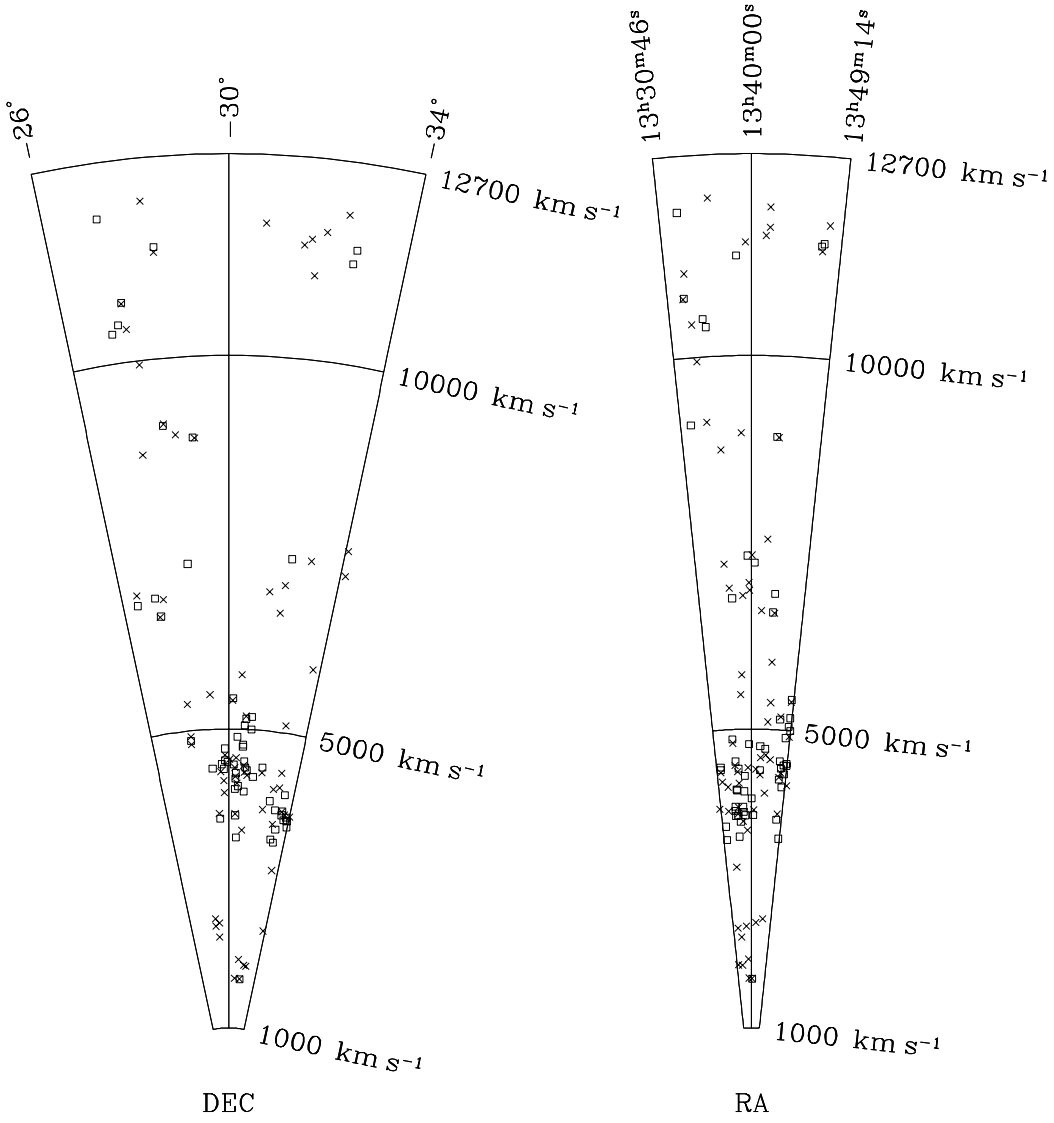

Figure 2.15: Slices in DEC and RA showing DEEP sources (crosses) and RC3 galaxies (open boxes). The angle of the slices has been expanded by a factor of 3 for clarity. It can be seen that DEEP and the RC3 generally trace the same structure, although the bright galaxies catalogued in the RC3 are often not the same sources as the HI rich galaxies catalogued in DEEP. The Centaurus cluster can be seen clearly as an over-density between 3000 and 5000 $\mathrm{km s^{-1}}$.

that the RC3 – in DEEP the Centaurus Cluster has just over twice as many galaxies as in the velocity range 5000 – 7000 $\mathrm{km\,s^{-1}}$, immediately behind the cluster, while in the RC3 the number of galaxies found in the cluster is well over five times greater than the number found between 5000 and 7000 $\mathrm{km\,s^{-1}}$.

In order to see whether the two data sets were significantly different, they were compared using the Kolmogorov-Smirnov test. This tests the null hypothesis that both data sets are from the same parent population (e.g. that they sample the same large scale structure). The test was carried out by examining numbers of galaxies along the velocity axis in the two surveys and gave the result that the null hypothesis has a significance of greater than 10%, e.g. they could not be shown to be from different parent populations at the 90% confidence level. The Centaurus Cluster is, like many clusters, rich in ellipticals and so it would not be surprising if the population in the RC3 was very different from that detected in DEEP, since ellipticals are generally HI poor. However, the samples in both catalogues are too small in number for the difference to be significant. This is not inconsistent with the higher ratio of galaxies in the Centaurus cluster to the region just beyond in the RC3 compared than in DEEP. Rather it says that although this difference exists the numbers involved are too small for it to be statistically significant.

2.9 Spectra from the DEEP survey

The spectra from the DEEP survey, as used to determine the total flux, peak flux, and velocity widths, are shown in Figure 2.16. These spectra were all produced using the MIRIAD routine *mbspect*. The baseline of each spectrum has had a fifth-order polynomial fitted and subtracted in order to remove residual ripple. A fifth-order polynomial was used as this allows four turning points, which is the expected maximum number for 5.7 MHz ripple across 2000 $\mathrm{km\,s^{-1}}$.

The dashed vertical lines on each spectrum delimit the regions which were excluded from the baseline fit, this is generally sources down to their 20% level although for NGC 5291 (DEEP J1347-3024) this was extended a further 2 channels either side due to the high flux of this source. For some spectra this region also includes parts of other sources or RFI lines which have been excluded from the baseline fit. The dotted vertical lines delimit the region used for parameter fitting to the source and is generally 2 channels (26.4 $\mathrm{km\,s^{-1}}$) outside the 20% level on each side, although for NGC 5291 four channels either side were taken. All the spectra are shown with radio velocity ($cz(1+z)^{-1}$) along their x-axis and flux on their y-axis. All the spectra except NGC 5291 have a baseline of 2000 $\mathrm{km\,s^{-1}}$, centred on the 20% velocity width of the source.

NGC 5291 has a baseline of 3000 $\mathrm{km\,s^{-1}}$ as it has too large a velocity width for a baseline to be fitted over 2000 $\mathrm{km\,s^{-1}}$.

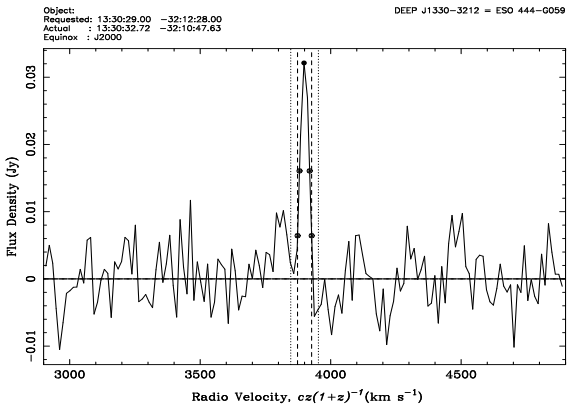

ESO 444-G059

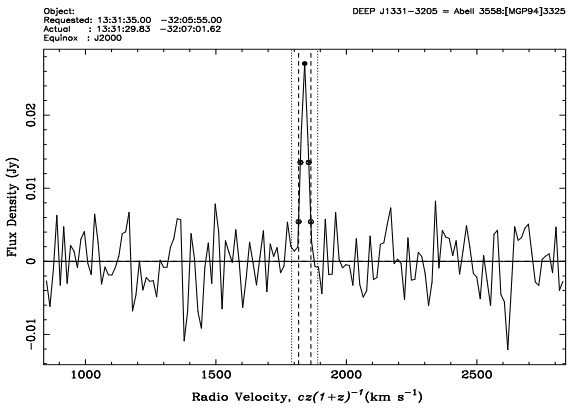

Abell 3558:[MGP94]3325

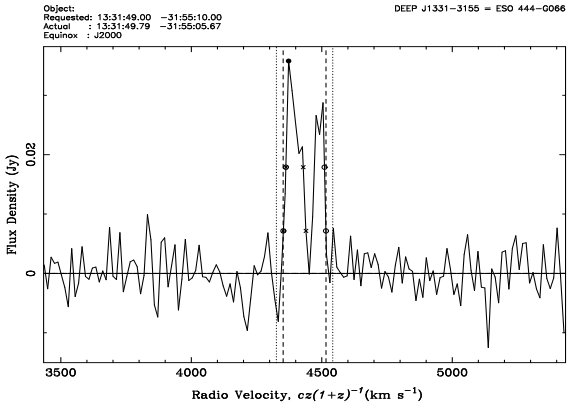

ESO 444-G066

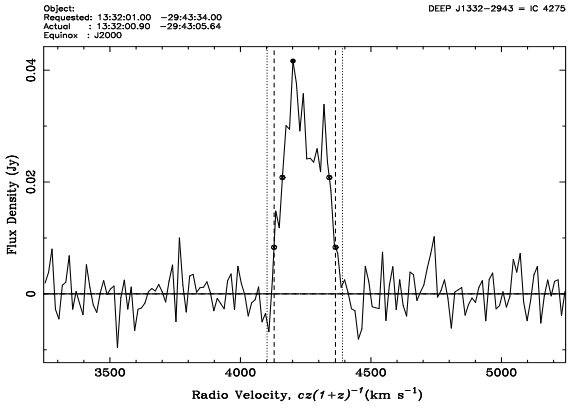

IC 4275

Figure 2.16: Spectra from the DEEP survey. Data above the spectra are output from *mbspect* – source name, requested position (fitted position of source), actual position of spectra (nearest pixel centre), and equinox of position (J2000). Dashed lines indicate areas removed from baseline fitting, while the dotted lines indicate the area used for fitting source parameters. Solid dots indicate the peak of the spectrum and the 50% and 20% points used to calculated ΔV_{50} and ΔV_{20}.

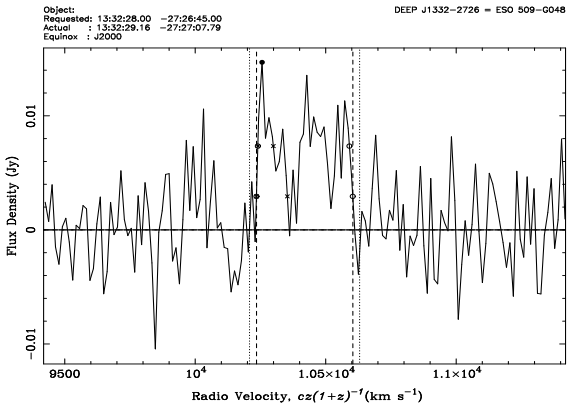

ESO 509-G048

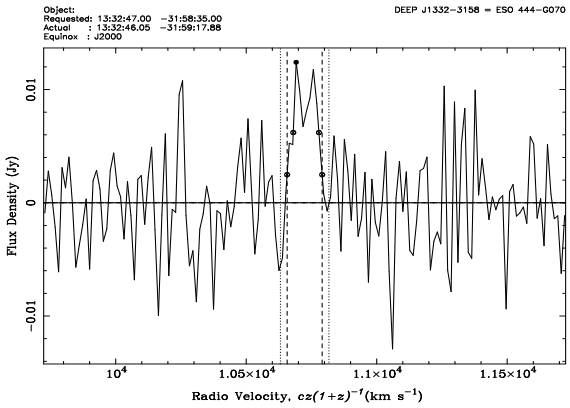

ESO 444-G070

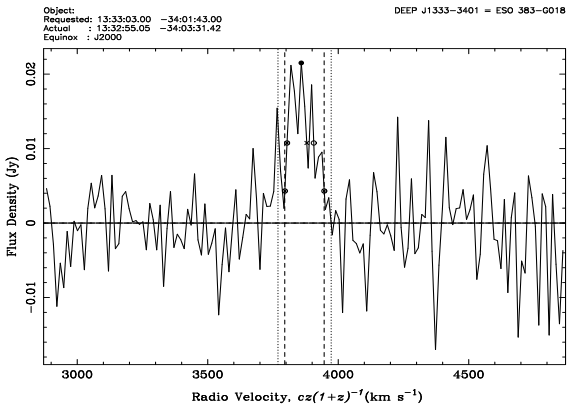

ESO 383-G018

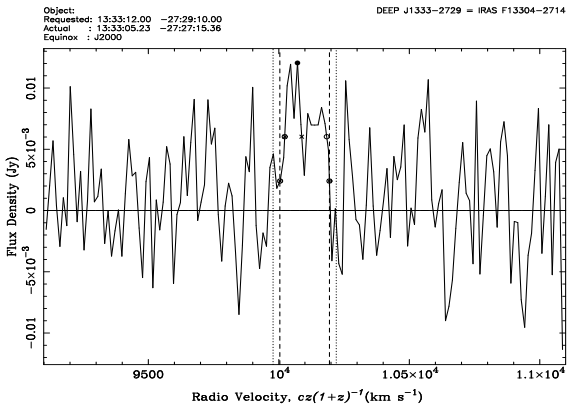

IRAS F13304-2714

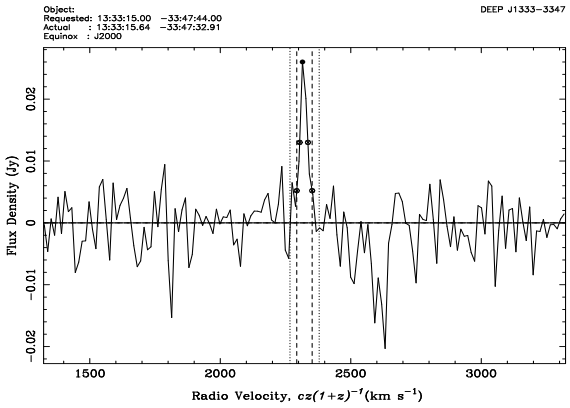

DEEP J1333-3347

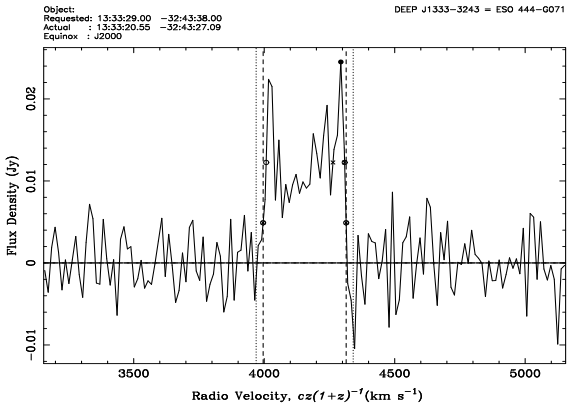

ESO 444-G071

Figure 2.16: Spectra from the DEEP survey (continued)

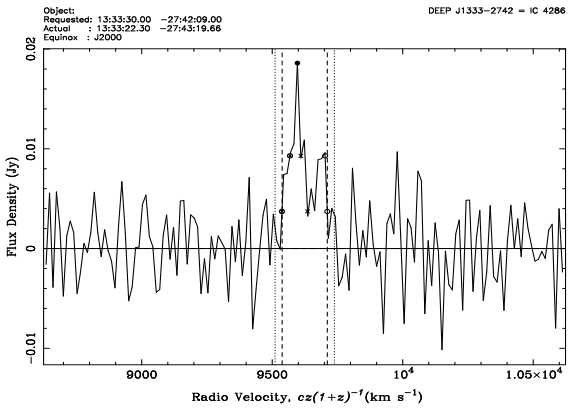

IC 4286

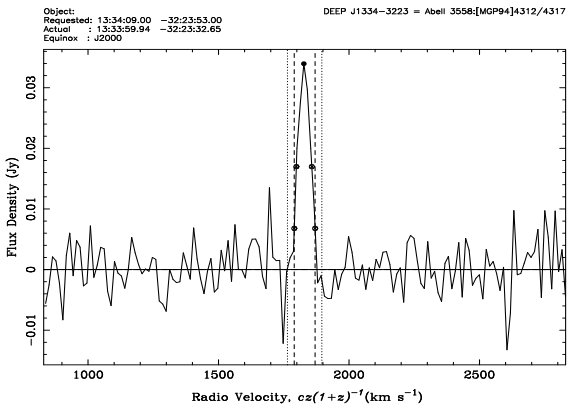

Abell 3558:[MGP94]4312/4317

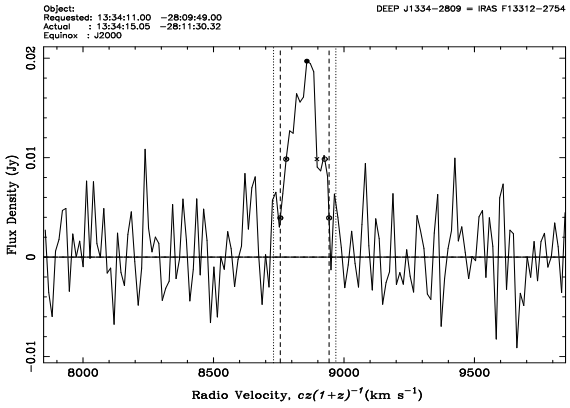

IRAS F13312-2754

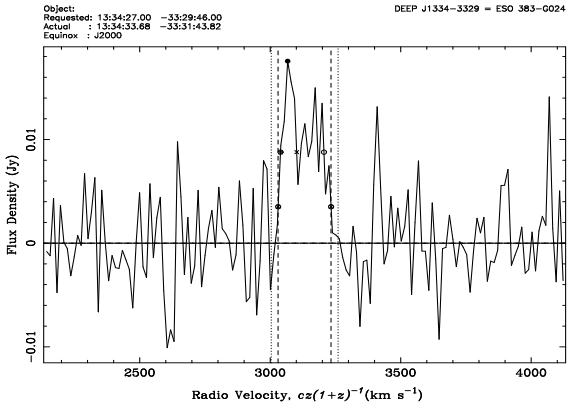

ESO 383-G024

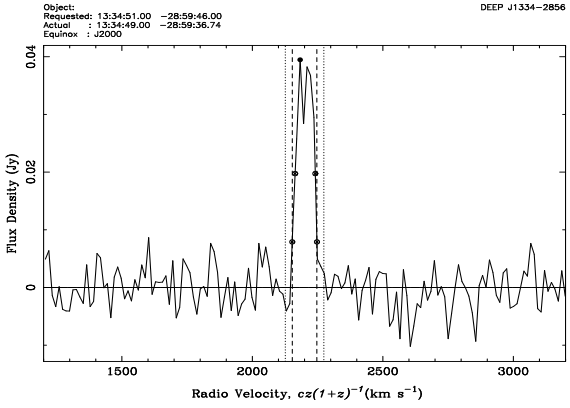

DEEP J1334-2859

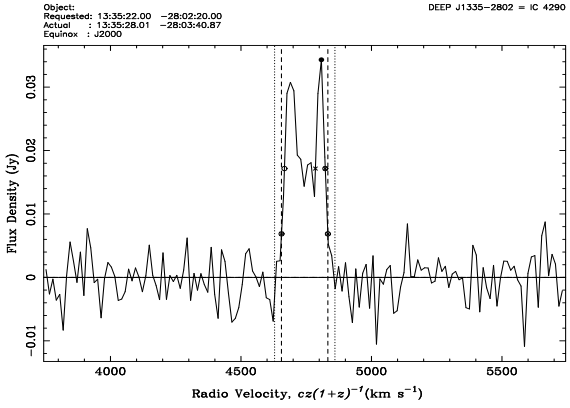

IC 4290

Figure 2.16: Spectra from the DEEP survey (continued)

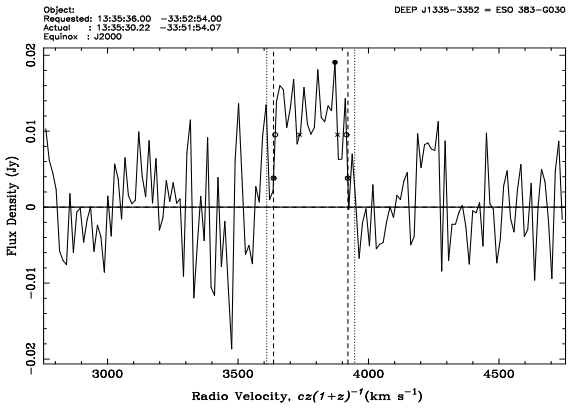

ESO 383-G030

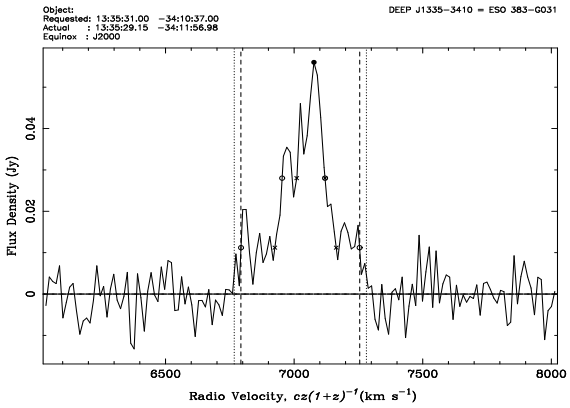

ESO 383-G031

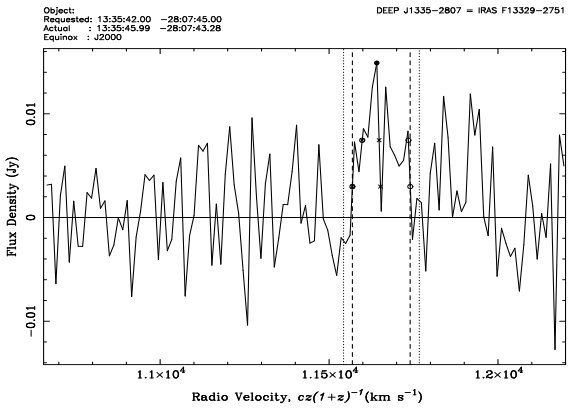

IRAS F13329-2751

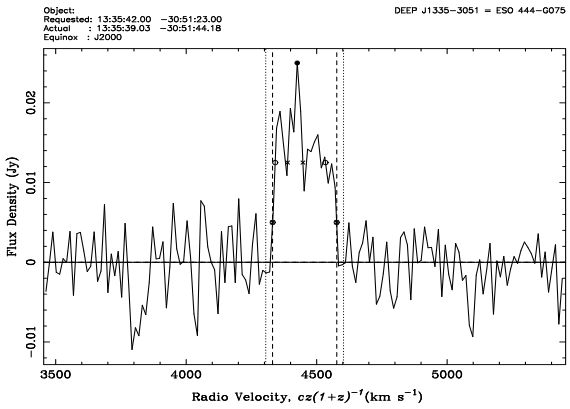

ESO 444-G075

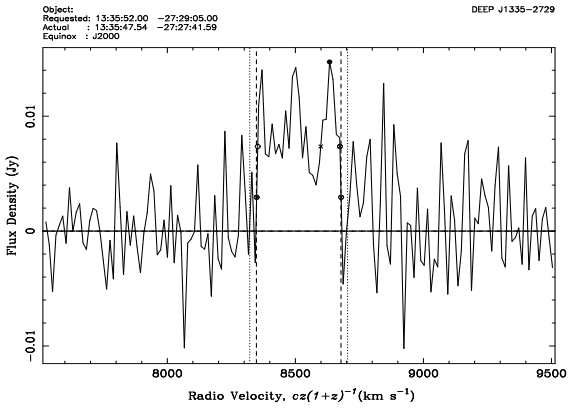

DEEP J1335-2729

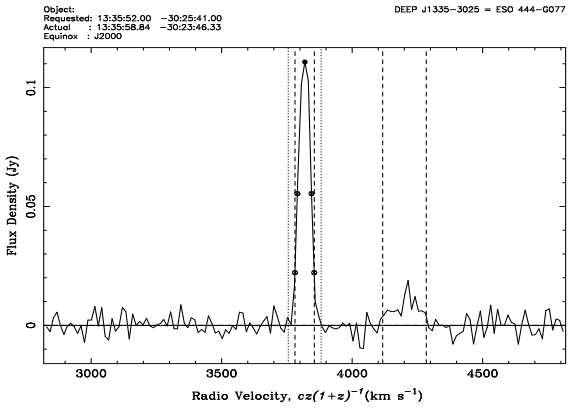

ESO 444-G077

Figure 2.16: Spectra from the DEEP survey (continued)

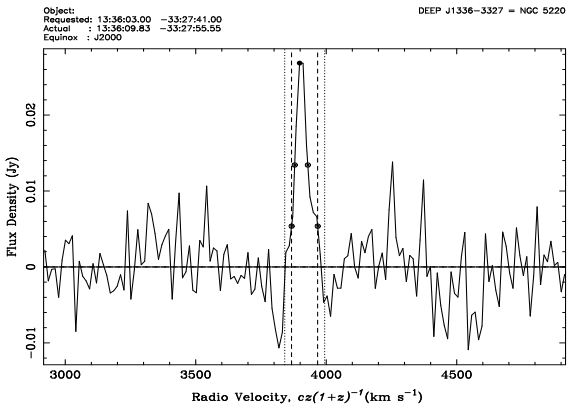

NGC 5220

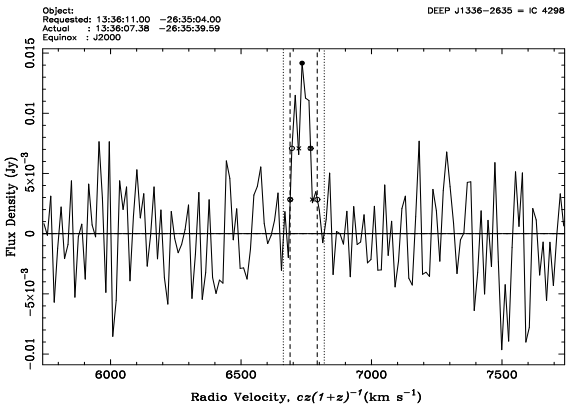

IC 4298

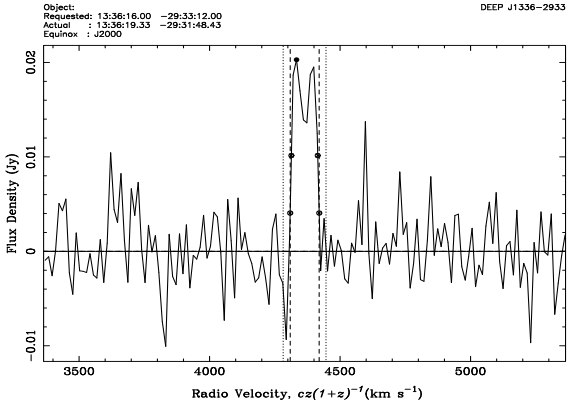

DEEP J1336-2933

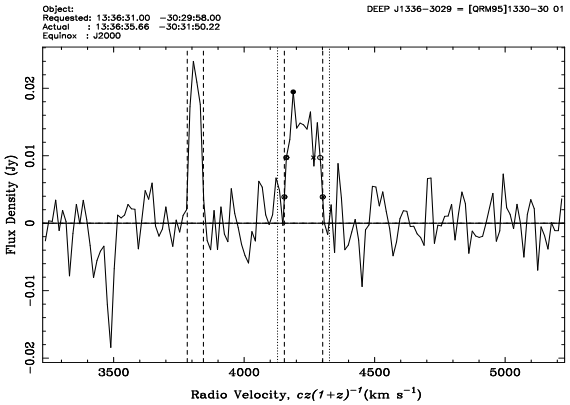

[QRM95]1330-30 01

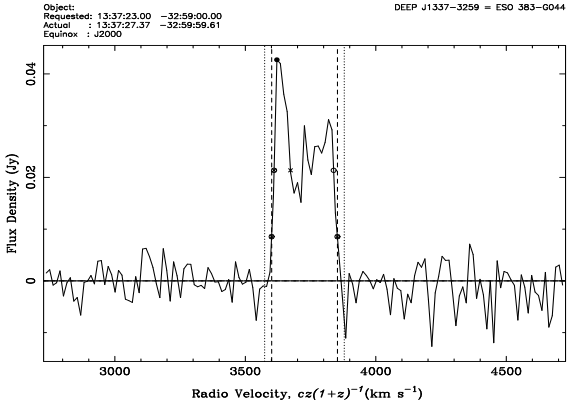

ESO 383-G044

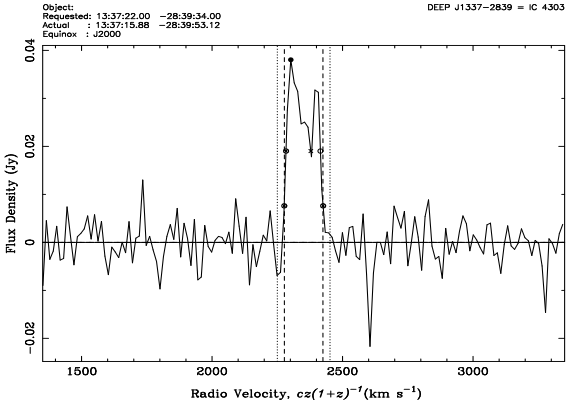

IC 4303

Figure 2.16: Spectra from the DEEP survey (continued)

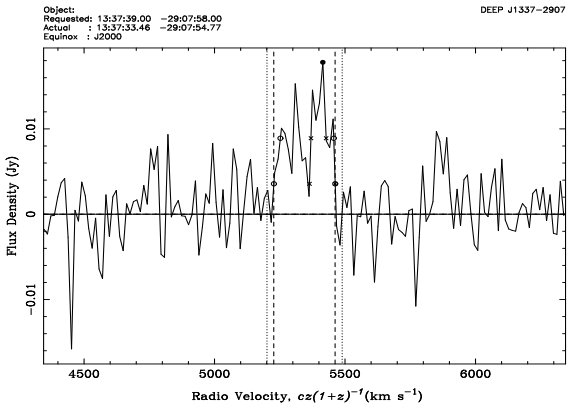

DEEP J1337-2907

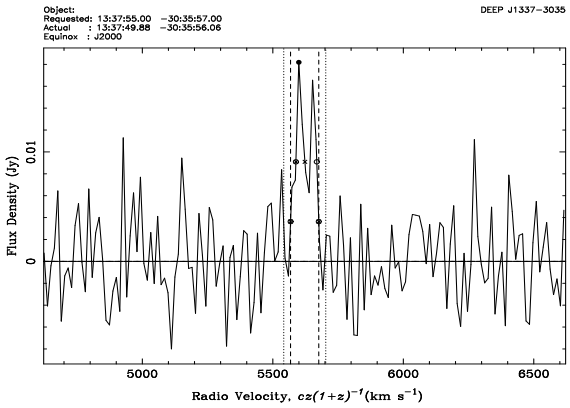

DEEP J1337-3035

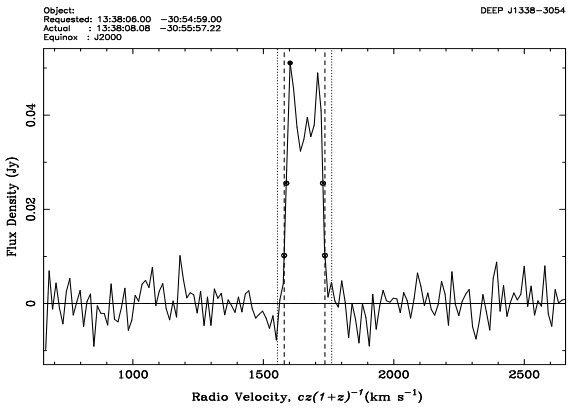

DEEP J1338-3054

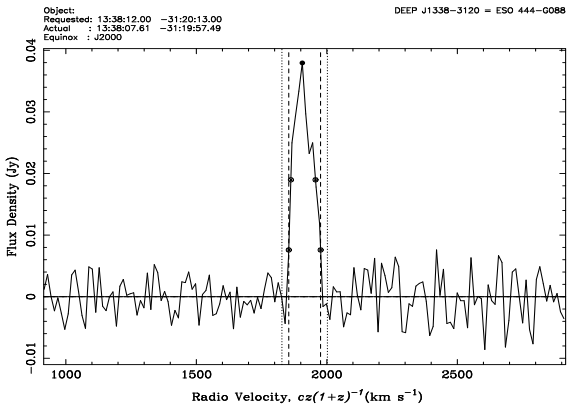

ESO 444-G088

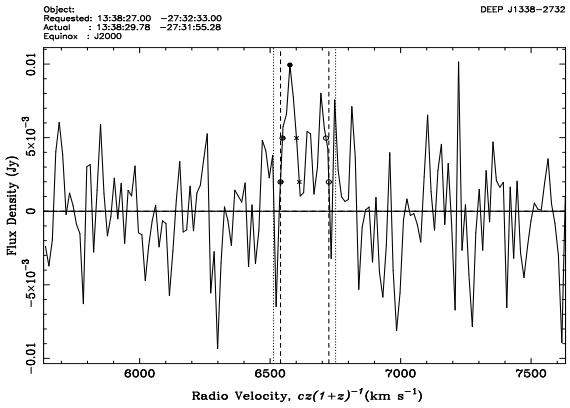

DEEP J1338-2732

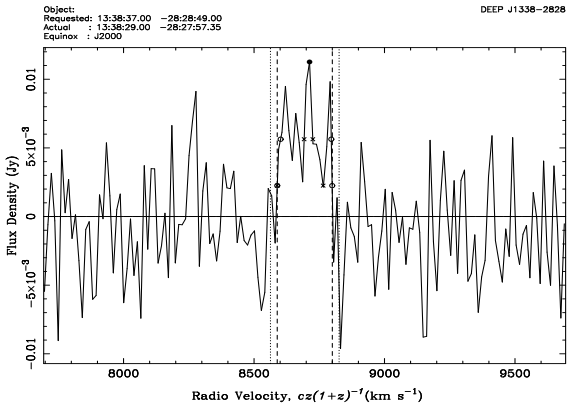

DEEP J1338-2828

Figure 2.16: Spectra from the DEEP survey (continued)

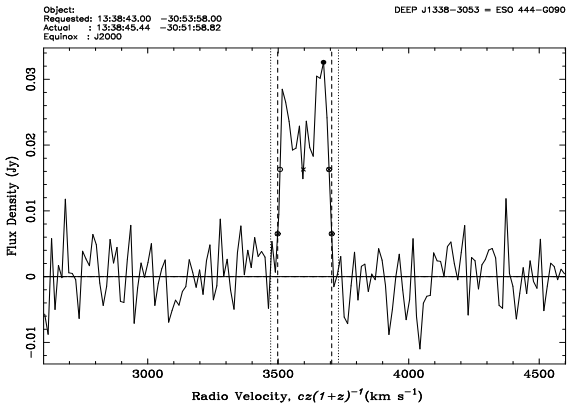

ESO 444-G090

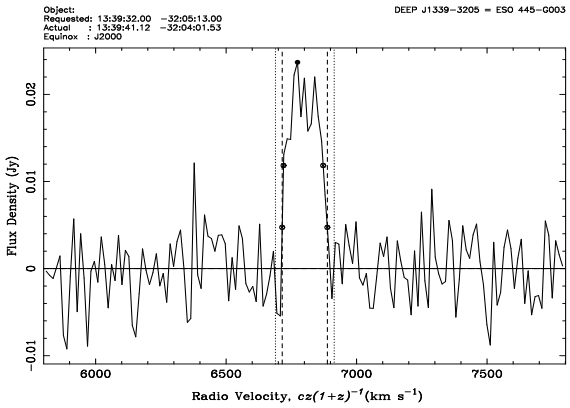

DEEP J1339-3021

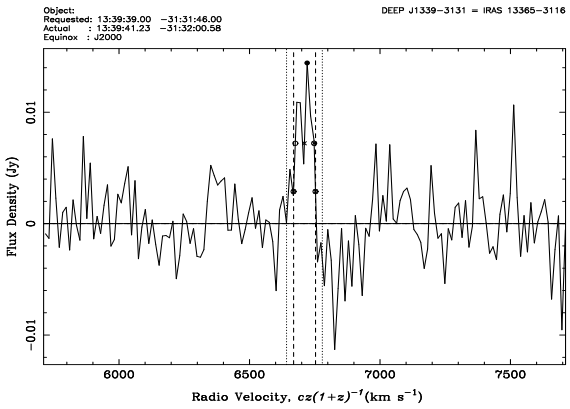

IRAS 13365-3116

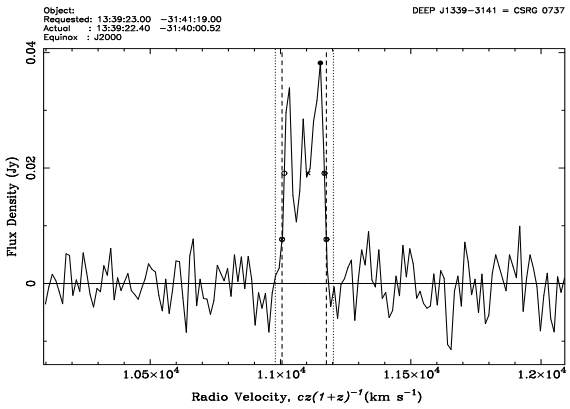

CSRG 0737

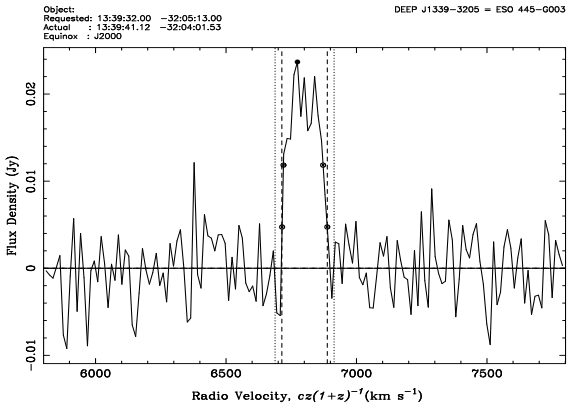

ESO 444-G003

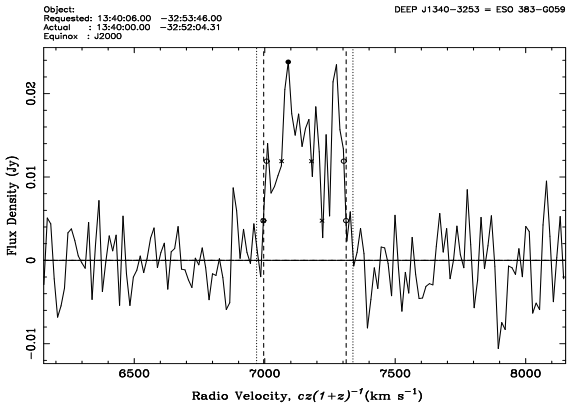

ESO 383-G059

Figure 2.16: Spectra from the DEEP survey (continued)

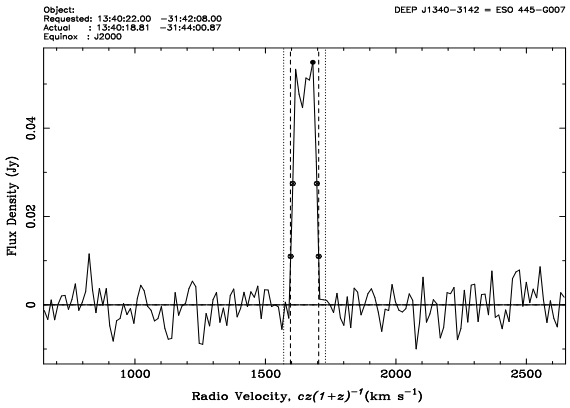

ESO 445-G007

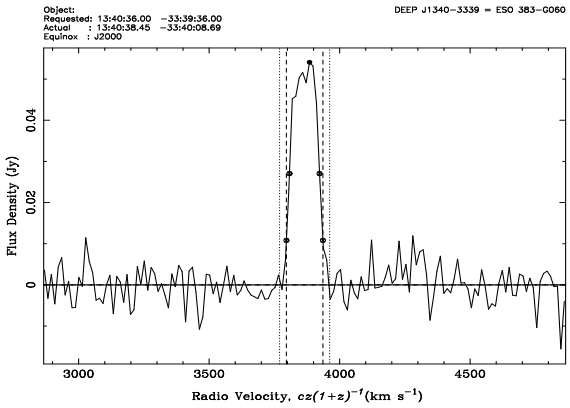

ESO 383-G060

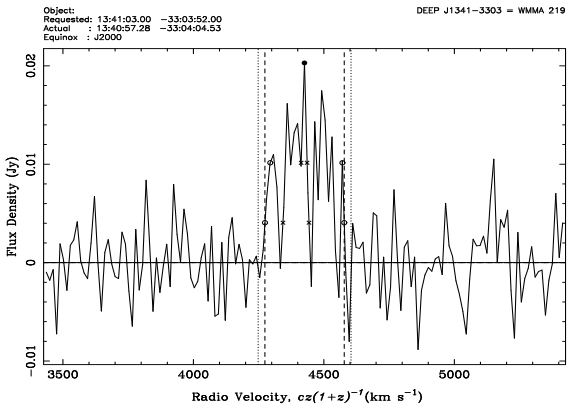

WMMA 219

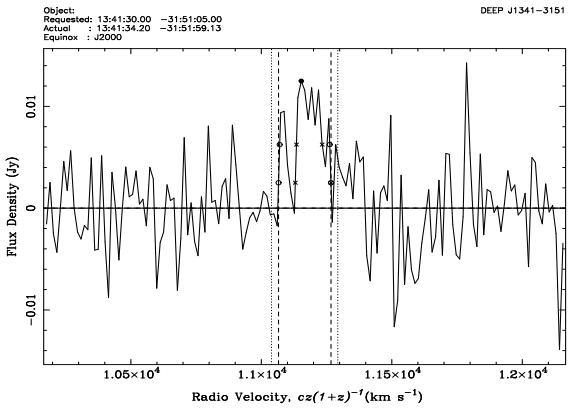

DEEP J1341-3151

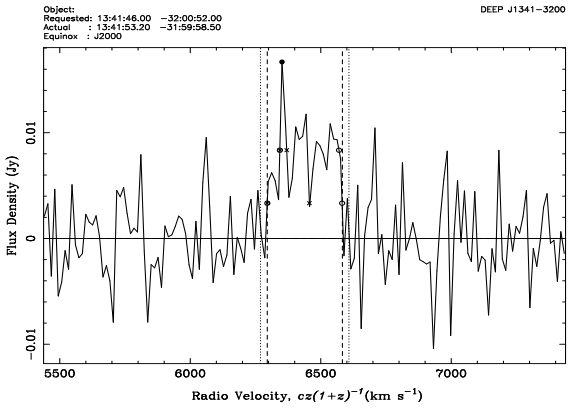

ESO 445-G011

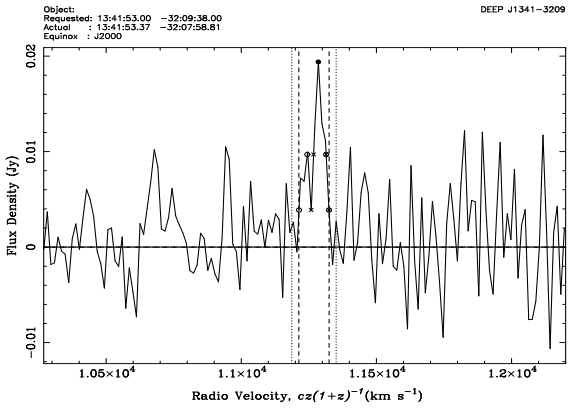

DEEP J1341-3209

Figure 2.16: Spectra from the DEEP survey (continued)

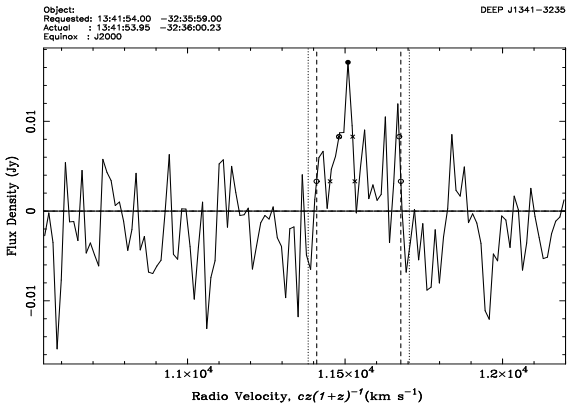

DEEP J1341-3235

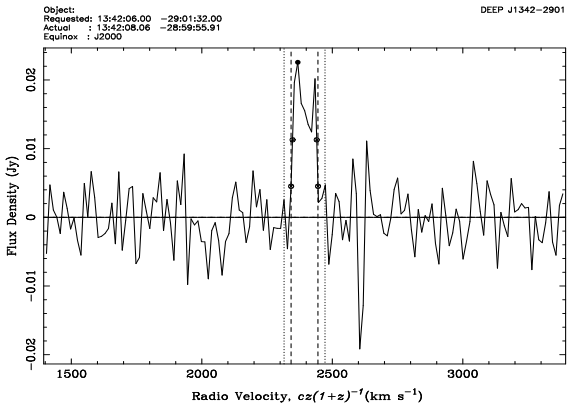

DEEP J1342-2901

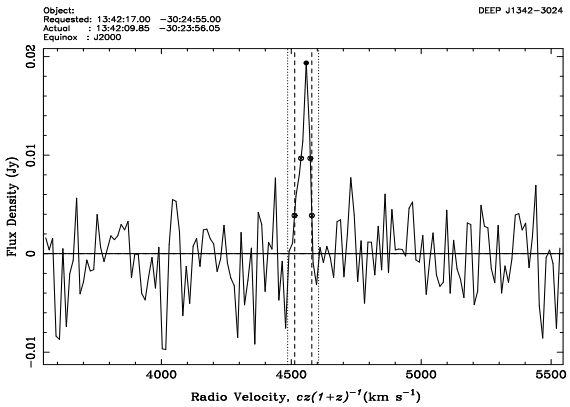

DEEP J1342-3024

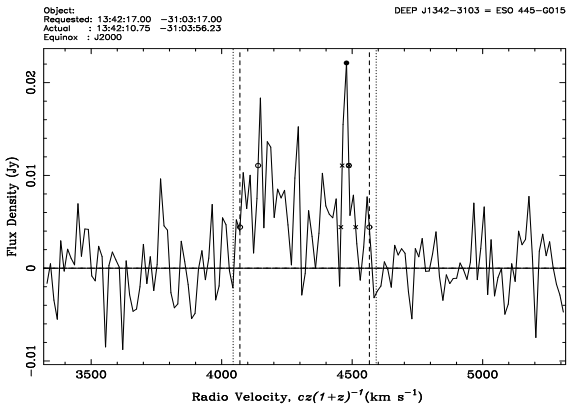

ESO 445-G015

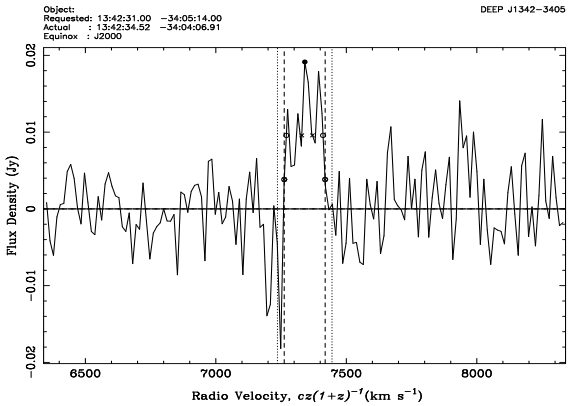

DEEP J1342-3405

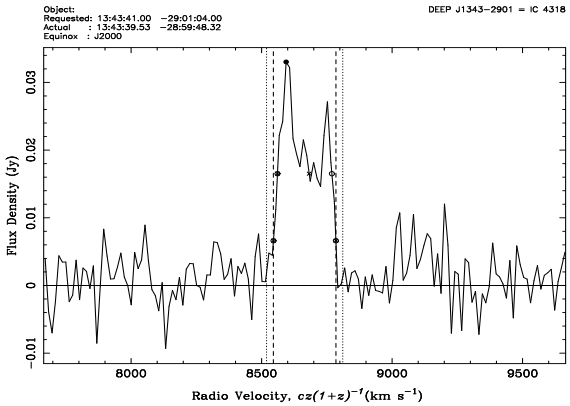

IC 4318

Figure 2.16: Spectra from the DEEP survey (continued)

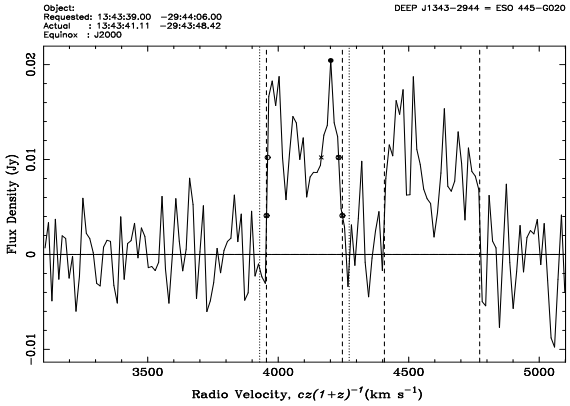

ESO 445-G020

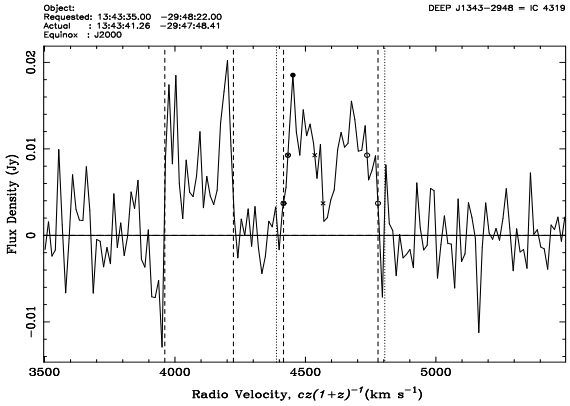

IC 4319

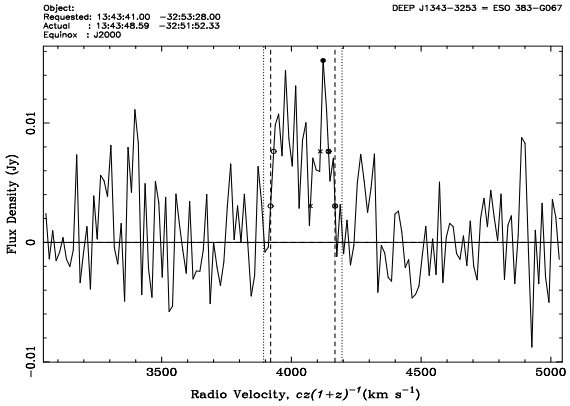

ESO 383-G067

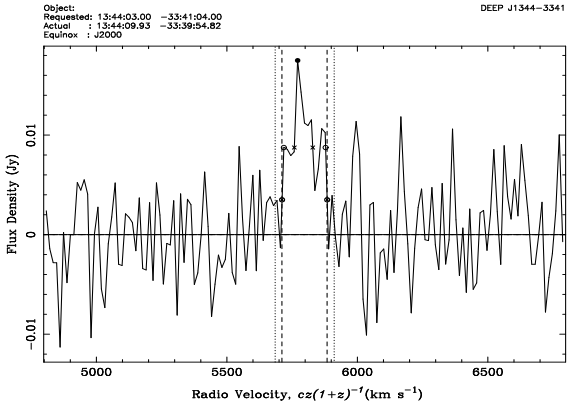

DEEP J1344-3341

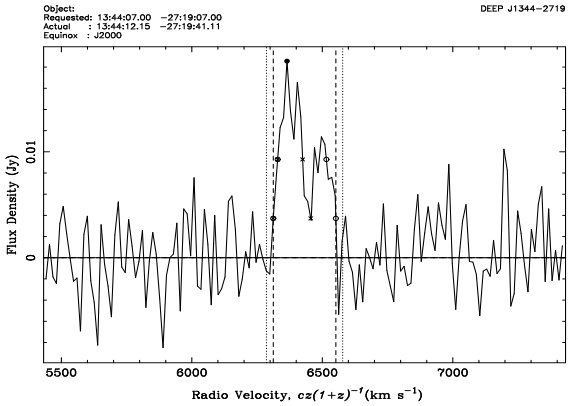

ESO 509-G100

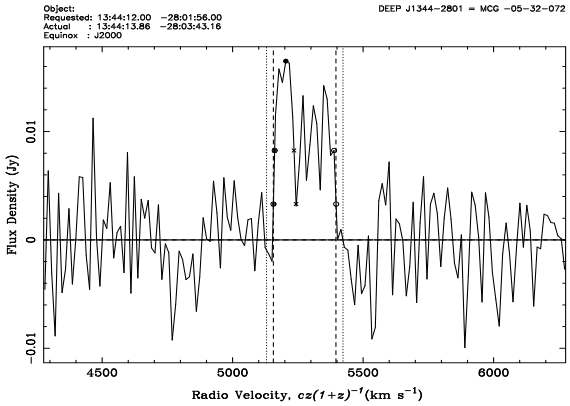

MGC -05-31-072

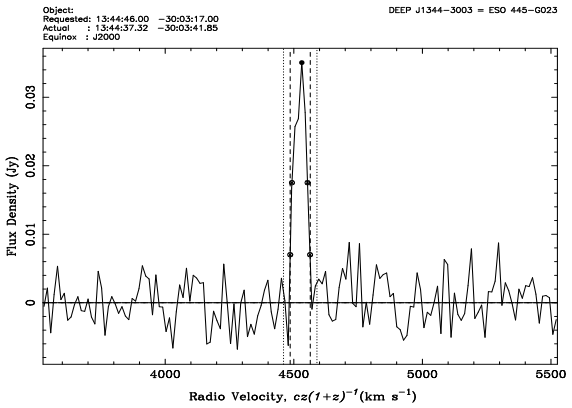

ESO 445-G023

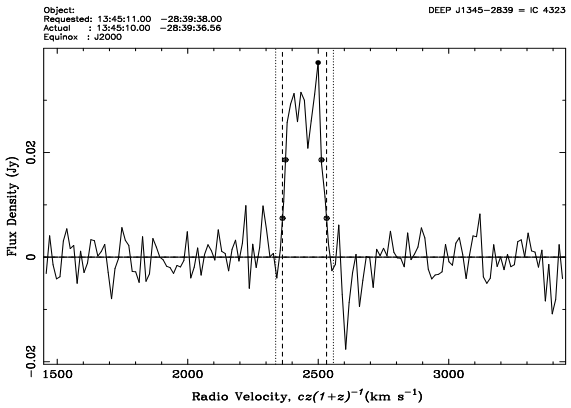

IC 4323

Figure 2.16: Spectra from the DEEP survey (continued)

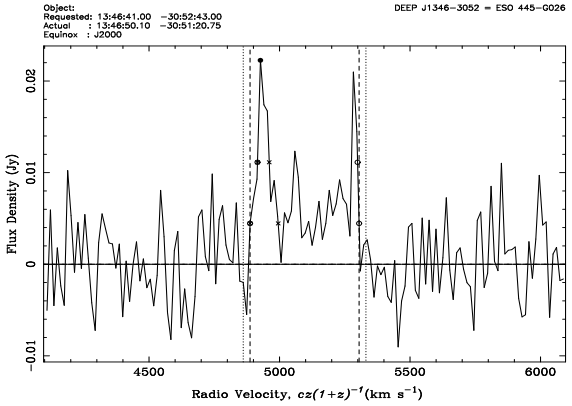

ESO 445-G026

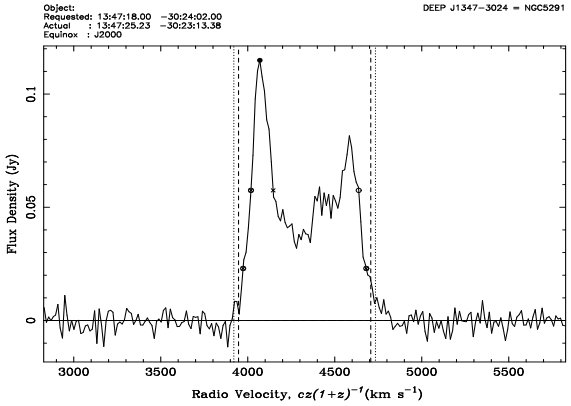

NGC 5291

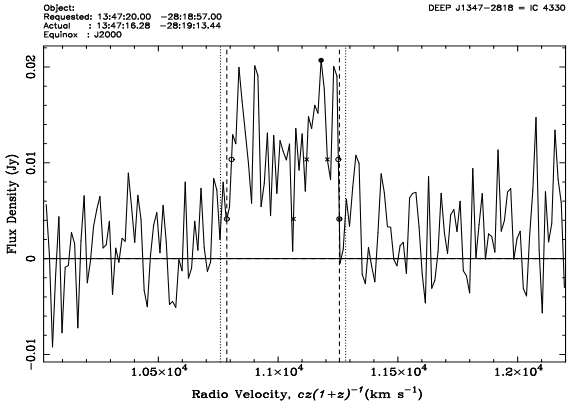

IC 4330

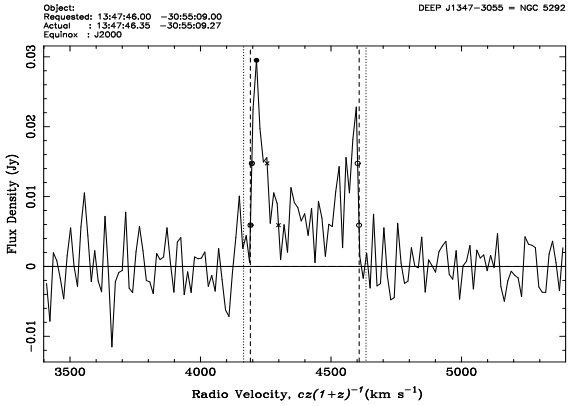

NGC 5292

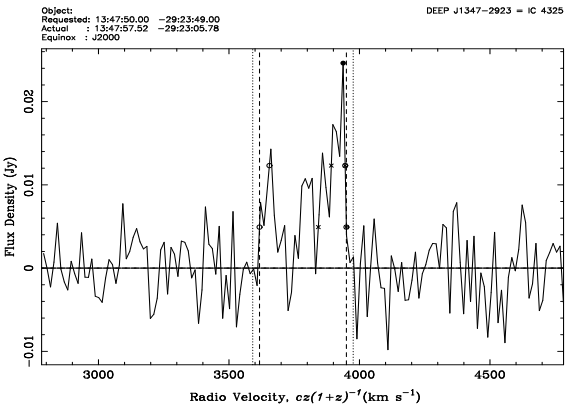

IC 4325

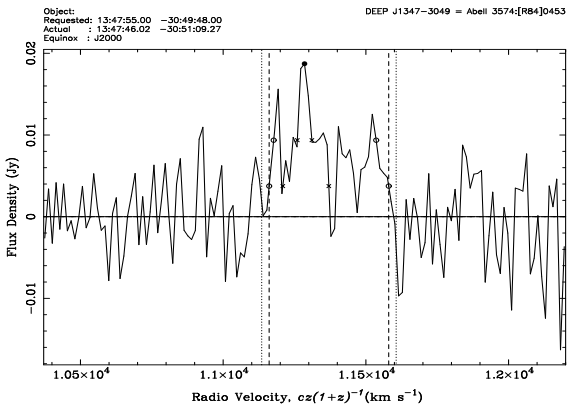

Abell 3574[R84]0453

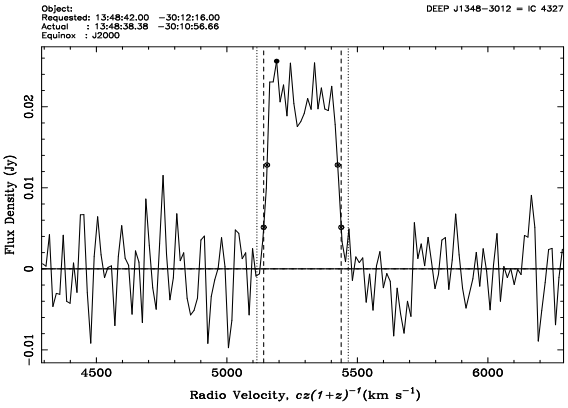

IC 4327

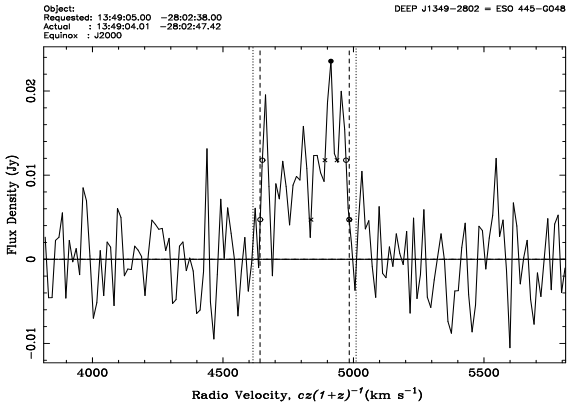

ESO 445-G048

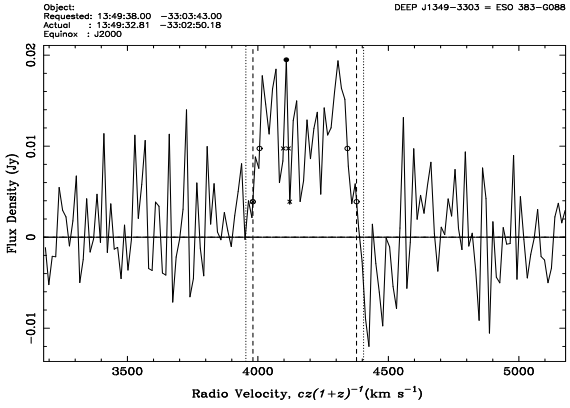

ESO 383-G088

Figure 2.16: Spectra from the DEEP survey (continued)

Chapter 3

Optical Data

3.1 Summary of chapter 3

Deep R-band tech pan images have been obtained of a large part of the survey area. Section 3.2 describes the reduction and analysis of this data and Section 3.3 describes the properties of the optical sample. Section 3.4 gives details of correlations between the optical properties of the samples, and Section 3.5 presents properties of DEEP galaxies from the literature and compares these to their optical and HI properties.

3.2 Reduction and Analysis

Optical observations of the DEEP survey region were made by Quentin Parker of the UK Schmidt Telescope (UKST). Eight R-band tech pan plates, each of 60 minutes integration time, were taken at the UKST and were stacked, digitised, and linearised using the SuperCOSMOS machine at Royal Observatory, Edinburgh. The tech pan plates cover an area of $6^\circ \times 6^\circ$, and therefore provide R-band information for 24 square degrees of the $4^\circ \times 8^\circ$ DEEP HI region. The tech pan data was calibrated by Peter J. Boyce of the University of Bristol using the magnitudes of unsaturated ESO-LV galaxies within the region.

Total magnitudes and optical positions for the programme galaxies were found using SExtractor (Bertin & Arnouts 1996). This supplies three alternative measures of the magnitude: mag_{iso}, mag_{isocor}, and mag_{auto}. These are found using neural networks, mag_{iso} being an isophotal magnitude at (for these plates) the 26.5

R mag arcsec^{-2} isophote, mag_{isocor} is a total magnitude found using a correction to mag_{iso} and mag_{auto} is an automated Kron magnitude. The neural network selects the best estimate of the total magnitude and calls this mag_{best}, this value (which was the same as mag_{isocor} for all the galaxies in DEEP) has been used as the measure of apparent magnitude for this project, however all three magnitudes normally agreed to well within the accuracy of the photometry. In order to get an estimate of the surface-brightness, surface photometry was performed using the *ellipse* task within IRAF and the radial profiles from this were used to determine the effective radius of the galaxies, the semi-major axis of the ellipse enclosing half the light of the galaxy, and the surface-brightness at this radius, the effective surface-brightness.

3.3 The Optical Sample

There are 56 DEEP sources within the tech pan area, of which 54 have been identified with a unique optical counterpart. One source (DEEP J1334-3223) is close to both Abell 3558:[MGP94]4312 and Abell 3558:[MGP94]4317, which are very nearly overlapping optically. It is not yet known which of these is the correct optical counterpart. One source (DEEP J1338-2828) is close to a number of small optical sources and, as it is at a distance of around 120 Mpc, it seems probable that this is a previously uncatalogued group and that the HI detected is from a number of different members of this group. The two brightest members of this group have been analysed here.

Of the 56 sources, 13 are previously uncatalogued objects. ESO 509-G100 has been analysed as the optical counterpart to DEEP J1335-2729, despite it having an incorrect optical redshift, as there is no other obvious counterpart in the field. A further ten are not included in the ESO-LV catalogue and, of those that are in the ESO-LV, two are too faint to have measured values of R_T (apparent R-band total magnitude). This leaves 30 galaxies with previously determined magnitudes from the ESO-LV as a comparison sample (see Section 3.5).

By comparing the literature values for R_T with the measured values of R-band magnitude (m_R), it was determined that the statistical error on m_R is approximately 0.21 magnitudes. This is too large to be due to the error on the ESO-LV measurements of R_T, which have a statistical error of 0.09 magnitudes. NGC 5292 appears to be badly affected by saturation on the tech pan plates as m_R for this galaxy is over a magnitude fainter than R_T from the ESO-LV, therefore it was excluded from the fit. The comparison between m_R and R_T can be seen in Figure 3.9 in Section 3.5.

3.3.1 Optical Properties

The optical properties of the DEEP galaxies in the tech pan area are given in Table 3.1. Columns 1 and 2 of this table give the DEEP programme ID and the catalogue ID (if previously catalogued), as in Table 2.1 for the HI properties. Columns 3 and 4 give the optical positions of the counterparts. Column 5 gives the magnitude (m_R) as measured by SExtractor (see Section 3.2) while columns 6 and 7 give the effective radius (r_{eff}), enclosing half the light of the galaxy, and the effective surface-brightness (μ_{eff} – the surface-brightness at this radius). Columns 8 gives the ellipticity ($\epsilon = 1 - \frac{b}{a}$) as measured by SExtractor and column 9 gives the R-band absorption due to dust in our galaxy from Schlegel et al. (1998), supplied by NED. Columns 10 and 11 give the absolute magnitude (M_R), including the correction for absorption from column 10 and the cosmological $(1+z)^2$ dimming, and the physical effective radius (R_{eff}), calculated from m_R and r_{eff} using the distances given in Table 2.1 and reproduced in column 12. Column 13 gives the effective surface-brightness μ_{eff}(c), corrected for cosmological $(1+z)^4$ dimming, absorption (column 19) and inclination.

3.4 Correlations in the optical data

The effective surface-brightness must be corrected for galactic absorption, for cosmological dimming ($(1+z)^4$), and for inclination. In principle a correction should also be made to account for the different portion of the galaxies spectrum that falls within the filter width at different redshifts, however this 'k-correction' is negligible over the redshift range of the DEEP sources. The galactic absorption has been found from Schlegel et al. (1998) using the tool provided by NED, cosmological dimming has been calculated using the velocities from the HI data, and the inclination correction was calculated using $2.5 \times C \times \log(a/b)$, where C is a band-dependent constant taken to be 0.5 for R-band (as in Graham & de Blok (2001) and Tully & Verheijen (1997)) and a/b is the axis ratio of the galaxy, found by SExtractor. Both the observed μ_{eff} and the corrected μ_{eff}(c) are given in Table 3.1. The uncorrected value is used for comparison with other observed properties, but the corrected value is used for comparison with absolute properties. The mean corrections across the sample are -0.15 ± 0.02 mags for galactic absorption, -0.17 ± 0.09 mags for cosmological dimming and 0.29 ± 0.24 mags for inclination correction, this gives a total correction of -0.03 ± 0.28. On average, therefore, the surface-brightness of the galaxies is slightly increased by these corrections, but the overall increase is negligible compared to the scatter in the correction – which is mainly due to the scatter in the

Table 3.1: Optical Properties of DEEP sources

ID	Catalogue Name	α_{J2000} h m s	δ_{J2000} ° ′ ″	m_R	r_{eff} ″	μ_{eff} Rμ	ϵ	A_R	M_R	R_{eff} kpc	D Mpc	μ_{eff}(c) Rμ
1	2	3	4	5	6	7	8	9	10	11	12	13
DEEP J1330-3212	ESO 444-G059	13 30 30	-32 12 26.7	16.77	12.12	25.12	0.110	0.136	-17.16	3.29	56	24.93
DEEP J1331-3205	Abell 3558:[MGP94]3325	13 31 31	-32 06 17.1	16.86	6.56	23.91	0.349	0.134	-15.54	0.89	28	23.96
DEEP J1331-3155	ESO 444-G066	13 31 51	-31 55 15.4	14.93	11.64	23.73	0.088	0.145	-19.31	3.61	64	23.51
DEEP J1332-2943	IC 4275	13 31 51	-29 43 55	13.13	11.36	21.25	0.388	0.152	-21.02	3.36	61	21.24
DEEP J1332-2726	ESO 509-G048	13 32 34	-27 26 55.0	14.00	9.30	22.46	0.399	0.169	-22.17	6.67	148	22.26
DEEP J1332-3158	ESO 444-G070	13 32 47	-31 57 59.0	14.02	8.40	21.87	0.200	0.144	-22.19	6.19	152	21.53
DEEP J1333-2729	IRAS F13304-2714	13 33 15	-27 30 09.7	16.34	4.46	22.88	0.345	0.175	-19.76	3.09	143	22.64
DEEP J1333-3243	ESO 444-G071	13 33 30	-32 43 12.9	13.42	15.89	21.61	0.675	0.153	-20.68	4.622	60	21.95
DEEP J1333-2742	IC 4286	13 33 36	-27 37 52.8	15.03	5.20	21.93	0.109	0.170	-20.95	3.43	136	21.54
DEEP J1334-3223A[1]	Abell 3558:[MGP94]4312	13 34 04	-32 22 01.0	15.71	4.19	21.69	0.486	0.149	-16.71	0.57	28	21.85
DEEP J1334-3223B[1]	Abell 3558:[MGP94]4317	13 34 04	-32 21 37.0	16.44	12.66	24.14	0.596	0.149	-15.97	1.72	28	24.43
DEEP J1334-2809	IRAS F13312-2754	13 34 05	-28 09 31.6	14.79	6.95	21.60	0.366	0.170	-20.99	4.21	125	21.42
DEEP J1334-2859		13 34 53	-29 00 08.2	15.12	9.41	22.78	0.174	0.146	-17.64	1.51	33	22.67
DEEP J1335-2802	IC 4290	13 35 20	-28 01 18.0	13.39	13.46	21.96	0.340	0.196	-21.04	4.44	68	21.85
DEEP J1335-2807	IRAS F13329-2751	13 35 48	-28 06 41.5	14.30	5.49	21.36	0.299	0.192	-22.16	4.39	165	21.02
DEEP J1335-3051	ESO 444-G075	13 35 47	-30 52 35.0	13.36	17.82	21.98	0.562	0.139	-20.88	5.53	64	22.16
DEEP J1335-2729	ESO 509-G075[2]	13 35 46	-27 29 21.6	13.61	6.45	20.74	0.161	0.162	-22.09	3.78	121	20.43
DEEP J1335-3025	ESO 444-G077	13 35 52	-30 25 48.4	15.25	12.12	23.96	0.285	0.125	-18.63	3.23	55	23.91
DEEP J1336-2933		13 36 08	-29 34 12.0	17.23	6.69	24.51	0.258	0.123	-16.95	2.04	63	24.42
DEEP J1336-3029	[QRM95]1330-30 01	13 36 37	-30 29 39	14.90	7.10	22.65	0.287	0.127	-19.22	5.79	61	22.58
DEEP J1337-2839	IC 4303	13 37 18	-28 39 28.3	14.63	8.26	22.35	0.350	0.162	-18.29	1.40	35	22.35
DEEP J1337-2907		13 37 40	-29 07 58.0	15.03	7.96	22.08	0.548	0.155	-19.60	2.93	76	22.20
DEEP J1337-3035		13 37 57	-30 35 10.9	17.20	5.84	24.60	0.103	0.131	-17.53	2.27	80	24.36
DEEP J1338-3054		13 38 08	-30 55 06.7	14.77	5.76	21.99	0.331	0.192	-17.52	0.73	26	21.97
DEEP J1338-3120	ESO 444-G088	13 38 20	-31 18 29.1	15.55	12.88	24.26	0.359	0.151	-16.94	1.81	29	24.30

Table 3.1: Optical Properties of DEEP sources (continued)

ID	Catalogue Name	α_{J2000} h m s	δ_{J2000} ° ′ ″	m_R	r_{eff} ″	μ_{eff} Rμ	ϵ	A_R	M_R	R_{eff} kpc	D Mpc	μ_{eff}(c) Rμ
1	2	3	4	5	6	7	8	9	10	11	12	13
DEEP J1338-2732		13 38 30	-27 32 08.9	15.96	6.00	23.31	0.097	0.193	-19.20	2.73	94	22.98
DEEP J1338-2828A[3]		13 38 32	-28 28 08.2	16.67	3.34	22.70	0.240	0.148	-19.06	1.99	123	22.45
DEEP J1338-2828B[3]		13 38 38	-28 27 57.4	17.19	3.40	23.14	0.069	0.148	-18.54	2.03	123	22.78
DEEP J1338-3053	ESO 444-G090	13 38 39	-30 53 30.3	15.22	11.41	23.19	0.716	0.147	-18.56	2.88	52	23.62
DEEP J1339-3021		13 39 08	-30 22 09.7	16.64	8.85	24.38	0.098	0.142	-17.57	2.70	63	24.16
DEEP J1339-3131	IRAS 13365-3116	13 39 22	-31 31 53.6	14.02	7.82	21.54	0.088	0.154	-21.12	3.60	95	21.24
DEEP J1339-3141	CSRG 0737	13 39 21	-31 40 39.2	13.87	6.92	21.62	0.057	0.144	-22.42	5.27	157	21.18
DEEP J1339-3205	ESO 445-G003	13 39 33	-32 06 15.0	14.88	10.50	22.99	0.209	0.134	-20.26	4.89	96	22.78
DEEP J1340-3253	ESO 383-G059	13 40 03	-32 53 47.3	15.44	15.10	22.99	0.834	0.111	-19.79	7.39	101	23.64
DEEP J1340-3142	ESO 445-G007	13 40 22	-31 41 58.1	16.45	16.57	24.72	0.586	0.148	-15.79	2.09	26	25.00
DEEP J1341-3151		13 41 36	-31 52 46.8	15.31	6.69	22.43	0.219	0.143	-20.99	5.13	158	22.09
DEEP J1341-3200	ESO 445-G011	13 41 27	-32 00 08.9	13.83	10.46	21.58	0.393	0.135	-21.20	4.62	91	21.53
DEEP J1341-3209		13 41 31	-32 11 00.4	15.37	7.47	23.16	0.067	0.143	-20.96	5.79	160	22.72
DEEP J1341-3235		13 41 52	-32 34 40.2	15.03	8.67	22.42	0.306	0.137	-21.34	6.85	163	22.14
DEEP J1342-2901		13 42 05	-29 01 20.5	17.40	8.90	24.56	0.674	0.151	-15.56	1.55	36	24.95
DEEP J1342-3024		13 42 21	-30 23 13.9	17.75	6.47	24.93	0.272	0.059	-16.44	2.04	65	24.91
DEEP J1342-3104	ESO 445-G015	13 42 15	-31 02 14.1	13.35	11.22	21.65	0.574	0.159	-20.83	3.37	62	21.83
DEEP J1343-2901	IC 4318	13 43 23	-28 58 05.4	13.44	10.15	21.87	0.234	0.148	-22.26	6.00	122	21.61
DEEP J1343-2944	ESO 445-G020	13 43 49	-29 44 40.3	14.66	13.92	22.53	0.776	0.150	-19.40	3.98	59	23.07
DEEP J1343-2948	IC 4319	13 43 27	-29 48 11.8	12.78	18.09	21.53	0.608	0.156	-21.54	5.79	66	21.75
DEEP J1343-3253	ESO 383-G067	13 43 39	-32 55 03.7	14.55	11.07	22.18	0.745	0.137	-19.47	3.11	58	22.67
DEEP J1344-2719	ESO 509-G100	13 43 51	-27 21 43.2	14.10	10.04	22.57	0.564	0.162	-20.96	4.43	91	22.67
DEEP J1344-2801	MCG -05-32-072	13 44 09	-28 01 24.8	13.80	8.78	21.68	0.213	0.190	-20.85	3.19	75	21.47
DEEP J1344-3003	ESO 445-G023	13 44 44	-30 03 28.6	15.00	11.55	23.44	0.104	0.152	-19.28	3.64	65	23.22
DEEP J1345-2839	IC 4323	13 45 07	-28 39 04.3	14.97	12.18	22.54	0.757	0.145	-18.05	2.19	37	23.09

Table 3.1: Optical Properties of DEEP sources (continued)

ID	Catalogue Name	α_{J2000} h m s	δ_{J2000} ° ′ ″	m_R	r_{eff} ″	μ_{eff} Rμ	ϵ	A_R	M_R	R_{eff} kpc	D Mpc	μ_{eff}(c) Rμ
1	2	3	4	5	6	7	8	9	10	11	12	13
DEEP J1346-3052	ESO 445-G026	13 46 33	-30 52 44.5	14.01	11.72	22.46	0.826	0.144	-20.49	4.09	72	23.12
DEEP J1347-3024	NGC 5291	13 47 24	-30 24 26.6	12.45	12.12	20.78	0.314	0.172	-21.75	3.64	62	20.69
DEEP J1347-2818	IC 4330	13 47 15	-28 19 54.3	13.41	15.96	21.95	0.533	0.162	-22.89	12.07	156	21.88
DEEP J1347-3055	NGC 5292	13 47 40	-30 56 22.0	12.26	11.77	20.69	0.265	0.158	-21.92	3.54	62	20.57
DEEP J1347-2923	IC 4325	13 47 40	-29 26 03.7	13.40	13.44	21.64	0.569	0.155	-20.55	3.65	56	21.83
DEEP J1347-3049	Abell 3574:[R84]0453	13 48 03	-30 47 02.3	14.46	6.17	21.73	0.445	0.152	-21.89	4.82	161	21.56
DEEP J1348-3012	IC 4327	13 48 44	-30 13 04.2	13.63	12.54	21.96	0.495	.0178	-21.00	4.56	75	22.00
DEEP J1349-2802	ESO 445-G048	13 49 07	-28 00 15.9	14.82	12.83	23.59	0.327	0.153	-19.59	4.29	69	23.51

[1] DEEP J1332-3223 has two possible counterparts separated by about 30″on the plates.

[2] ESO 509-G075 has an optical velocity twice the HI velocity of the source, but is the only obvious counterpart in the field.

[3] DEEP J1338-2828 is believed to be a group of galaxies. The two brightest members of the group are given here as optical counterparts.

inclination.

Figure 3.1 shows the distribution of surface-brightnesses and how this is changed by the corrections for absorption and cosmological dimming. It can be seen that the sample spans 5 magnitudes in surface-brightness, with most galaxies found being in the bin $21.5 \leq \mu_{eff} < 22$, both before and after the corrections are applied. This peak near the Freeman-law value is not present after volume-corrections have been carried out and is due to a correlation between $M_{\rm HI}$ and μ_{eff} (see Section 4.2). This correlation and the volume-corrections necessary to reconstruct the true surface-brightness distribution (SBD) are investigated further in Chapter 4.

Figure 3.2 shows the number of galaxies found in each apparent magnitude bin (panel (a)) and each absolute magnitude bin (panel (b)). It can be seen that both are fairly peaked distributions, with a peak at $14 \leq m_R < 15$ in apparent magnitude and at $-21 < M_R \leq -20$ in absolute magnitude. The distribution in absolute magnitude is wider than that in apparent magnitude and covers 8 magnitude bins. This is equivalent to 3.2 dex, and is also wider than the 2.75 dex width of the $M_{\rm HI}$ distribution (see Chapter 2), indicating that there is a wide range of values for $M_{\rm HI}/L_R$.

Figure 3.3 compares the apparent and absolute magnitude. Panel (a) shows that these are related – the apparently bright galaxies are also those which are actually bright. This may be thought to be quite worrying, as there would not normally be a relationship between apparent and absolute magnitude. However, panel (b) shows the distribution of distance moduli which illustrates why the apparent and absolute magnitudes are linked for this sample. The distance moduli are distributed as -34.32 ± 1.17, a very narrow distribution due to the small range of redshifts covered by the survey. As this is narrower than the range of apparent magnitudes covered, this leads to a relationship between apparent and absolute magnitude with the same size scatter. This result would not be expected in a flux-limited, optically-selected survey where bright galaxies would be detected much further out.

Figure 3.4 shows the distribution of galaxies by apparent and absolute effective radius. Most of the galaxies can be seen to fall in a range of apparent sizes (panel (a)) between $5''$ and $14''$, around a factor 3 wide. Within this range the distribution is fairly even with no one size dominating. The distribution of absolute sizes (panel (b)) is quite different – there is a strong peak centered in the 3 – 4 kpc bin which dominates the distribution. This implies that most galaxies in the DEEP sample have similar optical sizes – over two thirds of the galaxies have radii between 2 and 5 kpc, a similar fraction to that covering $6'$ to $13'$ in apparent size.

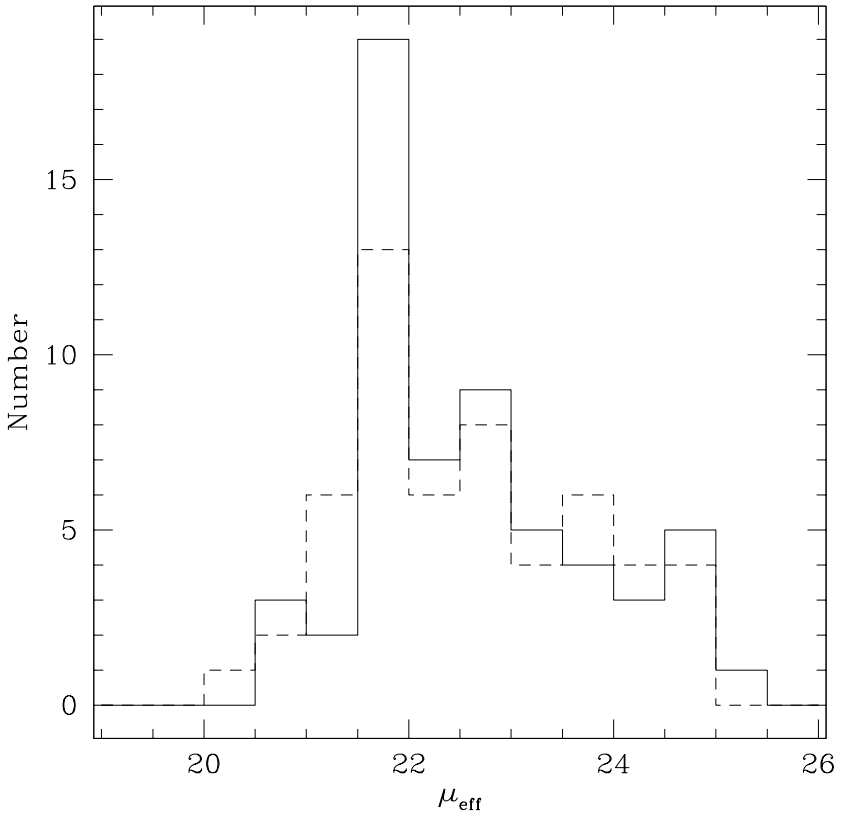

Figure 3.1: Number of galaxies found in each surface-brightness bin. The solid line shows the distribution of observed surface-brightness, the dashed line shows the distribution of surface-brightness corrected for galactic absorption, cosmological dimming, and inclination. It can be seen that the correction has the effect of slightly flattening out the distribution, although it is still quite strongly peaked in the bin $21.5 \leq \mu_{eff} < 22$.

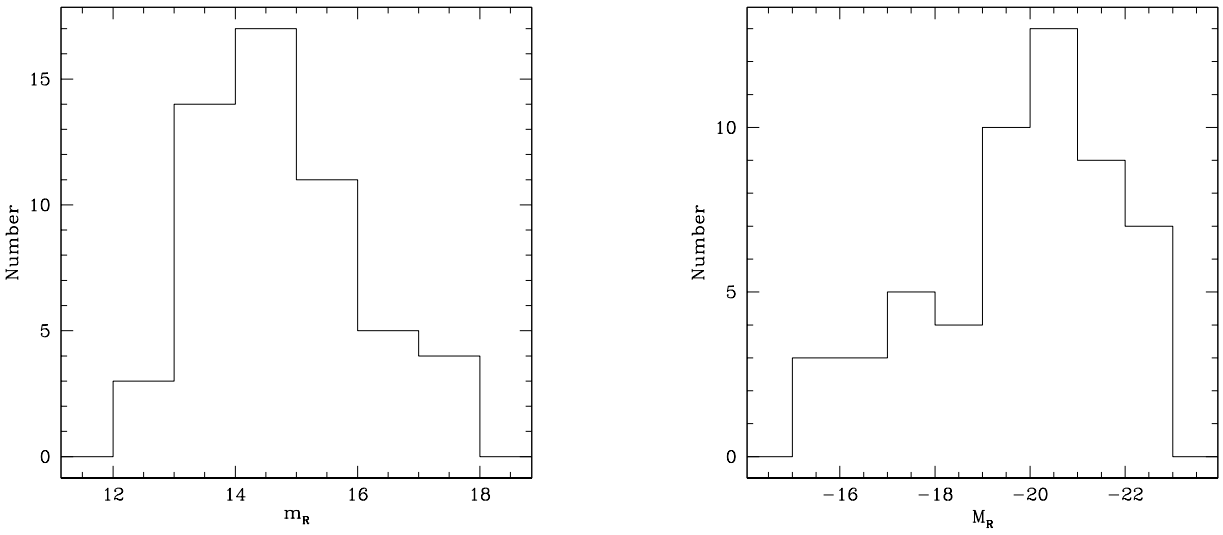

(a) Number of galaxies per apparent magnitude bin

(b) Number of galaxies per absolute magnitude bin

Figure 3.2: Number of galaxies in apparent and absolute magnitude bins. It can be seen that both distributions are fairly peaked, with a maximum in the bin $14 \leq m_R < 15$ for apparent magnitude (panel a) and in the bin $-21 < M_R \leq -20$ for absolute magnitude.

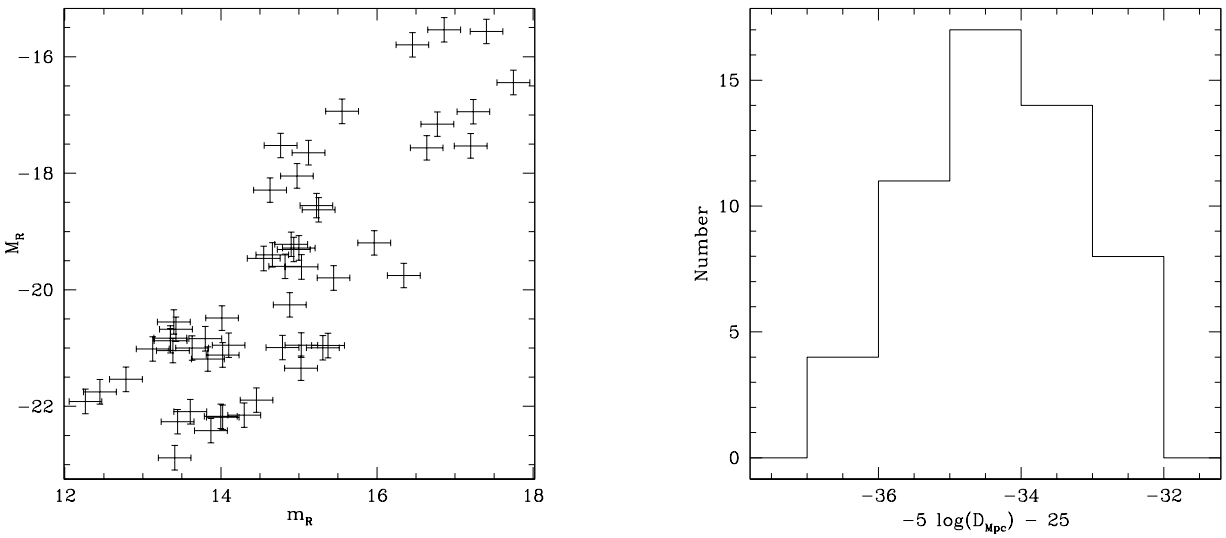

(a) Apparent magnitude versus absolute magnitude

(b) Distribution of distance moduli

Figure 3.3: Comparison between apparent and absolute magnitude of the DEEP sources. Panel (a) shows that apparent and absolute magnitude appear to be correlated, the reason for this correlation is shown in panel (b) – the DEEP survey covers only a small range of redshifts. This results in the range of distance moduli being smaller than the range or apparent magnitudes covered, so a correlation is seen between apparent and absolute magnitude with the same scatter as the distribution of distance moduli.

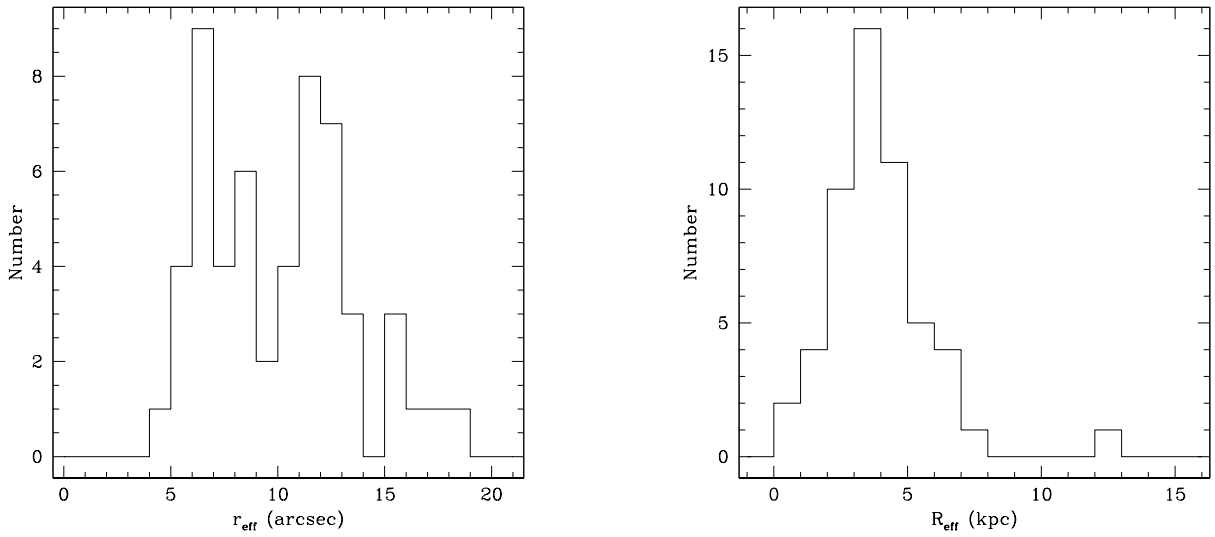

(a) Number of galaxies per arcsecond bin of apparent effective radius

(b) Number of galaxies per kiloparsec bin of absolute effective radius

Figure 3.4: Number of galaxies found in each bin of apparent and absolute effective radius. It can be seen that these are both fairly narrow distributions, the distribution of absolute effective radii is strongly peaked, while the distribution of apparent effective radii is considerably flatter. Most galaxies in DEEP appear to have similar optical sizes, with over two thirds of galaxies having absolute effective radii between 2 and 5 kpc.

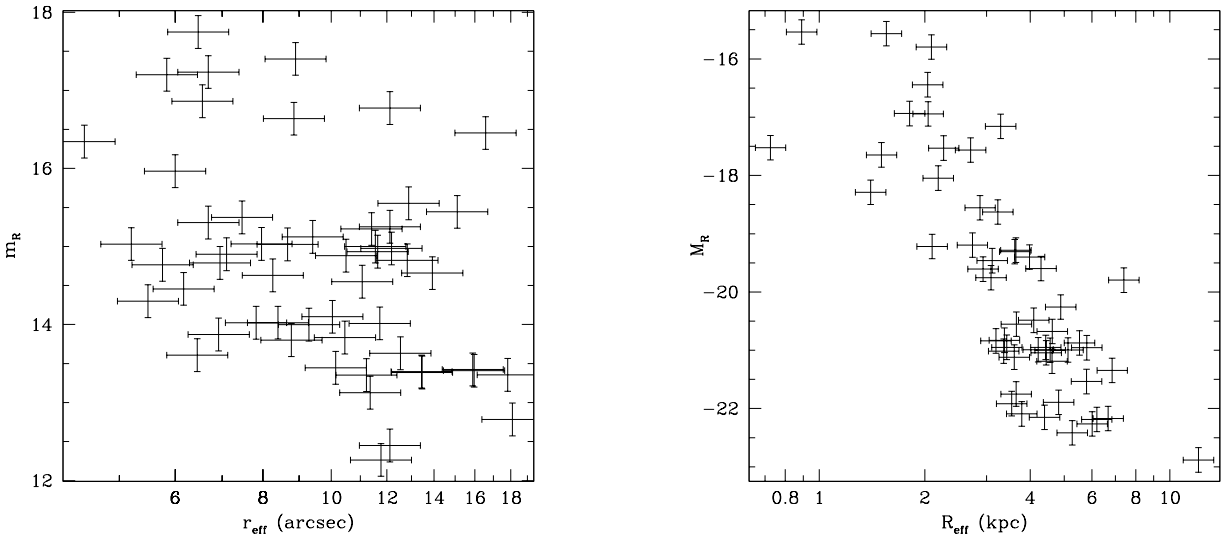

(a) Apparent magnitude versus apparent effective radius

(b) Absolute magnitude versus absolute effective radius

Figure 3.5: Comparison between effective radius and magnitude. It can be seen in panel (a) that there is little or no correlation between apparent effective radius and apparent magnitude. This implies that there is no preferred surface-brightness in DEEP. As $l \propto \Sigma r^2$, if Σ (the surface-brightness in intensity units) is constant then $l \propto r^2$, giving $m \propto -5 \log r$ which is not seen here. The weak relationship seen in panel (b) is expected as both quantities here are distance dependent, even so the relationship is not particularly strong.

Figure 3.5 examines these distributions in terms of apparent and absolute magnitude. It can be seen that there is no correlation between apparent effective radius and apparent magnitude (panel a). As no relationship is seen, it seems unlikely that there is a physical link between size and luminosity – implying that there is not a single preferred surface-brightness. Panel (b) shows the expected relationship between absolute effective radius and absolute magnitude. As both these quantities are distance-dependent, it would be surprising if they were not related. Even so, the relationship is not particularly strong, probably due to the wide range of surface-brightnesses found in DEEP.

Figure 3.6 shows the variation of apparent and absolute effective radii with effective surface-brightness. It can be seen that there is no relationship between apparent effective radius and effective surface-brightness (panel (a)). Panel (b) shows that there does not appear to be a particularly strong relationship between absolute effective radius and surface-brightness. From the relationship between M_R and $\mu_{eff}(c)$ seen in Figure 3.8 a relationship is expected between $\log R_{eff}$ and $\mu_{eff}(c)$ with a slope of -10.6. This is shown in the figure by a dashed line and can be seen to be consistent with the data – the full range of surface-brightnesses in DEEP is covered by a small range (about a factor 3 wide) in radius.

Figure 3.7 shows an interesting and unexpected correlation between apparent magnitude and effective surface-brightness. The line shows the best fit of $\mu_{eff} = (0.78 \pm 0.06)m_R + (11.1 \pm 0.8)$, which has a scatter of half a magnitude. This is too narrow for it to be explained by any relationship between μ_{eff} and M_R, as even a precise relationship would be expected to pick up a scatter of ~ 1.2 mags from the width of the distribution of distance moduli.

It is possible that this relationship could arise from a combination of observational selection and physical properties – if galaxies of a narrow range of flux are selected (as they are bound to be in a mainly flux-limited sample such as this), and the mean HI column densities of all these galaxies fall within a narrow range, then the HI sizes of these galaxies would also fall in a narrow range. If HI size is linked to optical size, as seems likely and has been found by Cayette et al. (1994) and Salpeter & Hoffman (1996), then this will lead to all the galaxies having similar optical sizes (as seen in Figure 3.4). This would lead to a 1:1 relationship between apparent magnitude and effective surface-brightness, slightly steeper than that observed. This could be due to the ratio of HI optical size increasing towards lower surface-brightnesses, which would not be unexpected as the mass to light ratio, $M_{\rm HI}/L_B$, increases towards lower surface-brightnesses (see Chapter 4).

Low column-density galaxies would be expected to occupy the top-left corner of this graph, and high column-density galaxies the bottom-right corner. If the hypothesis proposed to explain this relationship

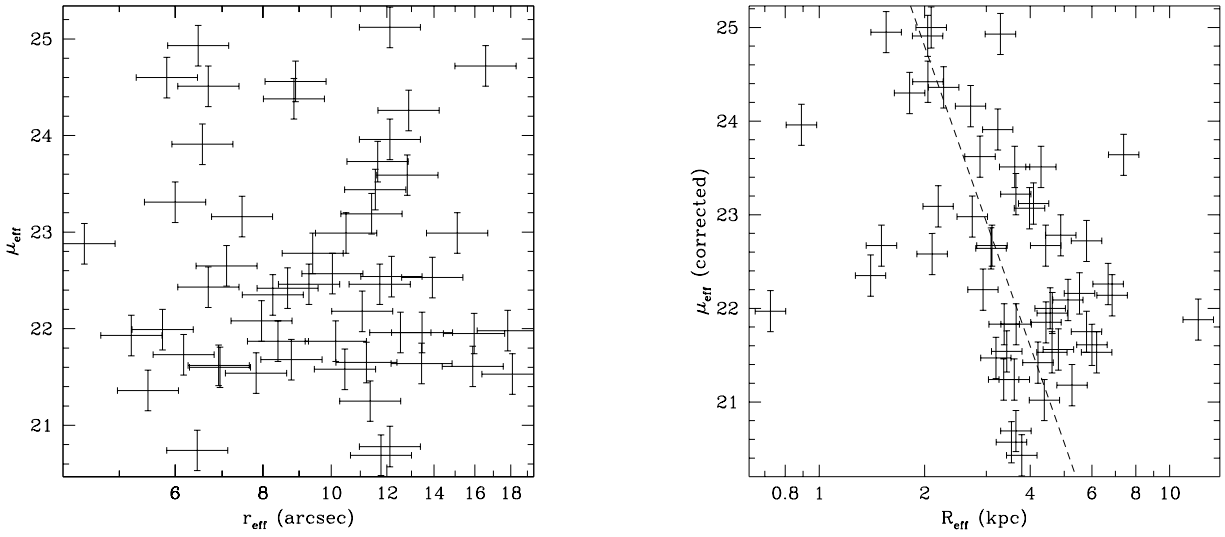

(a) Apparent effective radius versus effective surface-brightness

(b) Absolute effective radius versus effective surface-brightness

Figure 3.6: Variation of apparent and absolute effective radius with surface-brightness. There is no relationship seen in panel (a) between apparent effective radius and the uncorrected surface-brightness. This implies the relationship seen in Figure 3.7 between apparent magnitude and surface-brightness – as there is only a small range of angular sizes across the whole spread of surface-brightness (equivalent to $\simeq 1.2$ mags) the higher surface-brightness galaxies have higher apparent luminosities. Panel (b) shows a possible weak relationship between absolute effective radius and the corrected effective surface-brightness, although this is very nearly swamped by the scatter. The dashed line does not show the best-fit, bur rather the slope implied by the relationship seen between M_R and $\mu_{eff}(c)$ (Figure 3.8).

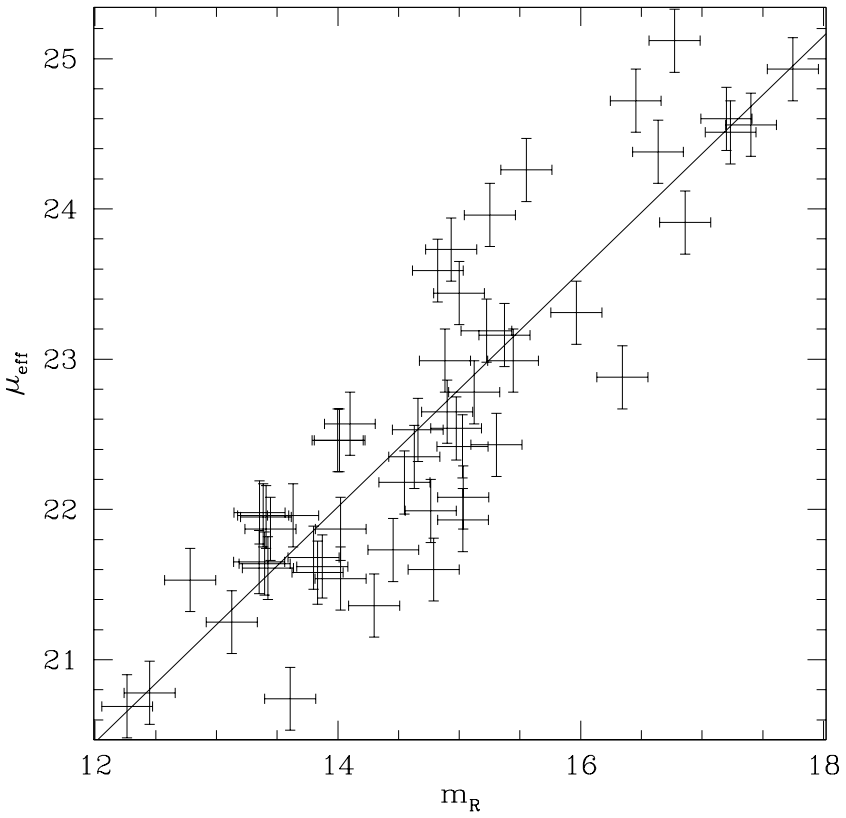

Figure 3.7: Correlation between apparent magnitude and effective surface-brightness. This interesting and unexpected correlation can be explained as being due to a near-constant HI surface-density and a near constant ratio of HI size to optical size.

is indeed true, this implies that galaxies with high or low mean column-densities do not exist or are not observed. For high column-density galaxies this is not unexpected as the mean column-density will always be lower than the peak. For low column-density galaxies, however, there is no reason why they should not be detected in DEEP if they do exist and have HI masses above the detection limit. This, therefore, implies that these galaxies do not exist, or that they have been ionised by the intergalactic UV field and no longer contain significant amounts of neutral hydrogen.

Figure 3.8 shows another interesting correlation, between absolute magnitude and effective surface-brightness. The line shows the best fit of $\mu_{eff} = (0.53 \pm 0.04)M_R + (33.1 \pm 0.9)$, with a scatter of 0.6 mags. This is too narrow to be explained as a translation of the relationship between surface-brightness and apparent magnitude and so must have a physical basis. There appears to be a lack of bright, low surface-brightness galaxies and a similar lack, although not as complete, of faint, high surface-brightness galaxies. This is investigated further in Chapter 4 where volume corrections for the HI mass are used to construct the bivariate brightness distribution.

The relationship between μ_{eff} and M_R found in DEEP is similar to that found by Bingelli & Cameron (1991) for galaxies in Virgo of $\langle\mu\rangle_{eff} \approx 0.75B_T + 11.5$, where B_T is the apparent B-band magnitude (at a constant distance-modulus for galaxies in Virgo), and $\langle\mu\rangle_{eff}$ is the mean B-band surface-brightness within the effective radius – different from the definition of μ_{eff} used for the DEEP project. The Bingelli & Cameron relationship has a similar scatter of 0.8 magnitudes but a steeper slope – the surface-brightness falls off considerably quicker with decreasing luminosity than has been found in DEEP. This is probably due to differences in the morphological types studied – the DEEP relationship has been found for gas-rich galaxies, which are mainly field spirals, while the Bingelli & Cameron relationship has been found for dwarf galaxies (mainly dwarf ellipticals) within the Virgo cluster.

3.5 Literature comparison

The literature values for all the previously catalogued DEEP galaxies are given in Table 3.2. This gives B- and R-band magnitudes from the ESO-LV catalogue (B_T and R_T), B-band magnitude from the RC3 (m_B) and 12, 25, 60, and 100 micron fluxes from IRAS (Beichman et al. 1988; Moshir et al. 1992). The errors in the ESO-LV magnitudes are 0.09 mags, the errors in the RC3 are 0.21 mags. Errors and upper limits for the IRAS fluxes are variable and are given in the table.

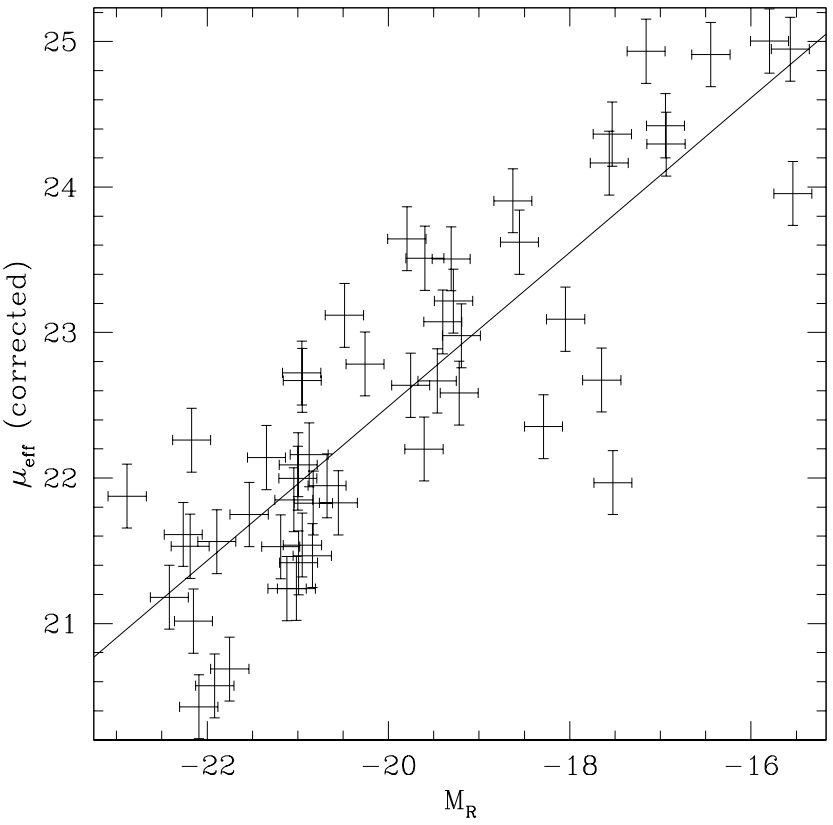

Figure 3.8: Correlation between absolute magnitude and effective surface-brightness. The scatter is too narrow for this to be due to the correlation seen in Figure 3.7 between apparent magnitude and effective surface-brightness combined with the narrow distribution of distance moduli seen in Figure 3.3 and so must be due to a physical effect. The slope, 0.53 ± 0.04, is shallower than that seen by Bingelli & Cameron (1991) in dwarf galaxies in the Virgo cluster.

Table 3.2: Literature values for optical / IRAS observations of the DEEP galaxies

Catalogue	ESO-LV		RC3	IRAS			
ID	B_T	R_T	m_B	12μm	25μm	60μm	100μm
ESO 444-G059	16.97	16.42	-	No IRAS data			
Abell 3558:[MGP94]3325	-	-	-	No IRAS data			
ESO 444-G066	15.45	14.78	15.39	No IRAS data			
IC 4275	14.23	13.41	14.20	< 0.137	< 0.1552	$0.7748 \pm 8\%$	$1.827 \pm 11\%$
ESO 509-G048	15.11	13.94	15.06	No IRAS data			
ESO 444-G070	15.47	14.15	-	< 0.1157	< 0.1602	$0.2469 \pm 18\%$	< 0.1046
IRAS F13304-2724	-	-	-	< 0.1602	< 0.2489	$0.6070 \pm 11\%$	$0.8364 \pm 22\%$
ESO 383-G018	15.29	14.30	-	$0.1360 \pm 21\%$	$0.4440 \pm 8\%$	$0.6164 \pm 9\%$	< 1.222
ESO 444-G071	14.79	-	14.74	< 0.1531	< 0.2281	$0.7994 \pm 9\%$	$1.593 \pm 13\%$
IC 4286	15.95	15.16	-	No IRAS data			
Abell 3558:[MGP94]4312[1]	-	-	-	No IRAS data			
Abell 3558:[MGP94]4317[1]	-	-	-	No IRAS data			
IRAS F13312-2754	-	-	-	< 0.1292	< 0.1069	$0.2836 \pm 16\%$	< 0.9450
ESO 383-G024	15.74	14.99	-	No IRAS data			
IC 4290	14.24	13.51	14.21	No IRAS data			
ESO 383-G030	14.20	-	14.17	No IRAS data			
ESO 383-G031	14.42	13.29	14.38	No IRAS data			
IRAS F13329-2751	-	-	-	< 0.1045	< 0.1221	$0.3437 \pm 13\%$	$0.8419 \pm 20\%$
ESO 444-G075	14.31	13.58	14.27	< 0.1758	< 0.1457	$0.6751 \pm 10\%$	$1.955 \pm 10\%$
ESO 509-G075[2]	15.33	14.02	-	No IRAS data			
ESO 444-G077	15.26	14.93	15.20	No IRAS data			
NGC 5220	13.12	12.07	13.11	$0.1811 \pm 16\%$	$0.1706 \pm 24\%$	$0.5871 \pm 9\%$	$2.258 \pm 12\%$
IC 4298	14.16	12.77	14.13	< 0.1160	< 0.1933	$0.2506 \pm 27\%$	$1.072 \pm 18\%$
[QRM95]1330-30 01	-	-	-	No IRAS data			
ESO 383-G044	14.09	13.20	14.06	$0.1059 \pm 26\%$	$0.1527 \pm 24\%$	$1.245 \pm 6\%$	$2.718 \pm 10\%$
IC 4303	15.27	14.09	-	No IRAS data			
ESO 444-G088	16.19	15.89	-	No IRAS data			
ESO 444-G090	15.93	15.47	-	No IRAS data			
IRAS 13365-3116	-	-	-	< 0.08642	< 0.1193	$0.4132 \pm 10\%$	$0.9714 \pm 20\%$
CSRG 0737	-	-	-	No IRAS data			
ESO 445-G003	15.53	14.95	-	No IRAS data			
ESO 383-G059	16.20	15.42	-	No IRAS data			
ESO 445-G007	16.65	-	16.57	No IRAS data			
ESO 383-G060	13.56	12.71	13.54	$0.1401 \pm 24\%$	$0.1549 \pm 26\%$	$1.330 \pm 7\%$	$3.147 \pm 9\%$
WMMA 219	-	-	-	No IRAS data			
ESO 445-G011	14.70	13.81	-	< 1.1101	< 0.1967	$0.5777 \pm 9\%$	$1.153 \pm 28\%$
ESO 445-G015	14.53	13.22	14.49	No IRAS data			

Table 3.2: Literature values for optical / IRAS observations of the DEEP galaxies (continued)

Catalogue	ESO-LV		RC3	IRAS			
ID	B_T	R_T	m_B	12μm	25μm	60μm	100μm
IC 4318	14.58	13.46	14.54	< 0.1453	< 0.1452	$0.6060 \pm 13\%$	$1.451 \pm 11\%$
ESO 445-G020	15.74	14.67	-	No IRAS data			
IC 4319	14.35	12.79	14.31	< 0.09306	< 0.1232	$0.4843 \pm 9\%$	$1.515 \pm 11\%$
ESO 383-G067	15.51	14.36	-	No IRAS data			
ESO 509-G100	15.13	14.08	15.08	< 0.1356	< 0.1490	$0.2569 \pm 16\%$	< 1.202
MCG -05-32-072	-	-	-	< 0.09873	< 0.1084	$0.2731 \pm 19\%$	$0.7372 \pm 21\%$
ESO 445-G023	15.59	14.88	-	< 0.08566	< 0.1505	$0.2259 \pm 18\%$	< 0.7216
IC 4323	15.91	15.06	-	No IRAS data			
ESO 445-G026	15.07	13.75	15.02	No IRAS data			
NGC 5291	14.09	12.39	15.13	No IRAS data			
IC 4330	14.75	13.48	14.70	< 0.05694	< 0.1718	$0.3497 \pm 14\%$	$0.8887 \pm 19\%$
NGC 5292	12.85	11.29	12.84	< 0.1744	< 0.1637	$0.7073 \pm 8\%$	$2.717 \pm 9\%$
IC 4325	14.76	13.51	14.71	< 0.1247	< 0.1768	$0.4419 \pm 12\%$	$1.266 \pm 25\%$
Abell 3574:[R84]0543	-	-	-	No IRAS data			
IC 4327	14.61	13.74	14.57	No IRAS data			
ESO 445-G048	15.58	14.42	-	No IRAS data			
ESO 383-G088	14.19	13.07	14.16	No IRAS data			

[1] Abell 3558:[MGP94]4312 and 4317 are the two possible optical counterparts for DEEP J1332-3223.

[2] ESO 509-G075 is treated as being the optical counterpart for DEEP J1335-2729 despite having an inconsistent optical velocity.

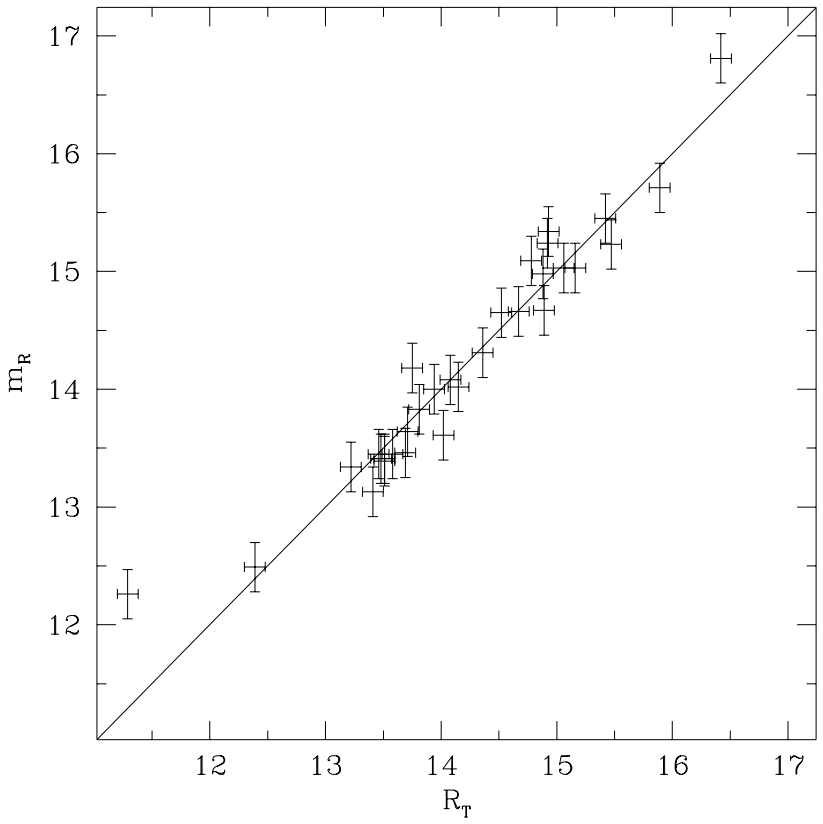

Figure 3.9: ESO-LV total R-band magnitude (R_T) versus the values from the tech pan plate (m_R). It can be seen that there is good agreement between the two, with the exception of NGC 5292 which is thought to have been affected by saturation. The error on m_R is found to be 0.21 mags.

Figure 3.9 shows the relationship between total R-band magnitudes from the ESO-LV catalogue and those found off the tech pan plates. The outlier to the bottom-left is NGC 5292, this galaxy has a high central surface-brightness and a significant fraction of its light has probably been lost on the tech pan plates due to saturation. The outlier to the top right is ESO 444-G059, a very low surface-brightness galaxy ($\mu_{eff} > 25$ Rμ) which has probably got a much larger error in the ESO-LV catalogue than the canonical 0.09 magnitudes. The line on this graph shows equality between the two magnitudes rather than a best-fit line, however the best-fit line, with a slope of 1.03 ± 0.04, lies within one standard deviation of this. Most of the points, with the exceptions noted above, lie clustered around this line, indicating that the photometry appears generally reliable. However, as ESO-LV galaxies were used to calibrate the plates this test only demonstrates that the calibration is consistent and has an error of 0.21 mags, the absolute calibration is still dependent on the ESO-LV.

3.5.1 Inclusion in catalogues

Figure 3.10 shows the number of DEEP galaxies from the tech pan region included in the ESO-LV and RC3 catalogues and in the IRAS 60 μm and 100 μm samples as a function of the optical (R-band) magnitude of these galaxies. It can be seen that the proportion of galaxies included in all four catalogues decreases with magnitude, as is expected, with the ESO-LV and RC3 only being 100% complete as regards the DEEP sample for galaxies brighter than 13^{th} magnitude. The IRAS samples never become fully complete, but this is expected as not all galaxies are strong IR sources, although there is a trend towards inclusion of brighter galaxies.

Figure 3.11 shows the number of DEEP galaxies included in the ESO-LV and RC3 catalogues and in the IRAS 60 μm and 100 μm samples as a function of the integrated HI flux of these galaxies. It can be seen that, as with optical magnitudes, the proportion included in all four catalogues decreases with decreasing flux. The ESO-LV and RC3 are complete for $\int S \, dv > 6$ Jy km s^{-1}. However the IRAS sample once again does not reach full completeness, missing the highest HI flux galaxy in the survey, NGC 5291.

Figure 3.12 shows the number of DEEP galaxies from the tech pan region included in the ESO-LV and RC3 catalogues and in the IRAS 60 μm and 100 μm samples as a function of the R-band effective surface-brightness of these galaxies. There is a general trend in all the catalogues to include proportionally more HSB than LSB galaxies. A much stronger trend is seen in the IRAS samples and the RC3 than in the ESO-LV, although none of these ever reach 100% completeness in any surface-brightness bin. The ESO-LV

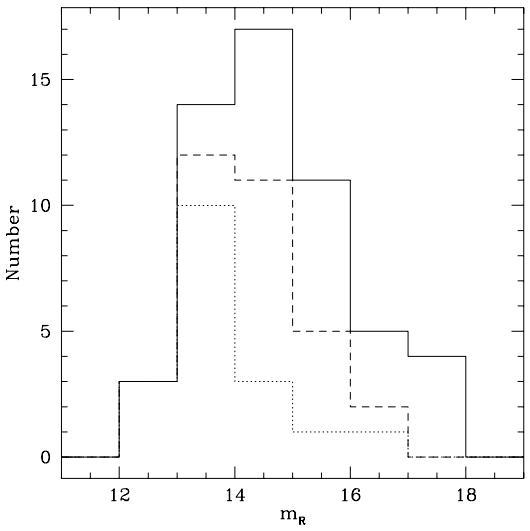

(a) Number of galaxies included in the ESO-LV (dashed line) and RC3 (dotted line) catalogues as a function of optical (R-band) magnitude. Total number of galaxies in DEEP is shown as a solid line.

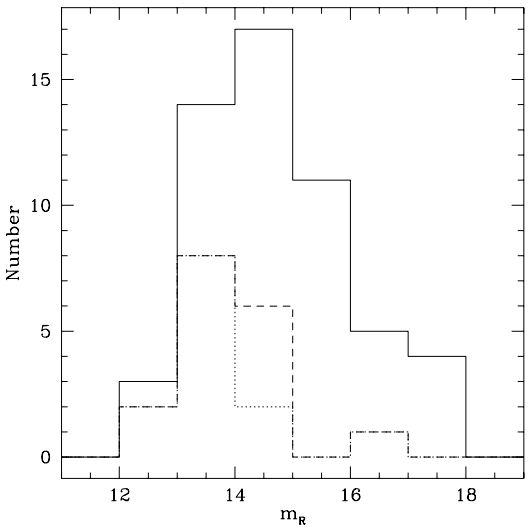

(b) Number of galaxies included in the IRAS 60 μm (dashed line) and 100 μm (dotted line) samples as a function of optical (R-band) magnitude. Total number of galaxies in DEEP is shown as a solid line.

Figure 3.10: Number of galaxies from the DEEP sample included in catalogues as a function of their R-band apparent magnitude. It can be seen that there is a trend for proportionally more brighter galaxies to be included in catalogues than fainter galaxies, however the ESO-LV and RC3 only become 100% complete brighter than 13^{th} magnitude.

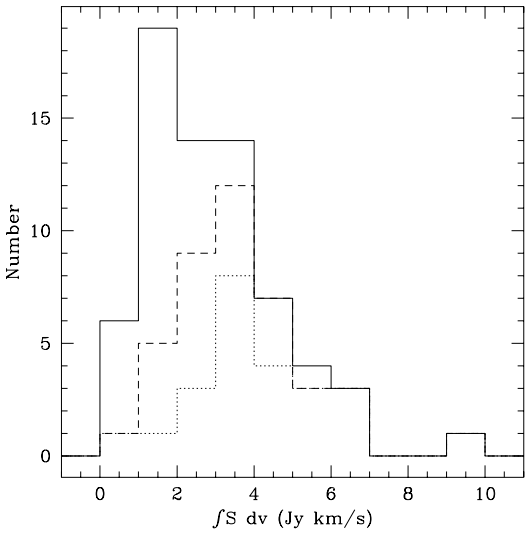

(a) Number of galaxies included in the ESO-LV (dashed line) and RC3 (dotted line) catalogues as a function of HI flux. Total number of galaxies in DEEP is shown as a solid line.

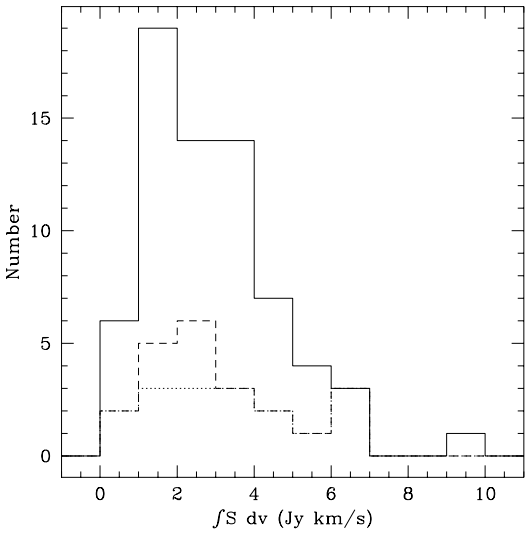

(b) Number of galaxies included in the IRAS 60 μm (dashed line) and 100 μm (dotted line) samples as a function of HI flux. Total number of galaxies in DEEP is shown as a solid line.

Figure 3.11: Number of galaxies from the DEEP sample included in catalogues as a function of their HI flux. As for apparent magnitude, there is a trend for proportionally more higher flux galaxies to be included in catalogues than lower flux ones. The ESO-LV and RC3 are complete for $\int S\,\mathrm{d}v > 6$ Jy km s^{-1}, but the IRAS catalogues omit NGC 5291, the highest flux galaxy in DEEP.

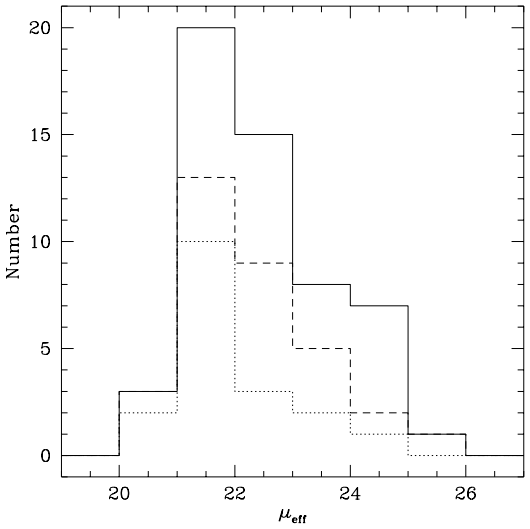

(a) Number of galaxies included in the ESO-LV (dashed line) and RC3 (dotted line) catalogues versus optical (R-band) effective surface-brightness. Total number of galaxies in DEEP is shown as a solid line.

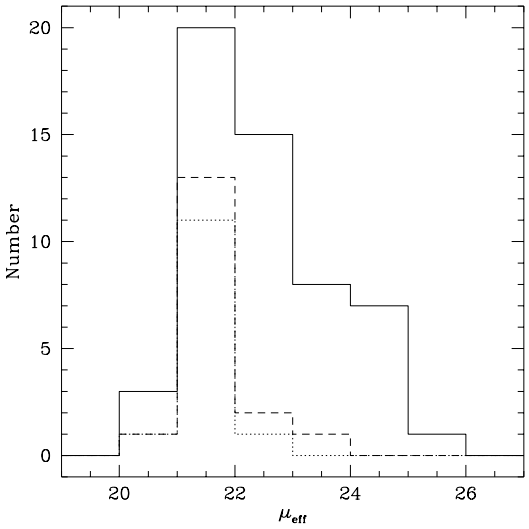

(b) Number of galaxies included in the IRAS 60 μm (dashed line) and 100 μm (dotted line) samples versus optical (R-band) effective surface-brightness. Total number of galaxies in DEEP is shown as a solid line.

Figure 3.12: Number of galaxies from the DEEP sample included in catalogues as a function of their R-band effective surface-brightness. It can be seen that there is a trend to include proportionally more higher surface-brightness than LSB galaxies, with few galaxies fainter than 22 Rμ being included in the RC3 or IRAS catalogues. The ESO-LV covers the full range of surface-brightnesses, although the trend is still in evidence and it only reaches full completeness above 21 Rμ.

includes galaxies over the whole range of surface brightnesses, and is fully complete for $\mu_{eff} < 21$. It also included the galaxy with the lowest (uncorrected) surface-brightness in the sample (ESO 444-G059) which is the only galaxy with $\mu_{eff} > 25$ Rμ.

3.5.2 Comparison of IRAS properties

This section examines the relationships between IRAS 60 μm and 100 μm fluxes from the literature and various properties determined for the DEEP galaxies. For the comparison with HI flux, the full DEEP sample is used, while for the comparison with apparent magnitude, effective surface-brightness, and HI mass to light ratio, only the DEEP galaxies from the tech pan region are used.

Figure 3.13 compares optical magnitudes and IR fluxes. It can be seen that there is a fairly good relationship between the two, for those galaxies detected by IRAS, except for IRAS F13304-2714 which is very faint optically for its IR flux. Other than this, IR flux would appear to be a fairly good estimator of R-band apparent magnitude – although the non-detection of many galaxies by IRAS indicates that the converse is not true.

Figure 3.14 compares HI and IRAS fluxes. There appears to be little correlation for the 100 μm fluxes, but for the 60 μm sample there appears to be a lack of high IR flux, low HI flux galaxies. This lack may be present at 100 μm, but there are not enough galaxies in the sample to be sure one way or the other.

Figure 3.15 compares the HI mass to light ratio with IRAS fluxes. Most of the IRAS galaxies have $M_{\rm HI}/L_R < 0.5$, but there are a few with higher values. The median value for the 60 μm data is $M_{\rm HI}/L_R = 0.36$ with a semi inter-quartile range of ± 0.12, this is statistically indistinguishable from the canonical value of $M_{\rm HI}/L_B = 0.31$ for optically-selected spiral galaxies (Roberts & Haynes 1994).

Figure 3.16 compares effective surface-brightness with IRAS fluxes. The IRAS galaxies can be seen to be strongly clustered around 21.5 – 22 Rμ, with few galaxies fainter than this. This is consistent with the result of Davies, Phillipps, & Disney (1989b) in their analysis of IRAS galaxies in the RC2 catalogue (de Vaucouleurs, de Vaucouleurs, & Corwin 1976) that galaxies with higher far infra-red fluxes tend to have higher surface-brightnesses.

However, it is possible that the cut-off in surface-brightness is due to lower surface-brightness galaxies being fainter optically – a faint galaxy that had the same ratio of optical luminosity to IR flux as the brighter galaxies detected by IRAS would remain undetected as its IR flux would be below the detection

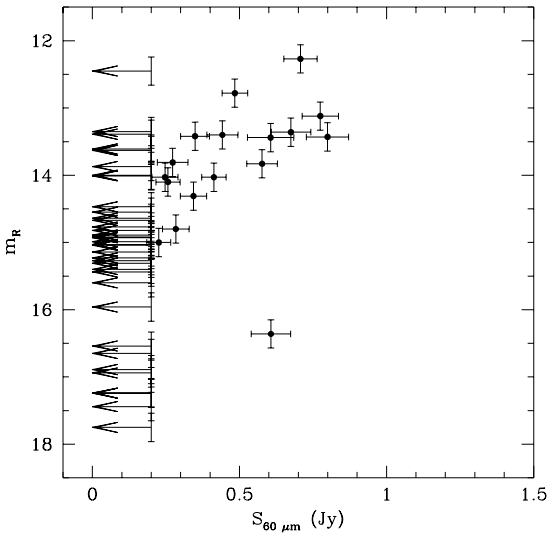

(a) IRAS 60μm flux as a function of optical (R-band) magnitude. For those galaxies not detected at 60 μm by IRAS, upper limits are shown at 0.2 Jy – the detection limit given by Moshir et al. (1992) for the IRAS Faint Source Catalogue at 60 μm.

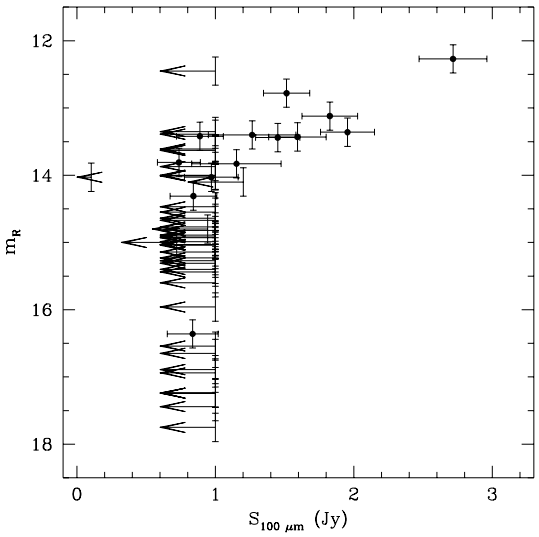

(b) IRAS 100μm flux as a function of optical (R-band) magnitude. For those galaxies not detected at 100 μm by IRAS, upper limits are shown as given in NED where these are available (for those galaxies detected at 60 μm but not at 100 μm), otherwise they are shown at 1.0 Jy – the detection limit given by Moshir et al. (1992) for the IRAS Faint Source Catalogue at 100 μm.

Figure 3.13: Comparison betweem IR fluxes from IRAS and optical magnitudes. It can be seen that for those galaxies which are detected by IRAS, there is a fairly good correlation between IR flux and apparent magnitude, and that the almost total non-detection of IRAS sources fainter than 15^{th} magnitude is due, if the correlation holds, to their IR fluxes being too low to be detected. The one outlier is IRAS F13304-2714

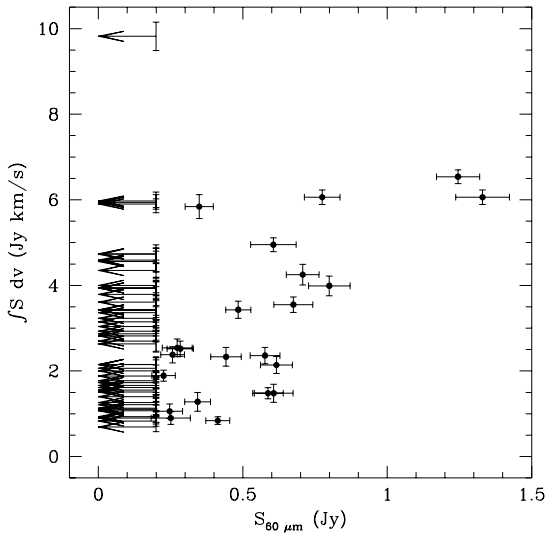

(a) IRAS 60μm flux as a function of HI flux. Upper limits are shown as in Figure 3.13, NGC 5291 (HI flux of 41 Jy km s^{-1}) which is not detected by IRAS is not shown as it is off the scale.

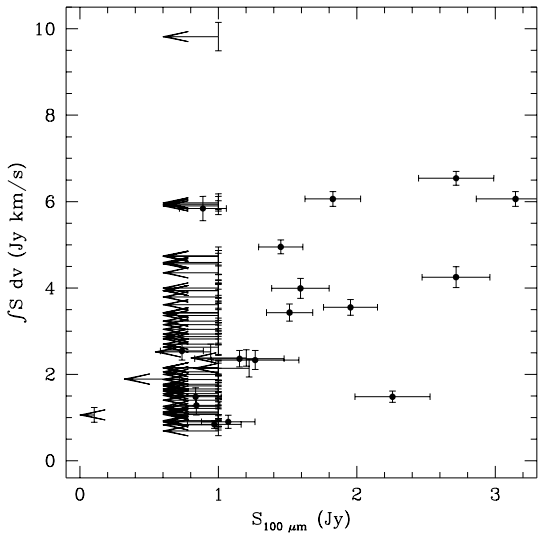

(b) IRAS 100μm flux as a function of HI flux. Upper limits are shown as in Figure 3.13, NGC 5291 (HI flux of 41 Jy km s^{-1}) which is not detected by IRAS is not shown as it is off the scale.

Figure 3.14: Comparison between IR and HI fluxes. It can be seen that there is little correlation, although there may be a lack of high 60 μm flux, low HI flux sources (panel a).

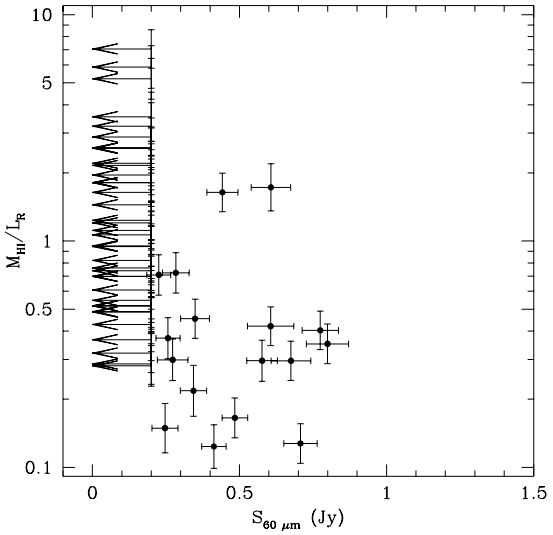

(a) IRAS 60μm flux as a function of $M_{\rm HI}/L_R$, limits as in Figure 3.13.

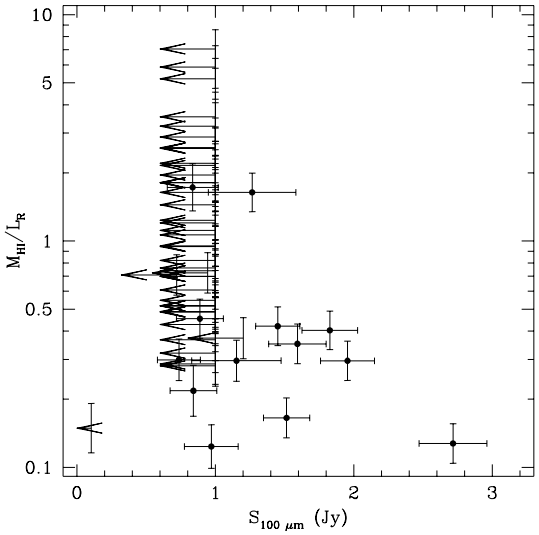

(b) IRAS 100μm flux versus $M_{\rm HI}/L_R$, limits as in Figure 3.13.

Figure 3.15: Comparison of IR flux with HI mass to light ratio. It can be seen that IRAS galaxies tend to have fairly low (for the DEEP sample) values of $M_{\rm HI}/L_R$. This is similar to the result seen in optically selected catalogues.

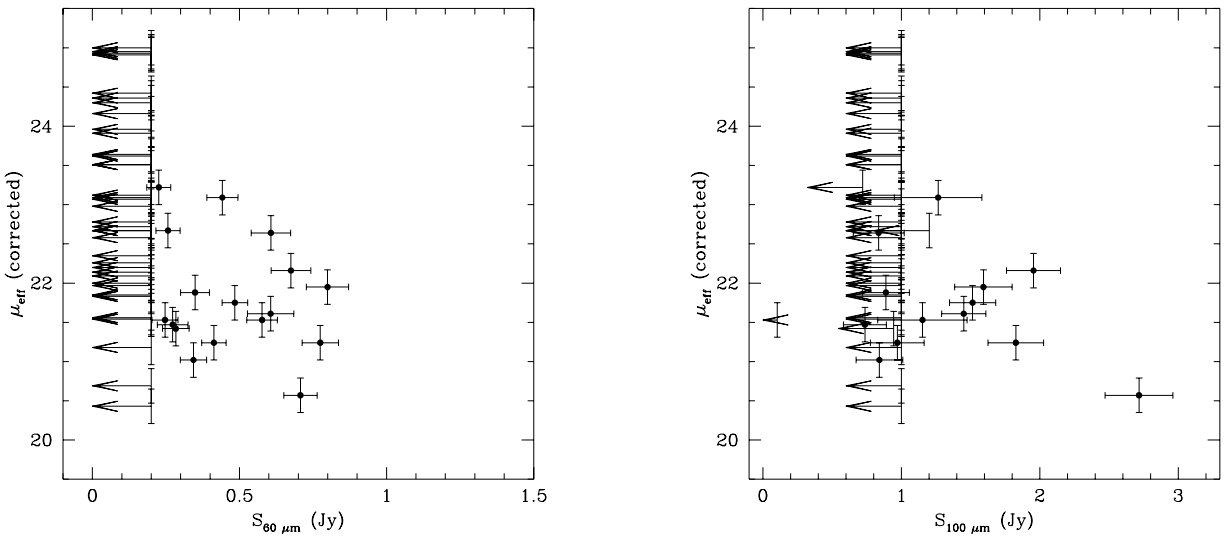

(a) IRAS 60μm flux versus effective surface-brightness, upper limits as in Figure 3.13.

(b) IRAS 100μm flux versus effective surface-brightness, upper limits as in Figure 3.13.

Figure 3.16: Comparison of IRAS flux with effective surface-brightness

threshold. If IRAS F13304-2714 is ignored, the best-fit to 60 μm flux versus apparent magnitude gives $m_R = (-2.78 \pm 0.68) \times \log(S_{60\mu\mathrm{m}}) + 12.69 \pm 0.28$, with a scatter of 0.46. This is statistically indistinguishable from a fit of $m_R = -2.5 \times \log(S_{60\mu\mathrm{m}}) + K$, which would imply a constant ratio of IR flux to optical luminosity, with K best fitted as 12.77 ± 0.48 magnitudes. Figure 3.17 plots optical – IR colour ($m_R - 2.5 \times \log(S_{60\mu\mathrm{m}})$) against effective surface-brightness. It can be seen that the lower limits to this colour (calculated using the 0.2 Jy detection limit of the IRAS Faint Source Catalogue from Moshir (1992)) come diagonally across the plot and form a selection limit to galaxies with the normal proportion of IR flux to apparent luminosity. This acts to remove most galaxies with $\mu_{eff} \gtrsim 22$ Rμ and all galaxies with $\mu_{eff} > 23.2$ Rμ. That very few of the LSB galaxies in DEEP are detected by IRAS can therefore be explained as a selection effect rather than LSB galaxies being poorer in warm dust than 'normal' galaxies – the LSB galaxies would have to be substantially more dust-rich (in proportion to their optical luminosity) than is normal in order to be detected.

Figure 3.18 shows the distribution of IRAS colours (60 μm flux / 100 μm flux)/ The colours have a distribution of $\langle S_{60}/S_{100} \rangle = 0.40 \pm 0.12$, including the outlier IRAS F13304-2714, or $\langle S_{60}/S_{100} \rangle = 0.38 \pm 0.08$

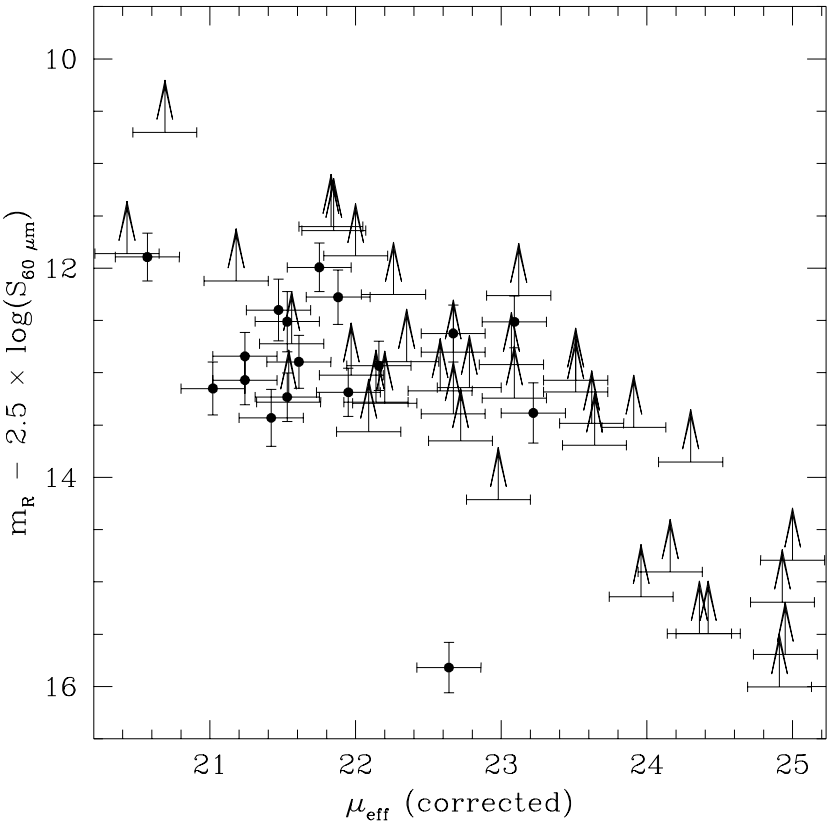

Figure 3.17: Censorship of low surface-brightness, dusty galaxies in the IRAS 60 μm sample. It can be seen that the optical – IR colour remains fairly constant, with $m_R - 2.5 \times \log(S_{60\mu m}) = 12.77 \pm 0.48$, and that there is a detection cut-off for galaxies with this colour which operates in a broad band to remove most galaxies below ~ 22 Rμ and all galaxies below 23.2 Rμ from the IRAS 60 μm sample, shown here by lower limits to the colours of non-detected galaxies calculated from the 0.2 Jy detection limit for the IRAS Faint Source Catalogue (Moshir et al. 1992). The non-detection of most of the LSB galaxies from DEEP by IRAS can therefore be explained simply as a selection effect due to the smaller size of the LSB galaxies and the fairly constant optical – IR colour across the range of surface-brightnesses. That LSB galaxies contain similar proportions of dust to 'normal' galaxies can not be ruled out as these galaxies would not be detected by IRAS.

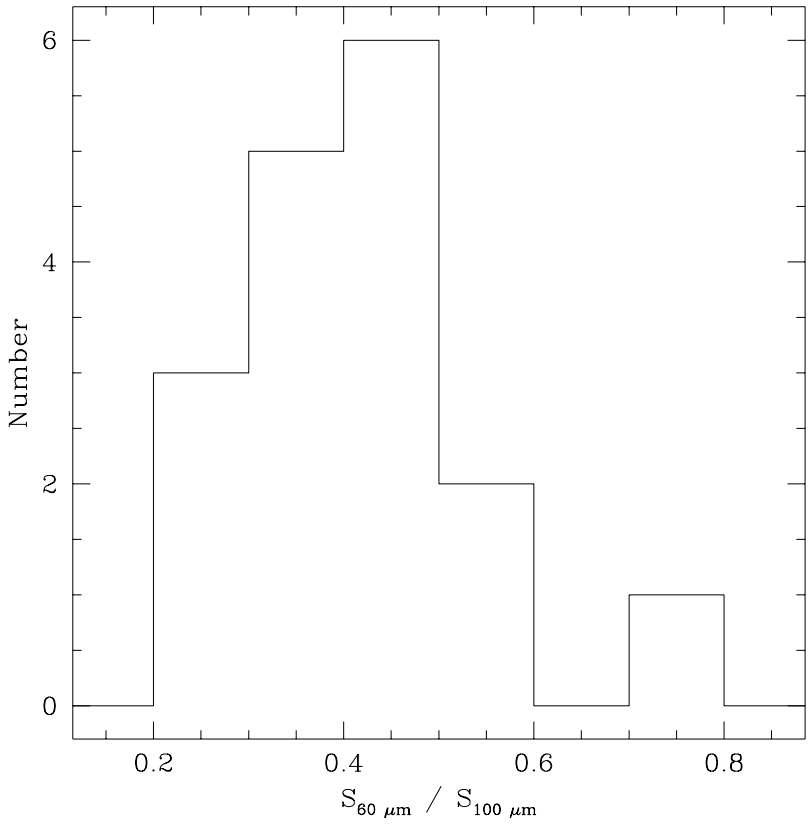

Figure 3.18: Distribution of IRAS colour ($S_{60\mu}$m/$S_{100\mu}$m). It can be seen that, with the exception of IRAS F13304-2714, most of the DEEP galaxies detected have colours near the average of 0.42 for the IRAS faint source catalogue (Moshir et al. 1992).

with this outlier excluded. This is comparable to the mean for sources in the IRAS faint source catalogue of 0.42 (Moshir et al. 1992), it would appear that the HI survey picks out a fairly unbiased sample of IRAS galaxies at least with regards to their colour.

Figure 3.19 compares the IRAS colour ($S_{60\mu}\mathrm{m}/S_{100\mu}\mathrm{m}$) with various optical and HI parameters from the DEEP survey. Panel (a) shows the comparison between colour and HI mass, panel (b) shows the comparison between colour and absolute R-band magnitude, panel (c) shows the IRAS colour versus effective surface-brightness, and Panel (d) shows a comparison between the IRAS colour and the HI mass to light ratio. The high IRAS colour outlier on all these plots is IRAS F13304-2714, which is also an outlier on many other plots. Little correlation can be seen, in particular the correlation by Davies, Phillipps, & Disney (1989b) between IRAS colour and surface-brightness – that LSB galaxies tend to have lower IRAS colour (implying they have cooler dust) is not seen in panel (c). If there is a weak correlation between colour and μ_{eff} it would appear to be, rather, that LSB galaxies have hotter colours.

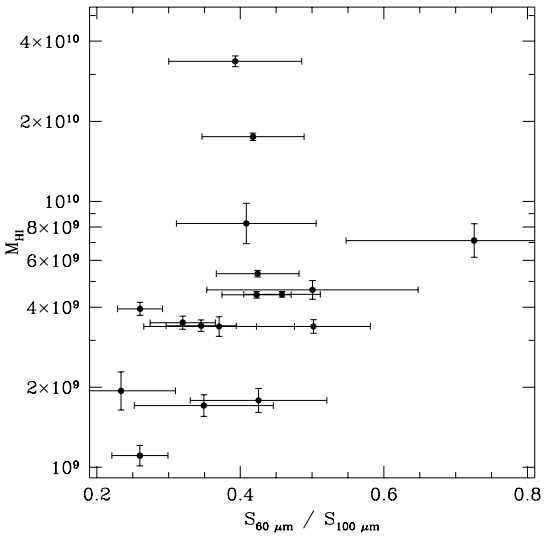

(a) HI mass as a function of IRAS colour

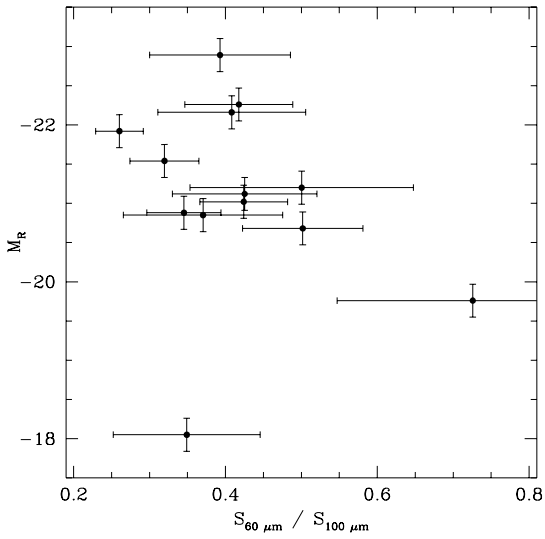

(b) R-band absolute magnitude as a function of IRAS colour

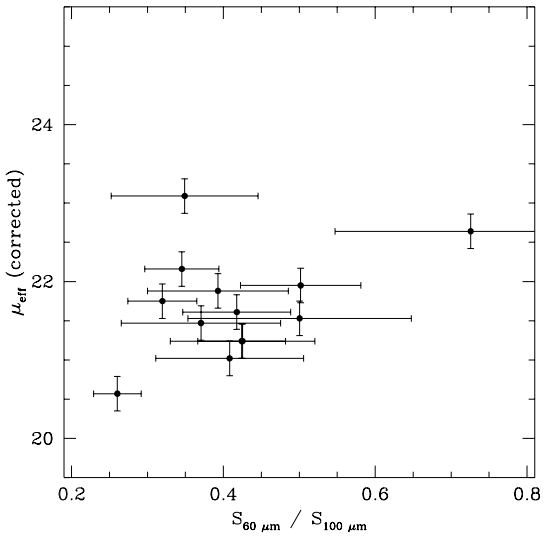

(c) Effective surface-brightness as a function of IRAS colour

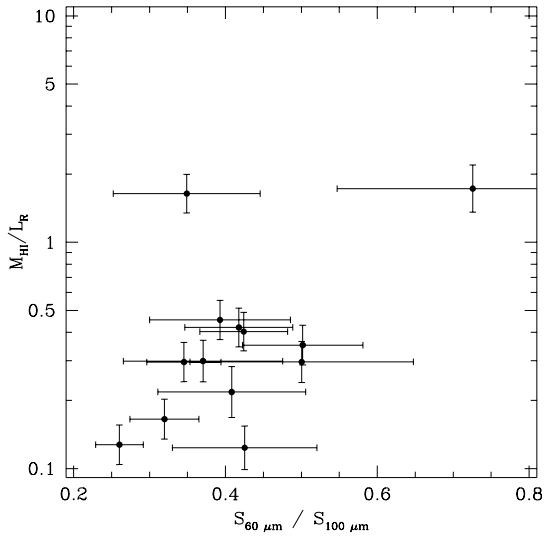

(d) Ratio of HI mass to optical luminosity as a function of IRAS colour

Figure 3.19: Comparision of IRAS colour ($S_{60\mu}$m/$S_{100\mu}$m) and other properties of DEEP galaxies. It can be seen that there is little correlation between the IRAS colour and the other HI and optical properties.

Chapter 4

Discussion and analysis

The combination of optical and HI information for an HI selected sample is a powerful tool for analysing the properties of gas-rich galaxies. As the only selection-effect in DEEP is selection by HI mass, once this is corrected for the sample gives an optically unbiased look at the luminosity function, the surface-brightness distribution, and the bivariate luminosity – surface-brightness distribution. The combination of HI and optical information also allows the Tully-Fisher relationships for these galaxies to be investigated, both the traditional velocity-width – optical magnitude relationship and the recently proposed velocity-width – baryonic mass relationship are investigated. By estimating the HI radii of the sources from the optical radii of the galaxies, their column-densities and dynamical masses can be estimated.

The cosmological importance of LSB galaxies can be estimated by combining the SBD with relationships found between surface-brightness and optical luminosity, HI mass, baryonic mass, and dynamical mass. This allows the contribution of LSB galaxies to the luminosity density, neutral hydrogen density, baryon density, and mass density of the Universe to be calculated.

4.1 Correlations with HI mass to light ratio

Roberts & Haynes (1994) found that for a roughly flux-limited sample of galaxies included in both the UGC and RC3 and for a roughly volume-limited sample of galaxies in the RC3 with a redshift relative to the local group of $V_{LG} < 3000\text{kms}^{-1}$ (implying membership of the Local Supercluster), the median value of M_{HI}/L_B

Table 4.1: $M_{\rm HI}/L_B$ along the Hubble Sequence, from Roberts & Haynes (1994)

Hubble	$B-R$		UGC			LSc	
Types	(de Jong 1996c)	$M_{\rm HI}/L_B$	$M_{\rm HI}/L_R$	Number	$M_{\rm HI}/L_B$	$M_{\rm HI}/L_R$	Number
E, S0	N/A	0.04	N/A	314	0.03	N/A	283
S0a, Sa	1.35 ± 0.22	0.12	0.10	510	0.10	0.09	201
Sab, Sb	1.20 ± 0.19	0.21	0.21	1126	0.20	0.20	325
Sbc, Sc	1.20 ± 0.13	0.29	0.29	955	0.30	0.30	513
Scd, Sd	1.06 ± 0.26	0.36	0.41	1444	0.47	0.53	780
Sm, Im	1.10 ± 0.10	0.66	0.72	406	0.78	0.85	555

increased with Hubble type as shown in Table 4.1. Here 'UGC' denotes galaxies in the flux-limited sample and 'LSc' denotes galaxies from the Local Supercluster.

For galaxies in the 'UGC' sample, this gives an average of $M_{\rm HI}/L_B = 0.29$ or 0.31 if E and S0 galaxies are excluded, while for galaxies in the 'LSc' sample, this gives an average of $M_{\rm HI}/L_B = 0.39$ or 0.44 if E and S0 galaxies are excluded. For the late-type galaxies, the colours from de Jong (1996c) can be used to convert this to R-band, giving $M_{\rm HI}/L_R = 0.33$ for the 'UGC' sample and $M_{\rm HI}/L_R = 0.47$ for the 'LSc' sample. It can be seen that the correction is small as the colours for all morphological types are close to the solar colour, $(B-R)_\odot = 1.19$. This value lies within the scatter of the colours for every morphological type.

The distribution of $M_{\rm HI}/L_R$ for the DEEP sample is shown in Figure 4.1. This sample has a median of $M_{\rm HI}/L_R = 0.75^{+1.83}_{-0.44}$ (where the errors include 68% of the sample), which is considerably more gas-rich than the optically selected samples. However this is not surprising as gas-rich galaxies are much more likely to be found in an HI survey than in an optical survey.

The sample can be divided (arbitrarily) into 4 sections:

- Moderately gas-poor galaxies with $0 < M_{\rm HI}/L_R \leq 0.316$ ($-1 < \log(M_{\rm HI}/L_R) \leq -0.5$). These galaxies have HI mass to light ratios lower than the average of the sample of Roberts & Haynes, yet still higher than 10%. There are 11 galaxies in this division out of the DEEP sample of 54 galaxies, or 20%.

- Moderately gas-rich galaxies with $0.316 < M_{\rm HI}/L_R \leq 1.0$ ($-0.5 < \log(M_{\rm HI}/L_R) \leq 0.0$). These galaxies have HI mass to light ratios higher than the average of the sample of Roberts & Haynes. However there is probably still more mass in stars than in the gas. This is the largest division in the DEEP

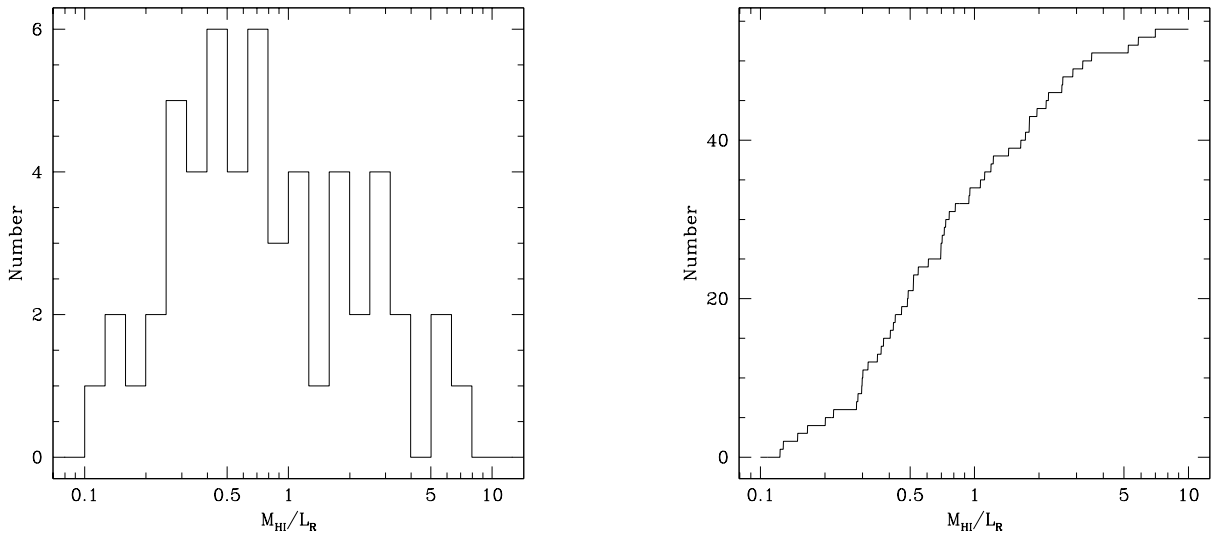

(a) Distribution of $M_{\rm HI}/L_R$

(b) Cumulative distribution of $M_{\rm HI}/L_R$

Figure 4.1: Distribution of HI mass to light ratios. It can be seen that this sample is considerably more gas-rich than optically selected samples, as selection by HI flux will preferentially pick out gas-rich galaxies. The median of the sample is $M_{\rm HI}/L_R = 0.75^{+1.83}_{-0.44}$, where the errors take in 68% of the galaxies.

sample with 23 galaxies, or 43%.

- Gas-rich galaxies with $1.0 < M_{\rm HI}/L_R \leq 3.16$ ($0.0 < \log(M_{\rm HI}/L_R) \leq 0.5$). These galaxies probably have more mass in their gas than in their stars and are uncommon in optically-selected samples. This is the second largest division, with 15 galaxies in DEEP, or 28%.

- Very gas-rich galaxies with $3.16 < M_{\rm HI}/L_R \leq 10.0$ ($0.5 < \log(M_{\rm HI}/L_R) \leq 1.0$). The baryonic mass of these galaxies is dominated by their gas, with the proportions of mass in stars and gas being reversed from the 'ordinary' galaxies in optically-selected samples. These galaxies are very rare in optical samples, and not particularly common even in HI selected samples, implying that their rarity is not entirely an optical selection effect. This is the smallest division in DEEP with 5 galaxies, or 9%.

Figure 4.2 shows how $M_{\rm HI}/L_R$ varies with HI mass. It can be seen that there is a suggestive but weak trend for less massive galaxies to have higher HI mass to light ratios. Certainly all the moderately gas-rich and gas-poor galaxies have $M_{\rm HI} > 10^9 M_\odot$, while all the very gas-rich galaxies have $M_{\rm HI} < 10^{9.5} M_\odot$. However, there is no strong correlation seen here: gas-rich galaxies are seen across the whole range of masses, and there are no moderately gas-poor galaxies with $M_{\rm HI} > 10^{10} M_\odot$.

There is a much stronger correlation seen between $M_{\rm HI}/L_R$ and absolute magnitude (Figure 4.3). It is clear that the higher mass to light ratios are seen in the fainter galaxies. The relationship found is

$$M_R = (5.40 \pm 0.52) \times \log\left(\frac{M_{\rm HI}}{L_R}\right) - (19.23 \pm 0.07) \tag{4.1}$$

which has a scatter of 1.3 magnitudes. This shows that the luminosity of the galaxies falls faster than the HI mass as the size of galaxies decreases, possibly indicating that these smaller galaxies are less efficient in converting their gas into stars.

A similarly good correlation can be seen between $M_{\rm HI}/L_R$ and effective surface-brightness (Figure 4.4. This relationship is

$$\mu_{eff} = (3.38 \pm 0.33) \times \log\left(\frac{M_{\rm HI}}{L_R}\right) + (22.95 \pm 0.04) \tag{4.2}$$

which has a scatter of 0.8 magnitudes. This is in agreement with previous results, e.g. de Blok, McGaugh, & van der Hulst (1996) in B and I band data, which indicated that the HI mass to light ratio increased at

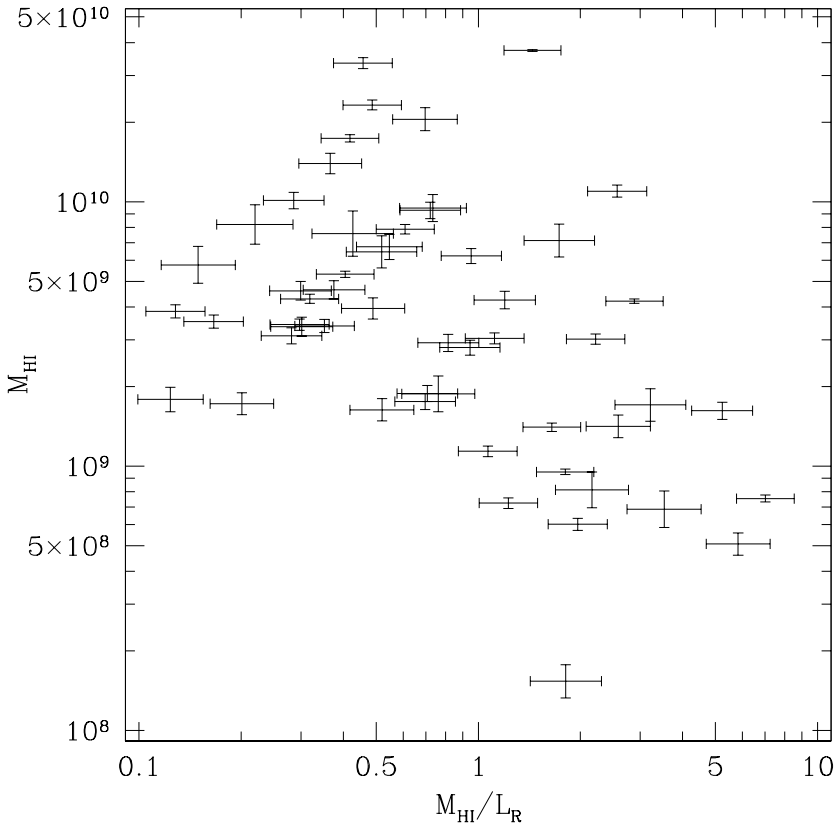

Figure 4.2: Correlation of HI mass with HI mass to light ratio. It can be seen that there is a total lack of low mass, low $M_{\rm HI}/L_R$ galaxies, with all the galaxies with $M_{\rm HI}/L_R < 1$ having $M_{\rm HI} > 10^9 M_\odot$, and a similar lack of high mass, high $M_{\rm HI}/L_R$ galaxies, with all the galaxies with $M_{\rm HI}/L_R > 3.16$ having $M_{\rm HI} < 10^{10} M_\odot$.

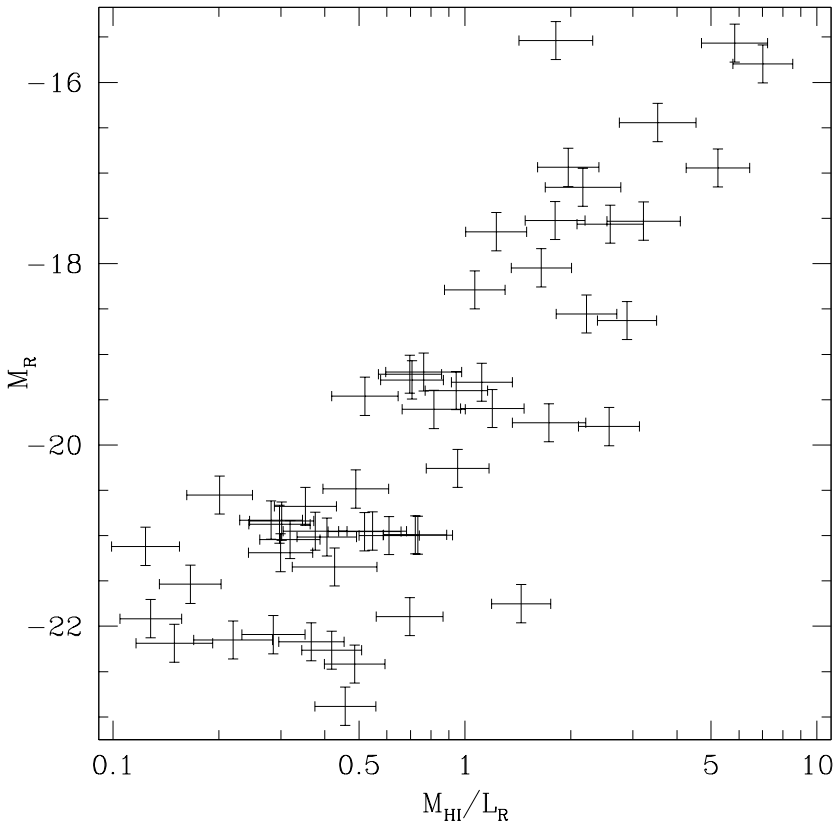

Figure 4.3: Correlation of absolute R-band magnitude with HI mass to light ratio. The correlation between M_R and $\log(M_{\rm HI}/L_R)$ has a slope of 5.40 ± 0.52 and a scatter of 1.3 magnitudes.

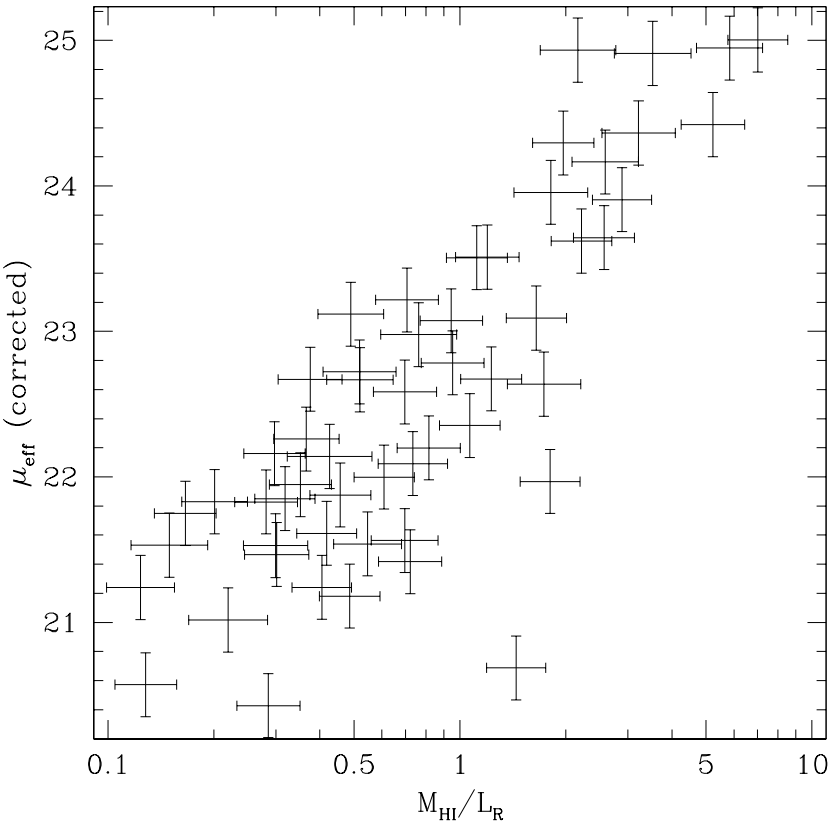

Figure 4.4: Correlation of effective surface-brightness with HI mass to light ratio. The correlation between μ_{eff} and $\log(M_{\rm HI}/L_R)$ has a slope of 3.38 ± 0.33 and a scatter of 0.8 magnitudes.

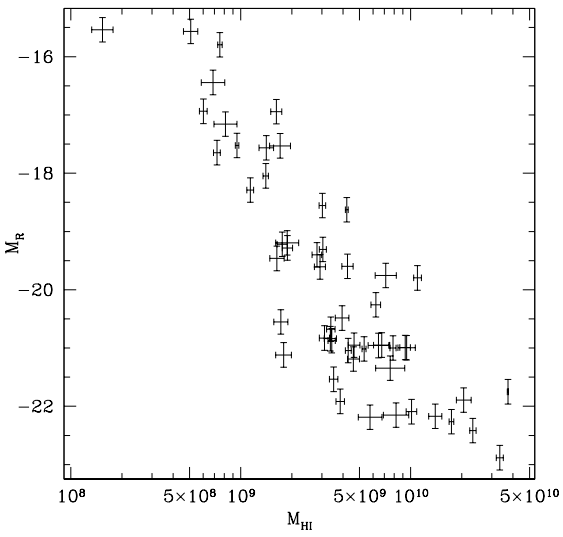

(a) Correlation of absolute R-band magnitude with HI mass.

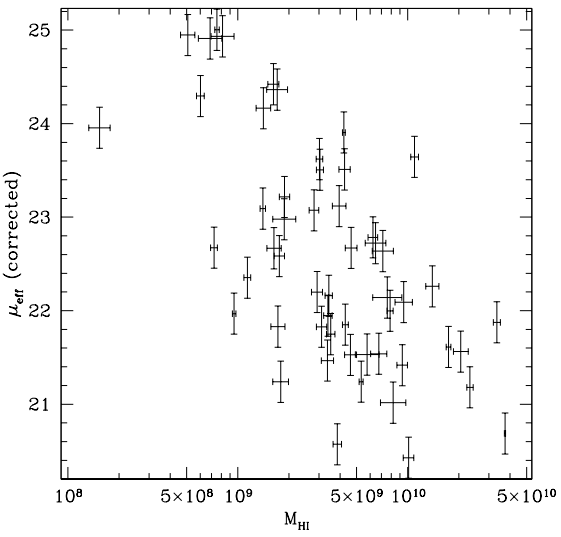

(b) Correlation of effective surface-brightness with HI mass.

Figure 4.5: Correlations between optical properties and HI mass. As both absolute R-band magnitude and effective surface-brightness are correlated with HI mass, selection by HI mass will give a biased distribution of these properties unless a correction is made.

lower surface-brightnesses. This could imply that these galaxies are relatively unevolved, and have not yet converted a large fraction of their mass to stars. It also indicates that luminosity is not a good guide to the mass of LSB galaxies as it will under-estimate the mass of baryons and, for a fairly constant baryonic to total mass ratio, it will also under-estimate the total mass of LSB galaxies. The luminosity is therefore not a good guide to the cosmological importance of LSB galaxies.

4.2 HI mass weighted correlations

Both absolute magnitude and effective surface-brightness appear to correlate with HI mass, as shown in Figure 4.5. This means that the distributions of absolute magnitude and surface-brightness given in Chapter 3 are *not* sampling the same volume in each bin – the fainter bins, corresponding to lower HI masses,

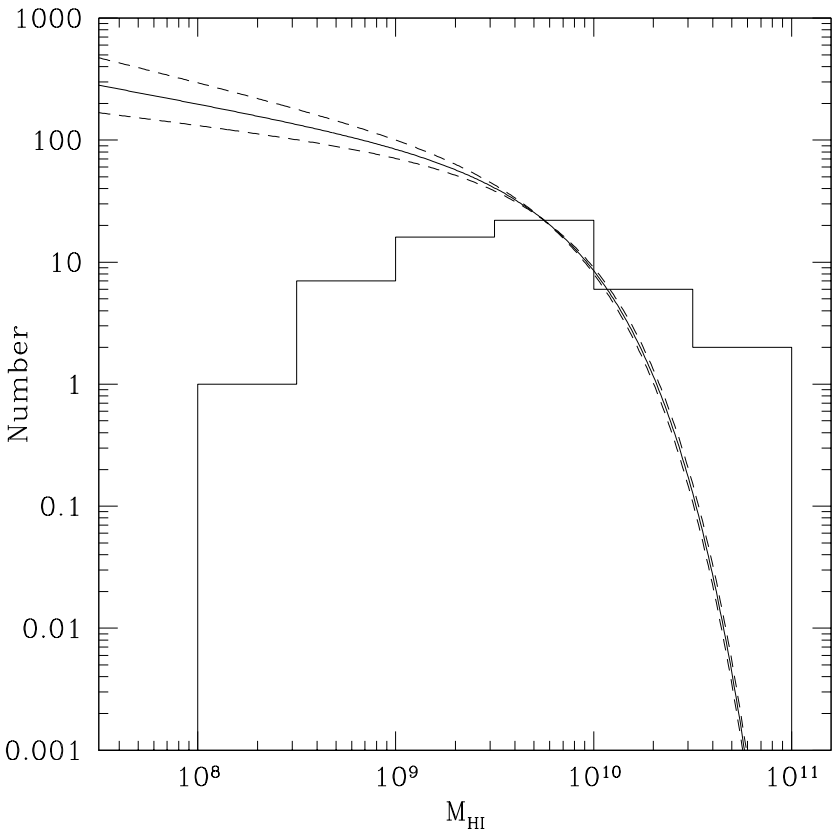

Figure 4.6: HI Mass Function used for weighting, with distribution of HI masses overlaid. The solid line shows a HIMF with $\alpha = -1.3$, while the dashed lines show HIMFs with $\alpha = -1.4$ and $\alpha = -1.2$, all with $M^{\star}_{\rm HI} = 10^{9.75}$ and normalised to the height of the bin on the histogram centred on this $M^{\star}_{\rm HI}$.

cover a smaller volume. In order to correctly determine the luminosity function and the surface-brightness distribution, it is necessary to correct for this selection effect.

This can be made using an assumed HI Mass Function (HIMF). Figure 4.6 shows a HIMF with $\alpha = -1.3 \pm 0.1$ and $M^{\star}_{\rm HI} = 10^{9.75} M_{\odot}$ (equivalent to $M^{\star}_{\rm HI} = 10^{9.5} M_{\odot}$ for $\rm H_0 = 100\ Mpc^{-1}\ kms^{-1}$) superimposed on the distribution of HI masses for galaxies in the tech-pan region. This HIMF shows how many galaxies would be expected in each bin if all bins sampled the same volume in the absence of large-scale structure and has been normalised to pass through $M^{\star}_{\rm HI}$ on the histogram. This can be used to correct each bin by weighting it according to the number of galaxies actually found in that bin divided by the number expected

from the HIMF, thus giving distributions of absolute magnitude and effective surface-brightness where all bins are sampling the same volume (Minchin 1999).

As long as there is no selection in favour of either higher luminosity or higher surface-brightness galaxies at any given mass, this method will correct for the selection effects in DEEP. It is unimportant for this method whether the selection is primarily by signal to noise ratio or by peak flux as the correction is made purely by comparing the observed distribution of HI masses with the theoretical distribution for a volume-limited sample.

4.2.1 Luminosity function

Figure 4.7 shows the absolute magnitude distributions of galaxies in each of six HI mass bins. These bins have been weighted as described above, in order to form a luminosity function (LF) for the DEEP galaxies. This LF (with the vertical scale in arbitrary units) is shown in Figure 4.8 and has a slope of $\alpha = -1.14 \pm 0.05$, which is consistent with determinations of the LF from optically-selected field samples, e.g. Blanton et al. (2001) who found $\alpha = -1.20 \pm 0.03$ for r-band SDSS commissioning data. There may be a down-turn in the brightest bin ($-23 < M_R \leq -22$), but it is not particularly apparent so $M_R^\star$ has not been fitted. This bin has, however, been omitted from the fitting of α. There may also be the start of an up-turn in the faintest bin ($-16 < M_R \leq -15$), but this is even less significant.

4.2.2 Surface brightness distribution

Similarly, the surface-brightness distribution can be re-weighted to give a more accurate picture of the space-density of low surface-brightness galaxies. Figure 4.9 shows the surface-brightness distributions of galaxies in the six different HI mass bins. The re-weighted surface-brightness distribution is given in Figure 4.10, it is similar in appearance to the broken power-law proposed by McGaugh (1996), with the break-point denoted by $\mu_B^\star = 21.9$ Bμ. I have therefore fitted a broken power-law to the SBD, with both fits taking in the $21.4 < \mu_{eff} < 22$ bin where the break-point seems to occur. The precise position of the break-point, which I refer to as $\mu_{eff}^\star$ following the convention of McGaugh (1996), is found by finding the intersection of the two power-laws.

This fitting gives a slowly rising number density of galaxies towards lower surface-brightnesses ($\phi \propto \mu_{eff}^{0.17 \pm 0.15}$ for $\mu_{eff} > \mu_{eff}^\star$) and a sharp fall in the number density towards higher surface-brightnesses

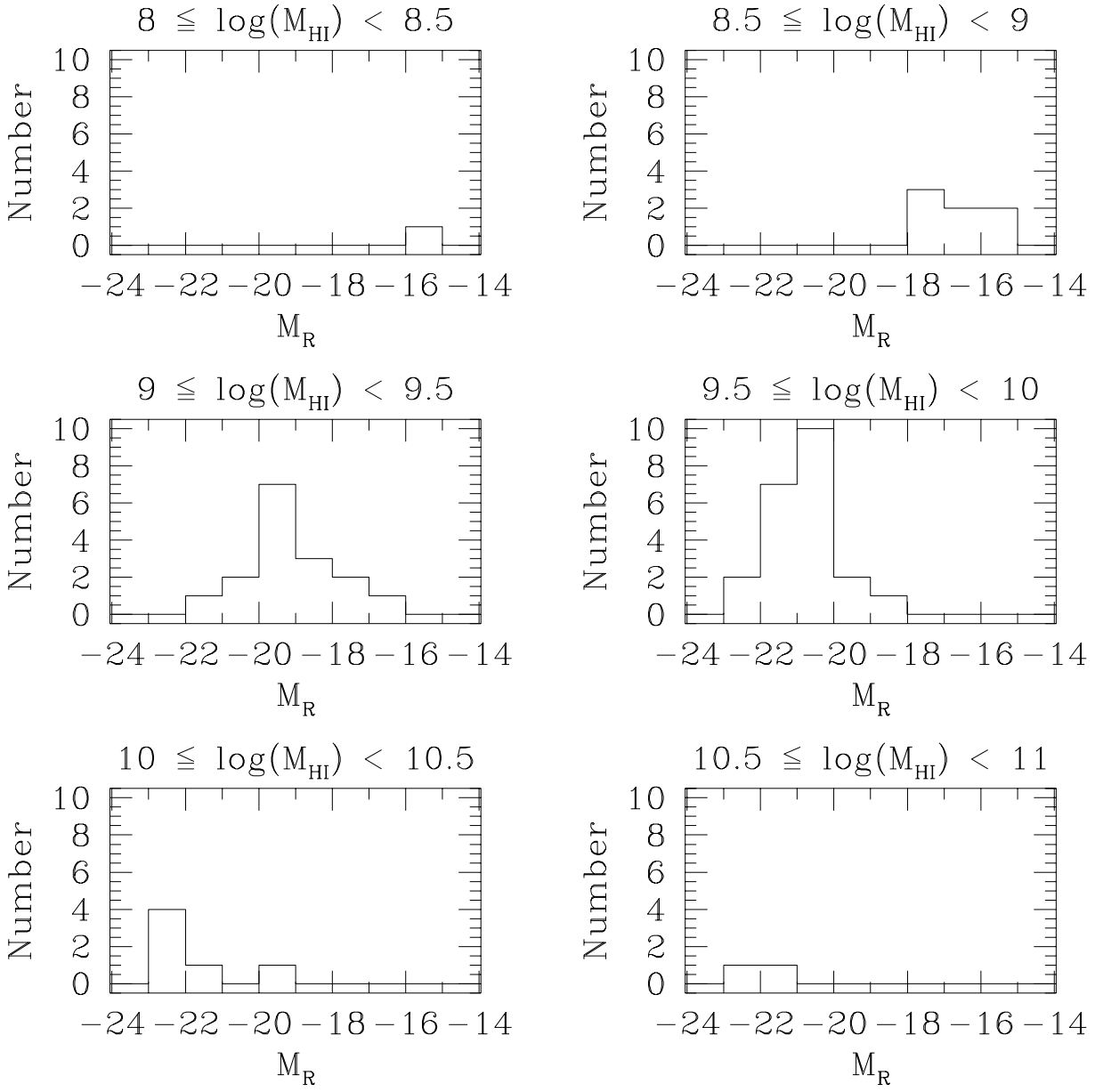

Figure 4.7: Absolute magnitude distributions in different HI mass bins. Each bin is weighted by a factor calculated from the HIMF and the number of galaxies in that bin in order to produce the Luminosity Function.

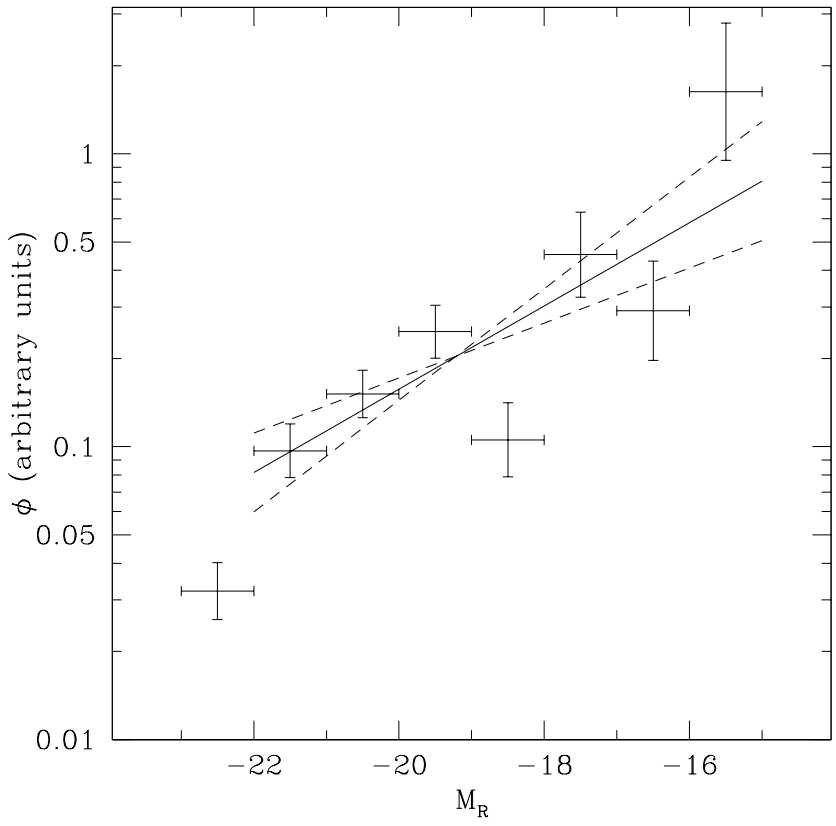

Figure 4.8: Corrected luminosity function of DEEP galaxies, density in arbitrary units. The fitted slope gives $\alpha = -1.14 \pm 0.05$ which is consistent with optically-selected field samples, e.g. Blanton et al. 2001 who found $\alpha = -1.2 \pm 0.03$ for r-band SDSS commissioning data.

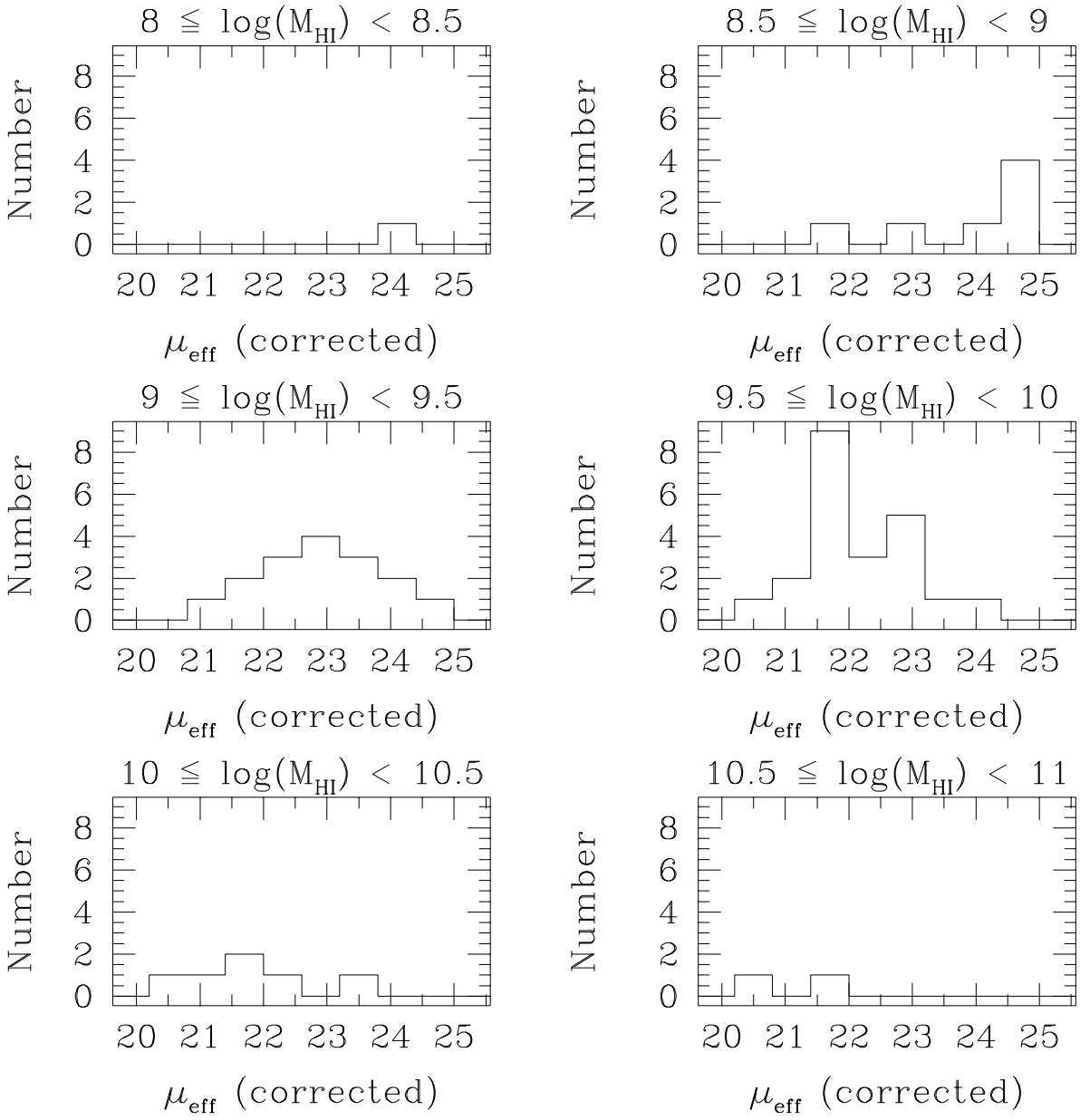

Figure 4.9: Surface brightness distributions in different HI mass bins. Each bin is weighted by a factor calculated from the HIMF and the number of galaxies in that bin in order to produce the Surface Brightness Distribution.

($\phi \propto \mu_{eff}^{1.13\pm0.04}$). The break point is at $\mu^{\star}_{eff} = 21.56^{+0.18}_{-0.26}$ Rμ.

The general shape of the SBD is comparable to that found by Davies (1990), with a nearly flat slope towards the LSB end and a sharp drop-off at the HSB end. However there are differences in the details: McGaugh's fitting of a broken power-law through the data of Davies (1990) gave $\phi \propto \mu_0^{-0.3}$ for $\mu_0 > 21.9$ Bμ) and $\phi \propto \mu_0^{2.6}$ at the HSB end. The differences here are unlikely to be due to over-weighting of the low-mass end of the HI mass function – a slope of $\alpha = -1.2$ instead of -1.3 barely alters the faint end slope of the surface-brightness distribution, therefore it would appear to be a real difference between the data. Davies (1990) was an optical survey of the Fornax group, whereas DEEP is an HI survey which is primarily in the field (although taking in part of the Centaurus cluster). It would be surprising if the two surveys had given exactly the same results.

4.2.3 Bivariate brightness distribution

The bivariate brightness distribution (BBD) is the bivariate distribution of galaxies as a function of luminosity and surface-brightness. It combines the SBD and the LF and contains the information from both of these as well as information about the relationship between them. If it can be determined, it ensures that surface-brightness selection effects have not affected the determination of the luminosity function – there is normally an implicit (and incorrect) assumption that these selection effects can be ignored in construction the LF (e.g. Ferguson & McGaugh 1995). The BBD also gives important information on the contribution of LSB galaxies to the Universe – if LSB galaxies are generally faint dwarf galaxies, then their contribution to the total light and mass of the Universe is not great compared to that of the 'normal' surface-brightness giant galaxies, but if LSB galaxies occupy the same range of luminosities as 'normal' galaxies, then they could make a significant contribution. The accurate determination of the BBD from an optical sample is very difficult (e.g. Boyce & Phillipps 1993), but it should be much easier from an HI selected sample as there is only the selection by HI mass to correct for.

Figure 4.11 shows the BBD of galaxies discovered in DEEP, without any weighting for HI mass being applied. The cells are one magnitude wide in luminosity and 0.6 magnitudes wide in surface-brightness, giving 8 bins along each axis, and the greyscale here is linear. It can clearly be seen that the most populated region is that of ordinary, $\sim M^{\star}_{R}$, 'normal' surface-brightness galaxies. However, these are also galaxies around $M^{\star}_{\rm HI}$, and are found preferentially by the DEEP survey.

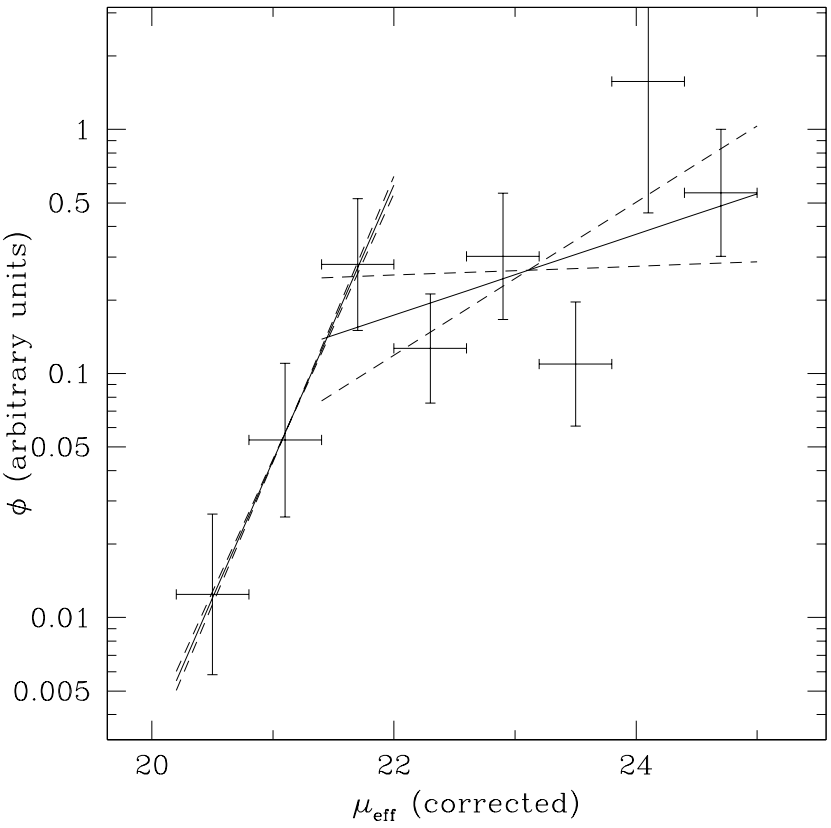

Figure 4.10: Corrected surface-brightness distribution of DEEP galaxies, density in arbitrary units. This gives a slowly rising number density towards lower surface-brightnesses, with a slope of $\phi \propto \mu_{eff}^{0.17\pm0.15}$ and a sharp down-turn at higher surface-brightnesses.

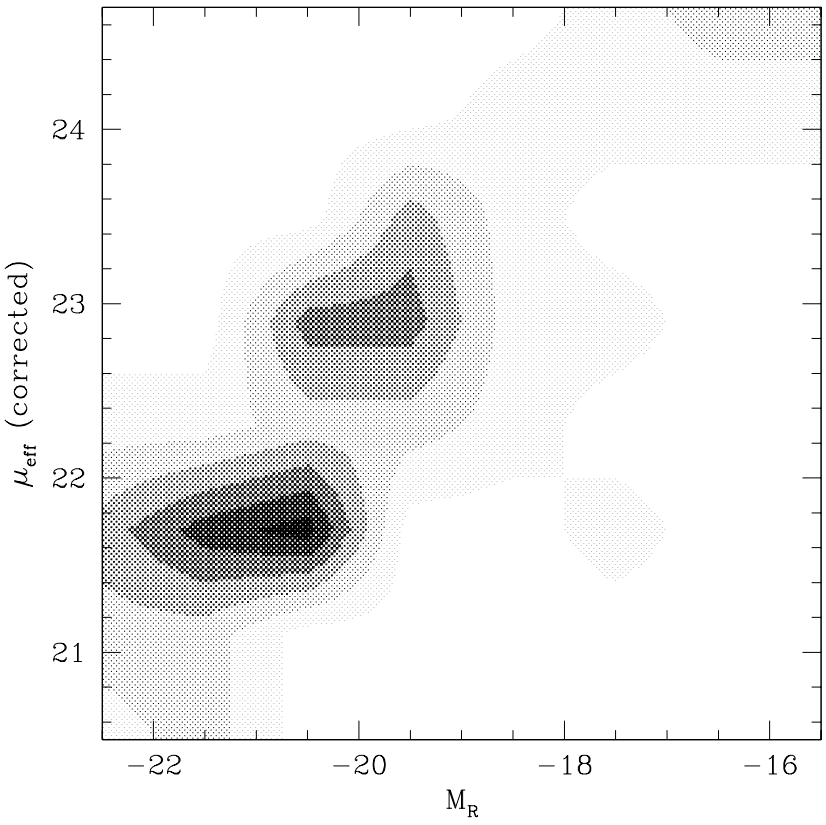

Figure 4.11: Uncorrected bivariate brightness distribution of DEEP galaxies. The scale is linear, ranging from 0 galaxies per bin (white) to 6 galaxies per bin (black) in steps of 1.

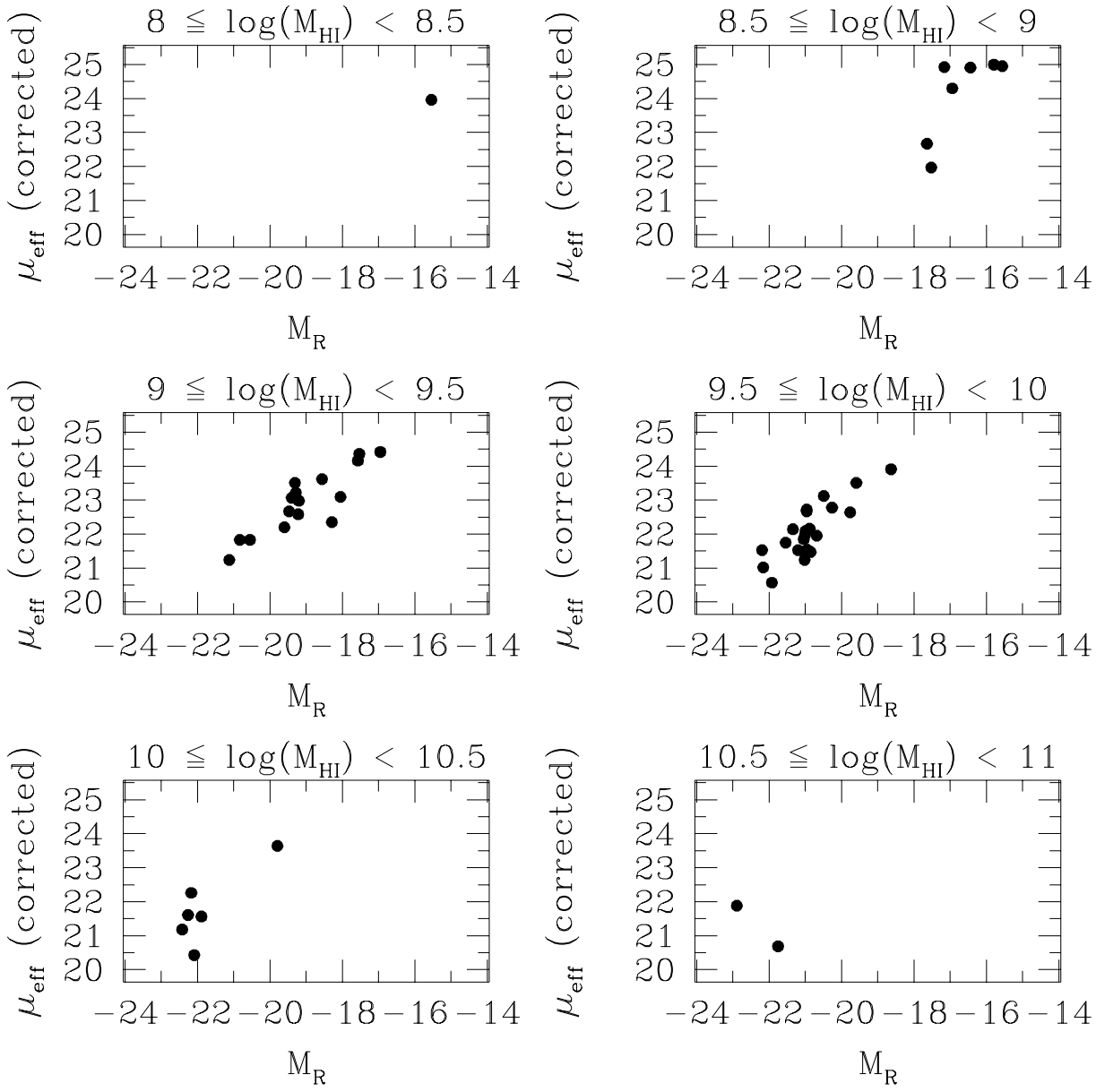

Figure 4.12: Distribution of galaxies by absolute magnitude and effective surface brightness in different HI mass bins. Each bin is weighted by a factor calculated from the HIMF and the number of galaxies in that bin in order to produce the Bivariate Brightness Distribution.

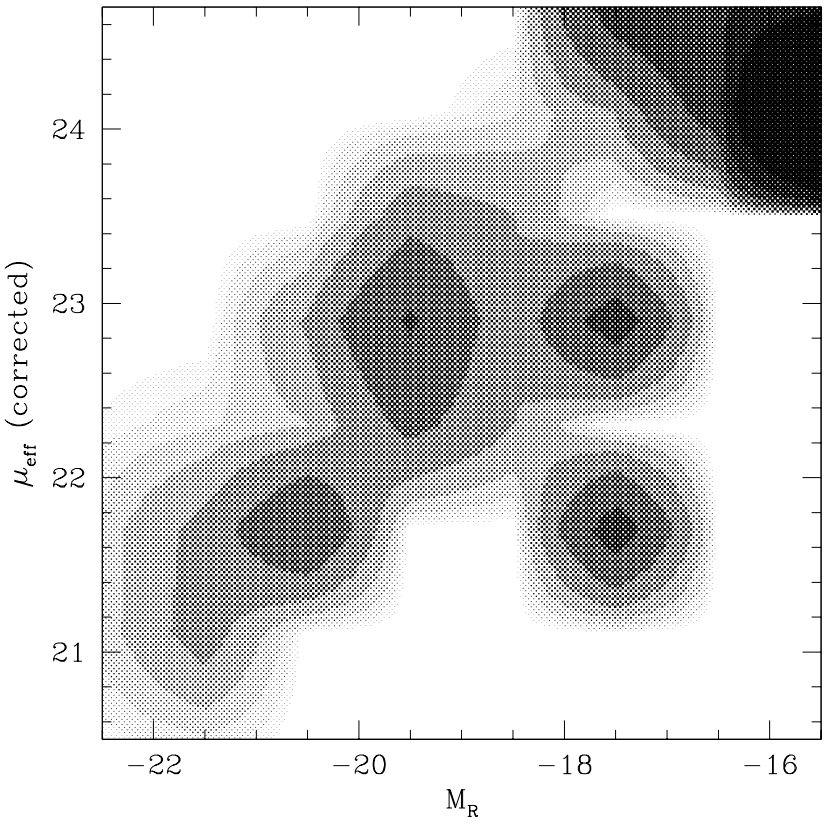

Figure 4.13: Corrected bivariate brightness distribution of DEEP galaxies, logarithmic greyscale in arbitrary units at intervals of 0.25 dex. It can be seen that there is a fairly uniform population except for bright, LSB galaxies which are not found.

The distribution of galaxies in the absolute magnitude – surface-brightness plane for different HI mass bins is shown in Figure 4.12. It can be seen that the trend is for low mass galaxies to also be faint, low surface-brightness galaxies. When these are weighted by the HIMF, as described earlier, the resulting BBD is that shown in Figure 4.13. Here it can be seen that there is much more uniform population of the absolute magnitude – surface-brightness plane than was seen in the unweighted BBD. Once again the cells are one magnitude wide in luminosity and 0.6 magnitudes wide in surface-brightness, but the greyscale used here is logarithmic in order to properly cover the range of densities, with a step size of 0.25 dex.

It is not possible to show error-bars on this map, but the errors can be estimated from the number per

cell shown in Figure 4.11. The peak in density at $M_R < -17$ and $\mu_{eff} > 23.6$ Rμ has only three galaxies across two cells and so is not particularly significant, and the extensions at $M_R \sim 18.5$ and $\mu_{eff} \sim 21.6$ Rμ and ~ 23 have only one galaxy per cell.

The BBD appears to show that high surface-brightness galaxies are generally bright galaxies, while low surface-brightness galaxies are almost all fairly low luminosity. Whether there is a large population of HI rich, relatively high surface-brightness, relatively low luminosity galaxies is uncertain due to the small number of galaxies found in this region and the high weighting given to them. It is likely that the paucity of low surface-brightness, high luminosity galaxies, Disney's "Crouching Giants", is real as these should have been easily detected if they had similar HI masses to other bright galaxies – these could only exist if they were particularly HI poor, possibly due to ionisation by the intergalactic UV flux. Out of 25 galaxies with $L_R > 10^{10} L_\odot$, none have $\mu_{eff}(c) > 23$ Rμ. That high-luminosity, low surface-brightness galaxies make up more than 11.5% of the high-luminosity population (here defined as those galaxies with $L_R > 10^{10} L_\odot$), can be therefore be ruled out with 95% confidence and that LSB galaxies make up more than 17% of high-luminosity galaxies can be ruled out with 99% confidence.

However, of the eight HI massive ($M_{\rm HI} > 10^{10} M_\odot$) galaxies found in DEEP, one (ESO 383-G059), is an LSB galaxy with $\mu_{eff}(corrected) = 23.6$ Rμ – but the high HI mass of this galaxy does not translate to a high optical luminosity. The concept of using optical luminosity as a measure of the mass of a galaxy appears somewhat shaky when applies to LSB galaxies, where most of the gas has often not been converted to stars. The lack of high-luminosity LSB galaxies may not, therefore, indicate a real lack of giant (in a baryonic sense) LSB galaxies.

Figure 4.14 goes some way to explaining the blank areas of the BBD. This shows the distribution of galaxies in absolute magnitude and effective surface-brightness with contours of constant HI mass overlaid. These contours have been calculated using the relationship $\log(M_{\rm HI}/L_R) = 0.3 \times \mu_{eff} - 6.8$ found earlier. If there is a dependence of $M_{\rm HI}/L_R$ on M_R independent of the relationship between $M_{\rm HI}/L_R$ and μ_{eff} then these contours will be inaccurate, however they seem to match the actual data for the galaxies fairly well. The HSB, low-luminosity galaxies can be seen here to fall in the same mass-range as the lower luminosity, LSB galaxies in the corner of the plot – these HSB galaxies could not be detected at much fainter luminosities due to their lower $M_{\rm HI}/L_R$ ratios, explaining why that corner of the BBD appears relatively underpopulated.

The unpopulated high-luminosity, LSB galaxies region is partly explained by the relationship between $M_{\rm HI}/L_R$ and μ_{eff} – these galaxies would have to have HI masses much greater than $M^\star_{\rm HI}$ and so would be

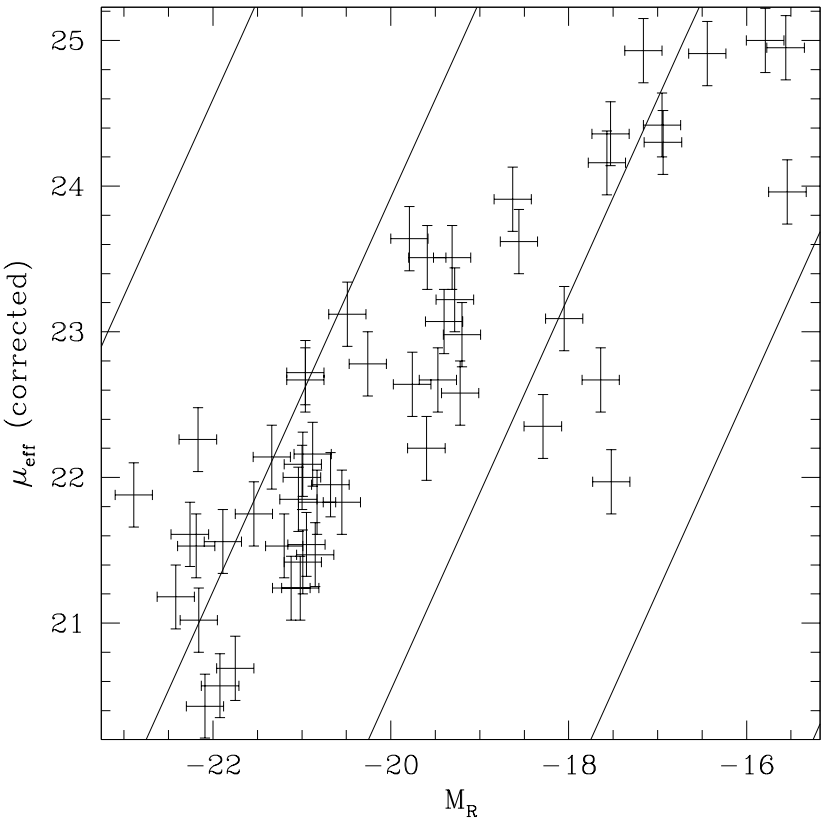

Figure 4.14: Distribution of galaxies by absolute R-band magnitude and effective surface-brightness, overlaid with contours of equal HI mass calculated using the relationship between $M_{\rm HI}/L_R$ and μ_{eff} found earlier. Contours go from $10^{11}M_\odot$ on the left through $10^{10}M_\odot$ and $10^9M_\odot$ to $10^8M_\odot$ on the right. It can be seen that this seems to explain the lack of HSB, low-luminosity galaxies as these have a lower HI mass and may partly explain the lack of LSB, high-luminosity galaxies, as these would be rare, high HI mass objects. There is still a definite lack of LSB, high-luminosity galaxies, however, that can not be explained in this way.

expected to be rare. However, it can be seen that those high HI mass galaxies that are found are almost entirely HSB galaxies and the slope of the limit of populated space is substantially shallower than the slope of constant HI mass, implying that the lack of high-luminosity, LSB galaxies can only be partly explained as an HI selection effect and that there is a real under-density of giant LSB galaxies compared to their HSB counterparts.

4.3 Optical parameters, HI flux, and estimated column densities

4.3.1 Dependence of HI flux on optical parameters

The unexpected result, described in Chapter 3, that the effective surface-brightness and the apparent magnitude are linked suggests that there is not a straight correlation between apparent magnitude and HI flux, but rather that the HI flux may depend on other parameters – in particular the size of the galaxy. Figure 4.15 shows the relationship between flux and apparent magnitude, it can be seen that although there is a trend for apparently brighter galaxies to have higher fluxes, this relationship has a very wide scatter.

Figure 4.16 shows that there is at least as good a correlation between effective radius and HI flux. This supports the idea that the average surface-density of HI does not change much, so optically larger galaxies with correspondingly larger HI discs have higher HI fluxes. If the central surface-brightness of galaxies was constant and the average surface-density of HI was constant, then a correspondence between optical and HI sizes would lead to a correspondence between optical luminosity and HI flux. However, the central surface-brightness of galaxies is not constant – although the observed central surface-brightness of a sample of galaxies often is. It is possible that observed correlations between luminosity and HI flux in optically-selected samples are due to surface-brightness selection effects.

4.3.2 Estimated HI column densities

It is possible to estimate the size of the HI disc from the optical size, and thus get an estimate of the HI column density. To do this, it is necessary to rely on data from optically-selected samples in order to relate the HI size of the galaxy to the effective radius. These relationships will therefore have been derived from samples with surface-brightnesses close to the Freeman value, and they may not be applicable to LSB galaxies.

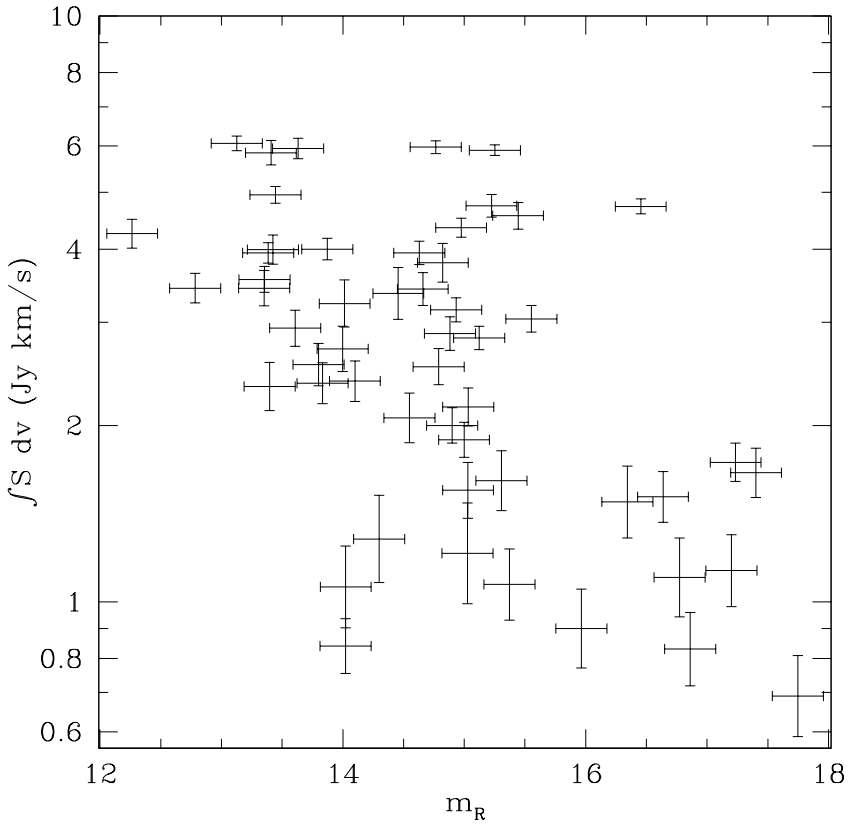

Figure 4.15: Correlation between apparent magnitude and HI flux. It can be seen that there is some correlation, although the scatter is large.

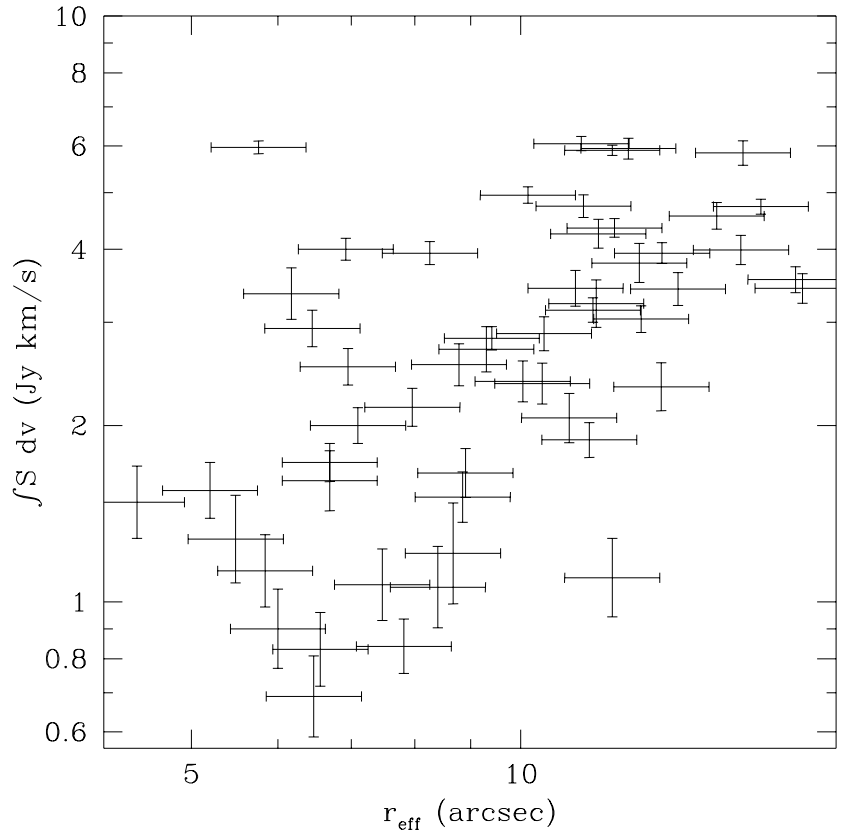

Figure 4.16: Correlation between effective radius and HI flux. As for apparent magnitude, there is some correlation but the scatter is large.

From the ESO-LV, which gives effective diameters and the diameter to the 25 Bμ isophote, it is possible to calculate that $r_{B25} \approx (2.15 \pm 0.67) \times r_{eff}$. Salpeter & Hoffman (1996) found that $r_{\rm HI} \approx (2.34 \pm 0.14) \times r_{B25}$, combining these gives:

$$r_{\rm HI} \approx (5.03 \pm 1.59) \times r_{eff} \tag{4.3}$$

This has been used to calculate the HI radius of the galaxies in DEEP and thus, by combining with their HI fluxes, the average column-density of HI in these galaxies. Figure 4.17 compares this to the effective surface-brightness of these galaxies. It can be seen that no galaxies have particularly low average column densities – even if the radii of the HI discs used are too small by a factor of 2 then the lowest column densities would still be around $10^{19.6}$ cm^{-2} and in order to reach the limiting column density of $\simeq 2 \times 10^{18}$ cm^{-2} the radii would have to be around 8 times larger or more.

Giovanelli & Haynes (1988) give values of $\log M_{\rm HI}/D^2_{Holm}$ (where D_{Holm} is the Holmberg diameter in kpc) for galaxies of different morphological types which are consistently around 6.8, or $\simeq 8 \times 10^{20}$ cm^{-2}. This should be approximately twice the value calculated here for $N_{\rm HI}$, and it does appear from the figures that most of the galaxies in DEEP have $N_{\rm HI} \simeq 4 \times 10^{20}$ cm^{-2}. The column densities from the DEEP sample appear, therefore, to be consistent with those from the optically-selected sample of Giovanelli & Haynes, despite having considerably higher values of $M_{\rm HI}/L_R$.

There is only a weak trend seen in Figure 4.17 for lower surface-brightness galaxies to have lower column densities. It could be that there is also a trend for $R_{\rm HI}/R_{eff}$ to increase with surface-brightness which would not be seen in this estimate. There is a lack of high column-density, low surface-brightness galaxies, but there are lower column-density galaxies seen across the whole range of surface-brightnesses. The best-fit gives $\log(N_{\rm HI}) = -0.09 \times \mu_{eff} + 22.2$ with a large scatter of 0.25 dex, or about a sixth of the total range in column densities.

Other comparisons with the estimated HI column density are given in Figure 4.18. Panel (a) shows a comparison between absolute magnitude and $N_{\rm HI}$: it can be seen that there is virtually no change in column-density across the range of brightnesses. There is a weak best-fit slope with $\log(N_{\rm HI}) \propto -0.03 \times M_R$, but this has an even larger scatter than the comparison with effective surface-brightness. Panel (b) shows HI mass against column-density: there does appear to be a possible relationship here with more massive galaxies having higher column-densities. The best-fit to this graph has $\log(N_{\rm HI}) = 0.26 \times \log(M_{\rm HI}) + 17.7$, again with a scatter of 0.25 dex.

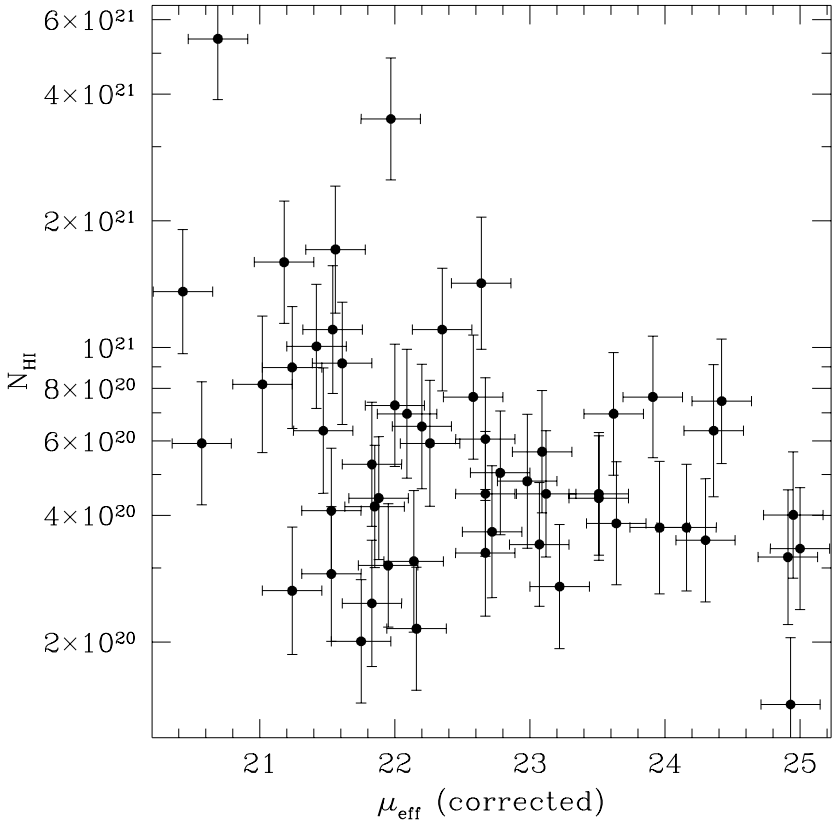

Figure 4.17: Comparison between effective surface-brightness and estimated average HI column-density. It can be seen that the lowest column densities are well above the detection limit for DEEP of $\simeq 2 \times 10^{18}$ cm^{-2}. This implies that there is no low column-density population of HI rich galaxies that would be missed in shallower surveys.

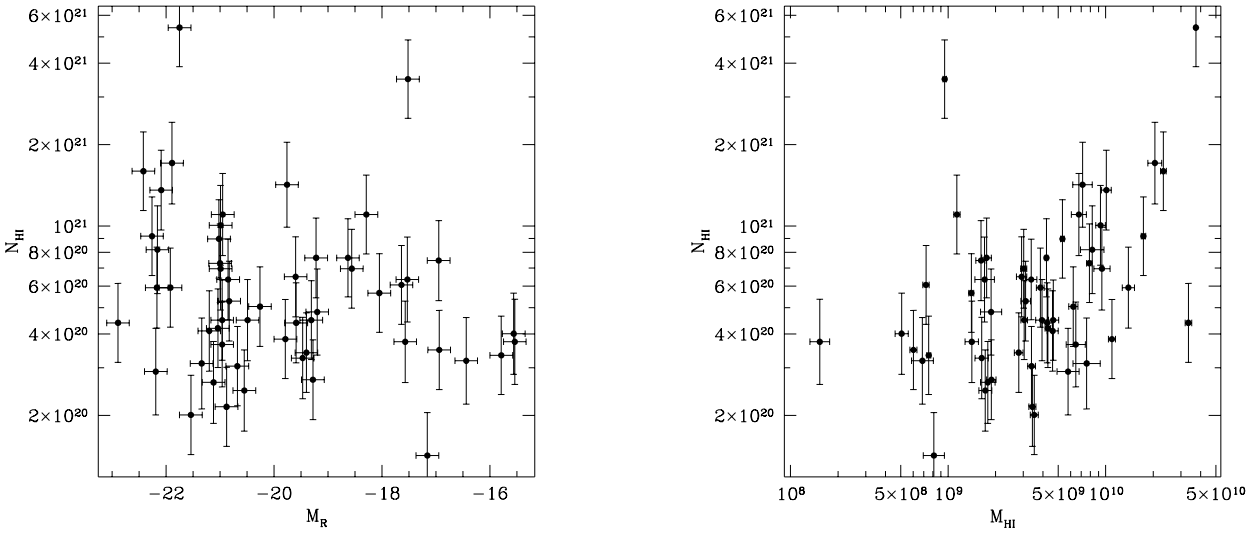

(a) Comparison between absolute magnitude and estimated average HI column-density

(b) Comparison between HI mass and estimated average column-density

Figure 4.18: Comparisons between other properties and estimated average HI column-density. It can be seen that there is no recognisable trend of column-density with absolute magnitude and only a very week trend with HI mass.

The scatter of 0.25 dex seen in two of these correlations is equivalent to a factor of 1.8 in column-density and so could be given by a scatter in $R_{\rm HI}/R_{eff}$ of 33%. This is not beyond the realms of possibility, Salpeter & Hoffman find a scatter of 10% in $R_{\rm HI}/R_{B25}$. so it is possible that either of these relationships could be tightened by a correlation of $R_{\rm HI}/R_{eff}$ with $M_{\rm HI}$ or μ_{eff}. Given the higher ratios of $M_{\rm HI}/L_R$ seen at lower surface-brightnesses, it would not seem unreasonable that there could be a similar change in the ratio of the radii. However, this is unlikely to cause a large enough change for any of these galaxies to be a truly low column-density system – it would appear that these do not exist or that if they do they have been ionized and can not be detected in HI.

4.4 'Peakiness' of HI profiles

It is possible that the HI profile shape is related to its surface-brightness. De Blok, McGaugh, & van der Hulst (1995) found that LSB galaxies are dominated by dark matter and have rotation curves which are rising at all radii, while 'normal' galaxies have flat rotation curves. This would be expected to lead to considerably more pronounced peaks on the HI profiles of 'normal' galaxies, where a large portion of the gas is travelling at the same velocity, than in LSB galaxies, where the gas is spread over a range of velocities.

In order to investigate this, I have defined a 'top hat' peak flux for each galaxy. This is the peak flux of a top hat profile with the same integrated flux and velocity width as the galaxy in question, e.g. $S_{tophat} = \int S\,{\rm d}v/\Delta V_{20}$. The 'peakiness' of the galaxy is then defined as its measured peak flux (S_{peak}) divided by the peak flux it would have if it had a top hat profile (S_{tophat}). For galaxies which have no well-defined peaks and approach a top hat shape this will be close to one, while for galaxies which have very pronounced peaks it will be considerably higher.

Figure 4.19 shows a comparison between the 'top hat' peak flux and the measured peak flux for each galaxy in DEEP. It can be seen that there is a general relationship between the two parameters, with some outliers above the line. However, the line does not appear to be a simple fit of the form $S_{peak} = k \times S_{tophat}$, which would imply the same general 'peakiness' at all peak fluxes, instead the line is best fit by $S_{peak} = 3.5 \times S_{tophat}^{3/4}$.

This implies that the peakiness is higher at lower peak fluxes, as is shown in Figure 4.20. The unpopulated region at low peak flux and low peakiness is consistent with this relationship between S_{peak} and S_{tophat}. However, it is hard to see what physical mechanism could cause this relationship, the unpopulated

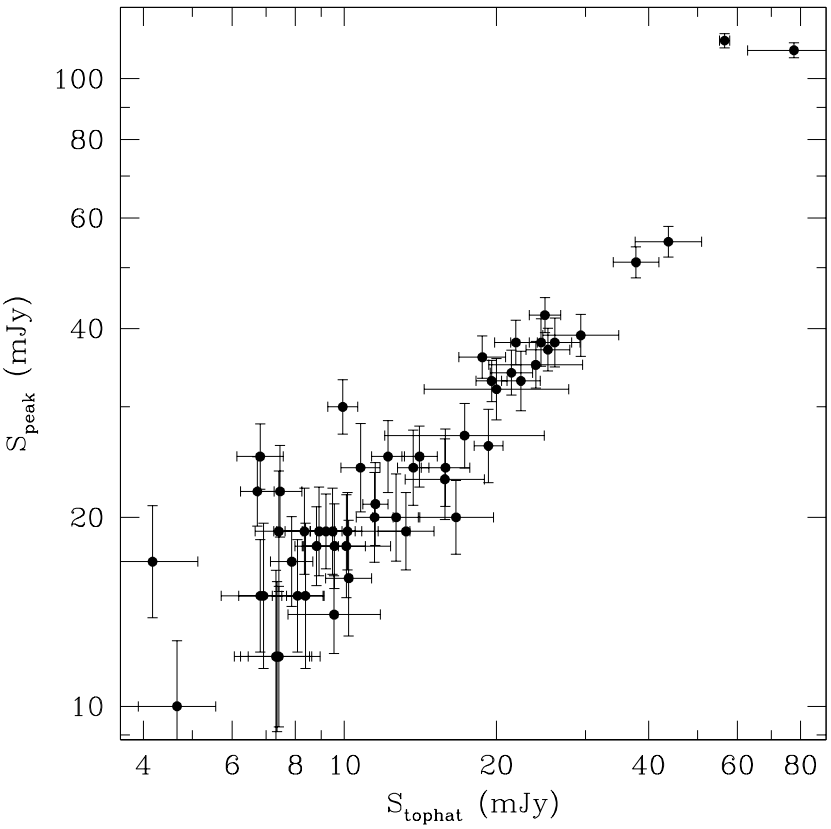

Figure 4.19: Top hat peak fluxes versus measured peak fluxes. It can be seen that there is a relationship between the two values, as would be expected. However, it is not linear but is rather $S_{peak} = 3.5 \times S_{tophat}^{3/4}$. This implies that the peakiness falls with increasing peak flux.

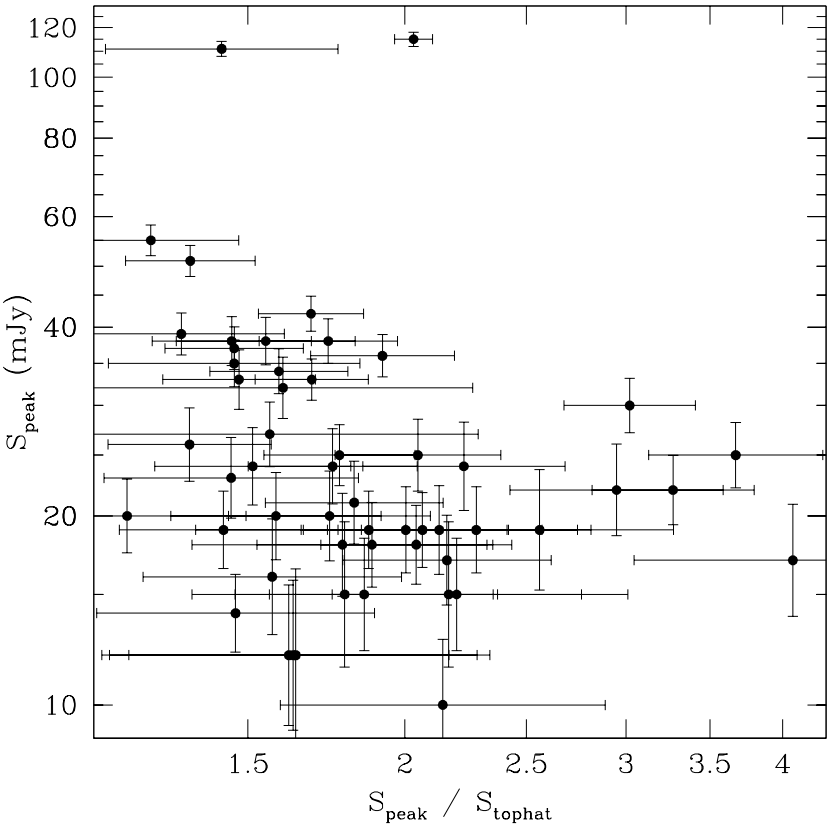

Figure 4.20: Variation of peakiness with peak flux. This shows more clearly than Figure 4.19 that galaxies with higher peak fluxes have a lower peakiness – implying that they are closer to top hat profiles in shape.

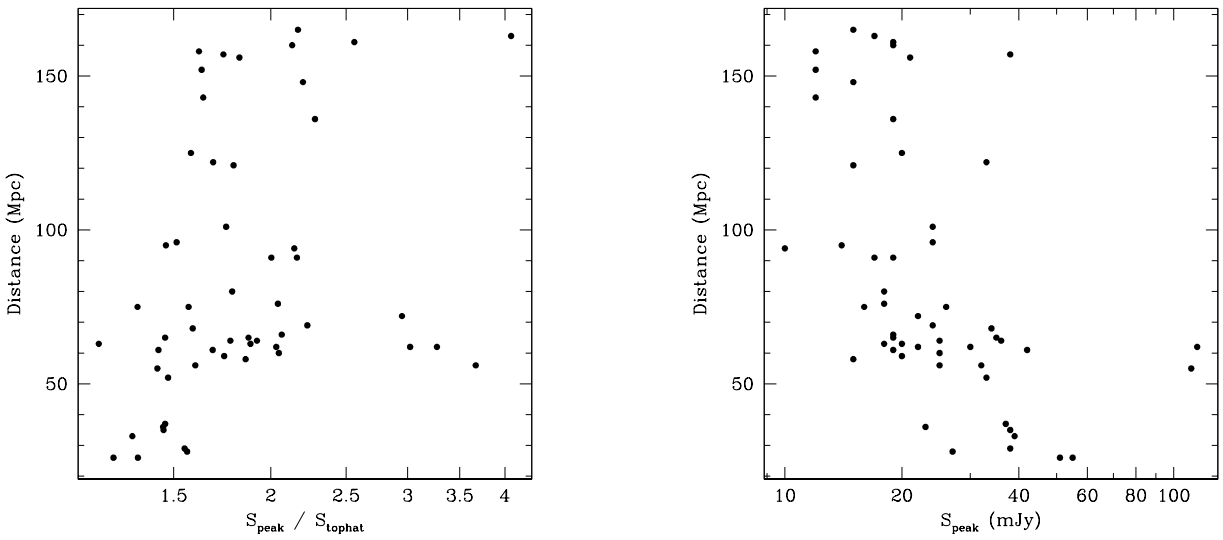

(a) Variation of peakiness with distance

(b) Correlation of peak flux with distance

Figure 4.21: Effect of distance on peakiness and peak flux. This demonstrates that the lower peak flux, higher peakiness sources are found at greater distances. As the DEEP galaxies are selected primarily by signal to noise rather than by peak flux, wider galaxies will have lower peak fluxes. Due to the relationship between $M_{\rm HI}$ and ΔV, these wider galaxies will be more massive and will generally be seen at greater distances. If these more massive galaxies also tend to be more peaky, this then explains the relationship between peakiness and distance and the selection effect that causes galaxies with higher peak fluxes to have relatively lower peakiness.

region cannot be explained by signal to noise considerations. These would be expected to depopulate the high peakiness, low peak flux corner of the graph. It would appear that it is a selection effect. Panel (a) of Figure 4.21 shows that the low peakiness sources which are absent from the low peak flux region are also absent from the more distant regions of the survey. Panel (b) shows also that the peak fluxes of these more distant sources are lower, confirming this result.

So, why do we find this result in Figure 4.21? The answer is quite simple – the DEEP sample has been selected by signal to noise ratio rather than peak flux, therefore wider galaxies will have lower peak fluxes. These wider galaxies are normally more massive galaxies, due to the relationship between $M_{\rm HI}$ and ΔV,

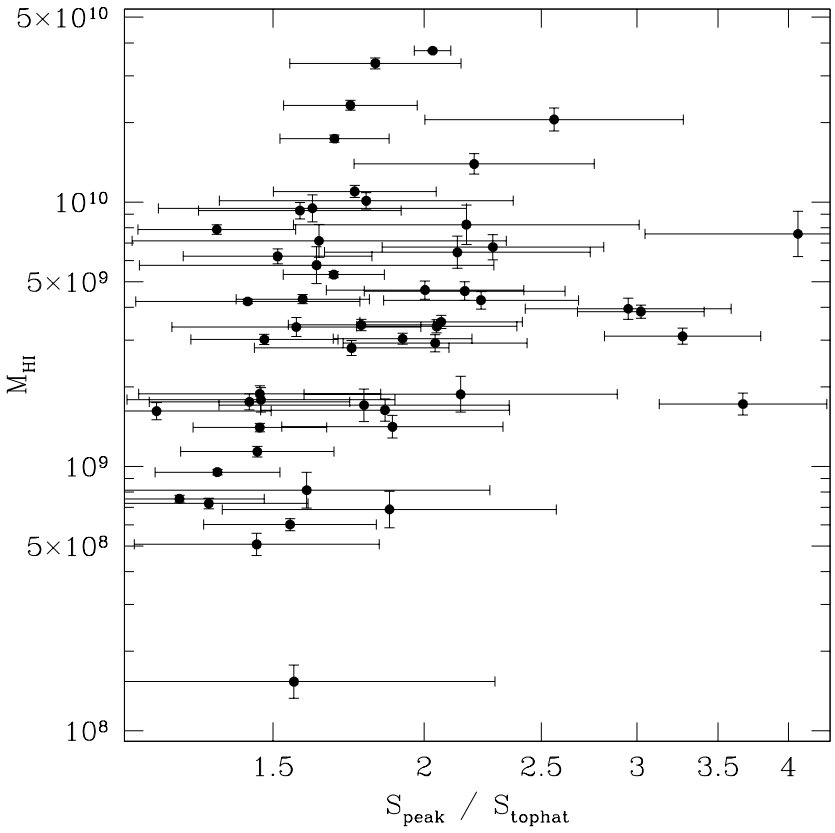

Figure 4.22: Peakiness versus HI mass. There may be a weak trend in this graph – all the sources with peakiness > 2 have $M_{\rm HI} > 10^9 M_\odot$ and all the sources with peakiness < 1.5 have $M_{\rm HI} < 10^{10} M_\odot$ – but it is inconclusive.

which will generally be seen further away. This explains the relationship between peak flux and distance, but the relationship between peakiness and distance requires one further step – more massive galaxies must be more peaky. This may be the case, as can be seen in Figure 4.22.

This would fit in with the hypothesis that peaky galaxies tend to be higher surface-brightness galaxies, as we have already seen that more massive galaxies tend to have higher surface-brightnesses. That peakiness and surface-brightness are related is investigated in Figure 4.23. It appears that there is a paucity of peaky, LSB galaxies, however it can not be statistically shown that there is a difference between the surface-brightness distributions of the full sample and of a high-peakiness sub-sample. It seems likely that a larger

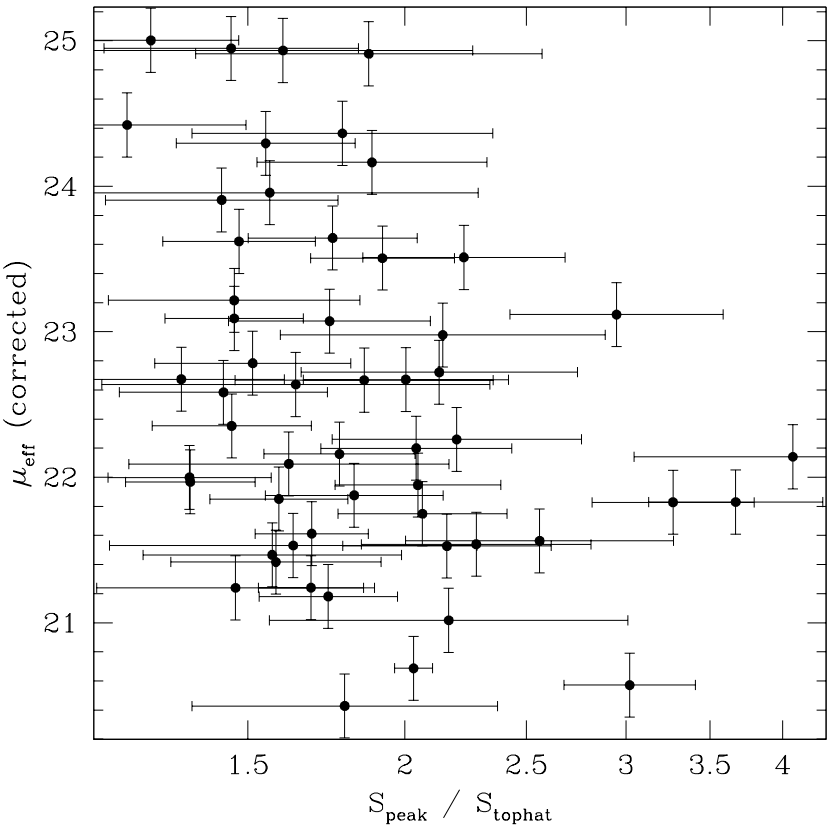

Figure 4.23: Comparison between peakiness and effective surface-brightness. There may be a very weak trend here – there definitely seems to be a lack of very peaky LSB galaxies – but there is no statistically significant difference between the distribution of surface brightnesses from a high peakiness (> 2.5) sub-sample and that of the full DEEP sample.

sample would allow a statistical difference to be shown.

If massive, high surface-brightness galaxies were peakier, they would be more easily detected in a peak flux limited sample, such as the HIPASS Bright Galaxy Catalogue (Koribalski 2001; BGC). Dwarf and low surface-brightness galaxies with the same total flux would be less likely to be detected, and those that were would tend to have relatively high total fluxes and are thus likely to have fairly large optical sizes and bright optical magnitudes, and therefore likely to be previously catalogued. This would lead to the result that a larger proportion of galaxies in an HI catalogue such as the BGC would be previously catalogued than in a

signal to noise limited catalogue.

4.5 Tully–Fisher relationships

The Tully–Fisher relationship is a relationship between the inclination-corrected optical magnitude of galaxies and their inclination-corrected rotation velocity. It was originally calibrated by Tully & Fisher (1977) using photographic magnitudes for local group, M81, and M101 group galaxies from Holmberg (1958), and HI observations from a number of sources. It can be used as a distance indicator, as the velocity width is measured independently of distance, while the absolute magnitude is distance dependent. The distance to the galaxy can be estimated by finding the distance necessary to correct the observed apparent magnitude to the absolute magnitude predicted by the velocity width.

The application of the Tully-Fisher (TF) relationship to various types of galaxies has been discussed recently. Zwaan et al. (1995) found that LSB galaxies seemed to fall on the same TF relationship as 'normal' galaxies, however other authors have found types of galaxies that deviate from this. Matthews, van Driel, & Gallagher (1998) found that most of their sample of extremely late-type, low-luminosity spirals fell below the standard TF relationship, with the deviation increasing with decreasing size and luminosity. O'Neil, Bothun, & Schombert (2000) found deviations in high velocity-width ($\Delta V > 200 \mathrm{km s}^{-1}$) galaxies, with these deviations increasing with increasing HI mass to light ratio, and McGaugh et al. (2000) found deviations from the TF relationship for galaxies widths less than 180 $\mathrm{km s}^{-1}$.

McGaugh et al. (2000) proposed a baryonic TF relationship to account for the deviations they saw. They found that if the TF relationship was constructed using $M_{bary} = M_{\star} + M_{gas}$ rather than the optical luminosity, the deviations vanished. The TF relationship for the DEEP galaxies has been investigated both in R-band, where the results of Courteau (1997) and Burton et al. (2001) are used for comparison, and as a baryonic relationship, following the method of McGaugh et al. (2000). The results of this are presented below.

In order to investigate the Tully-Fisher relationship for the DEEP sources, it is necessary to make an estimate of their inclination. This has been done from the optical axis ratio given by SExtractor (see Chapter 3) and equation 4.4 from Holmberg (1958)

$$\cos^2 i = \frac{(b/a)^2 - r_0^2}{1 - r_0^2} \tag{4.4}$$

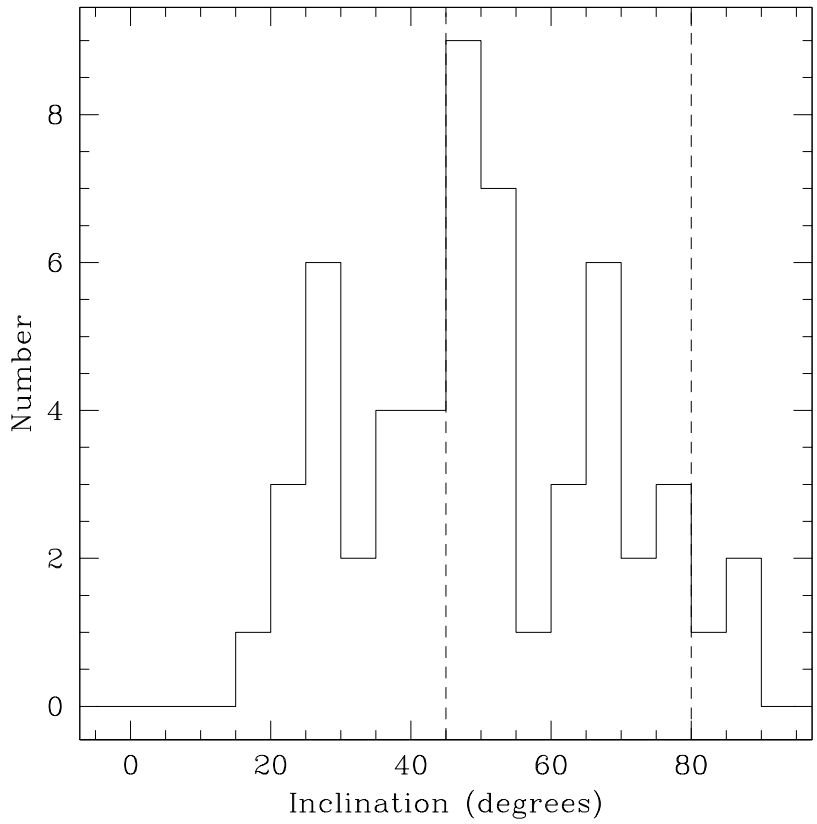

Figure 4.24: Distribution of inclinations. The dashed lines at 45° and 80° indicate the boundaries of the range of inclinations taken as useful for analysing Tully-Fisher relationships, only the 31 galaxies within this region were used to determine the R-band and baryonic TF relationships for DEEP.

where r_0 is the assumed axial ratio of an edge-on system. This is an unknown value which falls in the range 0.11 – 0.20. I have assumed a value of 0.16 with the errors on the inclinations modified to take the possible range of values into account – this makes very little difference except for very edge-on systems. Only those systems where the implied inclination was between 45° and 80° were used for defining the Tully-Fisher relationship, as this is where the inclinations are most reliable, but inclinations have been found for all the DEEP galaxies. The distribution of inclinations is given in Figure 4.24. The velocity widths were corrected using equation 4.5 from Tully & Fisher (1977)

$$\Delta V(0) = \frac{\Delta V_{20}}{\sin i} \tag{4.5}$$

where $\Delta V(0)$ is the corrected velocity width. The errors of $\Delta V(0)$ have been estimated using the error of 16 $\mathrm{km\,s^{-1}}$ on the velocity width and an assumed error of 10% in b/a. I follow Burton et al (2001) by using $\eta = \log \Delta V(0) - 2.5$ in defining the TF relationship as $M_R(c) = \Delta TF + \alpha_{TF}\eta$. The absolute magnitudes of the galaxies were corrected according to the prescription of Courteau (1997), who used $M_R(c) = M_R - A_{i,R}$ where the internal absorption, $A_{i,R}$ is given by

$$A_{i,R} = 0.95\,[\log(a/b) - 0.418] \tag{4.6}$$

This corrects all the galaxies to the magnitude they would have at an inclination of 70°. However, this makes no allowance for the surface-brightness of galaxies – LSB galaxies are thought to contain less dust than 'normal' galaxies, which would lead to them having a smaller internal extinction and thus being overcorrected here and appearing brighter than they truely are. As most LSB galaxies are low-luminosity galaxies, this would have the effect of making the slope of the TF relationship shallower.

The Tully-Fisher relationship found is given in Figure 4.25. The filled circles with solid error bars indicate galaxies in the inclination range of 45° – 80°, while the open circles with dotted error bars indicate galaxies outside this useful range. The weighted best-fit relationship, found using only the galaxies in the useful inclination range, is indicated by the solid line, while the long dashed line indicates the best-fit line of Courteau (1997) and the short dashed line indicates the 3σ scatter around this line. It can be seen that the DEEP data is fairly strongly inconsistent with the fit of Courteau (1997), with 9 out of 31 galaxies in the inclination range 45° – 80° falling outside these 3σ limits. However, this may be due to the Courteau sample being selected strictly by morphological type while no such selection has been placed on the DEEP sample.

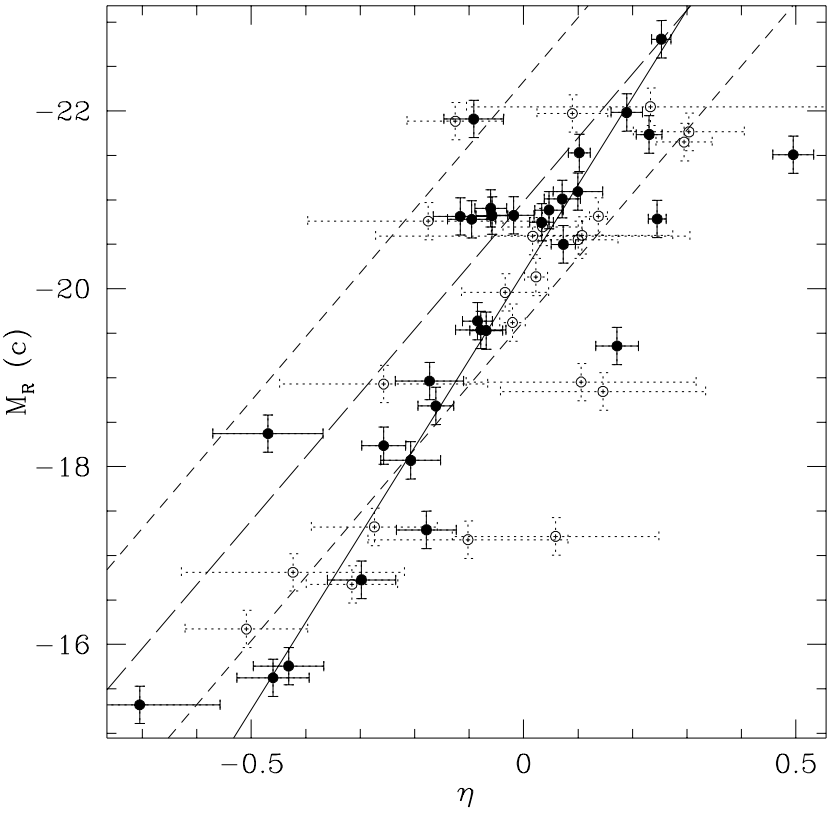

Figure 4.25: Tully–Fisher relationship for DEEP galaxies. Filled circles with solid error-bars indicate galaxies in the range 45° – 80° used for fitting, open circles with dotted error-bars indicate galaxies outside this useful range. The solid line indicates the weighted best-fit to the DEEP galaxies, the long-dashed line indicates the best-fit of Courteau (1997) and the short-dashed lines indicate the 3σ scatter around this best-fit. 9 out of 31 DEEP galaxies within the useful inclination range fall outside of this 3σ limits, however the slopes of the best fit lines are consistent at the 2σ level.

Table 4.2: Tully-Fisher parameters

Sample	α_{TF}	Δ_{TF}	σ_{TF}
DEEP	-9.84 ± 1.32	-20.18 ± 0.03	1.19
B01	-3.77 ± 0.55	-20.27 ± 0.40	0.94 ± 0.15
B01 (no outliers)	-5.58 ± 0.50	-20.76 ± 0.15	0.56 ± 0.07
C97	-7.18 ± 0.26	-20.98 ± 0.05	0.45 ± 0.03

The details of the best fit are given in Table 4.2, with the scatter around the best fit given as σ_{TF}. The table also gives the parameters from Burton et al. (2001; B01) and Courteau (1997; C97), as corrected to R-band by Burton et al., as a comparison. Burton et al. used $H_0 = 70$ Mpc^{-1} km s^{-1}, while I have used $H_0 = 75$ Mpc^{-1} km s^{-1}, the zero-points (Δ_{TF}) from the literature have therefore been corrected by 0.15 mags to bring them in line with this. It should be noted that the very small error in Δ_{TF} is primarily due to the weighted mean of the DEEP data being very close to $\eta = 0$, the scatter in magnitudes is given by σ_{TF}. The best fit slope is less than 1.5σ from best fit of Courteau (1997), and just over 2σ from the 'no-outliers' slope of Burton et al (2001). The TF relationship found for the DEEP galaxies is therefore not inconsistent with previous values from the literature. The TF relationship for DEEP is also statistically indistinguishable from a slope of -10, which would give $L_R \propto V(0)^4$ – fitting theoretical predictions of what the TF relationship should be.

It is possible that a 'baryonic' TF relationship for the DEEP galaxies may provide a better fit. The residuals of the DEEP galaxies to the the Courteau (1997) TF relationship are given in Figure 4.26 and show a weak trend for the residuals to increase with increasing HI mass to light ratio, implying that a baryonic correction may well bring the DEEP data closer to the literature values for the TF relationship.

The baryonic mass for the DEEP galaxies has been found by combining the HI mass and optical luminosity using:

$$M_{bary} = 1.4 M_{\rm HI} + \Upsilon^R_\star L_R \tag{4.7}$$

where $\Upsilon^R_\star$ is the stellar mass to R-band light. This has been estimated, as in McGaugh et al. (2000) using the model of de Jong (1996) for a 12 Gyr old, solar metallicity stellar population with a constant star formation rate and a Salpeter initial mass function, corrected to R-band using the average colours in that paper (also

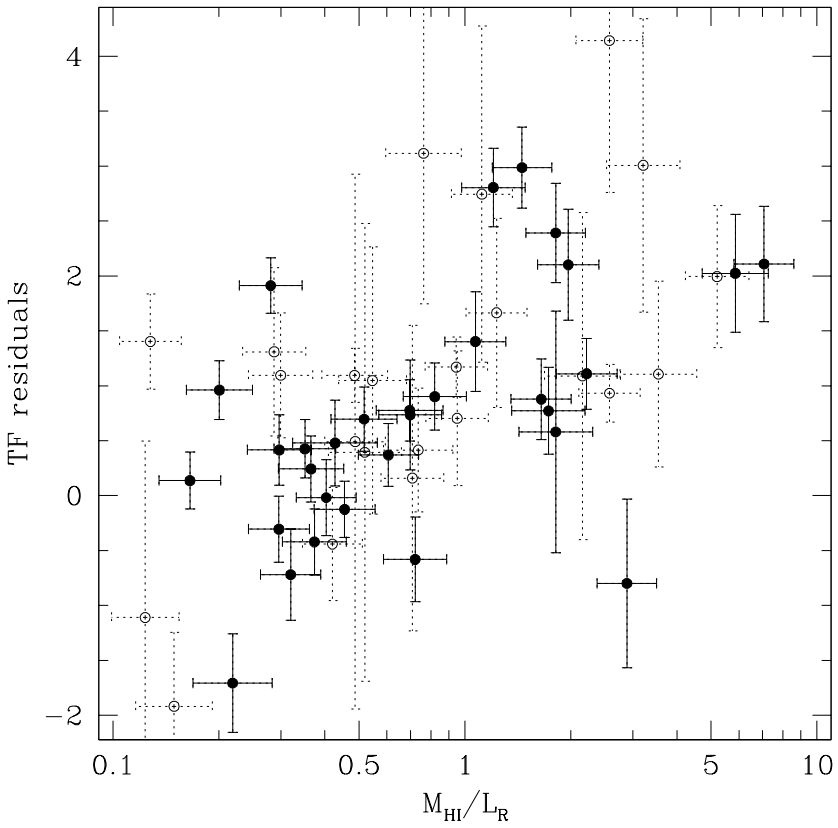

Figure 4.26: Residuals of the DEEP galaxies to the Courteau (1997) TF relationship against HI mass to light ratio. It can be seen that there is a trend of increasing residuals with increasing $M_{\rm HI}/L_R$, implying that a baryonic correction may well reduce the residuals.

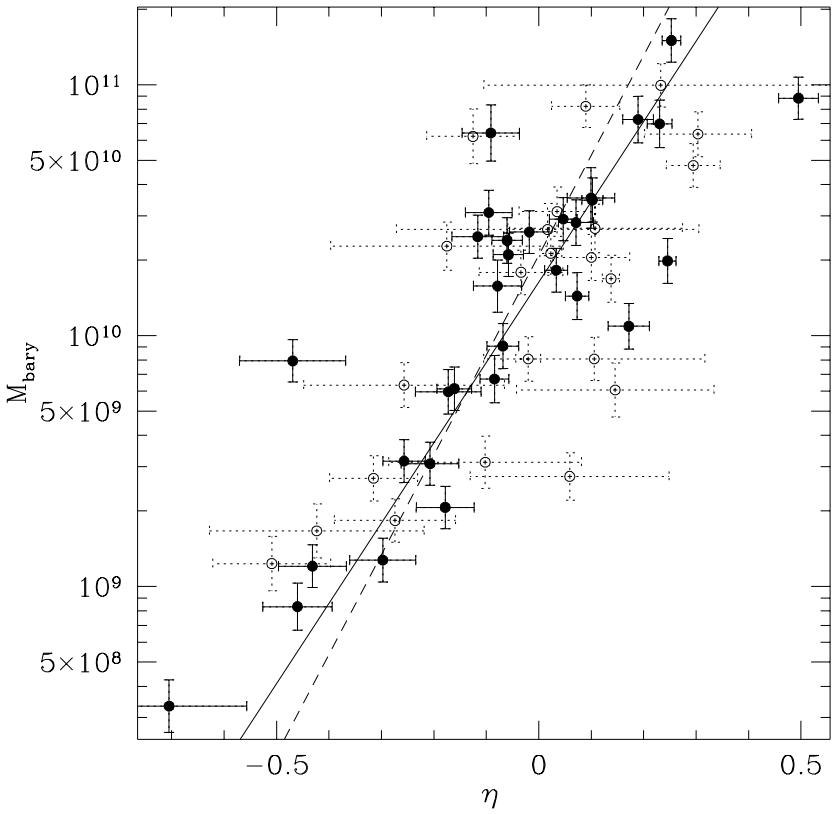

Figure 4.27: Baryonic Tully-Fisher relationship for DEEP galaxies. The solid and open circles indicate galaxies within and outside the useful inclination ranges respectively, as in Figure 4.25. The solid line shows the best-fit to the DEEP data, and the dashed line shows the best-fit of McGaugh et al. (2000).

used by McGaugh et al. for their correction to H-band). This gives a value of $\Upsilon_\star^R \approx 1.4$, which I have used in my calculations.

Once the baryonic mass has been calculated, the baryonic TF relationship may be found. This is given in Figure 4.27. The line indicates the weighted best-fit, which gives $\log(M_{bary}) = (3.20 \pm 0.42) \times \eta + (10.213 \pm 0.068) \pm 0.379$. The dashed line indicates the best-fit of McGaugh et al. (2000) who found $\log(M_{bary}) = (3.98 \pm 0.12) \times V_c + (1.57 \pm 0.25)$ (or $\log(M_{bary}) = (3.98 \pm 0.12) \times \eta + (10.32 \pm 0.01)$), where V_c is the circular velocity of the galaxies, $V_c = \Delta V(0)/2$. The best-fit line is within 2σ of both the best-fit of McGaugh et al. (2000) and a slope of precisely 4. For a slope of 4, McGaugh et al. find $M_{bary} = 35V_c^4$,

while the DEEP data gives $M_{bary} = 25V_c^4$. As the DEEP data has a scatter of 0.379 dex (or $\approx 240\%$) these normalisations are statistically indistinguishable.

The DEEP data is consistent with both previous optical and baryonic TF relationships. The baryonic TF found appears too shallow, indicating possibly that the correction to the optical luminosity and HI mass has not been made correctly – it would not be particularly surprising if this was the case. Were a higher value of $\Upsilon_\star^R$ to be used, the slope would be steeper and thus closer to that of McGaugh et al. (2000). The trend in the residuals to the optical TF relationship definitely implies that a correction of some form should be made for the HI content of the DEEP galaxies. This effect is more pronounced in the DEEP sample than it would be in an optically-selected sample due to the higher proportion of HI rich galaxies.

4.6 Dynamical masses

It is possibly to make a rough estimate of the dynamical masses of the DEEP galaxies using the equation:

$$M_{dyn} = \frac{R_{\rm HI} \times (\Delta V(0))^2}{\rm G} \tag{4.8}$$

I have estimated $R_{\rm HI}$ as in Section 4.3 using $r_{\rm HI} = 5.03 \pm 1.59 \times r_{eff}$ and converted the result to kpc using the distances to the DEEP galaxies. $\Delta V(0)$ has been calculated using the same method as for the Tully-Fisher relationship in Section 4.5. The distribution of dynamical masses is shown in Figure 4.28.

Figure 4.29 shows the relationship between the approximate dynamical mass of the DEEP galaxies and HI mass to light ratio of these galaxies. As $M_{\rm HI}/L_R$ is distance independent, this correlation could not be directly due to distance dependence. However, that the HI mass to light ratio is larger in galaxies with smaller dynamical masses is expected, as similar relationships between the HI mass to light ratio and luminosity HI mass have already been seen.

Figure 4.30 shows how the surface-brightness of galaxies varies with dynamical mass. It can be seen that there is a loose correlation here, with the more massive galaxies having higher surface-brightnesses. This is expected, as similar correlations have already been seen between surface-brightness and HI mass and optical luminosity. However, there are some giant galaxies with low effective surface-brightnesses – ESO 445-G048, one of the 12 galaxies with $M_{dyn} > 10^{12} M_\odot$, is an LSB galaxies with $\mu_{eff}(corrected) = 23.5$ Rμ and other LSB galaxies (including the galaxy ESO 383-G059 identified as an LSB giant by HI mass) are only a little smaller than this. While this is similar to the result for $M_{\rm HI}$, it is very different from the result for L_R. It

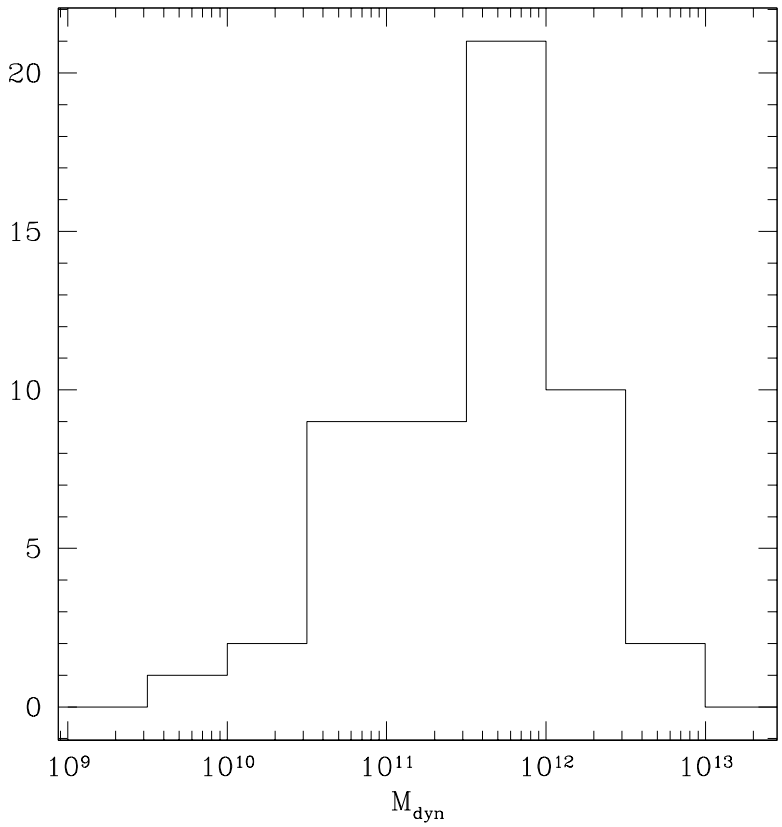

Figure 4.28: Distribution of approximate dynamical masses in units of solar mass. The distribution is similar in shape to the distributions of HI mass and of absolute magnitude and has a total width of 3.5 dex.

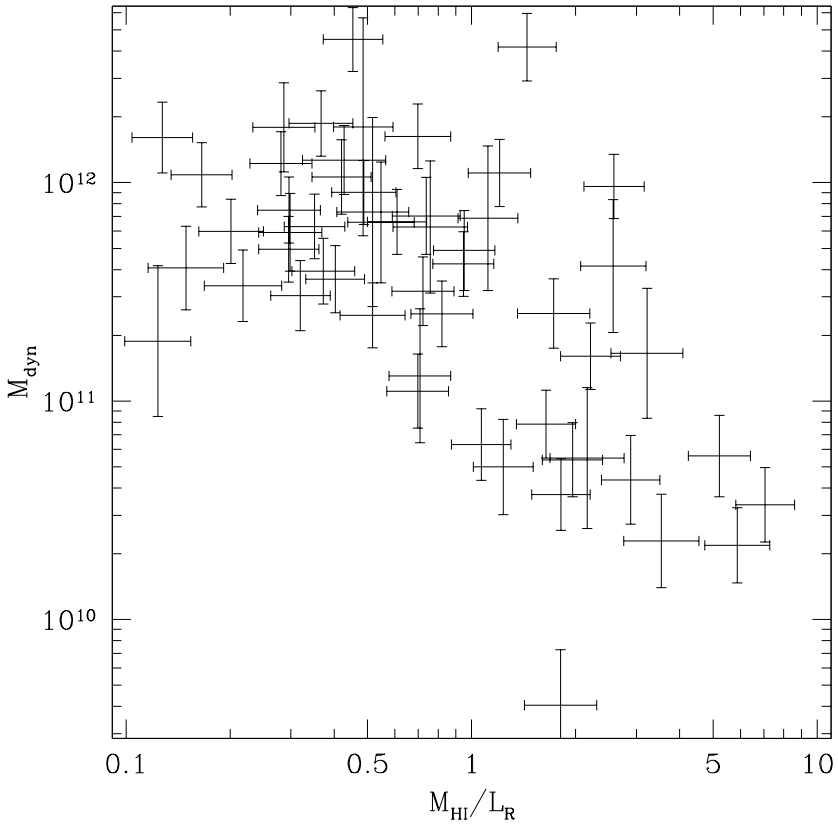

Figure 4.29: Variation of HI mass to light ratio with approximate dynamical mass. It can be seen that there is a trend for less massive galaxies to have higher HI mass to light ratios, although there are some large, HI rich galaxies – including the second most massive galaxy in DEEP. There are no low-mass ($M_{dyn} < 10^{11} M_{\odot}$) galaxies with $M_{\rm HI}/L_R < 1$ – all the low-mass galaxies found in DEEP are gas-rich.

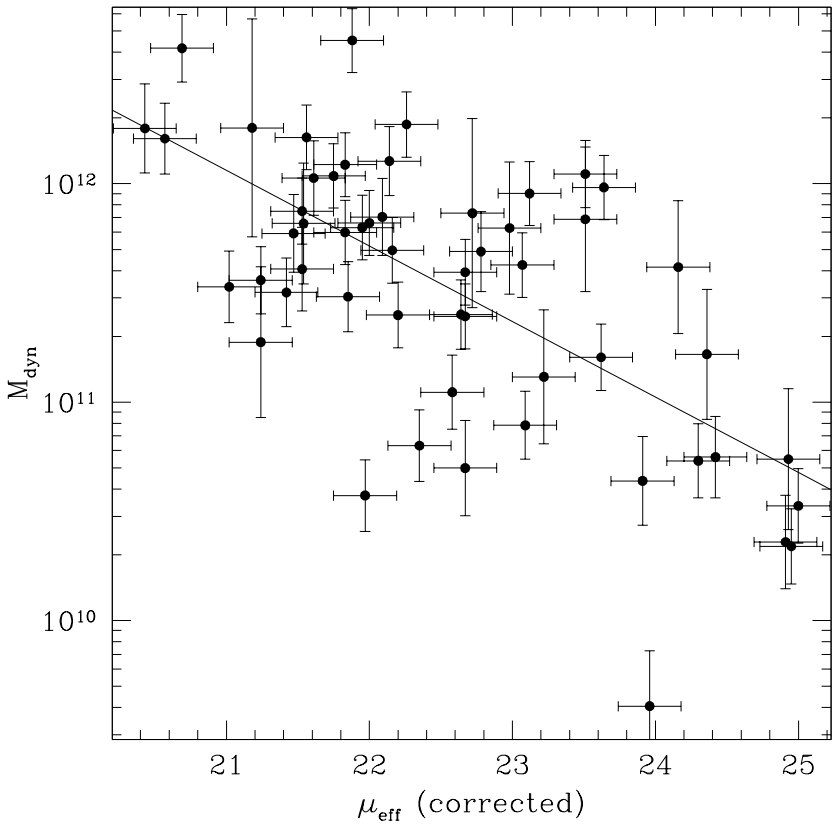

Figure 4.30: Variation of surface-brightness with approximate dynamical mass. There is a loose correlation seen here, however giant galaxies with $M_{dyn} \gtrsim 10^{12} M_{\odot}$ can be found. ESO 445-G048, with $\mu_{eff}(corrected) = 23.5$ Rμ is the largest LSB galaxy, but others, including the HI-Giant ESO 383-G059, also have masses close to $10^{12} M_{\odot}$. This rather loose correlation is similar to that seen for $M_{\rm HI}$ but very different from that seen for L_R – large LSB galaxies are not identified as such by their optical properties, even when they contain very large amounts of neutral hydrogen or have very high dynamical masses.

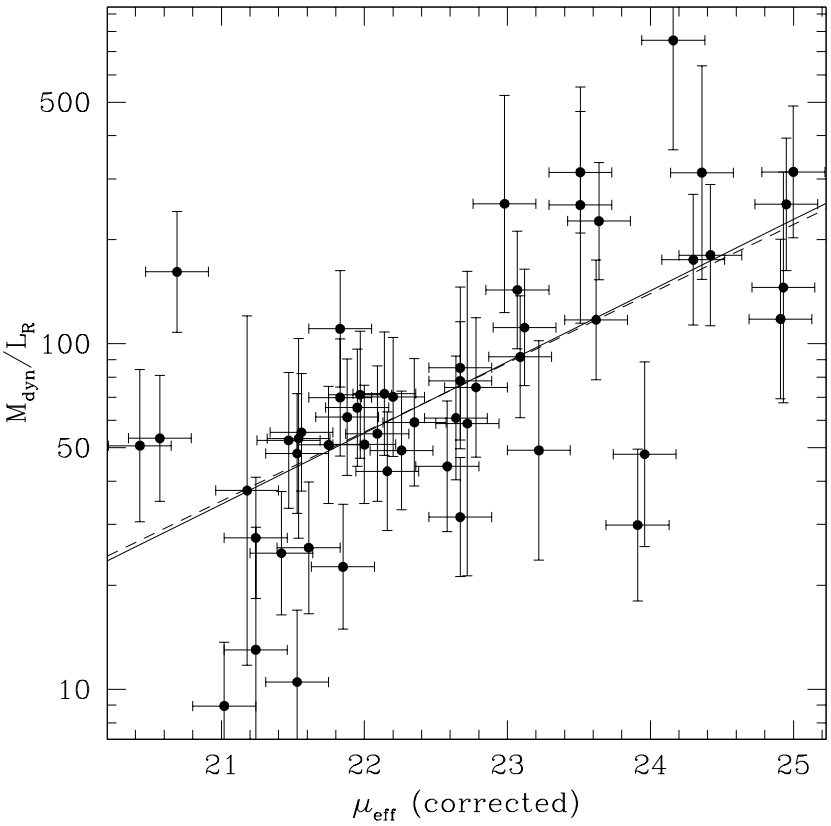

Figure 4.31: Variation of the mass to light ratio with effective surface-brightness. Solid line shows the best-fit to the data, dashed line shows the slope predicted by the $\Upsilon\Sigma$-relation ($\Upsilon^2\Sigma$ = constant, where $\mu \propto -2.5 \log \Sigma$), scaled to pass through the mean of the data.

appears that LSB galaxies can be 'giant' in the sense of containing a lot of mass or neutral hydrogen without meeting the standard definition of a giant galaxy – having a high luminosity.

Figure 4.31 shows the relationship between the dynamical mass to light ratio (M_{dyn}/L_R) and the effective surface-brightness. There is a lot of scatter in this relationship, but it is clearly present. The best-fit is shown by a solid line and the prediction from the $\Upsilon\Sigma$-relation (Zwaan et al. 1995) is shown as a dashed line, scaled to pass through the mean of the data points. The best fit, with a gradient of 0.21 ± 0.03 is statistically indistinguishable from the predicted gradient of 0.2. This is in agreement with the result found by de Blok, McGaugh, & van der Hulst (1996) using radio synthesis imaging to map the HI distribution of

galaxies and thus accurately determine their dynamical masses.

The $\Upsilon\Sigma$ relation was derived by Zwaan et al. 1995 as a necessary consequence of their result that LSB and 'normal' galaxies sat on the same TF relationship. It is derived from $M_{dyn} \propto V(0)^2 h$, where h is the scale-length of the disc and thus indicitive of the size of the galaxy, and $L_T \propto \Sigma_0 h^2$, where Σ_0 is the central surface-brightness in linear intensity units and L_T is the total luminosity of the galaxy. From these, it can be seen that

$$V(0)^4 \propto \frac{M_{dyn}^2}{h^2} \propto \frac{M_{dyn}^2 \Sigma_0}{L_T} \tag{4.9}$$

(Equation 1 in Zwaan et al. 1995) which can be rearranged to give

$$L_T \propto \frac{V(0)^4}{\Sigma_0 (M_{dyn}/L_T)^2} \tag{4.10}$$

(Equation 2 in Zwaan et al. 1995). For the Tully-Fisher relation, $L_T \propto V(0)^4$, to hold for all galaxies as Σ_0 varies, it is therefore necessary that $\Sigma_0 (M_{dyn}/L_T)^2$ (or $\Sigma\Upsilon^2$) remains constant.

Figure 4.32 shows the variation of the ratio of dynamical mass to baryonic mass with surface-brightness. The best fit is shown as a solid line, this has the form $\log(M_{dyn}/M_{bary}) = (0.06 \pm 0.03) \times \mu_{eff}(c) - (0.2 \pm 0.7) \pm 0.3$. There is a lot of scatter in the relationship, which slightly favours a baryon fraction falling towards lower surface-brightnesses but is only 2σ away from being totally flat. The total contribution of the baryonic matter, both in stars and in gas, therefore remains almost constant at around 2 – 5% although there is a very large scatter with values in DEEP ranging from around 20% down to less than 1%.

4.7 Importance of LSB galaxies

The SBD for the DEEP galaxies found in Section 4.2 has the form of

$$\log(\phi) = (1.13 \pm 0.04) \times \mu_{eff} - (25.1 \pm 0.9) \text{ for } \mu_{eff} < \mu_{eff}^{\star} \tag{4.11}$$

and

$$\log(\phi) = (0.17 \pm 0.15) \times \mu_{eff} - (4.4 \pm 3.4) \text{ for } \mu_{eff} > \mu_{eff}^{\star} \tag{4.12}$$

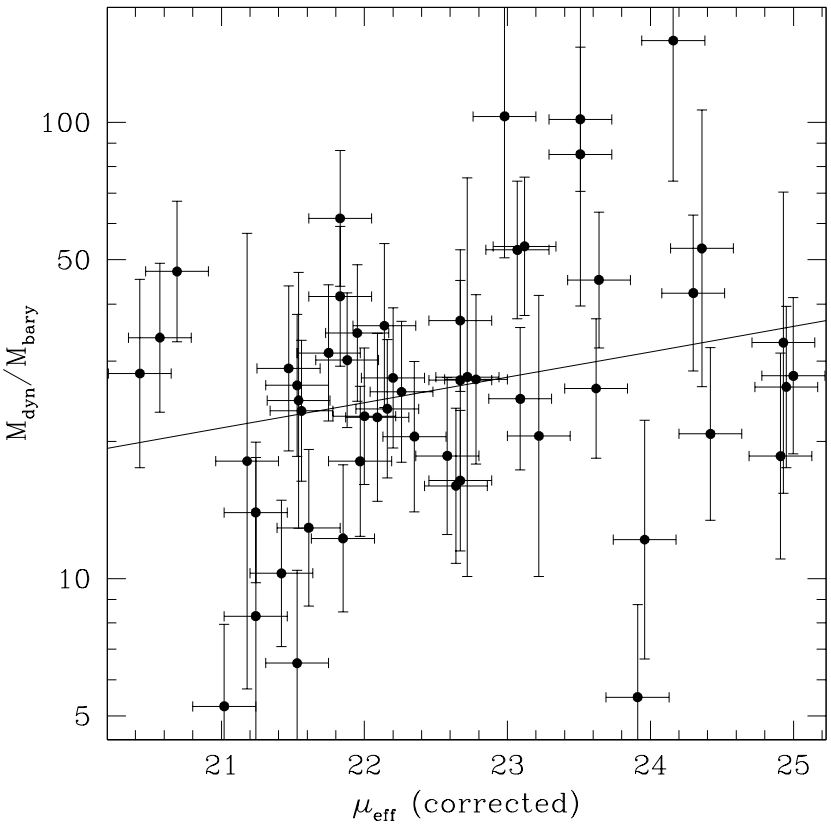

Figure 4.32: Variation of the ratio of dynamical mass to baryonic mass with surface-brightness. The solid line indicates the best fit, it can be seen that this favours the baryon fraction to be slowly falling towards lower surface-brightnesses, but this is only 2σ away from a constant baryon fraction.

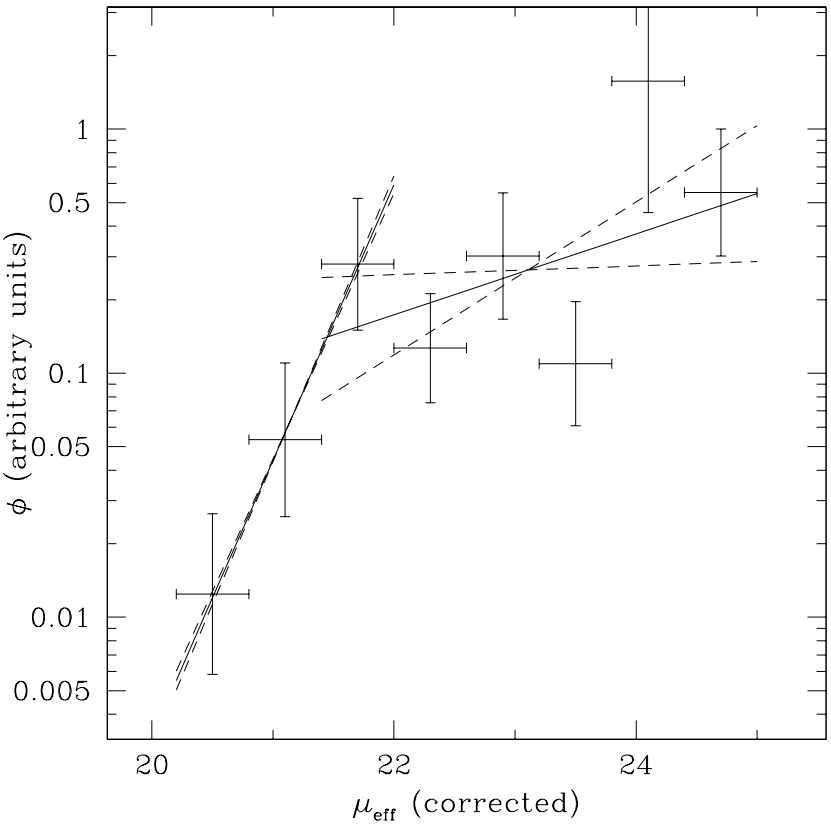

Figure 4.33: Surface-brightness distribution of DEEP galaxies. The rising slope towards lower surface-brightnesses implies that if this continues indefinitely the number of LSB galaxies would be infinite – an obviously not physical situation. However, even within the range of surface-brightnesses here LSB galaxies make up the majority ofgas-rich galaxies in the Universe.

where ϕ is in arbitrary units of number of galaxies per logarithmic surface-brightness bin.

This SBD (Figure 4.33) implies that the number density of galaxies is divergent towards lower surface-brightnesses, the integral under the SBD is infinite. This is still the case at the 1σ limits of the SBD as the numbers per logarithmic mass bin are still rising , albeit more slowly. Although this is obviously non-physical – there cannot be an infinite number density of extremely LSB galaxies – the implication is that LSB galaxies dominate the number density of gas-rich galaxies in the Universe. A similar situation can be seen in the luminosity function where low-luminosity galaxies dominate the number density (although not

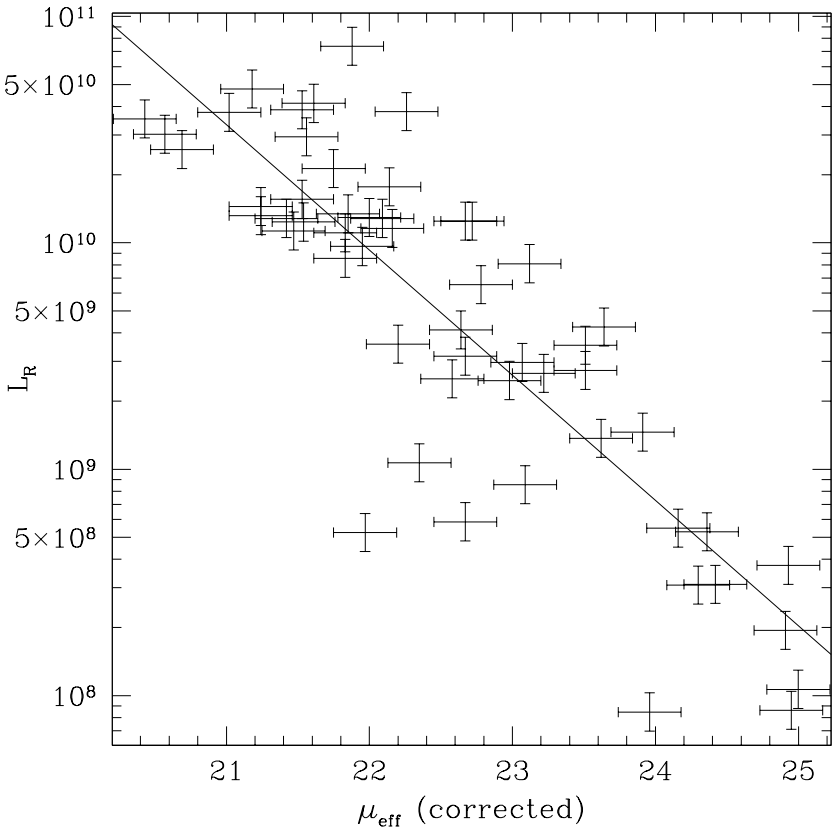

Figure 4.34: Luminosity – surface-brightness relationship for DEEP galaxies. This can be combined with the SBD to find how the luminosity density varies with surface-brightness.

the luminosity density).

By finding a relation between the luminosity and the effective surface-brightness and combining this with the SBD, the luminosity density contributed by galaxies at different surface-brightnesses can be found. Figure 4.34 shows the relationship found between luminosity and effective surface-brightness:

$$\log(L_R) = (-0.55 \pm 0.05) \times \mu_{eff} + (22.1 \pm 1.0) \tag{4.13}$$

This can be combined with the equation for ϕ to give

$$\log(L_R \times \phi) = (0.58 \pm 0.06) \times \mu_{eff} - (3.0 \pm 1.3) \text{ for } \mu_{eff} < \mu^{\star}_{eff} \tag{4.14}$$

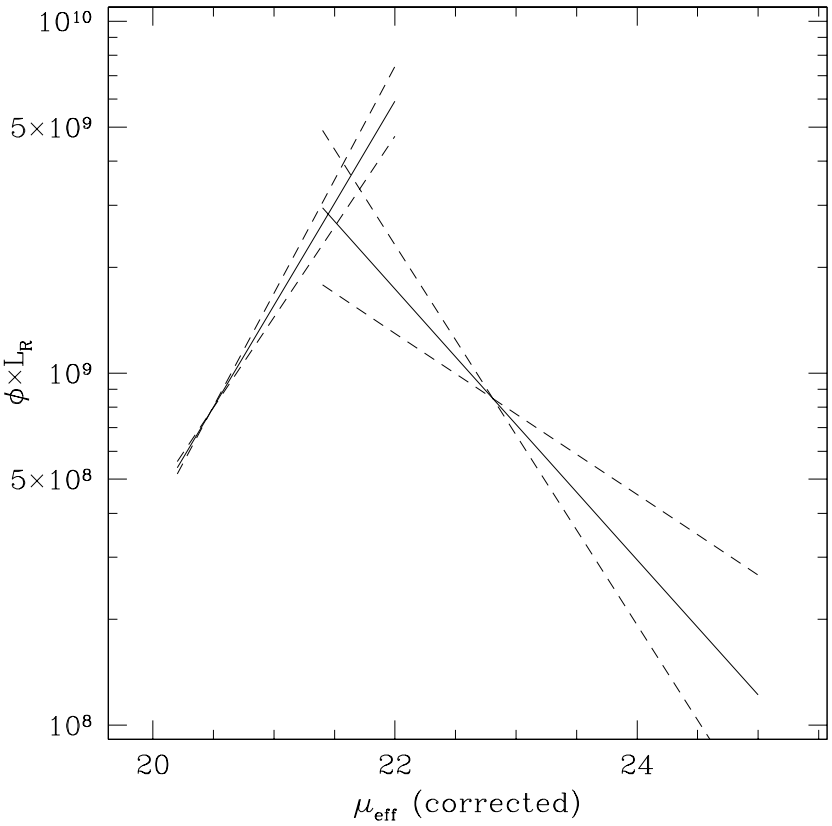

Figure 4.35: Luminosity density – surface-brightness distribution for DEEP galaxies. The luminosity density can be seen to fall sharply either side of a peak at $\mu^{\star}_{eff}$, close to the Freeman value. If this is extrapolated, it is implied that LSB galaxies ($\mu_{eff} > 23$) contribute 17% of the luminosity density of HI-rich galaxies in the Universe.

and

$$\log(L_R \times \phi) = (-0.38 \pm 0.16) \times \mu_{eff} + (17.7 \pm 3.6) \text{ for } \mu_{eff} > \mu^{\star}_{eff} \tag{4.15}$$

This is shown in Figure 4.35, it can be seen that the luminosity density distribution is sharply peaked at $\mu^{\star}_{eff}$, very close to the Freeman value – implying that the greatest contribution to the luminosity density (for gas-rich galaxies) comes from Freeman-law galaxies.

The variation of luminosity density, $\phi \times L_R$, with surface-brightness can be used to assess the contribution

of LSB galaxies to the total luminosity density of gas-rich galaxies in the Universe by integrating under the curve of luminosity density as a function of effective surface-brightness in linear intensity units (Σ_{eff}) from $\Sigma_{eff} = 0$ to ∞ for the total luminosity density and from $\Sigma_{eff} = 0$ to an arbitrarily defined limit for 'low surface-brightness' for the luminosity density due to LSB galaxies. The total luminosity density is given by

$$\rho(L) = \int_0^{\infty} \Psi(\Sigma_{eff}) \times X(\Sigma_{eff})\ \mathrm{d}\Sigma_{eff} \tag{4.16}$$

where Ψ is the number of galaxies per linear surface-brightness bin, $\Psi = \phi/\Sigma_{eff}$. As the SBD is a broken power law, Ψ can be split into two parts, Ψ_{LSB} for $\mu_{eff} > \mu^{\star}_{eff}$ (or $\Sigma_{eff} < \Sigma^{\star}_{eff}$) and Ψ_{HSB} for $\mu_{eff} < \mu^{\star}_{eff}$ (or $\Sigma_{eff} > \Sigma^{\star}_{eff}$). The total density is then given by:

$$\int_{\Sigma^{\star}_{eff}}^{\infty} \Psi_{HSB}(\Sigma_{eff}) \times L(\Sigma_{eff})\ \mathrm{d}\Sigma_{eff} + \int_0^{\Sigma^{\star}_{eff}} \Psi_{LSB}(\Sigma_{eff}) \times L(\Sigma_{eff})\ \mathrm{d}\Sigma_{eff} \tag{4.17}$$

and the LSB contribution to the total luminosity density, where LSB galaxies are defined as those with an effective (R-band) surface-brightness $\mu_{eff} > 23$, or $\Sigma_{eff} < 10^{-0.4\times 23} = 6.31 \times 10^{-10}$, is given by:

$$\int_0^{6.31\times 10^{-10}} \Psi_{LSB}(\Sigma_{eff}) \times L(\Sigma_{eff})\ \mathrm{d}\Sigma_{eff} \tag{4.18}$$

This gives the contribution of LSB galaxies to the total luminosity density of HI rich galaxies to be between 11 and 30% (1σ limits) with a best-fit value of 17%.

Figure 4.36 shows the relationship between HI mass and effective surface-brightness for the DEEP galaxies:

$$\log(M_{\mathrm{HI}}) = (-0.30 \pm 0.04) \times \mu_{eff} + (16.5 \pm 1.0) \tag{4.19}$$

In the same way as the luminosity density contribution at different surface-brightnesses has been found, this relationship can be combined with the SBD to find the contributions to neutral hydrogen density. This gives

$$\log(M_{\mathrm{HI}} \times \phi) = (0.82 \pm 0.06) \times \mu_{eff} - (8.6 \pm 1.3) \text{ for } \mu_{eff} < \mu^{\star}_{eff} \tag{4.20}$$

and

$$\log(M_{\mathrm{HI}} \times \phi) = (-0.13 \pm 0.15) \times \mu_{eff} + (12.1 \pm 3.6) \text{ for } \mu_{eff} > \mu^{\star}_{eff} \tag{4.21}$$

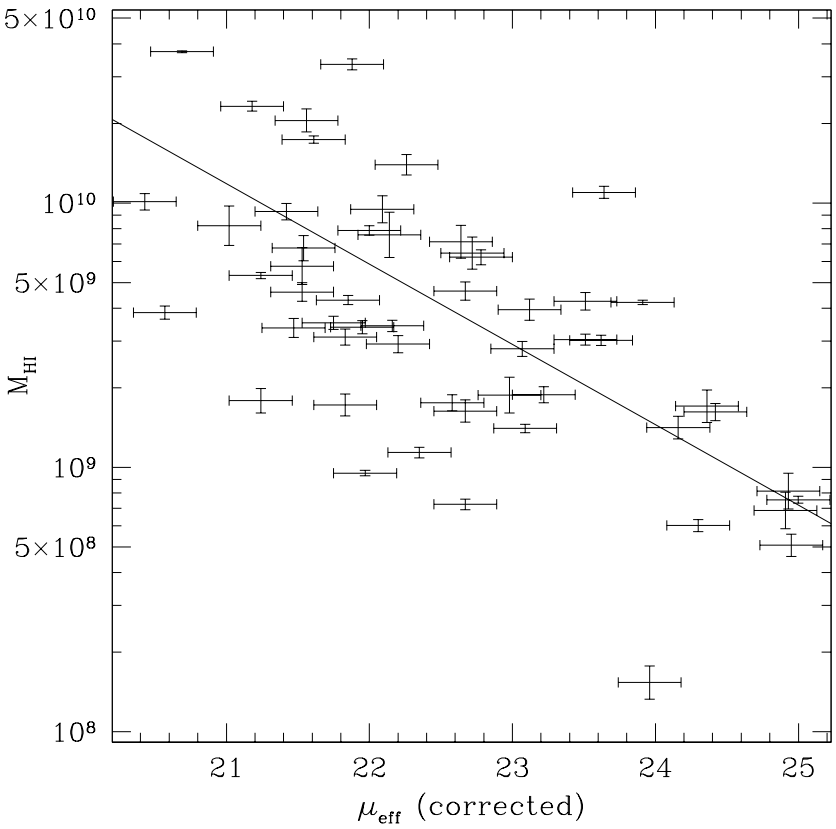

Figure 4.36: HI mass – surface-brightness relationship for DEEP galaxies. This can be combined with the SBD to find how the neutral hydrogen density varies with surface-brightness.

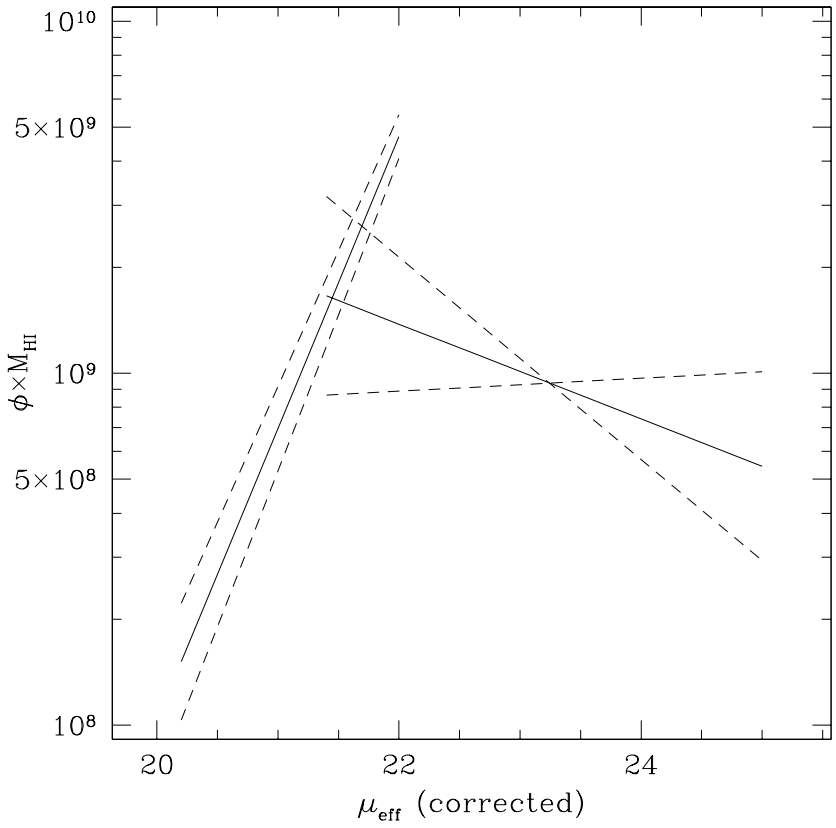

Figure 4.37: Neutral hydrogen density – surface-brightness distribution for DEEP galaxies. It can be seen that there is only a slow fall in HI density towards lower surface-brightnesses, while there is a sharp cut-off towards higher surface-brightnesses. If this is extrapolated, it implies that LSB galaxies contribute 59% of the neutral hydrogen density of the Universe.

Figure 4.37 shows how the neutral hydrogen density varies with effective surface-brightness, it can be seen that there is only a slow decrease towards lower surface-brightnesses while there is a sharp cut-off brighter than $\mu^{\star}_{eff}$. Analysing this in a similar manner to the luminosity density shows that LSB galaxies contribute at least 29% of the neutral hydrogen density of the Universe (1σ limit), with a best-fit value of 59%. That the neutral hydrogen density is divergent, with increasing density towards lower surface-brightnesses, cannot be ruled out at 1σ.

The relationship between the baryonic mass of galaxies (as calculated in Section 4.5) and their effective

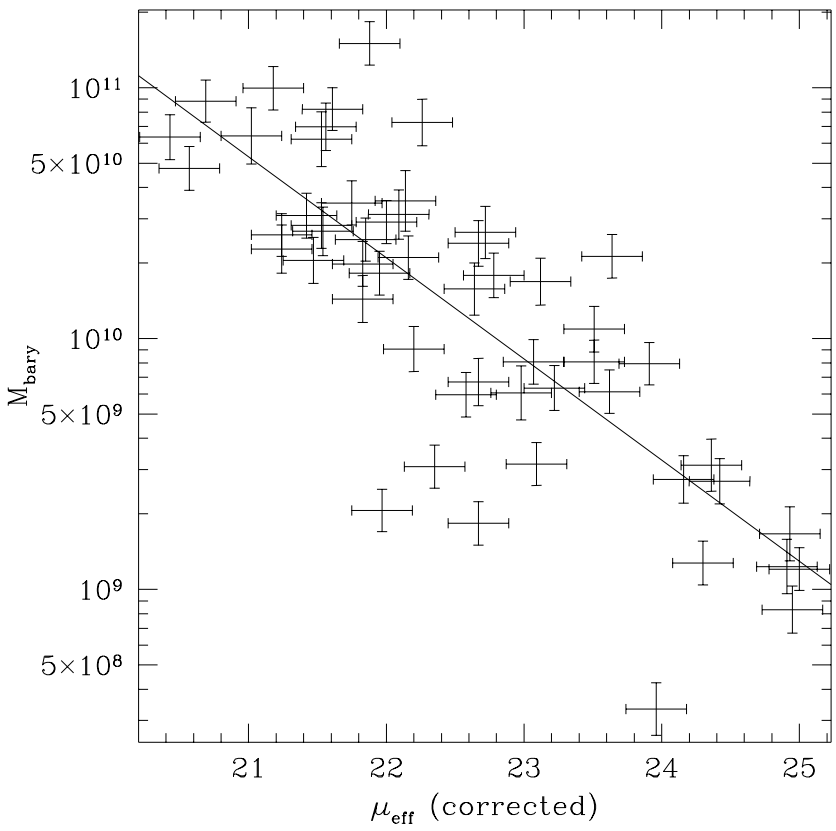

Figure 4.38: Baryonic mass – surface-brightness relationship for DEEP galaxies. This can be combined with the SBD to find how the baryon density varies with surface-brightness.

surface-brightness is shown in Figure 4.38. The best-fit line is

$$\log(M_{bary}) = (-0.40 \pm 0.04) \times \mu_{eff} + (19.2 \pm 1.0) \tag{4.22}$$

As for luminosity and neutral hydrogen, this can be combined with the SBD to give the baryon density contribution from galaxies at different surface-brightnesses. This gives

$$\log(M_{bary} \times \phi) = (0.73 \pm 0.06) \times \mu_{eff} - (5.9 \pm 1.3) \text{ for } \mu_{eff} < \mu^{\star}_{eff} \tag{4.23}$$

and

$$\log(M_{bary} \times \phi) = (-0.23 \pm 0.16) \times \mu_{eff} + (14.8 \pm 3.5) \text{ for } \mu_{eff} > \mu^{\star}_{eff} \tag{4.24}$$

This is shown in figure 4.39, it can be seen that the baryon contribution falls off slowly towards lower surface-brightnesses and is truncated by the down-turn in the SBD towards higher surface-brightnesses. Integrating this in the same way as before implies that the contribution of LSB galaxies to the baryon density of gas-rich galaxies in the Universe is between 19 and 71% (1σ limits), with a best-fit of 36%.

Figure 4.40 shows the relationship between dynamical mass and effective surface-brightness. The best fit is given by

$$\log(M_{dyn}) = (-0.35 \pm 0.06) \times \mu_{eff} + (19.3 \pm 1.3) \tag{4.25}$$

which can be combined with the SBD to give the mass density as a function of effective surface-brightness:

$$\log(M_{bary} \times \phi) = (0.78 \pm 0.07) \times \mu_{eff} - (5.8 \pm 1.6) \text{ for } \mu_{eff} < \mu^{\star}_{eff} \tag{4.26}$$

and

$$\log(M_{bary} \times \phi) = (-0.18 \pm 0.16) \times \mu_{eff} + (14.9 \pm 3.6) \text{ for } \mu_{eff} > \mu^{\star}_{eff} \tag{4.27}$$

Figure 4.41 shows how the mass density varies as a function of effective surface-brightness. Integrating this as previously gives an LSB contribution to the total mass density of gas-rich galaxies in the Universe of between 27 and 90%, with a best fit value of 45%.

Table 4.3 summarises the findings of this section. It can be seen that LSB galaxies make significant contributions to all the cosmological densities investigated, and may contain over half of all but the luminosity

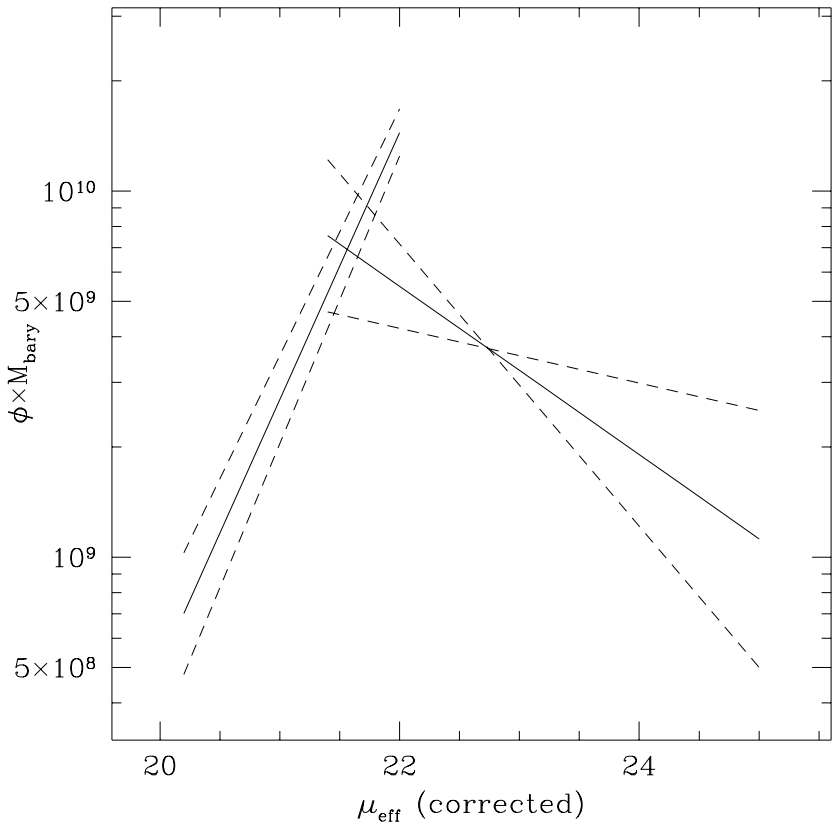

Figure 4.39: Baryon density – surface-brightness distribution for DEEP galaxies. It can be seen that the greatest contribution to the baryon density is made by Freeman-law galaxies around $\mu^{\star}_{eff}$, with the density falling of slowly towards lower surface-brightnesses and quickly towards higher surface-brightnesses. When this is extrapolated, it implies that the contribution to the total baryon density of gas-rich galaxies in the Universe from LSB galaxies to be 36%.

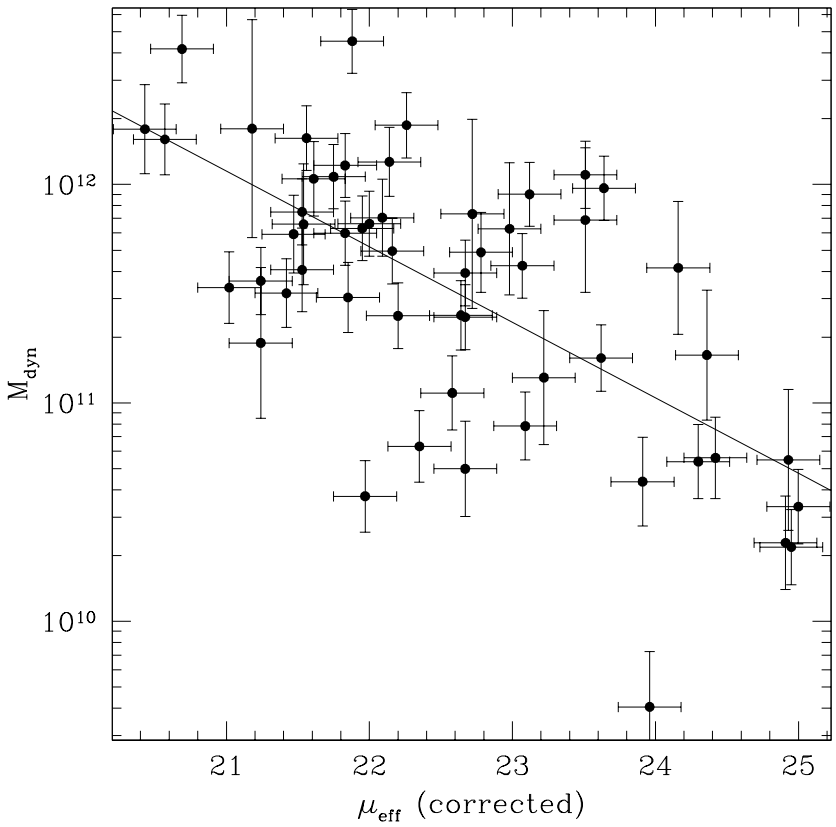

Figure 4.40: Dynamical mass – surface-brightness relationship for DEEP galaxies. This can be combined with the SBD to find how the mass density varies with surface-brightness.

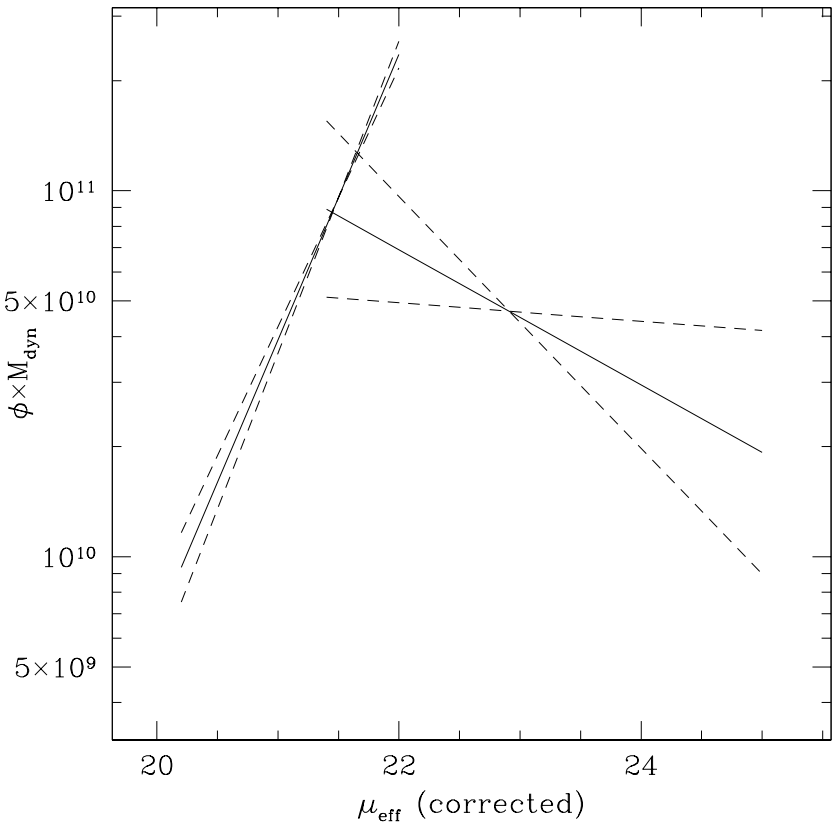

Figure 4.41: Mass density – surface-brightness distribution for DEEP galaxies. The greatest contribution is again made by Freeman-law galaxies $\mu^{\star}_{eff}$, and the mass density falls away more slowly towards lower surface-brightnesses than towards higher surface-brightnesses due to the shape of the SBD. When this is extrapolated, it implies that the contribution of LSB galaxies to the total mass density of gas-rich galaxies in the Universe is 45%.

Table 4.3: Summary of the implied contribution of LSB galaxies to the Universal density of various quantities in gas-rich galaxies. Best fit values and 1σ limits are given, (100%) indicating that the integral under the distribution of that quantity with surface-brightness is divergent implying that it is totally dominated by LSB galaxies.

Quantity	1σ low	Best fit	1σ high
Number density	(100%)	(100%)	(100%)
Luminosity density	11%	17%	30%
Neutral Hydrogen density	29%	59%	(100%)
Baryon density	19%	36%	71%
Mass density	27%	45%	90%

density. The luminosity density of LSB galaxies can be seen to be a very poor indicator of their cosmological importance, yet it is the indicator most commonly used (e.g. McGaugh 1999). The higher HI mass to light ratios of LSB galaxies means that they have more gas and more baryons than would be indicated by their light on a straight extrapolation of $M_{\rm HI}/L$ from Freeman-law galaxies. Similarly, LSB galaxies are dominated by dark matter, so their contribution to the total mass density of the Universe is much higher than their contribution to its luminosity density.

Chapter 5

Conclusions and Future Work

5.1 Conclusions

I have studied a small $4° \times 8°$ region of space using the Parkes HI multibeam system to reach a greater depth than any previous HI survey. The survey revealed 69 sources over almost three decades in HI mass in a volume between 1000 and 12,700kms^{-1}. Follow-up on deep tech pan plates at the UKST has given R-band optical data for 54 galaxies which have been identified as the optical counterparts to the HI sources, these cover a range of 5 magnitudes in effective surface-brightness (μ_{eff}) and 8 magnitudes in absolute magnitude (M_R).

Defining low surface-brightness (LSB) galaxies as those with $\mu_{eff} > 23$ Rμ, there are no high luminosity ($L_R > 10^{10} L_\odot$), LSB 'crouching giant' galaxies. There are 25 high luminosity galaxies in the sample. This gives an upper limit at the 95% confidence level to the contribution of LSB galaxies to the population of gas-rich, high-luminosity galaxies of 12.3%.

A relationship has been found in Section 3.4 between M_R and μ_{eff} in the sense that more luminous galaxies have higher surface-brightnesses. The best-fit slope is 0.53 ± 0.04, significantly shallower than the slope of 0.75 found by Bingelli & Cameron (1991) for dwarf galaxies in the Virgo cluster. This relationship implies that a relationship should be seen between the physical effective radius of the galaxies, R_{eff}, and μ_{eff}, as the luminosity, surface-brightness, and size of galaxies is related by $L \propto \mu \times R^2$. The slope predicted is consistent with the data, although the relationship is almost hidden by the scatter as the slope is very

steep: $\mu_{eff} = -10.6 \times \log R_{eff} + K$.

No relationship has been found, however, between the angular size of the galaxies, r_{eff} and their apparent magnitude, m_R. This indicates that there is no preferred surface-brightness in the DEEP survey. If all galaxies had the same surface-brightness, then a correlation would be seen between these two variables.

An unexpected correlation was found in the optical data between m_r and μ_{eff} – lower surface-brightness galaxies are seen to have lower apparent luminosities. The scatter in this relationship is too low for it to be due to the small redshift range covered by DEEP, therefore another explanation must be found. The correlation found implies that all of the galaxies of DEEP are of a similar angular size in the optical. If the ratio of HI size to optical size is reasonably constant, then this implies that the HI discs of all the DEEP galaxies are of similar angular sizes. All the DEEP galaxies also have similar HI fluxes – the majority of sources in any catalogue will be close to the limit of that catalogue. Together these two results imply that all the galaxies in DEEP have similar values for their HI column density, $N_{\rm HI}$. This may be due to lower column-density galaxies being ionised by the intergalactic UV flux, as proposed by Corbelli & Salpeter (1993).

Although no high luminosity, LSB galaxies have been foud in DEEP, a high HI mass ($M_{\rm HI} > 10^{10} M_{\odot}$), LSB galaxy was found. There were only 8 such high HI mass galaxies in the optical sample, that one of these is an LSB galaxies implies up to 45.9% of high HI mass galaxies in the Universe could be LSB galaxies (to 95% confidence limits).

A relationship has been found between $M_{\rm HI}$ and μ_{eff} in Section 4.2 and Section 4.7. Although this is similar in appearance to the relationship between M_R and μ_{eff}, with more HI-massive galaxies having higher surface-brightnesses, there is more scatter and the slope is less steep: $\log M_{\rm HI} = (-0.30 \pm 0.04) \times \mu_{eff} + K$ while $\log L_R = (-0.55 \pm 0.05) \times \mu_{eff} + K$. This implies that the HI mass to light ratio, $M_{\rm HI}/L_R$, increases towards lower surface-brightnesses. This is indeed what is observed. It is shown in Section 4.1 that there is a correlation between the surface-brightness and the HI mass to light ratio of $\mu_{eff} = (3.38 \pm 0.33) \times \log(M_{\rm HI}/L_R) + K$. This is in agreement with the results of previous studies (e.g. de Blok et al. 1997) that LSB galaxies have higher HI mass to light ratios than 'normal' galaxies. The implication of this is that, for LSB galaxies, the luminosity is not a good tracer of the total baryonic mass and thus of the cosmological importance of these galaxies. 'Crouching Giant' galaxies may indeed exist, but they are giant in their total baryon content rather than in their luminosity.

In Section 4.3, I have attempted to derive HI column-densities for the DEEP galaxies using their measured HI masses and relationships found in the literature between optical and HI radii of optically-selected samples of galaxies. These relationships may not be applicable to the DEEP galaxies, but this is the best that can be done without carrying out deep synthesis mapping of all the sources. This gives the result that most galaxies in DEEP have average column densities of around 4×10^{20} atoms cm^{-2}, with even the lowest being above 10^{20} atoms cm^{-2}. This is well above the column-density limit for DEEP of $\simeq 2 \times 10^{18}$ atoms cm^{-2} for a realistic galaxy with $\Delta V = 200 \mathrm{km s}^{-1}$. The estimated radii would have to be too small by a factor of around 8 for the lowest column-density galaxies to be near this limit. This implies that there is no large population of low column-density galaxies that would be missed in HIPASS and other HI surveys. To the 95% confidence level, galaxies with average values of $N_{\mathrm{HI}} < 10^{20}$ atoms cm^{-2} make up less than 5.4% of all gas-rich galaxies.

The column-densities found are consistent, when the differences of method are taken into account, with the measures of $M_{\mathrm{HI}}/D^2_{Holm}$ of Giovanelli & Haynes (1989). That all the column-densities are approximately equal is also consistent with the explanation for the relationship between m_R and μ_{eff} found in Section 3.4.

The same radii used to calculate the column-densities were used, with the optical inclinations and the HI velocity widths, to calculate the dynamical mass, M_{dyn} of the DEEP galaxies (Section 4.6). Again, it was found that LSB galaxies were generally less massive than 'normal' galaxies. However out of the 12 galaxies with $M_{dyn} > 10^{12} M_{\odot}$, one is an LSB galaxy. This implies that the upper limit on the LSB proportion of gas rich, high mass galaxies is 32.8% (to 95% confidence limits).

It can also be seen that the luminosity is a poor tracer of the dynamical mass of LSB galaxies in the same way that it is a poor tracer of the baryonic mass. Zwaan et al. (1997) found that in order to explain their observation that LSB galaxies fall on the same Tully-Fisher (TF) relationship as 'normal' galaxies, the product $\Upsilon^2\Sigma$ must remain constant (where Υ is the mass to light ratio, and Σ is the surface-brightness in linear units of intensity). This means that as the surface-brightness falls, the luminosity is an increasingly bad indicator of the true mass, and thus importance, of the galaxies. That $\Upsilon^2\Sigma$ remains constant is also seen in the DEEP data (Section 4.6).

That the $\Upsilon^2\Sigma$ relation is seen to hold in the DEEP data implies that the DEEP galaxies should all fall on a single TF relationship. This has been investigated in Section 4.5, where it has been found that the DEEP data can be fitted with a single slope. This slope is consistent (at the 2σ level) with the R-band TF relationship of Courteau (1997) although with a much wider scatter, which may be due to the wider

spread of morphological types. The data is also consistent with the baryonic TF relationship of McGaugh et al. (2000). It appears possible that the match with this relationship could be improved by altering the estimated value of $\Upsilon^{\star}_{R}$, the stellar mass to light ratio in R-band.

Section 4.2 presents an analysis of this data set using a weighting based on an HI Mass Function (HIMF) with $\alpha = -1.3 \pm 0.1$ and $M^{\star}_{\rm HI} = 10^{9.75} M_{\odot}$. The sample was divided into six bins of 0.5 dex in HI mass. These bins were then weighted to bring them in line with the HIMF, thus correcting for discrimination based on HI mass regardless of whether selection is by peak-flux, signal to noise, or some combination of these. As long as there is no discrimination against low luminosity or LSB galaxies apart from the dependence of these quantities on HI mass, this weighting corrects the sample to that expected if all galaxies were seen over the same volume. This has allowed the faint-end slope of the R-band luminosity function (LF) and the surface-brightness distribution (SBD) to be determined for gas-rich galaxies.

If the HIMF is steeper (such as $\alpha = -1.52$ as found by Kilborn 2001) this will serve to steepen the LF and the low surface-brightness (LSB) end slope of the SBD. The faint-end slope of the LF was found to be $\alpha = -1.14 \pm 0.05$, which is fairly flat and is consistent with the LF for field galaxies found in optically selected field samples, such as $\alpha = -1.20 \pm 0.03$ found in the r-band Sloan Digital Sky Survey commissioning data (Blanton et al. 2001).

The SBD was found to be fitted by a broken power-law, with the break at $\mu^{\star}_{eff} = 21.56^{+0.18}_{-0.26}$ Rμ, close to the Freeman-law value. This is similar to the form for the SBD found by McGaugh (1996) using the data of Davies (1990). The SBD is then given by $\phi \propto \mu_{eff}^{1.13 \pm 0.04}$ towards high surface-brightnesses ($\mu_{eff} < \mu^{\star}_{eff}$) and $\phi \propto \mu_{eff}^{0.17 \pm 0.14}$ towards low surface-brightnesses ($\mu_{eff} > \mu^{\star}_{eff}$), where ϕ is the number of galaxies per logarithmic bin of surface-brightness. This LSB end slope is steeper than that normally found by optical surveys, which are generally fairly close to flat or slowly falling while this slope gives an increasing number of galaxies towards lower surface-brightnesses. The high surface-brightness (HSB) slope is shallower than that of McGaugh (1996), but is consistent with other surveys (Phillipps et al. 1987, de Jong 1996) which also found shallower HSB end slopes.

This surface-brightness distribution is used in Section 4.7 to estimate the cosmological importance of LSB galaxies. By combining relationships found between the effective surface-brightness and luminosity, HI mass, baryonic mass, and dynamical mass with the SBD the contribution of LSB galaxies to the luminosity density, neutral hydrogen density, baryon density, and mass density of gas-rich galaxies in the Universe has been derived. This implies that, to one standard-error, LSB galaxies contribute between 11% and 30% of

the luminosity density of gas-rich galaxies in the Universe, with a best-fit of 17%. They contribute over 29% of the neutral-hydrogen density of the Universe, with a best-fit of 59%, and between 19% and 71% of the baryon density of gas-rich galaxies in the Universe, with a best-fit of 36%. They also contribute between 27% and 90% of the mass density of gas-rich galaxies in the Universe, with a best-fit of 45%. It can be seen that LSB galaxies are in important component of the Universe, in particular with regard to their content of neutral hydrogen and total dynamical mass. Despite being generally less massive individually than 'normal' surface-brightness galaxies, LSB galaxies are much more numerous and can thus make a large contribution to cosmic densities.

Section 3.5 investigates the properties of DEEP galaxies which are already in the literature. As expected, discrimination against low luminosity and LSB galaxies is seen in optically-selected and IRAS samples. The lack of LSB galaxies in IRAS has been investigated further. It appears that this lack may well be a selection effect due to the generally lower luminosity of LSB galaxies rather than due to an intrinsic lack of dust in LSB galaxies. The ratio of IR luminosity to R-band luminosity appears to remain constant for those galaxies detected in IRAS as the surface-brightnesses changes, which would lead to low-luminosity, LSB galaxies having IR fluxes below the detection limit of IRAS. However, if this is the case then the contribution of LSB galaxies to the total IR flux of the Universe is likely to be small, as their contribution to the total R-band luminosity is small.

5.2 Future work

The DEEP region has now been observed to an integration time of 9000 seconds per pointing, or 20 $\times$ the integration time of HIPASS. Analysis of this new data will allow more sources to be found, increasing the accuracy to which the relationships presented here can be determined. The additional sources may also show up trends only hinted at in this work, such as the link between peakiness of galaxies and surface-brightness (Section 4.4).

Optical images obtained in B- and R-band with the CTIO Curtis-Schmidt telescope will allow multi-colour optical analysis of the whole of the DEEP area, rather than only the $4^\circ \times 6^\circ$ area which overlaps with the tech pan plates. This will increase the number of optical counterparts considerably, and therefore will both add to the accuracy of the relationships found and increase the possibility of finding interesting 'extreme' objects. Full profile analysis will allow decomposition of surface-brightness profiles in order to

separate out the components and accurately fit central surface-brightnesses to the galaxies, where they have regular profiles.

The greater numbers added both to the HI sample and to the number of galaxies with optical data will help improve the accuracy of the SBD and of the relationships between effective surface-brightness and luminosity, HI mass, baryonic mass, and dynamical mass. This will enable tighter limits to be put on the contributions of LSB galaxies to the cosmic luminosity, neutral hydrogen, baryonic and mass densities of gas-rich galaxies.

Optical spectroscopy has been carried out using the 2.3-m telescope of the Australian National University (ANU) at Siding Springs Observatory. When analysed, this will hopefully allow ESO 509-G075 to either be confirmed or rejected as the optical counterpart of DEEP J1335-2729 and either Abell 3558:[MGP94]4312 or 4317 to be determined to be the optical counterpart of DEEP J1332-3223. In addition, spectra of interesting sources with high luminosity of HI mass but no velocity in the literature have been obtained and will hopefully allow the optical counterparts of these sources to be confirmed.

Further follow-up is planned using the Australia Telescope Compact Array to investigate interesting LSB galaxies such as ESO 445-G048 and ESO 383-G059 and to accurately determine their dynamical masses along with any other interesting sources that turn up when the new HI and optical data is analysed.

REFERENCES

Allen, R. J. & Shu, F. H. 1979, ApJ, 227, 67

Arp, H. 1965, ApJ, 142, 402

Banks, G. D. 1998, Ph.D. Thesis, Cardiff University

Banks, G. D. et al. 1999, ApJ, 524, 612

Barnes, D. G. 1998, in "Astronomical Data Analysis Software and Systems VIII", ASP Conf. Ser. 145, p32, eds. R. Albrecht, R. N. Hook, & H. A. Bushouse

Barnes et al. 1998, in "Astronomical Data Analysis Software and Systems VIII", ASP Conf. Ser. 145, p89, eds. R. Albrecht, R. N. Hook, & H. A. Bushouse.

Barnes et al. 2001, MNRAS, 322, 486

Barton, E. J., Geller, M. J., Bromley, B. C., van Zee, L., & Kenyon, S. J. 2001, AJ, 121, 625

Bertin, E. & Arnouts, S. 1996, A&AS, 117, 393

Bingelli, B. & Cameron, L. M. 1991, A&A, 252, 27

Bingelli, B., Sandage, A., & Tammann, G. A. 1985, AJ, 90, 1681

Blanton et al. 2001, AJ, 121, 2358

Bothun, G., Impey, C., & McGaugh, S. 1997, PASP, 109, 745

Bothun, G. D.. Impey, C. D., Malin, D. F., & Mould, J. R. 1987, AJ, 94, 23

Briggs, F. H. & Rao, S. 1993, ApJ, 417, 494

Cawson, M. G. M., Kibblewhite, E. J., Disney, M. J., Phillipps, S. 1987, MNRAS¡ 224, 557

Cayatte, V., Kotanyl, C., Balkowski, C., van Gorkom, J.H. 1994, AJ, 107, 1003

Colgan, S. W. J., Salpeter, E. E., & Terzian, Y. 1990, ApJ, 351, 503

Corbelli, E. & Salpeter, E. E. 1993, ApJ, 419, 104

Corbelli, E., Schneider, S. E., & Salpeter, E. E. 1989, AJ 97, 390

Côté, S., Freeman, K. C., Carignan, C., & Quinn, P.J. 1997, AJ, 114, 1313

Courteau, S. 1997, AJ, 114, 2402

Dalcanton, J. J., Spergel, D. N., Gunn, J. E., Schmidt, M., Schneider, D. Pl 1997, AJ, 114, 1447

Davies, J. I. 1990, MNRAS, 244, 8

Davies, J. I., Phillipps, S., & Disney, M. J. 1989a, MNRAS, 239, 703

Davies, J. I., Phillipps, S., & Disney, M. J. 1989b, Ap&SS, 157, 299

Davies, J. I., Disney, M. J., Phillipps, S., Boylce, B. J., & Couch, W. J. 1994, MNRAS, 269, 349

da Costa, L. N., Numes, M. A., Pellegrini, P. S., Willmer, C., Chincarini, G., & Cowan, J. J. 1986, AJ, 91, 6

da Costa, L. N., Willmer, C., Pellegrini, P. S., & Chincarini, G. 1987, AJ, 93, 1338

Dekel, A. & Silk, J. 1986, ApJ, 303, 39

de Blok, W. J. G., McGaugh, S. S., & van der Hulst, J. M.. 1996, MNRAS, 283, 18

de Blok, W. J. G. & van der Hulst, J. M. 1998a, A&A, 335, 421

de Blok, W. J. G. & van der Hulst, J. M. 1998b, A&A, 336, 49

de Blok, W. J. G., van der Hulst, J. M., & Bothun, G. D. 1995, MNRAS, 274, 235

de Jong, R. S. 1996a, A&AS, 118, 557

de Jong, R. S. 1996b, A&A, 313, 45

de Jong, R. S. 1996c, A&A, 313 377

de Jong, R. S. & Lavey, C. 1999, Ap&SS, 269, 569

de Jong, R. S. & van der Kruit, P. C. 1994, A&AS, 106, 451

de Souza. R. E., de Mello, D. F., & Dos Anjos, S. 1997, A&AS, 135, 329

de Vaucouleurs, G. 1974, in "The Formation and Dynamics of Galaxies", IAU Symp. 58, p1, ed. J. R. Shakeshaft.

de Vaucouleurs, G., de Vaucouleurs, A., & Corwin, H. G. 1976 (RC2), "Second Reference Catalogue of Bright Galaxies", publ. University of Texas Press, Austin, US.

de Vaucouleurs, G., de Vaucouleurs, A., Corwin, H. G., Jr., Buta, R. J., Paturel, G., & Fouqué, P. 1991 (RC3) "Third Reference Catalogue of Bright Galaxies", vols 1-3, publ. Springer-Verlag, New York, US.

Disney, M. J., 1976, Nature, 263, 573

Disney, M. J. & Banks, G. D. 1997, PASA, 14, 69

Disney, M. J. & Phillipps, S. 1983 (DP 83), MNRAS, 205, 1253

Disney, M. J., Phillipps, S., Davies, J. I., Cawson, M. G. M., & Kibblewhite, E. J. 1990, MNRAS, 245, 175

Dressler, A. 1991, ApJS, 75, 241

Dreyer, J. L. E. 1888 (NGC), MmRAS, 49, 1

Dreyer, J. L. E. 1895 (IC, Part 1), MmRAS, 51, 185

Dreyer, J. L. E. 1908 (IC, Part 2), MmRAS, 59, 105

Drinkwater, M. J., Phillipps, S., Gregg, M. D., Parker, Q. A., Smith, R. M., Davies, J. I., Jones, J. B., Sadler, & E. M. 1999, ApJ, 511, 97

Drinkwater, M. J., Phillipps, S., Jones, J. B., Gregg, M. D., Dady, J. H., Davies, J. I., Parker, Q. A., Sadler, E. M., & Smith, R. M. 2000, A&A, 355, 900

Driver, S. P. 1994, Ph.D. Thesis, Cardiff University

Eder. J. A., Oemler, A., Jr., Schombert, J. M., & Delel, A. 1989, ApJ, 340, 29

Evans, Rh., Davies J. I., & Phillipps, S. 1990, MNRAS, 245, 164

Fairall, A. P., Vettolani, G., & Chincarini, G. 1989, A&AS, 78, 269

Ferguson, H. C. & McGaugh, S. S. 1995, ApJ, 440, 470

Fish, R. A. 1964, ApJ, 139, 284

Fouqué, P., Durand, N., Bottinelli, L., Gouguenheim, L., & Paturel, G. 1990, A&AS, 86, 473

Freeman, K. C. 1970, ApJ, 160, 811

Freeman, K. C. 1978, in "Structure and properties of nearby galaxies", IAU Symp. 77, p3, eds. E. M. Berkhuijsen & R. Wielebinski.

Fukugita, M., Hogan, C. J., & Peebles, P. J. E. 1998, ApJ, 503, 518

Giovanelli, R. & Haynes, M. P. 1988, in "Galactic and extragalactic radio astronomy (2nd edition)", eds. Verschuur, G. L., & Kellermann, K. L., publ. Springer-Verlag, Berlin & New York.

Henning, P. A. 1992, ApJS, 78, 365

Henning, P. A. 1995, ApJ, 450, 578

Henning, P. A. & Kerr, F. J. 1989, ApJ, 347L, 1

Holmberg, E. B. 1958, Lund Medd. Astron. Obs. Ser. II, 136, 1

Holmberg, E. 1966, in "Galaxies and the Universe", Stars and Stellar Systems vol IX, p123, eds A. Sandage, M. Sandage, & J. Kristian, publ. University of Chicago Press, US, 1975.

Huchtmeier, W. K, Karachentesev, I. D., Karachentseva, V. E., & Ehle, M. 2000, A&AS, 141, 469

Impey, C., & Bothun, G. 1997, ARA&A, 35, 267

Impey. C., Bothun, G., & Malin, D. 1988, ApJ, 330, 634

Impey, C. D., Sprayberry, D., Irwin, M. J., & Bothun, G. D. 1996, ApJS, 105, 209

Irwin, M. J., Davies, J. I., Disney, M. J., & Phillipps, S. 1990, MNRAS, 245, 289

Karachentsev, I. D., Karachentseva, V. E., & Parnovskij, S. L. 1993 (FGC), Astronomische Nachrichten, vol. 314, no. 3, p97.

Kerr, F. J. & Henning, P. A. 1987, ApJ, 320, 99

Kennicutt, R. C., Jr. 1989, ApJ, 344, 685

Kibblewhite, E. J., Bridgeland, M. T., Bunclark, P. S., & Irwin, M. J. 1984, in "Astronomical Microdensitometry Conference", eds. D. A. Klinglesmith, publ. National Aeronautic and Space Administration, US.

Kibblewhite, E. J., Cawson, M. G. M., Phillipps, S., Davies, J. I., & Disney, M. J. 1989, MNRAS¡ 236, 187

Kilborn, V. A. 2001, Ph.D. Thesis, University of Melbourne

Kilborn, V. A., Webster, R. L., & Staveley-Smith, L. 1999, PASA, 16, 8

Kilborn, V. A. et al. 2000, AJ, 120, 1342

Koribalski, B. S. 2001, in "Gas & Galaxy Evolution", ASP conf. ser., eds. J. E. Hibbard, M. P. Rupen, & J. H. van Gorkom, in press.

Kormendy, J. 1977, ApJ, 217, 406

Longmore, A. J., Hawarden, T. G., Cannon, R. D., Allen, D. A., Mebold, U., Goss, W. M., & Reif, K. 1979, MNRAS, 188, 285

Longmore, A. J., Hawarden, T. G., Goss, W. M., Mebold, U., & Webster, B. L. 1982, MNRAS, 200, 325

McGaugh, S. S. 1996, MNRAS¡ 280, 337

McGaugh, S. 1999, int "The Low Surface Brightness Universe", ASP Conf. Ser. 170, eds. J. I. Davies, C. Impey, & S. Phillipps.

McGaugh, S. S. & Bothun, G. D. 1994, AJ, 107, 530

McGaugh, Bothun, & Schombert 1995 (MBS 95)

McGaugh, S. S., Schombert, J. M., Bothun, G. D., & de Blok, W. J. G. 2000, ApJ, 533, 99

Maloney, P. 1993, ApJ, 414, 41

Mathewson. D. S., Cleary, M. N., & Murray, J. D. 1974, ApJ, 190, 291

Mathewson, D. S. & Ford, V. L. 1996, ApJS, 107, 97

Mathewson, D. S., Ford, V. L., & Buchhorn, M. 1992, ApJS, 81, 413

Matthews, van Driel, & Gallagher 1998, AJ, 116, 1169

Menzies, J. W., Coulson, I. M., & Sargent, W. L. W. 1989, AJ, 97, 1576

Minchin, R. F. 1999, PASA, 16, 12

Moore et al. 1998

Morshidi, Z. 1998, Ph.D. Thesis, Cardiff University

Morshidi-Esslinger, Z., Davies, J. I., & Smith, R. M. 1999a, MNRAS, 304, 297

Morshidi-Esslinger, Z., Davies, J. I., & Smith, R. M. 1999b, MNRAS, 304, 311

Nilson, P. 1973 (UGC), "Uppsala General Catalogue of Galaxies", publ. Royal Society of Science of Uppsala, Sweden.

O'Neil, K. & Bothun, G. 2000, ApJ, 529, 811

O'Neil, K., Bothun, G. D., & Cornell, M. E. 1997, AJ, 113, 1212

O'Neil, K., Bothun, G. D., & Schombert, J. 2000, AJ, 119, 136

O'Neil, K., Bothun, G. D., Schombert, J., Cornell, M. E., & Impey, C. D. 1997, AJ, 114, 2448

Penston, M. V., Fosbury, R. A. E., Ward, M. J., & Wilson, A. S. 1977, MNRAS, 180, 19

Phillipps, S. & Disney, M. J. 1983, MNRAS, 203, 55

Phillipps, S., Disney, M. J., Kibblewhite, E. J., & Cawson, M. G. M. 1987, MNRAS, 229, 505

Pickering, T. E., Impey, C. D., van Gorkom, J. H., & Bothun, G. D. 1997, AJ, 114, 1858

Quintana, H., Ramirez, A., Melnick, J., Raychaudhury, S., & Slezak, E. 1995, AJ, 110, 463

Richter, O.-G. 1984, A&AS, 58, 131

Richter, O.-G. 1987, A&AS, 67, 261

Roberts, M. S. 1975 in "Galaxies and the Universe", Stars and Stellar Systems vol IX, p309, eds A. Sandage, M. Sandage, & J. Kristian, publ. University of Chicago Press, US

Roberts, M .S. & Haynes, M. 1994, ARA&A, 32, 115

Romanishin, W., Krumm, N., Salpeter, E., Knapp, G., Strom, K. M., & Strom, S. E. 1982, ApJ, 263, 94

Rosenberg, J. L. & Schneider, S. E. 2000, ApJS, 130, 177

Sandage, A. 1978, AJ, 83, 904

Salpeter, E. E. 1955, ApJ, 121, 161

Salpeter, E. E. & Hoffman, G. L. 1996, ApJ, 465, 595

Schecter, P. 1976, ApJ, 203, 297

Schneider, S. E., Spitzak, J. G., & Rosenberg, J. L. 1998, ApJ, 507L, 9

Schombert, J. M. & Bothun, G. D. 1988, AJ, 95, 1389

Schombert.J. M., Bothun, G. D., Schneider, S. E., & McGaugh, S. S. 1992, AJ, 103, 1107

Schwartzenberg, J. M., Phillipps, S., Smith, R. M., Couch, W. J., & Boyle, B. J. 1995, MNRAS, 275, 121

Shostak, G. S. 1977, A&A, 54, 919

Solanes, J. M., Giovanelli, R., & Haynes, M. P. 1996, ApJ, 461, 609

Sorar, E. 1994, Ph.D. Thesis, Pittsburgh University

Spitzak, J. G. 1996, Ph.D. Thesis, University of Massachusetts

Spitzak, J. G. & Schneider, S. E. 1998, ApJS, 199, 159

Sprayberry, D. 1994, Ph.D. Thesis, University of Arizona

Sprayberry, D., Impey, C. D., Irwin, M. J., & Bothun , G. D. 1997, ApJ, 482, 104

Staveley-Smith, L., Wilson, W. E., Bird, T. S., Disney, M. J., Ekers, R. D., Freeman, K. C., Haynes, R. F., Sinclair, M. W., Vaile, R. A., Webster, R. L., & Wright, A. E. 1996, PASA, 13, 243

Theureau, G., Bottinelli, L., Coudreau-Durand, N., Gouguenheim, L., Hallet, N., Loulergue, M., Paturel, G., & Teerikorpi, P. 1998, A&AS, 130, 333

Tully, R. B. & Fisher, J. R. 1977, A&A, 54, 661

Turner, J. A., Phillipps, S., Davies, J. I., & Disney, M. J. 1993, MNRAS, 261, 39

Van den Bergh, S. 1959, in "Publications of the David Dunlap Observatory", vol. 2, No. 5, p147, publ. University of Toronto Press, Canada.

van der Hulst, J. M., Skillman, E. D., Smith, T. R., Bothun, G. D., McGaugh, S. S., & de Blok, W. J. G. 1993, AJ, 106, 548

van der Kruit, P. C. 1987, A&A, 173, 59

Vorontsov-Vel'Yaminov, B. A. & Arkhipova, V. P. 1974 (MCG, part 5), Trudy Gosud. Astron. Inst. Shtemberga, 46, 1

Vorontsov-Vel'Yaminov, B. A. & Arkhipova, V. P. 1968 (MCG, part 4), Trudy Gosud. Astron. Inst. Shtemberga, 38, 1

Vorontsov-Vel'Yaminov, B. A. & Arkhipova, V. P. 1964 (MCG, part 2), Trudy Gosud. Astron. Inst. Shtemberga, 34, 1

Vorontsov-Vel'Yaminov, B. A. & Arkhipova, V. P. 1963 (MCG, part 3), Trudy Gosud. Astron. Inst. Shtemberga, 33, 1

Vorontsov-Vel'Yaminov, B. A. & Krasnogorskaya, A. A.. 1962 (MCG, part 1), Trudy Gosud. Astron. Inst. Shtemberga, 32, 1

Willmer, C. N. A., Maia, M. A. G., Mendes, S. O., Alonso, M. V., Rios, L. A., Chaves, O. L., & de Mello, D. F. 1999, AJ, 118, 1131

Willmer, C. N. A., Focardi, P., Chan, R., Pilligrini, P. S., & da Cost, L. N. 1991, AJ, 101, 57

Wright, A. E. & Otrupcek, R. 1990 (PKSCAT 90), "Parkes Catalogue, 1990", publ. Australia Telescope National Facility, Australia.

Zwaan, M. A., van der Hulst, J. M., de Blok, W. J. G., & McGaugh, S. S. 1995, MNRAS, 273L, 35

Zwaan, M. A., Briggs, F. H., Sprayberry, D., & Sorar, E. 1997, ApJ, 490, 173

Zwaan, M. 2000, Ph.D. Thesis, Rijksuniversiteit Groningen, Netherlands

Zwicky , F.1957, "Morphological Astronomy', publ. Springer, Germany

Zwicky, F., Herzog, E., Wild, P., Karpowicz, M., & Kowal, C. T. 1968b (CGCG, vol. 6), "Catalogue of Galaxies and of Clusters of Galaxies", publ. California Institute of Technology, US.

Zwicky, F., Herzog, E., Wild, P., Karpowicz, M., & Kowal, C. T. 1968a (CGCG, vol. 4), "Catalogue of Galaxies and of Clusters of Galaxies", publ. California Institute of Technology, US.

Zwicky, F., Herzog, E., Wild, P., Karpowicz, M., & Kowal, C. T. 1966 (CGCG, vol. 3), "Catalogue of Galaxies and of Clusters of Galaxies", publ. California Institute of Technology, US.

Zwicky, F., Herzog, E., Wild, P., Karpowicz, M., & Kowal, C. T. 1965 (CGCG, vol. 5), "Catalogue of Galaxies and of Clusters of Galaxies", publ. California Institute of Technology, US.

Zwicky, F., Herzog, E., Wild, P., Karpowicz, M., & Kowal, C. T. 1963 (CGCG, vol. 2), "Catalogue of Galaxies and of Clusters of Galaxies", publ. California Institute of Technology, US.

Zwicky, F., Herzog, E., Wild, P., Karpowicz, M., & Kowal, C. T. 1961 (CGCG, vol. 1), "Catalogue of Galaxies and of Clusters of Galaxies", publ. California Institute of Technology, US.